Acute effects of Axin loss in the mouse liver and embryonic development

Anika D. Offergeld

PhD Thesis
2015

Cardiff University
School of Biosciences

Thesis Supervisors:
Prof Trevor C. Dale
Prof Alan R. Clarke

Declaration

This work has not been submitted in substance for any other degree or award at this or any other university or place of learning, nor is being submitted concurrently in candidature for any degree or other award.

Signed …….. (candidate) Date ……..

STATEMENT 1

This thesis is being submitted in partial fulfilment of the requirements for the degree of PhD.

Signed …….. (candidate) Date ……..

STATEMENT 2

This thesis is the result of my own independent work/investigation, except where otherwise stated. Other sources are acknowledged by explicit references. The views expressed are my own.

Signed …….. (candidate) Date ……..

STATEMENT 3

I hereby give consent for my thesis, if accepted, to be available online in the University's Open Access repository and for inter-library loan, and for the title and summary to be made available to outside organisations.

Signed …….. (candidate) Date ……..

STATEMENT 4: PREVIOUSLY APPROVED BAR ON ACCESS

I hereby give consent for my thesis, if accepted, to be available online in the University's Open Access repository and for inter-library loans **after expiry of a bar on access previously approved by the Academic Standards & Quality Committee.**

Signed …….. (candidate) Date ……..

Acknowledgement

First of all, I would like to thank my supervisors Dr Trevor Dale and Dr Alan Clarke for their time and effort in guiding the progress of this thesis, while leaving me the opportunity to pursue interesting aspects independently.

I also want to thank the whole 3rd floor east, past and present, and the members of Alan Clarke's lab at the ECSCRI (European cancer stem cell research institute) for all their valuable impute as part of 'team Axin'. Especial thanks have to go to Dr Gui-Jie Feng, Ken Ewan, Christine Calver, and Victoria Marsh Durban.

The research presented here would not have been possible without the technical assistance from many people. I would like to thank Derek Scarborough, and Mark Isaac for their histological services and the team from JBIOS and the barrier unit for their assistance with animal research. Without Patrick Mason, Helen Reed, Bridget Allen, Orosia Asby, Elaine Taylor and Michael Quirk, I would have endured many more laborious hours in the mouse facilities, weaning and ear-clipping mice. Special thanks also goes to Prof. Nick Alan and Dr. Susi Hunter for helping me with the generation of the many ES cell lines and Meritxell Huch-Ortega who patiently introduced me to the art of culturing primary liver cells in 3D. Additional thanks go to Oliver Poetz, Bram Herpers, and Leo Price all of whom were valuable collaborators during my PhD thesis. I was also very lucky to supervise many undergraduate students throughout the course of my thesis. The valuable work of William Hill, Ian Blackburn, and Kyle Hawker contributed to the successful progress of the Axin story.

On a personal note, I would also like to thank my Cardiff friends and lab mates, for wonderful meals and drinking sessions in the last few years; and also to my partner Matt without whom I would regularly go insane. Thanks for supporting and distracting me whenever I need it.

Many thanks also go to my family and friends in Germany. Ohne euch währe ich nicht da, wo ich heute bin! Danke für eure unerlässliche Unterstützung und Liebe.

The work presented here was funded by a studentship form Tenovus Cancer Care.

Contents

List of Figures

List of Tables

Abbreviations

SYMBOLE	
β-Gal	β-Galactosidase
β-NF	β-Naphthoflavone
β-TrCP	β Transducin repeat Containing Protein
Δ	Deletion (usually of exon 2 of Axin)
1i	ES medium containing ERK inhibitor
2i	ES medium containing GSK3 and ERK inhibitor
3Δ	Deletion of exon 2 to 10 of Axin
3fl	Axin allele containing three *loxP* sites
4-OHT	4-Hydroxytamoxifen

A	
$A1^{fl}$	Axin1 allele containing two *loxP* sites
$A1^{wt}$	Wild type Axin1 allele
$A2^{fl}$	Axin2 (Conductin) allele containing two *loxP* sites
$A2^{lacZ}$	Allele expressing lacZ under the control of the Axin2 (Conductin) promoter
$A2^{wt}$	Wild type Axin2 (Conductin) allele
aa	Amino acid
AFP	α-Fetoprotein
Ah	Aryl hydrocarbon
Ah-Cre	Aryl hydrocarbon Cre recombinase transgene
AhR	Aryl hydrocarbon receptor
Alb	Albumin
APC	Adenomatous Polyposis Coli
Axin	Axis Inhibitor

B	
Bcl2	B-cell leukaemia/lymphoma 2
BMP	Bone morphogenic protein
bp	Base Pair
BrdU	Bromodeoxyuridine (5-bromo-2'deoxyuridine)
BSA	Bovine Serum Albumin

C	
c-Myc	Celular-Myelocytomatosis oncogene
CARS	Coherent anti-Stokes Raman scattering
Ccd1	Coiled-coil-DIX 1
Cdc25a	Cell division cycle 25a
Cdh1	Cadherin1
cDNA	Complementary Deoxyribonucleic Acid
CHIR	CHIR99021, GSK3 inhibitor
Chk1	Checkpoint Kinase 1
CK1	Casein Kinase 1
CMV	Human Cytomegalovirus Promoter
Cre	Causes recombination
$CreER^T$	Causes recombination Estrogen Receptor fusion protein
CRISPR	Clustered regularly interspaced short palindromic repeats
C_t	Cycle time
CytP450	Cytochrome P450

D	
DAB	3,3'-diaminobenzidine
dATP	Deoxyadenosine Triphosphate
ddH_2O	Double distilled water
dH_2O	Deionized water
Dhh	Desert hedgehog
DI	Organoid differentiation medium with Cre inducer (i.e. β-NF or 4-OHT)
DIX	Dishevelled and Axin domain
Dkk1	Dickkopf-1
DM	Liver organoid differentiation medium
DMSO	Dimethyl sulfoxide
DNA	Deoxyribonucleic acid
DNase	Deoxyribonuclease
dNTP	Deoxynucelotid Triphosphate
DPEC	Diethylpyrocarbonate
Dsh	Dishevelled
DTT	Dithiothreitol
DU	Liver organoid differentiation medium with DMSO control

E	
E-Cad	E-Cadherin
EB	Embryoid body
ECL	Electrochemoluminiscence
ECM	Extracellular matrix
ECT	E-cadherin cytosolic tail
EDTA	Ethylenediaminetetraacetic acid
EdU	5-ethynyl-2'-deoxyuridine
EGF	Epidermal Growth Factor
EM	Organoids expansion medium
EMT	Epithelial-mesenchymal transition
EpCAM	Epithelial Cell Adhesion Molecule
ER	Estrogen receptor
ERK	Extracellular regulated Map kinase
ES cell	Embryonic stem cell
EtOH	Ethanol
EU	Liver organoid expansion medium with DMSO control

F

FBS	Fetal bovine serum
FGF	Fibroblast growth factor
fl	Flox, allele containing *loxP* sites
FLP	Flippase
Fox	Forkhead box transcription factor
FRT	FLP recognition target
FU	Fused
Fz	Frizzled

G

gDNA	Genomic DNA
GEF	Guanine Nucleotide Exchange Factor
GFP	Green Fluorescent Protein
GS	Glutamine Synthetase
GSK-3	Glycogen Synthetase kinase 3
GTP	Guanosin Triphosphate
GTPase	Guanosin Triphosphatase

H

H&E	Haematoxylin and Eosin
H2AX	Histone H2AX
H_2O_2	Hydrogen peroxide
HB	Hepatoblastoma
HBSS	Hank's balances salt solution
HBV	Hepatitis B virus
HDR	Homology-directed repair
HCC	Hepatocellular carcinoma
HCV	Hepatitis C virus
HGF	Hepatocyte Growth Factor
Hh	Hedgehog
HNF	Hepatocyte nuclear factor
HPRT	Hypoxanthine-guanosin phosphoribosyl transferase
HRP	Horseradish peroxidase
HSC	Hepatic stellate cell
HSEC	Hepatic endothelial cell

I

i.p.	Intra-peritoneal
ICAT	Inhibitor of β-Catenin and TCF-4
ICG	ICG001, Wnt inhibitor
ICM	Inner cell mass
IGF-1	Insulin-like-Growth-Factor 1
IHC	Immunohistochemistry
IRES	Internal ribosomal entry site
IκB	Inhibitor kappa-B

J

JAK	Janus kinase
JNK	c-Jun N-terminal kinase

K

kb	kilo base
kRAS	Kirsten Rat Sarcoma viral oncogene homolog
Krt 19	Cytokeratin 19

L

LDL	Low density lipoprotein
LEF/TCF	Lymphoid Enhancer Factor/T-Cell Factor
Lgr5	Leucin-rich repeat-containing G-protein coupled receptor 5
LN_2	Liquid Nitrogen
loxP	Locus of crossover of Bacteriophage P1
LRP	Low density lipoprotein receptor related protein

M

mAB	Monoclonal antibody
MAPK	Mitogen activated Protein Kinase
MEK	Mitogen activated ERK Kinase
MEKK	Mitogen activated ERK Kinase Kinase
Mg	Milligram
MIN	Multiple Intestinal Neoplasia
mRNA	Messenger RNA
MTOC	Microtubule-organising centre
mTERT	Mouse telomerase reverse transcriptase
mTOR	Mammalian Target or Rapamycin

N

N-Cad	N-Cadherin
NFκB	Nuclease Factor of kappa light polypeptide gene enhancer in B-cells
NGS	Normal goat serum
NHS	Normal horse serum
NRS	Normal rabbit serum

O

o/n	over night
Olfm4	Olfactomedin 4

P

pAB	Polyclonal antibody
pAkt	Phosphor-Akt
PBS	Phosphate Buffered Salin
PCR	Polymerase Chain Reaction
pERK	Phosphor-ERK
PFA	Paraformaldehyde
PI3K	Phosphatidylinositol 3-kinase
PKA	Protein Kinase A
PTEN	Phosphatase and Tensin Homologue on Chromosome 10
PP2A	Protein phosphatase 2
PP	Periportal
PV	Perivenous

Q	
qPCR	Quantitative PCR
qRT-PCR	Quantitative Real-Time PCR

R	
RFP	Red fluorescence protein
RGS	Regulator of G-Protein signalling
RNA	Ribonucleic acid
RNAse	Ribonuclease
Rpm	Revolutions per minute
RT	revers transcription

S	
SDS	Sodium Dodecyl Sulphate
SDS-Page	Sodium Dodecyl Sulphate Polyacrylamide Gel Electrophoresis
SEM	Standard error of the mean
Shh	Sonic Hedgehog
SMAD	Mother against decapentaplegic homolog
Smo	Smoothened
SOC	Super Optimal Broth
ssODN	Single-stranded DNA oligonucleotide
STAT	Signal Transducers and Activators of Transcription
SV40	Simian virus 40

T	
Tam	Tamoxifen
Taq	DNA polymerase from Thermus aquaticus
TAE	Tris-acetate-EDTA
TBS	Tris buffered saline
TBS/T	Tris buffered saline with Tween 20
Tcf/Lef	T-cell factor and Lymphoid enhancer factor
tetO	Tet Operon
TGF-β	Transforming Growth Factor-β
Tris	Tris(hydroxymethyl)aminomethane
tTA	Tetracycline-controlled Transactivator
TTR	Transthyretin
TTR-CreER^{T}	Transthyretin Cre recombinase ER fusion transgene

U	
u	Enzyme unit
UV	Ultra Violet

V	
V	Volts
v/v	Volume per volume

W	
w/v	Weight per Volume
Wnt	Wingless-type murine mammary tumour virus Integration site family
wt	Wild type

X	
x g	times gravity
X-gal	5-Bromo-4-Chloro-3-indolyl-β-D-Galactopyranoside

Abstract

Hepatocellular carcinomas carrying Axin1 mutations belong to a subset of tumours with an especially poor prognosis. Data obtained from an Axin1 mutant mouse line, challenged the traditional idea of Axin function; as simply a component of the β-Catenin-destruction complex. Axin1 deletion led to the development of highly proliferative HCC in the absence of an obvious Wnt/β-Catenin signature.

In order to uncover the mechanism(s) leading to Axin dependent tumourigenesis, this study focused on the role of Axin in two systems.

Firstly, we generated an allelic series of Axin mutant ES cell lines to analyse the role of Axin1 and 2 in ES cells. We could show, that single Axin mutants had a largely normal ES cell phenotype. In Axin double mutant ES cells, Wnt target gene expression was slightly upregulated, but cell proliferation stayed at normal levels. By contrast, upon differentiation into embryoid bodies, multiple readouts of the Wnt pathway were increased and a G2/M and cell cycle related gene expression profile was activated, accompanied by severe differentiation defects.

In the second system, we developed Axin1 mutant 3D liver cultures, which allow fate tracing of Axin mutant and wt cells in real time. We could show tightly regulatable gene deletion *in vitro* and produced preliminary evidence that Axin1 loss in culture closely mimics the *in vivo* situation in respect to G2/M gene expression in the absence of Wnt activation.

Overall, the effects of Axin loss on Wnt signalling and cell cycle regulation appeared to be tissue and cell cycle specific. Future use of the 3D culture system, together with the data obtained in Axin mutant ES cells and embryoid bodies, will not only advance our understanding of the involvement of Axin1 in hepatocellular carcinogenesis and cell cycle regulation; but may also be the starting point in the development of new therapeutic strategies.

"There is a theory which states that if ever anyone discovers exactly what the universe is for and why it is here, it will instantly disappear and be replaced by something even more bizarre and inexplicable."

"There is another theory which states that this has already happened."

(Adams 1980)

1 General Introduction

This thesis focuses on the role of Axin, a master scaffold protein for multiple signalling pathways and its role in embryonic development and carcinogenesis; specifically in hepatocellular carcinoma (HCC). In this introduction I will give a summary of the mammalian liver and (Wnt dependent) hepatocellular carcinogenesis. I will also discuss recent pertinent findings on the role of Axin in normal liver physiology and in HCC. These will be compared and contrasted with the roles of Axin/Wnt signalling in embryonic development.

1.1 The mammalian liver

1.1.1 Basic anatomy and function of the liver

The mammalian liver is the largest internal organ and the largest gland in the body. It has a major role in metabolism and a wide variety of associated functions. Portal blood coming from the capillaries of the small intestine, stomach, large intestine, spleen, and pancreas gets transported to the sinusoids of the liver, where it is filtered with the help of phagocytes (Kupffer cells). The hepatic portal system delivers substances absorbed by the digestive system (e.g. glucose and amino acid) for storage, metabolic conversion, and excretion. Oxygenated blood gets supplied via the hepatic artery. The liver assists with the assimilation of foods, detoxification, glycogen storage, production of bile, and hormone production. To accommodate all these functions the liver is capable of synthesising and breaking down a number of molecules vital for survival.

Macro-anatomically the mammalian liver is divided into four lobes, which are right, left, caudate and quadrate in humans; or right, left, median and caudate in rodents. The basic functional unit of the liver is the liver lobule (Figure 1-1 A-C). The lobule is classically described as a hexagon with the central vein in the centre and the portal triad, consisting of a portal vein, hepatic artery, and bile duct at each corner (Figure 1-1 A).

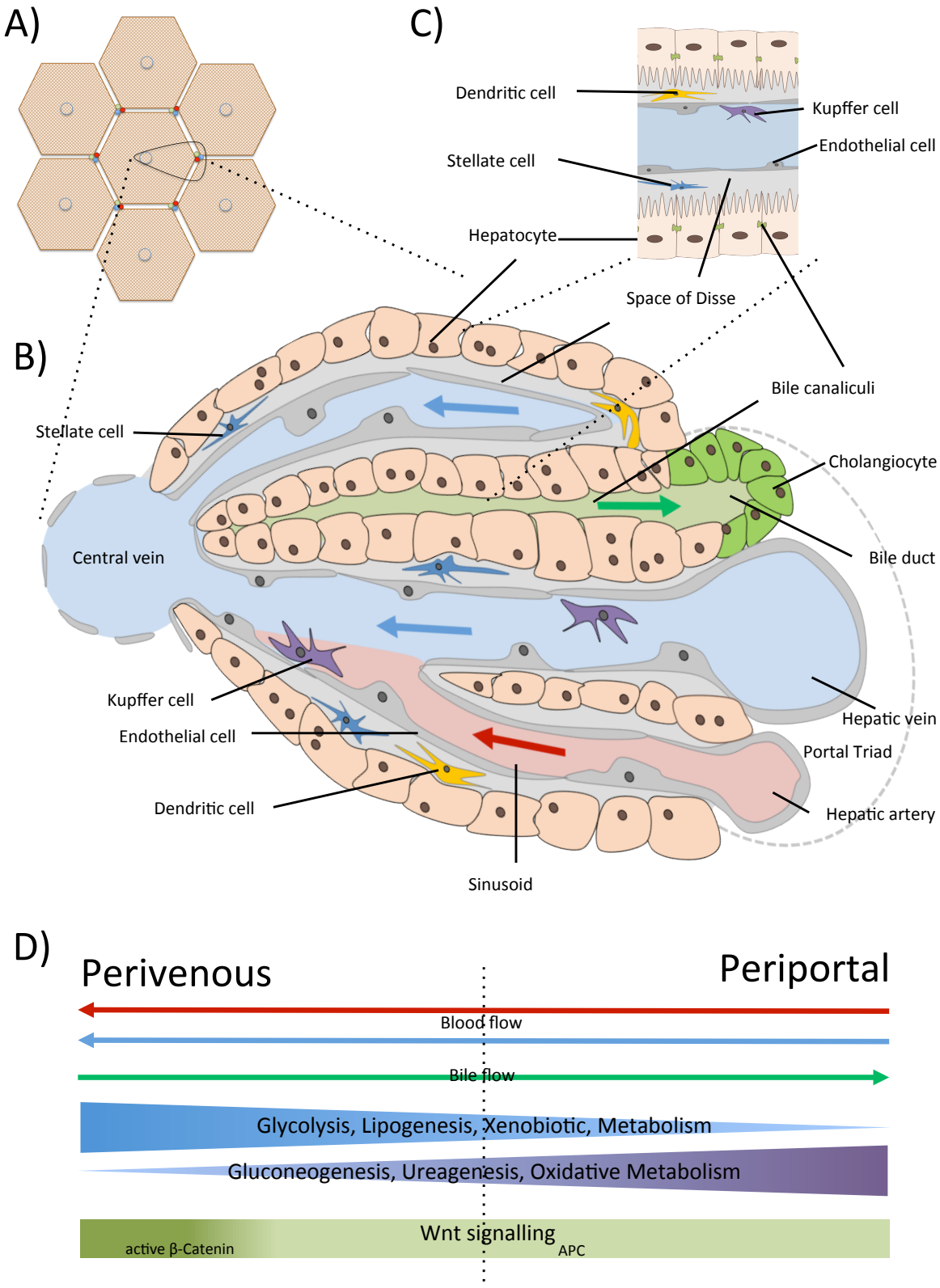
A)
C)
Dendritic cell
Kupffer cell
Endothelial cell
Stellate cell
Hepatocyte
Space of Disse
B)
Bile canaliculi
Stellate cell
Cholangiocyte
Central vein
Bile duct
Kupffer cell
Hepatic vein
Endothelial cell
Portal Triad
Dendritic cell
Hepatic artery
Sinusoid
D)
Perivenous
Periportal
Blood flow
Bile flow
Glycolysis, Lipogenesis, Xenobiotic, Metabolism
Gluconeogenesis, Ureagenesis, Oxidative Metabolism
Wnt signalling
active β-Catenin
APC

Figure 1-1. The liver lobule and liver zonation.

A) The liver is comprised of hexagonal shaped units called lobules, with a central vein in the centre and portal triads (bile duct, hepatic vein, and hepatic artery) at each corner. **B)** Magnification shows the blood (red and blue arrows) flowing from the portal vein and the hepatic artery to the central vein, passing through sinusoids lined with endothelial cells and cords of hepatocytes. Bile is secreted from the hepatocytes and flows through bile canaliculi towards the bile ducts (green arrow). Kupffer cells (liver macrophages) are located in the sinusoids, whereas hepatic stellate cells (liver fibroblasts) and dendritic cells are located in the space of Disse, between the endothelial cells and the hepatocytes. **C)** Detailed view of the sinusoid lined with fenestrated endothelial cells. The hepatocytes build cords and are linked by tight junctions that form the bile canaliculi. **D)** Hepatocytes differ in their functions depending on the location within the lobule (perivenous vs. pericentral) and can be divided into Zone 1 – 3 **(A)**. The zonated metabolic systems include the ammonia detoxification system, glucose and energy metabolism, and xenobiotic metabolism. Wnt signalling plays an important role in this zonation. Figure was adapted from Adams and Eksteen (2006); and Burke and Tosh (2006) and is not drawn to scale.

Blood flows from the portal vein and the hepatic artery through sinusoids toward the central vein. The sinusoids are composed of cords of hepatocytes lined with fenestrated hepatic sinusoidal endothelial cells (HSECs) that allow the exchange of materials between the hepatocyte and the blood. The macrophages of the liver (the Kupffer cells) are located on the luminal side of the sinusoids. Hepatic stellate cells (HSCs) populate the space of Disse, which is located between the HSECs and the hepatocytes. Bile produced by hepatocytes is first secreted into bile canaliculi; the space between hepatocytes formed by tight junctions. The bile is then collected in intrahepatic bile ducts, which are formed by cholangiocytes (ductal cells or biliary epithelial cells), flows on into the extrahepatic bile ducts and finally the duodenum.

Hepatocytes are the most abundant cell type in the liver, making up about 70 to 80% of the liver volume and 60% of total liver cells. Their function varies dramatically, depending on their position within the lobule, resulting in metabolic zonation (see Figure 1-1 A, D) (Jungermann 1986; Jungermann and Katz 1989). The zonation into periportal (PP) and perivenous (PV) hepatocytes affects ammonia detoxification, glucose and energy metabolism, and xenobiotic metabolism (Colnot and Perret 2010). The zones are usually numbered 1- 3 in line with the direction of blood flow (see Figure 1-1 A). In a recent publication Stefan Schuster and his group reviewed three hypothesis of liver zonation regulation: (1) the cell–cell/cell–matrix interaction hypothesis, (2) the upstream-downstream hypothesis, and (3) the concept of postdifferentiation patterning (Schleicher et al. 2015). The first hypothesis (1) proposes that cell-cell contact and extracellular matrix interaction distinguishes its metabolic function. Cells in contact with the central vein for example, express different genes than hepatocytes in other parts of the lobule. The upstream-downstream hypothesis (2) contributes metabolic zonation to the positioning of each hepatocyte in the lobule. The enzymatic composite of each cell differs because each hepatocyte exchanges metabolites and signalling molecules with the blood along the sinusoids, thus altering the concentration and composition for the next one in line. The third hypothesis (3) put forward by Gebhardt et al. explains metabolic zonation with

the presence of morphogens and the modulation through oxygen, nutrients and hormone gradients along the lobule (Gebhardt et al. 2007).

One of the main morphogens suggested to be involved in the zonation is the Wnt/β-Catenin pathway (see Section 1.3.1 for a summary of the Wnt signalling pathway). In the adult liver perivenous hepatocytes have high Wnt signalling activity leading to the expression of *glutamine synthetase* (GS) in the first to second layer of hepatocytes surrounding the central vein. In contrast, periportal hepatocytes with low Wnt signalling activity express *phosphoenolpyruvate carboxykinase* (PEPCK) for gluconeogenesis (Jungermann 1986). The expression of the urea cycle enzyme *carbamoylphosphate synthetase 1* (CPS 1) stretches from the periportal to the perivenous zone but is missing in the first to second cell layer of the pericentral zone, which is subject to high Wnt signalling activity. Additionally, enzymes related to the metabolism of drugs and xenobiotics have a high degree of zonation. The two major Cytochrome P450 enzymes *Cyp2e1* and *Cyp1a2* are only expressed in the perivenous zone in a β-Catenin dependent manner (Sekine et al. 2007; Oinonen and Lindros 1998). Furthermore, the xenosensor and transcription factor for drug-metabolizing enzymes aryl-hydrocarbon receptor (AhR), which is used as a tool to allow β-Naphthoflavone inducible gene activation (see Section 1.4.1.1 for further explanations), is expressed perivenously.

The importance of Wnt signalling for liver zonation was shown in several studies using conditional mouse mutants. Liver specific loss of β-Catenin and Lrp5/6 in knockout mice abolished the expression of perivenous enzymes (Sekine et al. 2006; Tan et al. 2006; Yang et al. 2014) whereas Wnt over activation in APC knockout mice led to the expression of perivenous enzymes in the whole liver (Benhamouche et al. 2006). The source of Wnt ligand remains unclear. Hepatocytes could act as an autocrine Wnt source or non-parenchymal cells could provide Wnt ligand in a paracrine fashion. A recent study by Yang et al. attempted to answer this question using conditional Wntless (Wls) knockout mice in which Wnt secretion could be blocked from either hepatocytes and cholangiocytes, Kupffer cells, or endothelial cells (Yang et al. 2014). Neither Wls loss from hepatocytes and cholangiocytes, nor from

Kupffer cells, resulted in any observable changes in liver zonation and Wls loss from endothelial cells was embryonically lethal preventing further analysis. These results led them to the conclusion that hepatocytes, cholangiocytes, or macrophages are not the source of Wnt in the liver. However, it remains to be shown if liver endothelial cells provide Wnt ligands; or if there is are multiple redundant Wnt sources.

1.1.2 Liver development and regeneration

1.1.2.1 The fetal liver

The mouse liver starts developing during gestation at embryonic day E 8.5. Hepatocytes and biliary epithelium cells are derived from the endoderm germ layer, specifically the endoderm of the ventral foregut (Tremblay and Zaret 2005). The commitment of endodermal cells in the foregut to develop into hepatoblasts and the formation of a liver bud is mediated by fibroblast growth factor (FGF) from the developing heart (Gualdi et al. 1996; Jung et al. 1999) and bone morphogenetic proteins (BMPs) produced in the mesenchyme of the septum transversum (Rossi et al. 2001). Simultaneously, Wnt and FGF4 signalling from the axial mesoderm inhibit hepatic fate in the dorsal endoderm (Zorn 2008). The hepatoblasts in the developing liver bud gain the expression of the transcription factors *Hex* and *HNF4α* (hematopoietically expressed homeobox and hepatocyte nuclear factor) as well as liver specific genes *α-fetoprotein* (AFP) and *albumin* (Alb) and can give rise to both hepatocytes and cholangiocytes. While hepatocytes and biliary epithelial cells are derived from the endodermal lineage, stromal cells including stellate cells, Kupffer cells, and blood vessels are of mesodermal origin. Figure 1-2 shows the stem cell lineage involved in liver development.

During further growth of the liver bud (E 9.5 to E 15), additional growth factors are secreted by the hepatic mesenchyme to promote hepatoblast migration, proliferation, and survival.

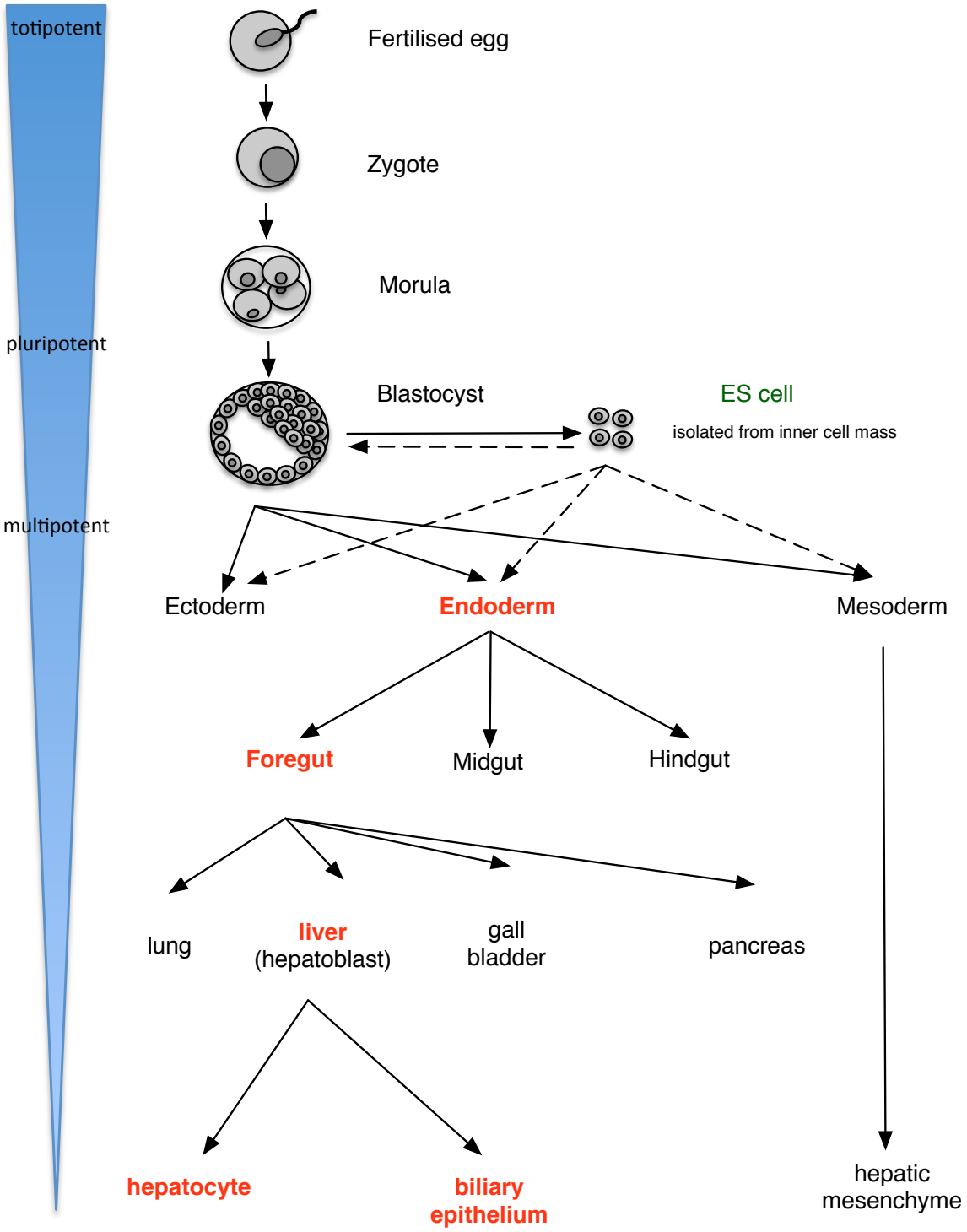

Figure 1-2. Stem cell lineage.
The zygote and the cells of the first cell divisions (blastomere), until the morula stage, are considered to be totipotent. They can generate a complete complex organism. The cells of the inner cell mass of the blastocyst are pluripotent, they can generate all three germ layers; meso-, ecto-, and endoderm; and the germ line. The cells of the inner cell mass can be isolated and grown *in vitro* as embryonic stem cells (ES cells, green) under culture conditions that maintain their pluripotency (dashed lines). The cells of the different germ layers are multipotent; they each generate a set of differed tissues. Here the lineage steps during hepatic development (red), from committed endoderm to functional hepatocytes and biliary epithelium are shown. Hepatic mesenchymal cells develop from the mesodermal germ layer (Figure adapted from Zorn 2008 and Wobus 2005).

These growth factors include FGF, BMP, HGF, Wnt, TGF-β and retinoic acid (Jung et al. 1999; Rossi et al. 2001; Berg et al. 2007; Iida et al. 2003; Ishikawa et al. 2001; Schmidt and Schibler 1995; Micsenyi et al. 2004; Monga et al. 2003; Pelton et al. 1991). During this phase of liver development the liver bud becomes the major site for fetal haematopoiesis. At embryonic day E 13 of mouse development, the hepatoblasts begin to differentiate into cholangiocytes furthered by TGF-β and Notch signalling (Tanimizu 2004; Lemaigre 2009). The cells in contact with the portal vein start expressing the biliary cell marker *cytokeratin-19* (*Krt19*) and down regulate hepatic genes. At E 17 the hepatocytes begin to establish epithelial morphology and arrange in the typical hepatocyte cords with bile canaliculi on the apical surface (Zorn 2008).

1.1.2.2 Adult liver stem cells and liver regeneration

Stem cells are usually defined by their capacity for self-renewal and the ability to differentiate into multiple lineages. The liver stem cell has been defined as the cell that gives rise to both hepatocytes and biliary epithelial cells (cholangiocytes), the two epithelial cell types in the liver (Miyajima et al. 2014). In most adult tissues and organs, stem cells are required for tissue turnover, as part of the homeostatic maintenance, and for repair and regeneration in pathologic conditions. Since hepatocytes have a very slow turnover compared to most other cells in the body (100 to 400 days in mice) (Magami et al. 2002) stem cells in the liver are mainly required for the purpose of regeneration.

Following surgical removal of up to 70% of the liver, it can regenerate its mass completely, making it possible to transplant liver tissue from a living donor. Even though the liver has an extraordinary regeneration potential, the mechanisms of regeneration and the identity of the liver stem cell is still highly debated. At least four different cell types have been implicated in the proliferative response following injury as the result of various fate-tracing experiments. These cells are the mature hepatocytes, the unipolar ductal cell, a bipolar ductal progenitor cell, and a multipotent periductular progenitor cell presumed to be of bone marrow origin.

There seems to be a cellular redundancy depending on the availability of cell types following different modes of injury.

The regeneration following acute liver damage, like partial hepatectomy (PHx), is mainly due to the proliferation of adult hepatocytes in a zonal manner beginning in the periportal area and ending in the pericentral zone (Michalopoulos 2010; Rabes 1977). Non-parenchymal liver cells secrete IL 6 (interleukin 6), priming mature hepatocytes for proliferation (Cressman et al. 1996). Kupffer cells provide secreted Wnt ligands to activated β-Catenin signalling and initiate regeneration (Yang et al. 2014). Then growth factors, including hepatocyte growth factor (HGF), are induced to drive hepatocytes into S phase. The regeneration is complete once non-parenchymal cells have proliferated as well. Information gained through experiments involving PHx induced regeneration can give valuable insight into liver transplantations and surgical removal of liver parts. However, pathological conditions of the liver that usually include hepatocyte death and inflammations might not be accurately recapitulated.

In many pathological conditions, including viral hepatitis, alcoholic liver disease, and non-alcoholic fatty liver disease, regeneration was suggested to be mediated by stem and progenitor cells instead of mature hepatocytes. The so-called oval cell, a bipotential, immature cell, is thought to be activated if hepatocyte proliferation is blocked. However, there was much controversy regarding the origin and fate of the oval cells. According to some research, the progenitor cell resides in the small terminal bile ducts (Fausto 2004; Lu et al. 2015). Part of the oval cell activation seems to be the secretion of Wnt3A and Wnt7A from macrophages in chronic liver diseases leading to canonical Wnt signalling in neighbouring cells which triggers regeneration of both hepatocytes and biliary epithelial cells (Boulter et al. 2012).

Given the potential to develop into both hepatocytes and ducal cells, it has been suggested that these progenitor cells originate from fetal hepatoblasts that remain undifferentiated in a stem cell niche within the bile duct (Schmelzer et al. 2006). Unfortunately, oval cells have not

been characterised thoroughly. Thus, the liver progenitor cells (LPCs) studied in a wide variety of rat and mouse liver injury models have all been termed oval cells, even though the cells observed in each model can differ widely. In recent years more and more groups set out to identify markers that faithfully identify LPC in rodents and humans. Flow cytometry based cell sorting using cell surface markers (e.g. EpCAM or CD133), followed by *in vitro* culture, are used to evaluate the proliferation and differentiation potential of many candidate cell types. Interestingly, it appears that activation of the LPCs and hepatocyte proliferation depends on the developmental pathways involved in embryonic hepatogenesis.

However, recently two independent fate tracing experiments following chronic liver injury argued against any involvement of LPCs to hepatocyte regeneration (Schaub et al. 2014; Yanger et al. 2014). According to this research hepatocytes are always generated by self-duplication. A study recently published in Nature claimed, that hepatocytes in the uninjured liver are all decedents of a *Axin2* expressing population of diploid cells around the central vein (Wang et al. 2015). This population of cells expressed known hepatocyte markers, as well as liver progenitor markers, and was exposed to high levels of Wnt.

Although, a review by Markus Grompe pointed out that so far this change in paradigm has only been shown in the mouse (Grompe 2014). He also raised the question of whether the injury models used are the right regime to activate an oval cell response in mice.

1.2 Hepatocellular carcinoma

The signalling pathways involved in liver development, homeostasis and regeneration must be tightly regulated to ensure normal liver function. Abnormal activation of signalling pathways can have drastic effects. For example aberrant β-Catenin activating throughout the liver leads to a significant increase in hepatocellular proliferation and the development of liver cancer (Colnot et al. 2004; Cadoret et al. 2001). The most common form of primary liver cancer is hepatocellular carcinoma (HCC), a tumour, which arises from hepatocytes.

1.2.1 Incidence and environmental risk factors or HCC

In humans, HCC is the most common form of primary liver cancer (90%), the fifth most common cause of cancer in men and the second most common cause of death from cancers worldwide (McGlynn et al. 2001; El-Serag and Rudolph 2007; Ferlay et al. 2012). In general, men are more often affected by HCC, than women (El-Serag and Rudolph 2007). Patients with pre-existing chronic liver diseases, as the result of hepatitis infections by Hepatitis B and C virus (HBV, HCV), alcoholism, type 2 diabetes or hepatic fibrosis have the highest risk of developing HCC (Bosch et al. 2004; Sherman 2010). In fact, 70-90% of HCCs are due to prior liver cirrhosis (Bréchot 2004; Kumagi et al. 2009). Other cases of liver cancer are linked to genetic, congenital, or metabolic factors.

Together with the incidences of childhood infection with HBV, HCCs are very common in developing countries in Asia and Africa (see Figure 1-3) (McGlynn et al. 2001; Leong and Leong 2005).

More than 75% of HCC can be found in South African countries and sub-Saharan Africa (Knudsen et al. 2014). In recent years the incidence of HCCs has been stable, or even decreasing in the developing world, probably due to the spread of vaccination programs (El-Serag and Rudolph 2007; Tajiri et al. 2010). In areas with previously low incidence rates like the USA, in contrast, incidence of HCC is rapidly rising probably together with a raise in chronic Hepatitis C (Altekruse et al. 2009).

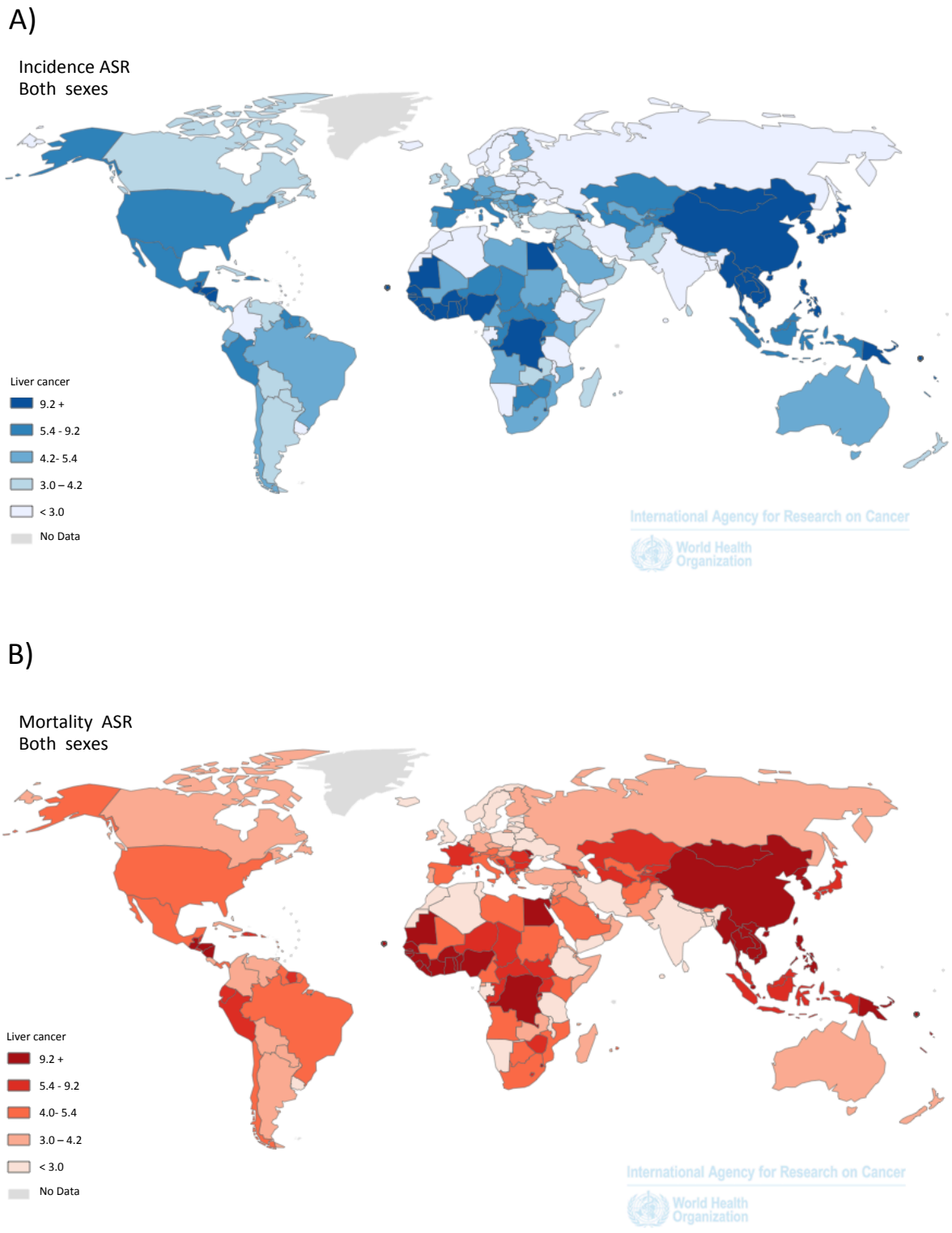

Figure 1-3. Incidence and mortality of liver cancer in the world.
Incidence **(A)** of liver cancer and liver cancer mortality **(B)** in the world, in both men and women, shown as an age-standardised rate (ASR)[a] (Ferlay et al. 2012).

[a] ASR is a summary measure of the rate in relation to a start age structure. Because age has a strong influence on the risk of dying from cancer, standardisation is necessary to compare populations with different age structures. ASR is expressed per 100,000.

Microscopically, liver tumours can either be well differentiated, with hepatocyte-like tumour cells, or poorly differentiated, with large and discohesive cells and sparse stroma and central necrosis (Yamaguchi et al., 2005). Although the outcomes of HCCs vary between different patients, the prognosis is generally very poor. A study conducted by Sheu et al. on asymptomatic Chinese patients showed that the tumour size doubled in 117 days on average; some extreme cases only needed one month (Lee et al. 2014; Sheu et al. 1985). Surgical cure is possible in less the 5% of all patients and the a median survival after diagnosis is 6 months (Lucey et al. 2006; Stuart and Stadler 2013). The five-year survival rate varies across different studies but are generally found to be between 10 and 20 % (Lee et al. 2014; Nguyen et al. 2009)

1.2.2 Genetic dispositions

Like most other solid tumours, tumourigenesis in HCC is usually a multistep process. The accumulation of genetic and epigenetic defects of oncogenes, tumour suppressors, DNA repair mechanisms, cell cycle regulators, cell adhesion molecules, and growth factors change the phenotype of hepatocytes one by one, leading to the development of dysplastic nodules and finally HCC (Moeini et al. 2012).

In the case of HBV, random integration of viral DNA into the host genome resulting in the activation of growth factors or the disruption of anti-oncogenes, is the presiding step to HCC. Other factors involved are chronic inflammation and HBV-specific proteins (Stuart and Stadler 2013; Bréchot 2004). How the single stranded RNA virus HCV contributes to tumourigenesis remains unclear (Nguyen et al. 2009). Even though risk factors like chronic HBV and HCV infections, alcoholic hepatitis, aflatoxin B1 and other disease are undeniably linked to HCC; they are not enough to explain the great difference in frequency and progression within the human population. Additional environmental and genetic factors play an important role in tumourigenesis.

In recent years, more and more signalling pathways have been identified to be involved in HCC tumour progression. Aberrant signalling pathway activity could potentially predict disease outcome and serve as a molecular-based target for novel therapeutic drugs (Frau et al. 2010; Moeini et al. 2012). However, the complex genetic alterations observed in HCC make it incredibly difficult to decipher causal genetic events from those accumulating during cancer progression. The most frequently mutated oncogenes identified are p53 and β-Catenin (Moeini et al. 2012). Other aberrantly activated signalling pathways found in HCC include the EGF, ERK, PiK/AKT, C-Met/HGF, Hedgehog, and apoptosis signalling.

A study conducted by Yujin Hoshida and colleagues in 603 patients, identified 3 different subclasses of human HCC depending on their tumour size, extent of cellular differentiation, and serum α-fetoprotein levels (Hoshida et al. 2009)(see Figure 1-4 A). The first subclass (S1) includes tumours with pathologically high Wnt signalling activity. The second subclass (S2) is extremely proliferative and shows c-Myc and Akt activation. The third subclass (S3) shows well-differentiated hepatocytes and usually includes low-grade tumours. Interestingly, mutations of most Wnt signalling components, but not of β-Catenin in exon 3, the exon containing the Serine and Threonine residues for phosphorylation by CK1 and GSK3 and subsequent degradation, leads to a Wnt active signature and the development of S1 tumours. Instead, β-Catenin mutations fail to activate Wnt target genes like Cyclin D1 and c-Myc and are often found in S3 tumours.

Another classification system by the Zucman-Rossi group distinguishes between 6 HCC subgroups based on transcriptome analysis of 57 HCCs and 3 hepatocellular adenomas and validation in 63 additional HCCs (Boyault et al. 2007) (see Figure 1-4 B). They also conclude that mutations of different members of the Wnt signalling pathway are found in different subsets of HCCs. They class mutations in *β-Catenin* in a different group than *Axin1* and show that *β-Catenin* mutant tumours are chromosomally stable whereas *Axin1* mutations tend to be involved in chromosomal instability and loss of heterozygosity (Boyault et al. 2007; Zucman-Rossi et al. 2007).

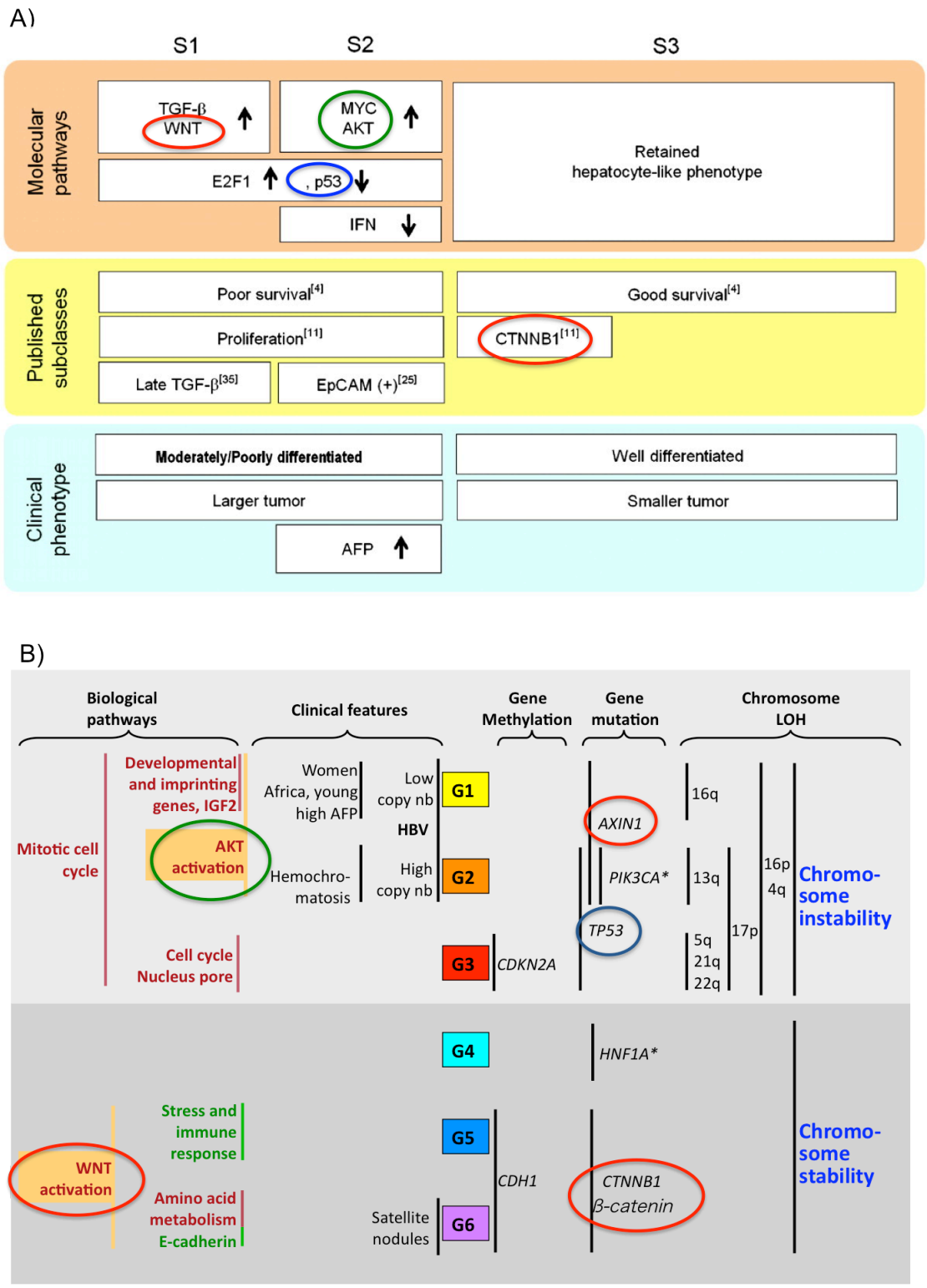

Figure 1-4. Classifications of HCC.
A) Classification of HCC into 3 subclasses (S1, S2 and S3) depending on tumour size, extent of cellular differentiation, and serum α-fetoprotein levels (Hoshida et al. 2009)[b]. **B)** Classification of HCC into 6 subgroups (G1-G6) based on transcriptome analysis (Boyault et al. 2007; Zucman-Rossi 2010)[c].

[b] Permission to reproduce this graph has been granted by the American Association for Cancer Research.
[c] Permission to reproduce this graph has been granted by John Wiley and Sons.

1.3 The scaffold protein Axin

Axin1 was originally identified as the product of the mouse *fused* locus by Zeng and his colleagues (Zeng et al. 1997). The name Axin originates from its involvement in embryonic Axis formation (Axis inhibition protein), since mutations in *Axin1* lead to the duplication of the embryonic axis and subsequent lethality. In mammals there are two known Axin genes, *Axin1* and *Axin2,* also known as *Conductin* or *Axil* (Axin-like protein) in rats, which are 44% identical. Axin2 was discovered in yeast two-hybrid screens, where it was found to efficiently bind to GSK3β (Glycogen-Synthase-Kinase 3β) and β-Catenin, in a similar way to Axin1 (Ikeda et al. 1998; Yamamoto et al. 1998; Behrens et al. 1998). These results suggested that both Axins act through inhibition of the Wnt/β-Catenin signalling pathway, where Axin forms a scaffold for a multi protein complex comprising APC (adenomatous polyposis coli), CK1 (Casein Kinase 1), and GSK3β, that targets β-Catenin for degradation (see Section 1.3.1 for more details about the Wnt signalling pathway).

As a result of alternative splicing of exon 8a[d], Axin1 has two isoforms (Zeng et al. 1997). Similarly, its homologue Axin2 also has two isoforms resulting from alternative splicing of exon 6a[d] (Li et al. 2015; and S Salahshor, unpublished data, 2004).

The known difference between the homologues Axin1 and Axin2 is mainly their expression pattern. While *Axin1* is expressed ubiquitously, *Axin2* is expressed in a tissue and developmental stage specific manner as the result of a negative feedback loop of canonical Wnt signalling activation (Jho et al. 2002; Leung et al. 2002; Lustig et al. 2002). By expressing *Axin2* from the *Axin1* locus, in genetically modified mice, Chia and Costantini could show that both proteins have equivalent functions *in vivo* (Chia and Costantini 2005).

As a scaffold protein, Axin is involved in multiple signalling pathways such as the TGF-β (transforming growth factor β), JNK (c-Jun N-terminal kinase), and the Wnt-signalling pathway (Salahshor and Woodgett 2005). Both Axins have various binding sites for proteins

[d] Exon labelling varies between publications, in this thesis exon 1 is counted as the non-coding region, and the protein starts with exon 2.

involved in these pathways and can therefore serve as a mediator for many different incoming signals (Chia and Costantini 2005). Protein interactions are mediated through multiple functional domains, most noticeably an N-terminal RGS (regulator of G-protein signalling) domain, and a C-terminal DIX domain (Dishevelled and Axin domain). Figure 1-5 shows a summary of Axin domains and interaction partners. The RGS domain, usually found in proteins involved in G-Protein signalling, mediates binding to APC (Zeng et al. 1997; Ikeda et al. 1998; Kishida et al. 1998) but does not have a known G-Protein related function (Mao et al. 1998). The C-terminal DIX domain is a binding site for other DIX domain containing proteins (i.e. Dsh or Axin itself) (Cadigan and Nusse 1997). Between these two very structured domains, with known crystal structure; is a highly flexible region containing binding sites for a number of different proteins, including β-Catenin, GSK3 and CK1 (Noutsou et al. 2011).

Other Axin interaction partners include negative or positive regulators of the Wnt-pathway and proteins involved in other cellular functions. Indeed, the list of known proteins being regulated, and/or directly binding to Axin, is constantly growing. An incomplete list, put together by Salahshor and Woodgett, using pathway assist software includes 46 interaction partners of Axin1 (Salahshor and Woodgett 2005). However, it remains unclear, which of these interactions are physiologically relevant. The focus of scientific research thus far has mainly been on the Wnt signalling pathway, while investigations into other integration partners have been widely neglected.

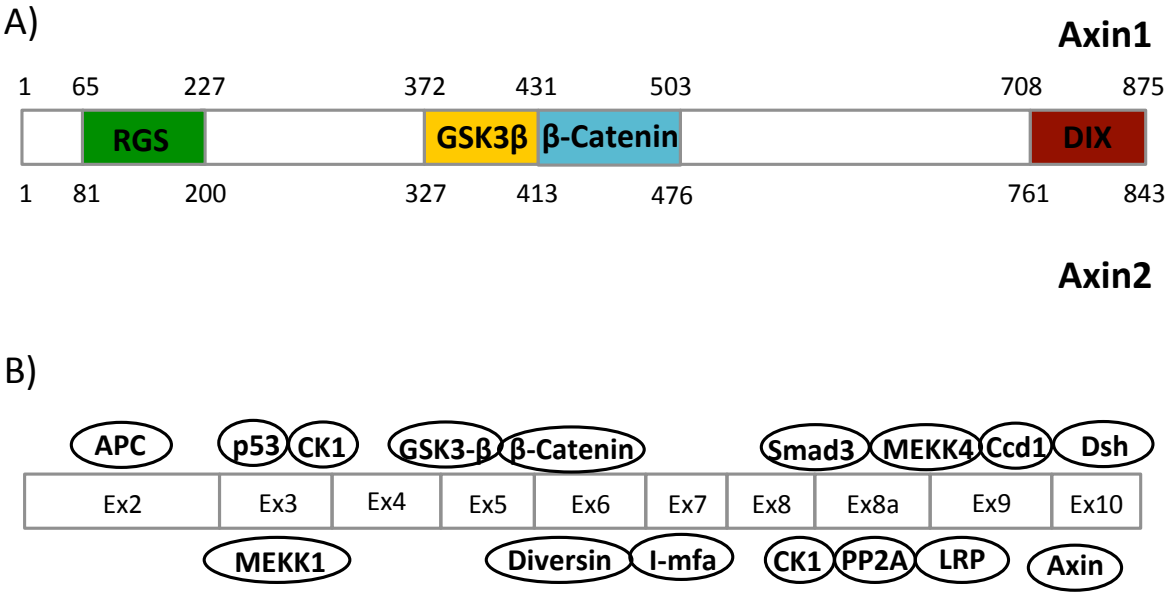
A)
Axin1
1
65
227
372
431
503
708
875
RGS
GSK3β
β-Catenin
DIX
1
81
200
327
413
476
761
843
Axin2
B)
APC
p53
CK1
GSK3-β
β-Catenin
Smad3
MEKK4
Ccd1
Dsh
Ex2
Ex3
Ex4
Ex5
Ex6
Ex7
Ex8
Ex8a
Ex9
Ex10
MEKK1
Diversin
I-mfa
CK1
PP2A
LRP
Axin

C)

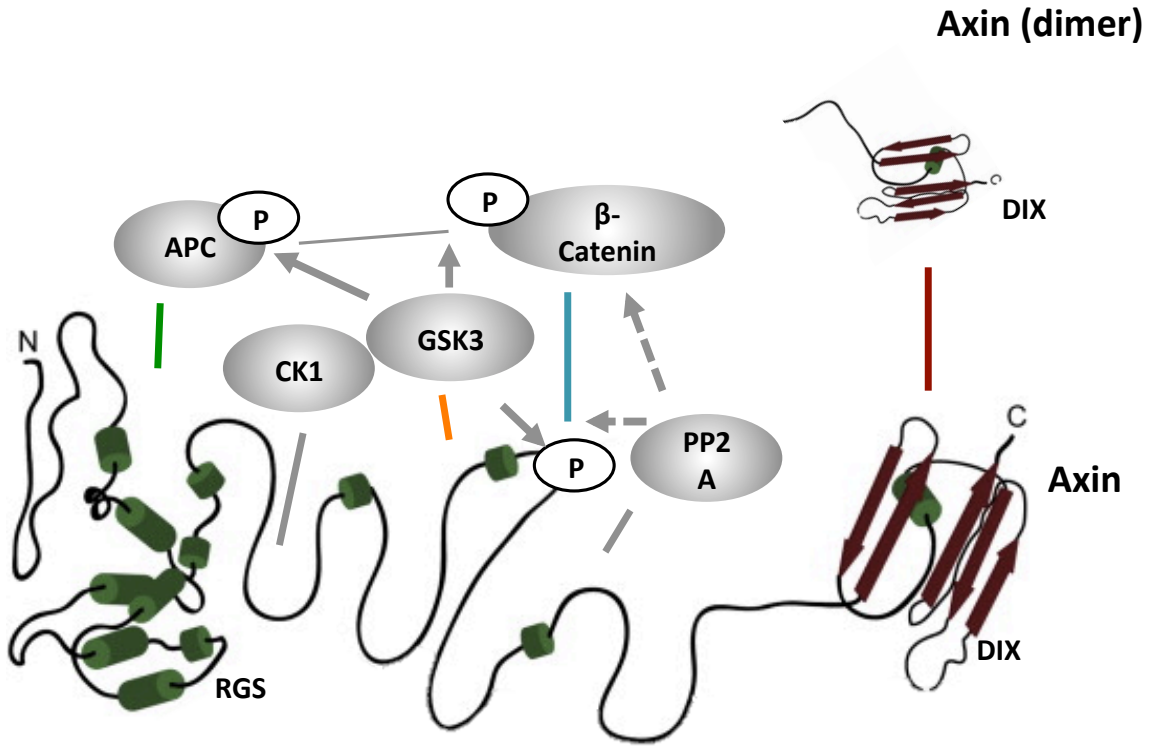
Axin (dimer)
DIX
P
APC
P
β-
Catenin
N
CK1
GSK3
P
PP2
A
C
Axin
RGS
DIX

Figure 1-5. Domain organisation of Axin.

Axin1 and Axin2 are multi-domain scaffold proteins; binding to a wide array of proteins. **A)** Schematic representation of Axin1 (top) and Axin2 (bottom) proteins and the amino acid regions of their major binding region; RGS domain, DIX domain and GSK3 and β-Catenin binding regions. **B)** Axin-interacting proteins with known relative binding positions in Axin1 according to the exon structure. Among those proteins are members of the Wnt, TGF-β, JNK, and p53 signalling pathways. **C)** Model of Axin as a highly flexible scaffolding protein, showing molecular interactions important for the β-Catenin destruction complex. Axin, APC, and β-Catenin bind to each other and form a complex. GSK3β binding to Axin is required for phosphorylation (grey arrows and P) of β-Catenin, APC and Axin itself. APC phosphorylation regulates APC-β-Catenin binding and phosphorylation of β-Catenin is required for its degradation. The phosphorylation of Axin enhances the binding efficiency to β–Catenin. The catalytic subunit of PP2A binds to a site adjacent to the β-Catenin binding site and may counteract the activity of GSK3β (dotted lines with arrows). Figures were adapted from Fagotto et al. (1999); Luo and Lin (2004); and Noutsou et al. (2011). Of note, exon labelling varies between publications, in this thesis exon 1 is counted as the non-coding region, and the protein starts with exon 2.

1.3.1 Axin and its role in Wnt-signalling

Wnt proteins are secreted glycoprotein ligands that regulate many processes in development and normal homeostasis. The name Wnt is derived from the drosophila *WG* (*Wingless*) (Sharma and Chopra 1976) and *Int-1 (integration1)* an integration site of the mouse mammary tumour virus (MMTV) (Nusse and Varmus 1982). To date, 19 members of the Wnt family are known (Katoh 2013). Different Wnt ligand/receptor combination can activate at least three distinct cell-signalling pathways; the canonical Wnt or Wnt/β-Catenin signalling pathway with β-Catenin as the major player, the planar cell polarity pathway (PCP) and intercellular Ca^{+} (Wnt/Ca^{+}) pathway. The following chapter will mainly focus on the canonical or Wnt/β-Catenin pathway; since Axin1 and Axin2 have known key regulatory functions in this pathway.

The Wnt/β-Catenin signalling pathway, also known as the canonical Wnt signalling pathway, is among the most conserved pathways in evolution. It is crucial for the development of organisms ranging from nematodes to mammals (Wordaz and Nusse 1998). In vertebrates it is involved in various processes ranging from organ development and axis formation, to cell proliferation, motility, and fate. Because of its many important roles in development; mutations in components of the Wnt signalling pathways are often linked to birth defects, cancer and other diseases (Clevers 2006).

The main player in canonical Wnt signalling is β-Catenin (MacDonald et al. 2009). Under un-stimulated conditions β-Catenin is constantly degraded by a multi-protein-complex (see Figure 1-5 C and Figure 1-6 A). This complex is built around Axin, which serves as a scaffold for the other components like the tumour suppressor APC, different members of the CK1 family and GSK3 (Behrens et al. 1998; Ikeda et al. 1998; Liu et al. 2002). β-Catenin is phosphorylated on Serine 33, 37 and 45 as well as Threonine 41 by GSK3 after a priming phosphorylation by CK1. Following this phosphorylation sequence at the amino terminal region of β-Catenin, it is ubiquitinated by β-TrCP (β transducing repeat containing protein), a

subunit of the E3 protein ligase complex SCF (Skp1 cullin F-box protein), and degraded by the Proteasome (Aberle et al. 1997; Liu et al. 2002).

In the presence of Wnt ligand, the destruction complex is inhibited following the binding of Wnt ligand to the receptor Frizzled (Fz, a family of G-protein coupled receptors) and its co-receptor LRP5 and 6 (Low-density lipoprotein receptor-related protein, Figure 1-6 B). Binding of R-Spondin to Lgr4/5/6 (Leucin-rich repeat containing G protein-coupled receptor) can further potentiate Wnt signalling activation (Schuijers and Clevers 2012). It has been suggested that upon Wnt binding, the receptors multimerise and a signalosome is formed (Bilic et al. 2007). Signalosome formation then leads to a phosphorylation cascade which ultimately leads to the inhibition of the β-Catenin destruction complex (Zeng et al. 2008). First, the cytoplasmic tail of Lrp6 is phosphorylated which leads to the recruitment of Axin and Dishevelled (Dsh) to the activated receptor complex at the cell membrane (Logan and Nusse 2004; Mao et al. 2001). There, Axin is dephosphorylated by protein phosphatase 1 (PP1) while GSK3 mediated phosphorylation of Axin is inhibited (Kim et al. 2013). As a result, Axin is in a closed state, unable to scaffold β-Catenin and Lrp6. The receptor is thus free to render more and more Axin molecules inactive. As a result of Wnt activation, β-Catenin can accumulate in the cell and translocate to the nucleus, thus leading to the expression of downstream targets through the activation of transcription factors belonging to the LEF/TCF family (lymphoid enhancer-binding factor 1 or T-cell-specific transcription factor) (Molenaar et al. 1996; van de Wetering et al. 1997). However, the exact mechanism of destruction complex inhibition is still highly debated (Li et al. 2012). Wnt target genes include genes important for proliferation and development. They are often cell type specific; commonly found genes include *Axin2*, *c-Myc*, and *Cyclin D1* (He et al. 1998; Lustig et al. 2002; Shtutman et al. 1999).

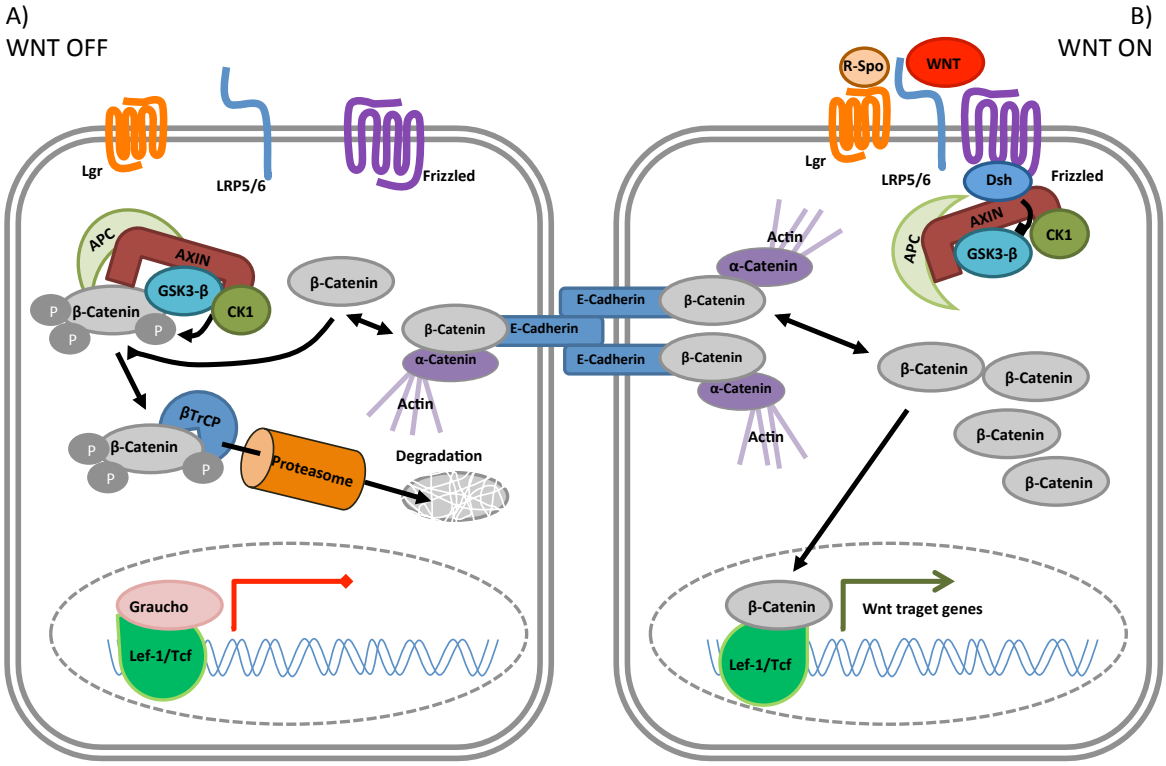

Figure 1-6. Overview of Wnt/β-Catenin signalling.
A complex containing Axin, APC, CK1, and GSK3 phosphorylates cytoplasmic β-Catenin in the absence of a Wnt ligand (**A,** Wnt OFF). This phosphorylated β-Catenin is recognized by the E3 ubiquitin ligase β-TrCP, and marked for proteasomal degradation. In the presence of Wnt ligand (**B**, Wnt ON), a receptor complex of Frizzled and LRP5/6 forms which leads to the recruitment of Axin and the other components of the destruction complex to the plasma membrane. This disrupts Axin-mediated degradation of β-Catenin, allowing β-Catenin to accumulate in the nucleus where it serves as a co-activator for TCF dependent transcription of Wnt target genes.

1.3.2 Axin regulation

Since Axin levels are generally very low compared to other Wnt signalling components, it is believed that regulation of Axin levels is critical in Wnt signalling (Kim and Jho 2010; Lee et al. 2003). The first level of Wnt signalling regulation is through a negative feedback loop as a result of upregulation of *Axin2* expression by TCF dependent transcription, leading to the subsequent down regulation of β-Catenin levels through a destruction complex surrounding Axin2 (Lustig et al. 2002). In line with this, Axin2 levels increase during the first 6 h following Wnt3a treatment, whereas Axin1 levels decrease during that time (Bernkopf et al. 2015). Additionally, Axin stability and localisation is tightly regulated through different processes of post-translational modifications, including phosphorylation, SUMOylation (Small Ubiquitin-like Modifier) and ubiquitination (Kim et al. 2008; Kim and Jho 2010; Callow et al. 2011; Zhang et al. 2011; Fei et al. 2013). Phosphorylation of Axin by GSK3β, CK1 or PPA2 (Protein phosphatase 2A) can enhance the binding efficiency of β-Catenin in the destruction complex (see Figure 1-5 C) and keeps Axin ready to engage with the Lrp6 (Yamamoto et al. 1999; Kim et al. 2013). Dephosphorylation of Axin by protein phosphatase-1 in response to the formation of the Wnt-receptor complex, on the other hand, leads to Axin degradation and activation of Wnt target genes (Strovel et al. 2000; Kim et al. 2013).

The proteasomal degradation of Axin is regulated by Tankyrase-mediated poly-ADP-ribose modification (PARsylation) followed by polyubiquitination through RNF146, a RING-domain E3 ubiquitin ligase (Huang et al. 2009). Alternatively, Axin can be ubiquitinated by other E3 ubiquitin ligases, like Smurf1 and Smurf2 (Smad ubiquitination regulatory factor) (Kim and Jho 2010; Fei et al. 2013). Notably, regulation of Axin through ubiquitination by the E3 protein ligase Smurf1 does not have proteolytic effects but only interrupts Axin binding to LRP5/6 in a cell cycle specific manner (Fei et al. 2014).

Furthermore, subcellular localisation and homo- and hetero-polymerisations mediated by the DIX domain have been reported to strongly influence the activity of the β–Catenin

destruction complex (Shiomi et al. 2003; Schwarz-Romond et al. 2007; Liu et al. 2011). The interaction of Axin and Dsh via both of their DIX domains for example, is believed to be a mechanism by which Axin function is inhibited (Kishida et al. 1999; Schwarz-Romond et al. 2007).

Although Axin is generally considered to be a cytoplasmic protein, it has been shown to shuttle between the cytoplasm and the nucleus. Axin1 has three nuclear localization signals (NLS) and two nuclear export signals (NES) (Salahshor and Woodgett 2005). Some data suggests that Axin1 and Axin2 bind β-Catenin in the nucleus and assists with its nuclear export (Wiechens 2003; Cong and Varmus 2004; Krieghoff et al. 2006). Following the just right hypothesis of Wnt signalling strength, the direct regulation of nuclear β-Catenin levels could have a major impact on downstream target activation (Albuquerque et al. 2002).

1.3.3 Other Axin interaction partners

The domain structure of Axin (see Section 1.3) does not only allow Axin to interact with member of the Wnt/β-Catenin signalling pathway, but also allows the crosstalk with many other interaction partners and complex signalling cascades (Noutsou et al. 2011) (Figure 1-7). The following paragraph lists a number of Axin interaction partners and a brief summary of the possible physiological role of those interactions.

As previously mentioned, aside from Wnt signalling Axin has been shown to interact with members of the TGF, JNK, and stress response pathways. Due to its numerous interaction partners, Axin has long been proposed to have integrative and crosstalk functions in the cytoplasm (Luo and Lin 2004) and was suggested to be important for signal integration in signalling endosomes (Pálfy et al. 2012). Many of the links to various signalling pathways seem to rely on a phosphorylation process, in a complex comprising Axin and GSK3, but not APC. GSK3β is a promiscuous kinase with nearly 100 proposed phosphorylation targets (Sutherland 2011).

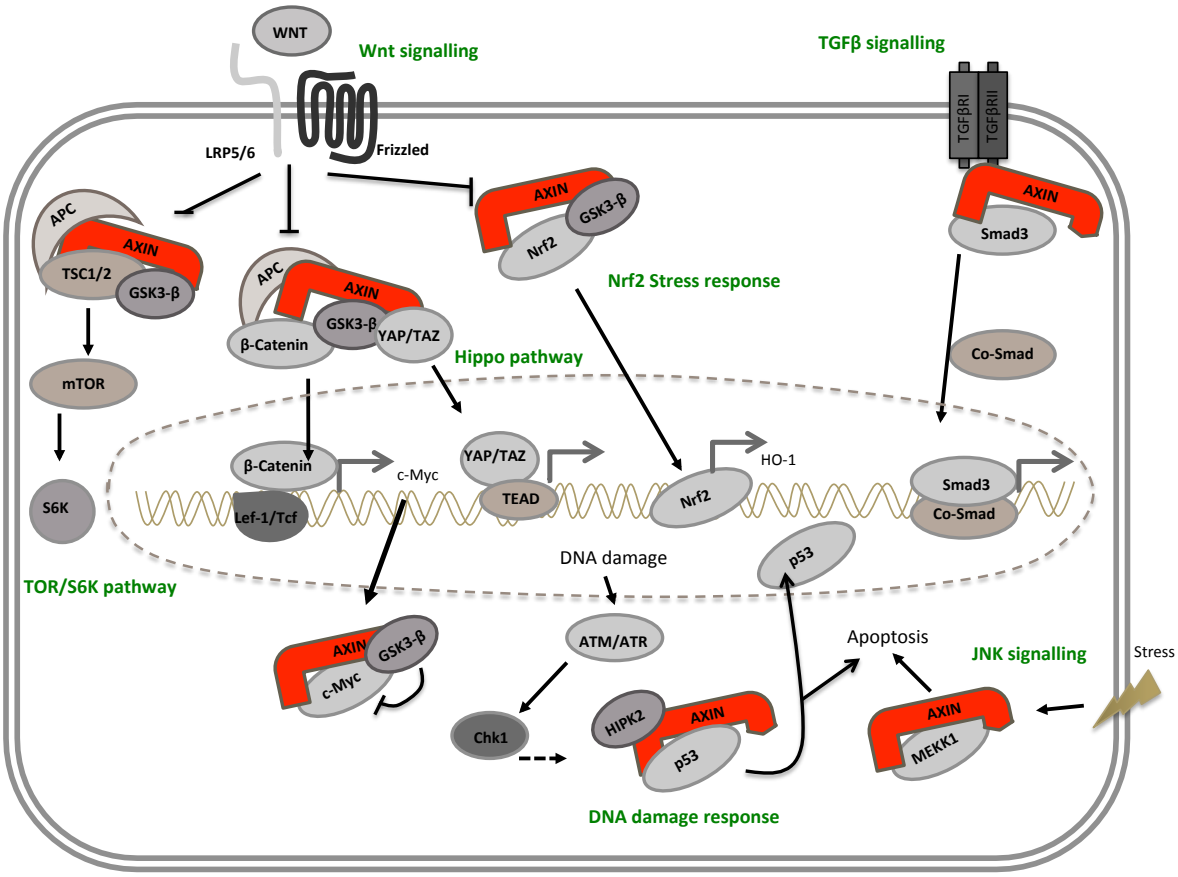

Figure 1-7. Regulation of different cellular pathways by Axin.
Axin serves as a scaffold protein in many signalling pathways including Wnt signalling, TGF-β signalling, the Hippo pathway, and Tor/S6K pathway. Additionally, Axin is linked to different stress responses as part of JNK signalling, DNA damage response, and the Nrf2 stress pathway.

Known GSK3 target proteins, outside core Wnt/β-Catenin signalling, include proteins involved in glycogen biogenesis, cell cycle regulation, inflammation response and microtubule stability and it seems likely that Axin plays a major role in target specification (Frame and Cohen 2001; Xu et al. 2009a).

Interestingly, the oncogene, transcription factor and direct Wnt target gene *c-Myc* is not only transcriptionally activated through Wnt signalling, but its protein levels are also directly regulated by an Axin/GSK3 destruction complex (Arnold et al. 2009). This provides an efficient negative feedback regulation on two levels. *Axin1* expression can inhibit β-Catenin dependent transcriptional activation of *c-Myc,* while simultaneously promoting a degradation complex for already existing c-Myc protein.

Other interesting Axin binding partners are the BMP signalling modulator Smad1 and the TGF-β-signalling mediator Smad3 (Sma and Mother against decapentaplegic homolog). BMP signalling strength can be negatively regulated through the proteasomal degradation of activated Smad1 by Axin/GSK3 (Fuentealba et al. 2007). The TGF-β signalling pathway regulates cell growth, cell proliferation, differentiation, and death. Axin1 together with GSK3 appears to facilitate Smad3 phosphorylation and degradation in the absence of TGF-β (Guo et al. 2008). Reduction in the activity of the Axin/GSK3 complex can activate TGF-β signalling targets without activation of the receptor or Smad2.

Based on experiments using *Axin* overexpression, other groups also suggest that Axin promoted TGF-β by facilitating the binding of Smad3 to the TGF receptor (Furuhashi et al. 2001) or through the degradation of the inhibitory Smad7 (Liu et al. 2006). However, the physiological significance of these findings remains unclear.

Recently, Axin has also been linked to the Hippo pathway. Immunoprecipitation of endogenous Axin1 in HEK293 cells and western blotting for possible associated proteins, revealed a strong association with endogenous Yes-associated protein (YAP) and transcriptional co-activator with PDZ-binding motive (TAZ) (Azzolin et al. 2014). The group around Stefano Piccolo hypothesised that YAP/TAZ are part of the β-Catenin destruction

complex, fulfilling a dual role in Wnt off conditions. Firstly, the destruction complex inhibits the transcriptional activity of YAP/TAZ on HIPPO pathway target proteins. Secondly, both YAP and TAZ are involved in the recruitment of β-TrCP to the destruction complex to enable β-Catenin degradation.

A connection of Wnt signalling, Axin and the TOR/S6K pathway was discovered by the group of Kun-Liang Guan. Following a priming phosphorylation by AMPK (AMP-activated protein kinase), TSC2 (Tuberous Sclerosis Complex) is phosphorylated by GSK3 in a Wnt dependent manner possibly by an Axin/GSK3 complex (Inoki et al. 2006). This in turn activates the TOR/S6K pathway regulating transcription, translation, protein and lipid synthesis, cell growth and size, and cell metabolism.

In addition to the involvement of Axin in the signalling cascades mentioned above; Axin has been linked to cellular stress response mechanisms and apoptosis regulation, as the result of various stressors including DNA damage and oxidative stress. The link between Axin and the apoptosis pathway JNK, or SAPK (stress-activated protein kinase) pathway, is through the interaction with MEKK1 and MEKK4 (Mitogen activated ERK Kinase Kinase). Axin MEKK interaction leads to the activation of JNK through a signalling cascade via MKK (Zhang et al. 2000). Another link of Axin to JNK signalling is through the interaction with Protein Inhibitor of Activated STAT (PIAS)(Rui 2002). Through JNK activation, Axin can regulate and induce apoptosis, which has been shown in many *Axin* overexpression studies (Xu et al. 2007; Neo et al. 2000).

We recently discovered a further link between Axin1 and stress responses through its interaction with Nrf2 (*Nuclear factor* E2-related factor 2) (Rada et al. 2015). As a response to oxidative stress, Nrf2 translocates from the cytoplasm into the nucleus, where it initiates the transcription of antioxidant genes (Yamamoto et al. 2008). Nrf2 activity is negatively regulated through several mechanisms under normal conditions. The most studied control of Nrf2 is though KEAP1 dependent proteasomal degradation (Hayes and Dinkova-Kostova 2014), but we showed that Nrf2 can also be regulated by Wnt signalling (Rada et al. 2015).

Wnt3a increases the Nrf2 levels and its transcriptional activity in hepatocytes, while a complex of Axin1, GSK3-β, and β-TrCP leads to the degradation of Nrf2.

Another interesting member of the long list of Axin interaction partners is p53. Yanning Rui and colleagues have shown that Axin1 can interact with, and facilitate p53 function through direct interaction with p53 and indirectly via homeodomain-interacting protein kinase 2 (HIPK2) (Rui et al. 2004). This interaction is vital for the activation of apoptosis following DNA damage (Li et al. 2009) and may be a crucial link between Axin mutations and carcinogenesis.

The scaffold protein Axin can integrate multiple signals from extracellular and intracellular cues by localizing important players in close proximity to each other. The crosstalk between multiple signalling cascades facilitated by Axin, allows the cell to react in the appropriate manner at the right time.

1.3.4 Axin and its links to cell cycle control

The cell cycle is the tightly regulated process, in which a cell undergoes a division and duplication process, leading to the production of two daughter cells. The cell cycle is commonly divided into distinct phases (see Figure 1-8).

The first stage of the cell cycle is the G_1 phase (Gap 1), in which the cell size is increased and mRNA and proteins, important for the replication, are synthesised. In the S phase (synthesis) the DNA is replicated before the cell undergoes a second Gap phase (G_2), where the cell continues to grow. This is followed by the Mitosis (M), in which the chromosomes are condensed and segregated, before the cell finally undergoes complete division into two daughter cells. Cells in the so-called G_0 (Gap 0) state are quiescent cells that have left the cell cycle and stopped dividing. Phases G_1, S and G_2 are also referred to as interphase.

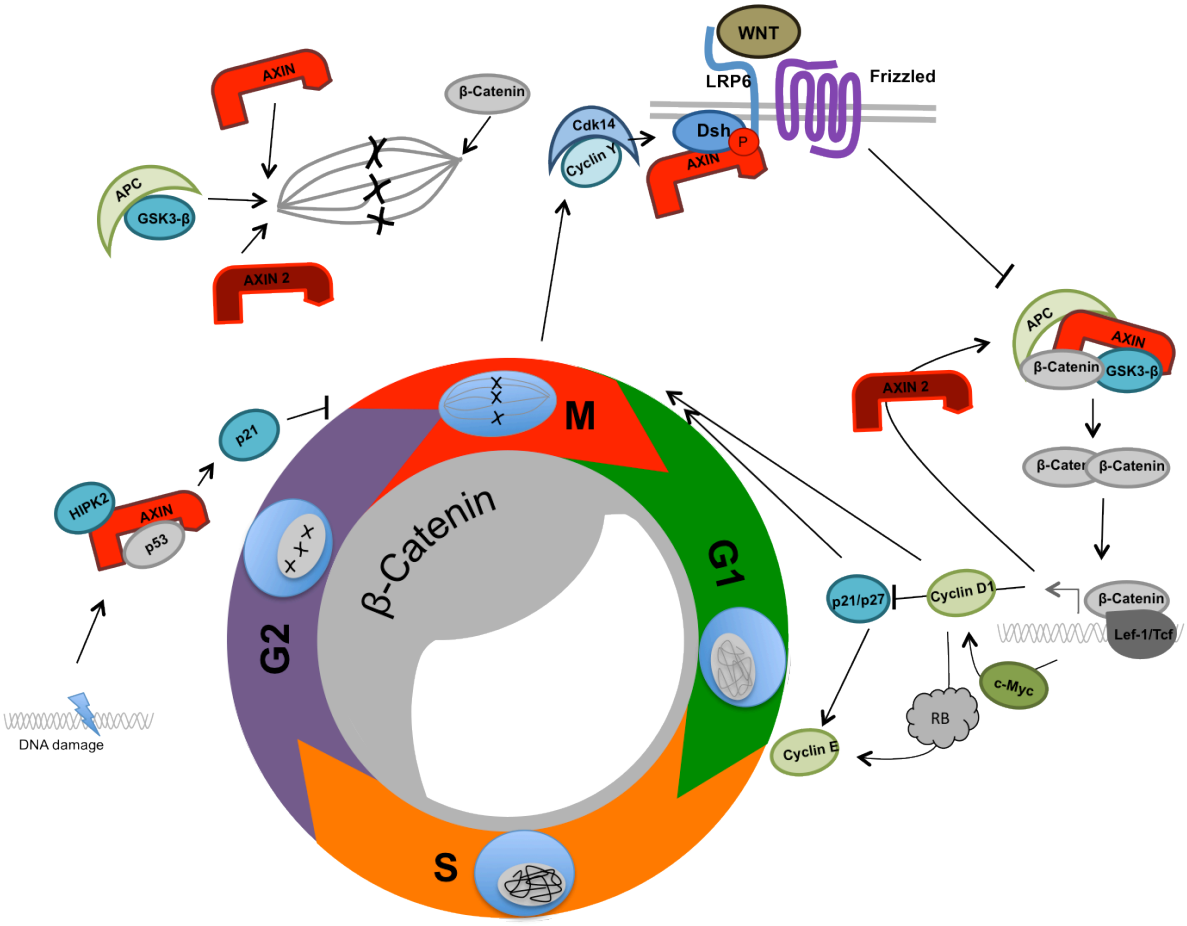

Figure 1-8. Overview over Wnt signalling in cell-cycle regulation.
Cell-cycle progression is controlled by cyclins and CDKs. In G_1, Cyclin D initiates Rb complex phosphorylation, which induces *cyclin E* transcription. Additionally, the CDK inhibitors p21 and p27 are repressed through Wnt pathway activation. After DNA replication in S phase, different quality controls ensure the integrity of the DNA. In case of DNA damage a complex of p53 and Axin activate p21 to inhibit cell cycle progression. The mitotic spindle is also regulated by Wnt signalling components. Wnt/GSK3 signalling promotes microtubule stabilization. APC and Dsh regulate the attachment of the mitotic spindle to the kinetochores;, and together with Fz and LRP6 modulate spindle orientation. GSK3, β-Catenin, and Axin2 are required at the centrosome to ensure a proper distribution of the chromosomes during division. (Figure adapted from Niehrs and Acebron 2012).

Cell cycle progression is tightly regulated at checkpoints to ensure that the different stages have been completed correctly, before the cell enters the next stage. The main focus of the checkpoint control is on DNA integrity. In the centre of this control mechanisms are cyclins and the cyclin dependent kinases (CDKs), with distinct sets of cyclins and CDKs coinciding with the different checkpoints (G_1/S; G_2/M; and M/G_1) (Pagano 1998; Moore 2013).
Any aberrant activation of the cell cycle and wrongly passed checkpoints can lead to serious consequences for the daughter cells and the whole organism.

Axin and other Wnt signalling components have often been implicated in cell cycle regulation in the past. This link is either through Wnt signalling dependent transcriptional activation of proteins involved in cell cycle regulation; or by Wnt signalling components, as well as Axin binding partners, directly participating in the regulation of cell cycle processes, for example, by localising at the mitotic spindle (see Figure 1-8). Similar to the cyclin and CDK waves during the cell cycle, Wnt components such as β-Catenin and Wnt target genes including *Axin*2 and *Cyclin D1* have been reported to oscillate in a cell cycle dependent manner (Tetsu and McCormick 1999; Olmeda et al. 2003; Davidson et al. 2009; Hadjihannas et al. 2012).

Wnt signalling promotes G_1 progression through its transcriptional targets *c-Myc* and *Cyclin D1*. C-Myc upregulates the G_1 cyclin *Cyclin D* and represses the CDK inhibitors *p21 and p27* (Gartel et al. 2001; Yang et al. 2001). Cyclin D1 is involved with the phosphoinhibition of the Retinoblastoma (Rb) complex leading to the increase of the G_1/S cyclin Cyclin E and marks the point of no return for cell proliferation by dividing G_1 and S phase of the cell cycle (Albrecht and Hansen 1999; Dulic et al. 1992; Saddic et al. 2011). Cyclin 1, Cyclin E1 and c-Myc proteins are also all direct targets of an Axin/GSK3 complex that controls protein degradation (Diehl et al. 1998; Welcker et al. 2003; Arnold et al. 2009). Thus, Wnt signalling and subsequent inhibition of the Axin/GSK3 complex induces transcription of G_1 mediators, while simultaneously increasing their stability, leading to the transition of G1 to S phase (Niehrs and Acebron 2012). The G_1/S checkpoint progression can additionally be regulated

by p53. The tumour suppressor protein can inhibit cell growth following DNA damage. Axin levels regulate p53 activity after genotoxic stress and determine if the cell undergoes p21 dependent cell cycle arrest or apoptosis (Li et al. 2009). The overall levels of Wnt signalling activity are highest at G2/M (Davidson et al. 2009). The abundance of 'free' β-Catenin drives the strong expression of Wnt target genes. Additionally, during mitosis many cellular proteins are stabilized in response to Wnt receptor activation, which is independent of the transcriptional activity of β-Catenin (Acebron et al. 2014). This newly discovered mode of Wnt signalling has been termed Wnt/STOP signalling (Wnt dependent stabilization of proteins) and has been suggested to provide the cell with increased mass following subsequent cell divisions and assures proper mitotic microtubule assembly and chromosome segregation (Stolz et al. 2015).

In the G2/M phase, there is also evidence that Axin stability itself is regulated by the cell cycle. Smurf1 mediates ubiquitination of Axin1, so that its inhibitory effects on Wnt signalling are attenuated in the G2/M phase of the cell cycle (Fei et al. 2014). At the same time; potentially also mediated by Axin inhibition and Cyclin Y, LRP6 phosphorylation is at a peak, which in turn leads to an increased responsiveness to the stimulation by Wnt ligands (Fei et al. 2014; Davidson et al. 2009). The Cyclin Y/CDK14 complex is most active in G2/M and phosphorylates LRP6 to drive GSK3 and Axin inhibition.

In the mitotic part of the cell cycle, Axin or Axin–binding proteins are involved in microtubule organisation, spindle formation, and centrosome division. GSK3β and APC, for example, can both be found at the plus-end of microtubules and at the MTOC (microtubule-organising centre). APC binding increases microtubules stability (Wen et al. 2004; Zumbrunn et al. 2001), while GSK3 promotes Par6-protein kinase dependent cell polarisation (Etienne-Manneville and Hall 2003). Axin2, APC and β-Catenin are required for chromosome segregation (Fodde et al. 2001; Hadjihannas et al. 2006; Bahmanyar et al. 2008) and the establishment of a bipolar mitotic spindle, necessary for the correct separation of daughter cells during cell division (Kaplan et al. 2004). Increased Axin2 levels have been linked to

Chromosomal instability by compromising spindle checkpoints (Hadjihannas et al. 2006). In fly embryos, Axin and APC2 have also been shown to be important for mitotic fidelity (Poulton et al. 2013). The loss of either protein increases chromosome segregation errors, due to their role in facilitating chromosomal separation and the fine-tuning of the cytoskeleton rearrangements. Axin1, but not Axin2, localises at the centrosome and facilitates microtubule nucleation by direct interaction with γ-tubulin, via a β-Catenin independent process (Fumoto et al. 2009). The Axin binding partner Dsh is vital for the establishment of spindle orientation dependent on LRP6/Fz localisation through a PLK1 dependent process (Kikuchi et al. 2010). This process might also explain the findings of the Nusse lab; that the localised Wnt signalling can lead to asymmetric cell division (Habib et al. 2013). Given the various links of Axin to Wnt signalling and cell cycle regulation, it is not surprising that Axin1 and Axin2 are both important tumour suppressors.

1.3.5 Axin and Wnt in embryonic development

The scaffold protein Axin has many roles in embryonic patterning. As previously described, *Axin* was identified through the effects of *Axin* mutation on axis duplications in mouse embryos (Zeng et al. 1997)(see Section 1.3). Additionally, *Axin1* overexpression in *Xenopus* embryos inhibits dorsal axis formation. In contrast, depletion of maternal *Axin1* mRNA with antisense oligonucleotides leads to hyperdorsalisation of embryos (Kofron et al. 2001). This phenotype is very similar to the one observed in cleavage stage embryos treated with the GSK3 inhibitor LiCl (Hedgepeth et al. 1997). Given this evidence, this effect was linked to the Axin dependent destabilisation of β-Catenin (Ikeda et al. 1998). Similarly, the *Drosophila* homologue Daxin produced a loss of *wg*-like phenotype, a cuticle covered with denticels, when overexpressed during embryogenesis (Willert et al. 1999). Disruption of Daxin through RNA interference, however, led to embryos with naked cuticles, similar to the overexpression of *wg*.

Complete removal of Axin1 in mice leads to an embryonic lethality between E 9.5 to E 10.5,

associated with a variety of defects such as forebrain truncation and axis duplication (Zeng et al. 1997). Similar phenotypes can also be found in *Axin1* mutants of the RGS or the DIX domain (Perry et al. 1995; Chia et al. 2009).

In contrast, *Axin2* mutants have been reported to be viable. The mostly studied Axin2 allele in mice is Axin2$^{lacZ/lacZ,}$ in which the *lacZ* gene was inserted into exon 2 of *Axin2* (Lustig et al. 2002) (see Figure 1-10 E). These mice show no obvious changes in embryonic patterning, with only minor defects in skull formation (Yu et al. 2005) and tooth development (Lammi et al. 2004). Furthermore, their body weight was significantly reduced in comparison to Axin2$^{lacZ/wt}$ and wild type littermates (Dao et al. 2010). Since the *lacZ* gene is inserted after the Axin2 promoter, the gene product β-Galactosidase can be used as a faithful reporter of *Axin2* expression and thus Wnt signalling activity. However, there is thus far no published evidence that the knock-in strategy completely deletes the *Axin2* gene. Other experiments were performed on the Axin2^{canp} mutant, which has a V26D substitution in the evolutionary preserved N-terminal Tankyrase binding motive (Qian et al. 2011). This mutant is lethal at mid-gestation and shows defects in heart, tail and primitive streak morphogenesis. In most tissues, Wnt signalling activity is decreased, due to the expression of a more stable Axin2 protein. However, in the primitive streak, Wnt signalling levels are even higher than in the wild type. This data suggests a positive role of Axin2 in canonical Wnt signalling.

The role of Axin in very early development and embryonic stem cells (ES cells) is, thus far, not well understood. Due to its role as a negative regulator of β-Catenin, it is widely believed that Axin mainly acts through Wnt signalling. The following paragraph will provide an overview of the suggested function of Axin and Wnt signalling in ES cells and early embryonic development. General information about ES cells and their use as a research tool can be found in Section 1.4.2.1.

The exact effect of Wnt signalling on early embryonic development is still highly disputed. This debate is probably due to the opposing context- and stage-specific effects that have been reported (Sokol 2011). Many agree that the Wnt target genes maintain the pluripotency of

stem cells (Nusse et al. 2008; Wend et al. 2010). Wnt/β-Catenin target gene expression in the early embryo in mainly mediated through depression of genes controlled by TCF3, among which are many key pluripotency factor genes (Merrill et al. 2004; Martello et al. 2012). Wnt3a is crucial for the self-renewal of many stem cell types, including ES cells (ten Berge et al. 2011). Hyperactivation of Wnt signalling, through the complete knockout of GSK3, blocks differentiation in mouse ES cells (Doble et al. 2007). Additionally, the inhibition of GSK3 with small molecules promotes self-renewal and prevents neural differentiation in mouse ES cells (Sato et al. 2004; Haegele et al. 2003). The role of Wnt signalling in blocking neural differentiation has also been shown in *Xenopus* (Heeg-Truesdell and LaBonne 2006).

By contrast, suppression of Wnt signalling leads to the differentiation towards Epiblast stem cells (EpiSCs) (ten Berge et al. 2011). In human ES cells GSK3 inhibition through small molecules promotes differentiation towards primitive streak, mesoderm, and definitive endoderm instead of maintaining pluripotency (Bone et al. 2009). Furthermore, *in vivo* studies in *Xenopus* and *in vitro* studies in mouse ES cells linked Wnt signalling to mesodermal differentiation (Gadue et al. 2006; Lindsley et al. 2006; Sokol 1993).

Through a very elegant method, in which ES cells are exposed to Wnt ligands bound to a bead; a group around Roel Nusse discovered that the location of Wnt source orients asymmetric cell division ES cells (Habib et al. 2013). They discovered, that the Wnt proximal daughter cell has high levels of nuclear β-Catenin while the distal daughter cell expresses markers of differentiation. This mechanism could be important for the stem cell niche in many tissues.

All these seemingly contradictory effects of Wnt signalling in mouse and human embryonic stem cells are probably linked to their developmental stage. While mouse ES cells are considered to be in a 'naïve' state of pluripotency, human ES cells resemble a 'primed' state of mEpiSCs (reviewed by Merrill 2012).

The difference between the role of Wnt signalling in maintaining pluripotency and driving differentiation could possibly be explained by a new idea brought forward by Austin Smith

and his group (Martello and Smith 2014). In their review about the nature of embryonic stem cells, they summarise current experimental evidence of how stem cell self-renewal and differentiation are governed. They describe a transcription factor circuit with Oct4 (*Pou5f1*) and Sox2 as the main regulators of pluripotency in the centre, surrounded by a network of factors that either favour differentiation or help to maintain pluripotency on self-renewal. Wnt/β-Catenin signalling is one of the network nodes involved in this circuit. Oct4 and Sox2 are not direct targets of self-renewal inputs. Pluripotency can be viewed as a balancing act between rival lineage specifies and extrinsic modulators that constantly compete (Loh and Lim 2011; Martello and Smith 2014). Activation or inhibition of any network components surrounding Oct4 and Sox2 can weaken the circuit substantially. The exact state of each of the other nodes in the network, determines if the balance of pluripotency can be maintained, or if a cell is driven down a specific lineage. In the case of Wnt activation, for example through GSK3 inhibition, the circuit maintaining pluripotency is usually stabilized. However, it is easy to imagine that the balance can still be tipped towards differentiation given the right combination of extrinsic signals. The context, timing, and identity of these signals remain to be elucidated.

1.3.6 Axin and Wnt in the liver and HCC

Misregulation of many members of the Wnt signalling cascade have been implicated in the development of cancers. The first discovery of a Wnt signalling pathway component in mammals was tumour related. Wnt1 was discovered because of an integration site of MMTV, which induced mammary gland tumours in mice (Nusse and Varmus 1982). Since then, deregulation of Wnt signalling components has been found in many other cancers (Polakis 2012).

Because Axin1 and Axin2 have a main regulatory function in Wnt signalling and due to their regulatory function in embryonic development, it is not surprising that *Axin* mutation has often been found in several different tumour types; including colon, ovarian,

endometrioid, adenocarcinoma and particularly hepatocellular carcinoma (HCC) (Lammi et al. 2004; Salahshor and Woodgett 2005; Marvin et al. 2011; Satoh et al. 2000; Liu et al. 2000). In HCC, mutations of Wnt signalling components, including *Axin*, are especially prevalent. Activating mutations in β-Catenin (*CTNNB1*) can be found in 5–50% of HCCs; mutations in A*XIN1* occur in 5 to 25% of HCCs; and *AXIN2* is mutated in 3 to 10% (Zucman-Rossi 2010). Interestingly, *APC* mutations are only found in 1.6% of HCCs (Guichard et al. 2012).

AXIN1 mutations were believed to lead to β-Catenin stabilization and thus the activation of β-Catenin/TCF dependent transcription, which in turn drives oncogenesis. However, mutations of *AXIN1* occurred in a subset of tumours with an especially poor prognosis. While *CTNNB1* mutations are found in a tumour subgroup that is well-differentiated and shows low proliferation rates accompanied by a defined acinus architectures, and a lack of steatosis and cholestasis; AXIN1 mutations are instead linked to a highly proliferative and chromosomally unstable subgroup of HCC (Laurent-Puig et al. 2001; Hoshida et al. 2009; Boyault et al. 2007; Zucman-Rossi 2010).

Mutations of *Axin1* and *Axin2* occur in all different domains of the tumour suppressors. In human HCC *AXIN1,* mutations have been found in exons 2 to 6 (see Figure 1-5 for the structure of Axin1). Among those are; insertion of stop codons, frame shift mutations, and deletion of substitutions of amino acids (Satoh et al. 2000; Taniguchi et al. 2002). Through biochemical analysis in different cancer cell lines, Marie-Therese Webster and her colleagues could show that a somatic Axin1 mutation, commonly found in patients and cancer cell lines, mainly interferes with GSK3 binding and the activation of TCF-dependent transcription through Frat1 and Dsh (Webster et al. 2000; Mazzoni and Fearon 2014; Klaus and Birchmeier 2008).

Mutations in AXIN2 mainly occur in exon 8, and are found in 20% of mismatch repair deficient colorectal tumours (Taniguchi et al. 2002; Salahshor and Woodgett 2005; Liu et al. 2000). Changes in DNA methylation levels in the promoter region of *Axin2* may also be important (Muto et al. 2014). Yuata Muto and colleagues found that DNA methylation

negatively correlates with *Axin2* expression, which in turn influences tumour progression. However, the exact role of Axin2 in tumourigenesis is unclear. Axin2 is generally considered a tumour suppressor because of its negative regulation of Wnt signalling. However, it has also been implicated as an efficient tumour promoting factor by activating a epithelial-mesenchymal transition (EMT) program and metastatic behaviour (Wu et al. 2012b). Additionally, high levels of Axin2 were shown to cause chromosomal instability in colon cancers (Hadjihannas et al. 2006).

To study the role of Axin1 post embryonically, Gui-Jie Feng et al. recently developed a conditional Axin1 mouse line (Feng et al. 2012). They showed that upon deletion of Axin1 in the liver of adult mice, using the β-Naphthoflavone (β-NF) inducible Ah-Cre transgene (Ireland et al. 2004), homozygous mice developed liver tumours within one year. But the acute effects observed, seem to differ from those of other mutations in Wnt pathway components, like *APC* knockouts or constitutively active *β-Catenin* mutations, which are linked to liver zonation changes and the strong activation of Wnt target genes (Benhamouche et al. 2006; Tan et al. 2006). Contrary to the prevailing view that Axin1 loss results in the disruption of the destruction complex, and thus in the stabilization of β-Catenin, Feng et al. did not observe widespread nuclear β−Catenin or a strong activation of Wnt target genes after Axin1 loss. Gene expression analysis revealed that only a small subset of Wnt target genes including *Axin2, c-Myc,* and *Cyclin D1* was induced following the deletion; while other liver specific Wnt target genes remained unchanged. The tumour development was preceded by an acute and persistent increase in hepatocyte cell volume, together with cell proliferation and a transcriptional program associated with induction of G2/M cell cycle (e.g. *CyclinsA2, B1, B2, Cdk1, Cdca3, Cdc20, Ki67* and *FoxM1*) and cytokinesis regulation (e.g. *Aurka, Prc1, Ect2, Plk* and *Cyk4/RacGap1*). Interestingly, these findings were consistent with a study published by Zucman-Rossi of human HCCs (Zucman-Rossi et al. 2007; Boyault et al. 2007). Their analysis of the gene expression profile in 45 human tumours and 4 cell lines, with either *AXIN1* or *CTNNB1* mutations, also strongly suggested that Axin loss of function is not equivalent to β-

Catenin gain of function mutations. They conclude that the tumour suppressor function of Axin1 is related to an non-Wnt pathway (Zucman-Rossi et al. 2007).

These observations raise some important questions regarding possible links between Axin1 loss and hepatocellular carcinogenesis:

I Are the effects of Axin1 loss mediated by β-Catenin?

Wnt dependent tumourigenesis was suggested to be dependent on a 'just right' level of canonical Wnt pathway activity (Albuquerque et al. 2002). The threshold of signalling level necessary to induce HCC might be very low (Buchert et al. 2010). Additionally, β-Catenin dependent transcription could only be upregulated in a small subset of cells that function as cancer stem cells and trigger tumour formation (Wend et al. 2010). Axin1 loss in the liver could lead to Wnt signalling activation below a detectable level but sufficient to induce tumourigenesis.

II Is there a functional β-Catenin destruction complex left?

The lack of an obvious β-Catenin dependent phenotype could be explained with the presence of a functional β–Catenin destruction complex. Following Axin1 loss, compensatory upregulation of *Axin2* would allow ongoing phosphorylation and degradation of β-Catenin by a destruction complex built around Axin2. The tumourigenesis could thus be linked to effects as the consequence of *Axin2* overexpression. Another possibility would be the presence of a β-Catenin destruction complex that functions completely without Axin; possibly build around APC.

The lack of free β-Catenin could further be explained with the incomplete loss of Axin1. Upon the induction of Cre recombinase exon 2 of Axin1 is removed. This is predicted to lead to a complete loss of Axin1 protein. Indeed, immunoblotting and immunoprecipitation with antibodies against different regions of the Axin1 molecule performed by Feng et al. failed to detect any region of remaining protein (Feng et al. 2012). However, the presence of a truncated form of Axin1 cannot be completely excluded.

III Is there a mechanism involving other Axin interaction partners?

Axin1 dependent tumourigenesis could also be linked to core Wnt/β-Catenin independent targets and interaction partners of Axin1. Section 1.3.3 of the introduction provides a summary of possible candidates.

The ultimate aim is to identify the mechanism by which Axin1 loss of function mutations drive the development of HCC and how its homologue Axin2 is involved in the process. Understanding this mechanism is vital in the development of potent anti-cancer agents.

1.4 Tool box

1.4.1 Mouse models for HCC

Mouse models for human cancers are invaluable to further the knowledge of basic disease biology, and to prove a platform to test potential therapeutic drugs. Importantly, mouse models need to recapitulate the disease situation in humans as accurately as possible, to provide maximal benefit.

In HCC research, a range of different chemically induced models, xenograft models and genetically modified mouse models are used. The chemically induced models rely on carcinogenic compounds that are either genotoxic, through their capacity to induce structural DNA changes, or indirectly enhance tumour formation after initiation by a hepatotoxic compound (reviewed by Pitot & Dragan 1991). Xenograft models develop HCC, by implanting human hematoma cell lines or biopsy material in immunocompromised mice, either ectopically or orthotopically (Leenders 2008). Xenografts of human HCC are predominantly used in preclinical drug studies.

In recent years, more and more genetically engineered mouse models (GEMMs) have been generated to mimic the mutation frequently observed in human cancers and to assess the relevance of candidate gene networks in tumour establishment, progression, and maintenance. GEMMS allow molecular and cellular manipulations impossible to perform in

patients, and have immensely improved our understanding of this complex disease (Bakiri and Wagner 2013).

1.4.1.1 The Cre-lox system

If a developmental process controlling proliferation, growth and differentiation is activated ectopically, the result is often hyper proliferation and ultimately cancer. Conversely, most of the genes involved in tumourigenesis are also important in developmental settings. Conventional mutants, i.e. of Wnt signalling components, are usually embryonically lethal, preventing any studies of their effect in adult mice. Furthermore, mutations, which are present in the germ line, affect the whole organism. The consequences of the mutation in one tissue can potentially mask the effects in the tissue of interest.

Axin1 is one of the genes, which is critical for embryonic development. *Axin1* has been found to be mutated in 13–43% of HCCs, in a tumour subset that has very poor prognosis. However, the mechanism leading to Axin dependent tumourigenesis remains unclear. Further investigations into the role of Axin in tumourigenesis are needed, to get into a position to design new effective therapies. But conventional mutants such as the $Axin1^{Tg1}$ mutant are embryonically lethal, preventing any analysis in the adult liver (Perry et al. 1995; Zeng et al. 1997).

Use of the Cre-loxP recombination system (Figure 1-9) has enabled the study of tissue specific mutants in detail. The Cre-loxP technology depends on two major components, the Cre recombinase, and its target sequences (*loxP* sites). Cre recombinase was originally isolated from Bacteriophage PI (Abremski and Hoess 1984) as a site-specific DNA recombinase that recognized specific DNA sequences termed *loxP* sites (Sternberg and Hamilton 1981; Hoess et al. 1982). When active Cre recombinase recognizes two *loxP* sites in the DNA it excises the segment in between (Figure 1-9 A). If these *loxP* sites are artificially integrated into the genome, specific DNA sequences can be targeted. Upon activation of a Cre recombinase the targeted region is excised, or 'floxed' out.

The Cre-loxP system can be used to inactivate and activate genes of interest. The inactivation usually depends on the removal of whole genes or important exons. Activation is usually achieved through a flox-Stop cassette (a stop codon flanked by two loxP sites) inserted between a promoter and the gene of interest. This cassette gets deleted upon Cre activation, removing the stop codon and permitting expression of the transgene. The activation of Cre recombines can be controlled through many different mechanisms. Tissue or cell type specific promoters are used to drive Cre recombinase only in the tissue of interests (Figure 1-9 B). Often, the promoters used are also inducible (see Figure 1-9 C).

In the case of Ah-Cre for example, Cre activation is driven by the promoter of Cytochrome P450 1A (CYP1A1) in the gastrointestinal tract in response to administration of aryl hydrocarbons such as β-Naphthoflavone (Campbell et al. 1996; Ireland et al. 2004).

A further level of Cre regulation is achieved through post-translational activation. The fusion of a Cre recombinase with a modified estrogen receptor (ER^T) prevents the translocation of transcribed, and translated Cre recombinase into the nucleus (Feil et al. 1996) (Figure 1-9 C). The estrogen receptor domain carries a point mutation, inhibiting the activation though endogenous estrogen present in the host animal.

However, binding of the estrogen analogue Tamoxifen to ER^T exposes the nuclear localization signal, allowing the translocation of the $CreER^T$ fusion protein to the nucleus to act upon target sequences. The liver specific TTR-$CreER^T$ is an example for this kind of Cre construct (Tannour-Louet et al. 2002). Alternative ways to achieve Cre mediated recombination on genomic loxP sites are the expression from transfected plasmids (*in vitro*) or mediated by viruses (both *in vitro* and *in vivo*).

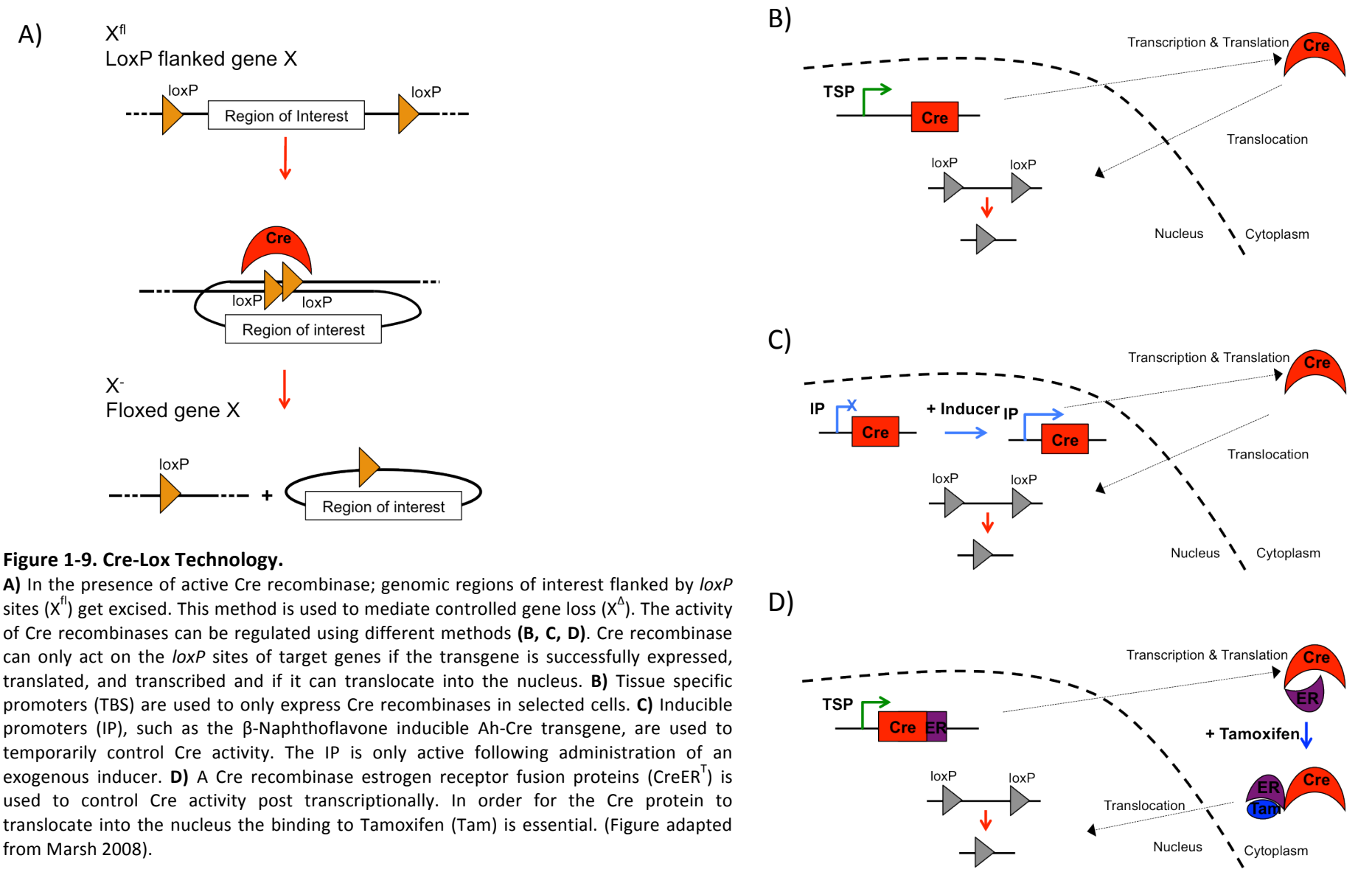

Figure 1-9. Cre-Lox Technology.

A) In the presence of active Cre recombinase; genomic regions of interest flanked by *loxP* sites (X^{fl}) get excised. This method is used to mediate controlled gene loss (X^{Δ}). The activity of Cre recombinases can be regulated using different methods **(B, C, D)**. Cre recombinase can only act on the *loxP* sites of target genes if the transgene is successfully expressed, translated, and transcribed and if it can translocate into the nucleus. **B)** Tissue specific promoters (TBS) are used to only express Cre recombinases in selected cells. **C)** Inducible promoters (IP), such as the β-Naphthoflavone inducible Ah-Cre transgene, are used to temporarily control Cre activity. The IP is only active following administration of an exogenous inducer. **D)** A Cre recombinase estrogen receptor fusion proteins ($CreER^{T}$) is used to control Cre activity post transcriptionally. In order for the Cre protein to translocate into the nucleus the binding to Tamoxifen (Tam) is essential. (Figure adapted from Marsh 2008).

1.4.1.2 Axin mutant mouse models used in this study

To study the role of Axin1 and Axin2 post embryonically Gui-Jie Feng recently developed conditional Axin1 and Axin2 mutant mouse lines, both of these lines will be used here (Feng et al. 2012, Feng, unpublished). In two independent experiments, exon 2 of each of the genes was targeted by homologue recombination with a construct containing the *loxP*-flanked exon 2. A Neomycin resistance cassette was subsequently removed by Flp mediated recombination, resulting in an allele containing a *loxP*-flanked exon 2 and a residual FRT site. Figure 1-10 A and B show both of the resulting alleles. In the presence of active Cre recombinase the *loxP*-flanked exons can be removed, leading to the loss of the start codon and thus any Axin protein (see Figure 1-10 D). Depending on the type of Cre construct used, recombination can be achieved in a time and tissue specific manner.

Axin1 deletion in the mouse liver, though Ah-Cre, led to the development of HCC within one year (Feng et al. 2012). Interestingly, this tumourigenesis was not associated with a raise in nuclear β-Catenin levels or changes in liver zonation that are found in mutants of other Wnt pathway components. Instead, a transcriptional program associated with G2/M cell cycle and cytokinesis regulators was activated, accompanied by increased proliferation, hepatomegaly, and an increase in hepatocyte cell volume. Conditional deletion of Axin2 in the liver has not yet been studied in detail, but Axin1 and Axin2 double knockout mice show accelerated HCC development at increased frequency, again without obvious changes in β – Catenin levels (Feng and Marsh, unpublished). Since Axin2 mutations have not been reported to be embryonically lethal, constitutive Axin2 mutants are available. In this study we also used the Axin2^{lacZ} allele (also known as Conductin^{lacZ} or *Axin2$^{tm1Wbm/J}$*) that carries a *lacZ* gene in frame with the endogens start codon of Axin2, replacing exon 2 (see Figure 1-10 E). The gene product of lacZ, β-Galactosidase, can be used as a faithful reporter of *Axin2* expression, and thus Wnt signalling activity.

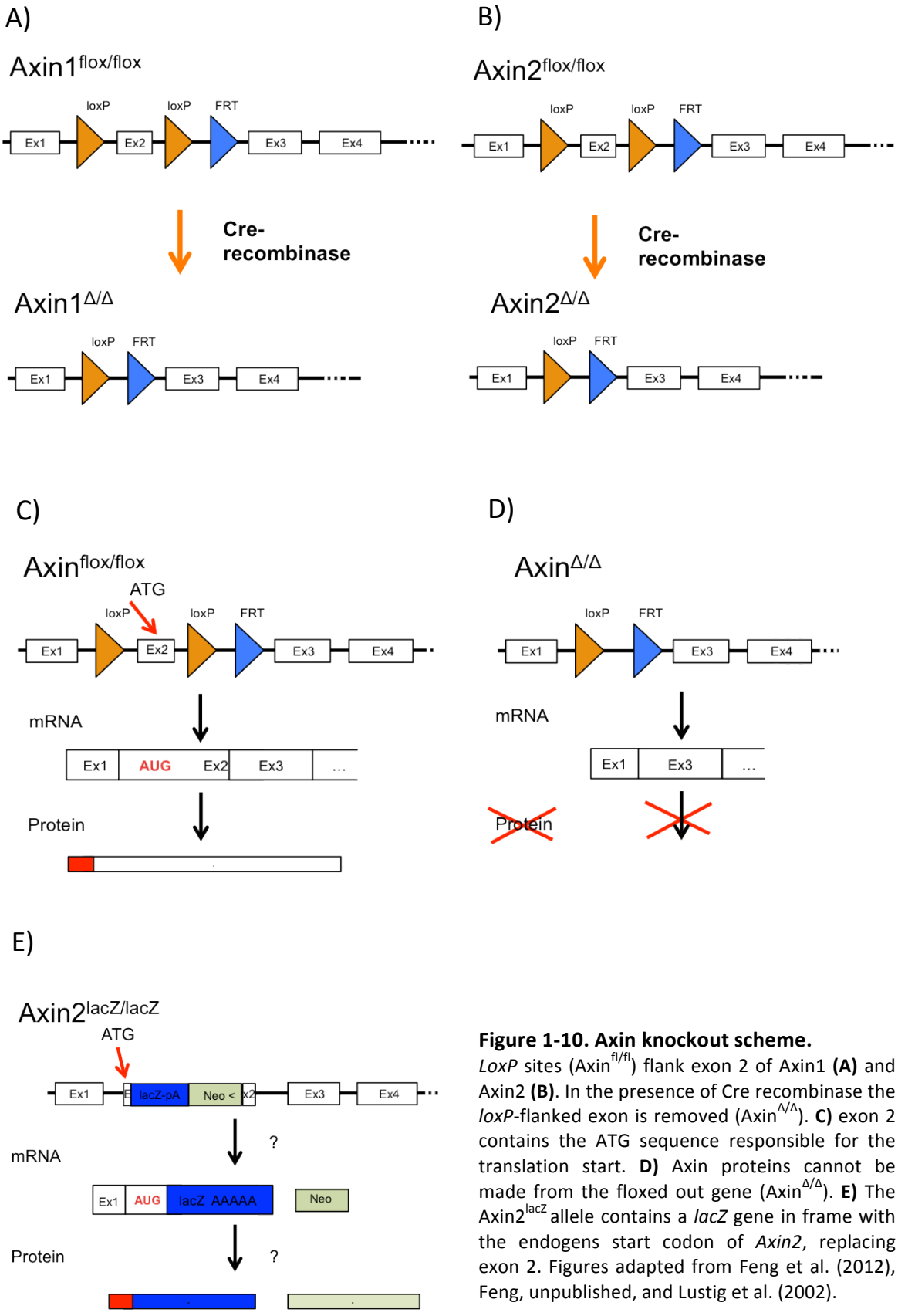

Figure 1-10. Axin knockout scheme.
LoxP sites (Axin$^{fl/fl}$) flank exon 2 of Axin1 **(A)** and Axin2 **(B)**. In the presence of Cre recombinase the *loxP*-flanked exon is removed (Axin$^{\Delta/\Delta}$). **C)** exon 2 contains the ATG sequence responsible for the translation start. **D)** Axin proteins cannot be made from the floxed out gene (Axin$^{\Delta/\Delta}$). **E)** The Axin2^{lacZ} allele contains a *lacZ* gene in frame with the endogens start codon of *Axin2*, replacing exon 2. Figures adapted from Feng et al. (2012), Feng, unpublished, and Lustig et al. (2002).

Indeed most studies utilising the Axin2^{lacZ} allele, use it to trace Wnt-responsive cells in normal or physiological conditions in heterozygous mice, which show no obvious phenotype. Mice carrying two copies of these alleles show minor defects in skull formation (Yu et al. 2005) and tooth development (Lammi et al. 2004). Furthermore their body weight is significantly reduced in comparison to Axin2$^{lacZ/wt}$ and wild type littermates (Dao et al. 2010).

1.4.2 In vitro models

1.4.2.1 Embryonic stem cells

The evolution and development of complex multicellular organisms was only possible by a hierarchic cellular system with tightly regulated proliferation and differentiation processes (Arendt 2008). Stem cells are the cellular origin of adult tissues and whole organisms. Stem cell are defined as cells with the intrinsic potential to self-renew and to differentiate along multiple cellular lineages (Reya et al. 2001; Bell and van Zant 2004). These cells can either be adult stem cells that contribute to tissue homeostasis and repair mechanisms in pathological situations (e.g. adult liver stem cells as described in Section 1.1.2.2) or precursor cells in embryonic development.

The fertilised egg of vertebrates (zygote) is the cell with the highest possible developmental potential. Figure 1-2 gives an overview of the differentiation potential of different cell types during embryonic development. The zygote undergoes several cell divisions to form the blastomere consistent of totipotent cells. The zygote and each of the blastomere cells have the potential to differentiate into an entire multicellular organism (Mitalipov and Wolf 2009). Further on in development, cells of the inner cell mass (ICM) lose part of their differentiation capacity. They can only give rise to all embryonic cell types, but cannot generate extra embryonic tissue anymore. These pluripotent cells can be isolated from the ICM of preimplantation mouth embryos and placed in *in vitro* culture as embryonic stem cell lines (ES cells) (Evans and Kaufman 1981; Martin 1981; Morrison et al. 1997). Of

note, human ES cells are suggested to be derived at a later stage of development (Nichols and Smith 2011). They are very similar to mouse epiblast-derived stem cells (EpiSCs) with a narrower developmental potential than ES cells.

Undifferentiated murine ES cells can be maintained *in vitro* for extended periods in media containing the cytokine, leukaemia-inhibitory factor (LIF) (Williams et al. 1988; Smith et al. 1988). LIF is a ligand of the gp130/LIF receptor that activates STAT3 though the JAK/STAT signalling pathway (Boeuf et al. 1997). STAT3 induces the expression of *Nanog, Klf4* and *c-Myc* and thus regulated the maintenance of pluripotency (Cartwright 2005; Suzuki et al. 2006; Hall et al. 2009). The addition of a MEK/Erk inhibitor (i.e. PD0325901) and a GSK3 inhibitor (i.e. CHIR99021) can further increase the ES cell self-renewal efficiency (Ying et al. 2008) (see Section 1.3.5 for more information about the use of a GSK3 inhibitor).

The undifferentiated state of ES cells can be characterized by high levels of alkaline phosphatase (AP) (Pease et al. 1990) and the expression of surface markers including SSEA and TRA antigens and the transcription factors Oct4 and Sox2. If the ES cells are injected into blastocysts they can take part in normal multicellular development, giving rise to endo-, ecto-, and mesoderm lineages as well as germ cells (Niwa 2007). This differentiation into the different germ layers can also be reproduced *in vitro* under certain culture conditions. When ES cells are allowed to aggregate, they form structures called embryoid bodies (EBs) that exhibit differentiation features similar to early embryos (Doetschman et al. 1985; Keller 1995).

ES cells are extremely interesting for basic and applied research. The ability of mouse ES cells to contribute to the germ line enabled the generation of transgenic mice and made them an important tool to study gene function. The inventors of this powerful technique, Mario R. Capecchi, Sir Martin J. Evans, and Oliver Smithies won the Nobel Prize in Physiology or Medicine 2007. Due to their theoretical ability to differentiate into all of the cell types in the body, ES cells also have an enormous potential in regenerative medicine.

In this study ES cells are used as a model system to study the role of Axin1 and its homologue Axin2 on embryonic development.

1.4.2.2 3D liver culture system

A major part of the investigation of the acute effects of Axin loss in the liver, in this study, was done using a novel primary 3D liver culture system (Sato et al. 2009; Huch et al. 2013). This culture system was the first that allowed the long-term clonal expansion of liver cells in culture.

For a long time, different labs all over the world tried to cultivate mature hepatocytes and hepatic stem cells *in vitro* with limited success (Zhou et al. 2015). Primary hepatocytes are often physiological and mitotically inactive and have been shown to rapidly lose metabolic function when grown in culture. The key to the new culture system was to grow liver stem cells in a tightly controlled 3D environment. Intrahepatic bile ducts derived cells are maintained as budding cyst-like structures embedded in Matrigel, which consists of extracellular matrix proteins, and in defined culture medium containing R-Spondin which potentiates Wnt signalling (Sato et al. 2009; Ruffner et al. 2012) (Figure 1-11). When the culture conditions are changed to low Wnt activation, as well as Notch and TGF-β inhibition though the small molecules DAPT and A8301, ductal cells can be differentiated along the hepatic lineage into functioning hepatocytes. This culture system provides a number of advantages over the *in vivo* analysis in mutant mice. In an *in vitro* culture, different parameters, including morphology and cell proliferation, can be measured and followed over a period of time. The organoid model also allows side-by-side comparison of normal and oncogenic cells of the same genetic background. The use of a 3D culture system becomes especially important in the study of cell cycle regulation. The analysis of spindle and centrosome formation and localisation is almost impossible *in vivo*. The 3D model allows the comparison of a range of different cell parameters while they happen.

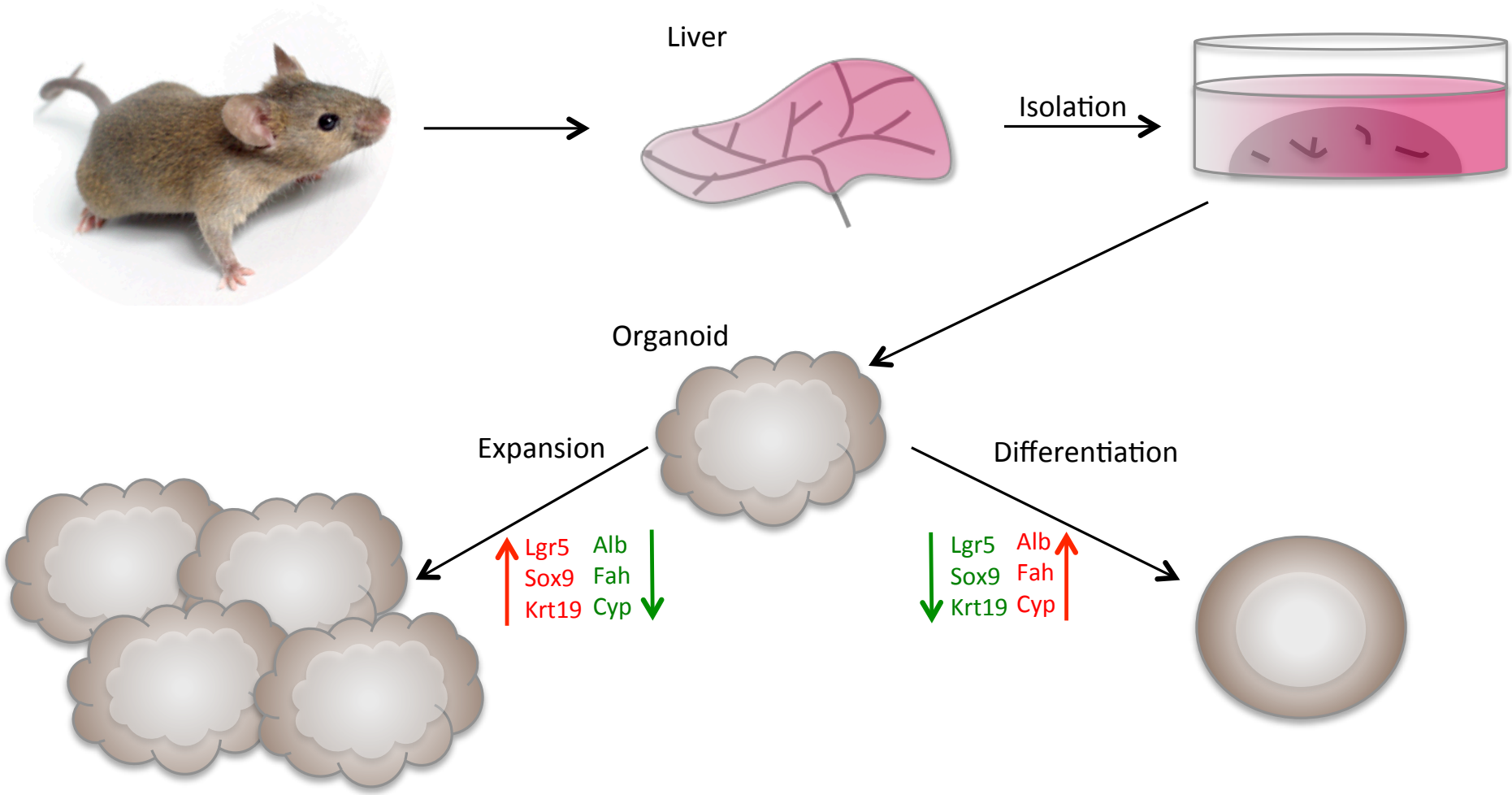

Figure 1-11. In vitro expansion and differentiation of ductal derived liver organoids.
Progenitor cells from intrahepatic bile duct can be isolated and grown as organoids. They can then be expanded or differentiated into hepatocytes *in vitro.* Figure adapted from Huch et al. (2013).

2 Aims and Objectives

There is a clear link between Axin mutations and the development of HCC with an especially poor prognosis. However, the mechanisms leading to Axin dependent tumourigenesis are currently highly debated. Given the important role of Axin in Wnt signalling regulation, the current dogma is that the loss of Axin function is oncogenic due to the subsequent activation of β-Catenin and Wnt target genes. However, evidence gathered in genetic screenings of human HCC and in knockout mouse models, suggests a role for Wnt/β-Catenin -independent mechanism(s) of Axin dependent development of HCC. While β-Catenin mutations are found in a tumour subgroup that is highly differentiated and shows low proliferation rates accompanied by a defined acinus architectures, and a lack of steatosis and cholestasis; Axin1 mutations are instead linked to a highly proliferative and chromosomally unstable subgroup of HCC (Hoshida et al. 2009; Zucman-Rossi et al. 2007; Boyault et al. 2007). A key paper in the understanding of Axin1 mutations in the mouse liver by Feng at al. shows that conditional loss of Axin1 through the β-Naphthoflavone inducible Ah-Cre (Ireland et al. 2005) leads to liver tumours after 12 months (Feng et al. 2012). Intriguingly, all the evidence gathered in this mouse model thus far showed a strong increase in proliferation, the upregulation of a G2/M and cell cycle gene expression profile in the absence of detectable levels of active, nuclear β-Catenin. Overexpression of *β-Catenin* was only found in some areas of the hepatic tumour that developed a year after Axin1 deletion in the mouse liver (see Section 1.3.6 for more details).

In order to develop potent and targeted anti-cancer agents, it is vital to understand the exact mechanism(s) leading to Axin dependent tumourigenesis.

This thesis aims to further the understanding by Axin gene deletion in two systems. Firstly, I generate an allelic series of Axin1 and Axin2 embryonic stem cell lines that I then use to study the loss of Axin1 and Axin2 specific functions in ES cells and their differentiated progeny. The objective of these studies was to identify redundant and non-redundant Axin1 /

2-dependent cellular processes. The results of this part of the analysis will be shown in Chapter 4.

Secondly, I develop a 3D liver organoid culture system to study the consequences of inducible Axin deletion in culture. The objective of these studies was to study the early cell biological and molecular events following Axin deletion in an experimentally accessible system. The results from these are shown in Chapter 5.

3 Materials and Methods

3.1 Experimental Animal

3.1.1 Animal Husbandry

All experiments in this thesis were performed in mice (*mus musculus*) or with tissues and cell cultures derived from the mouse. Animal experiments were conducted in accordance with the UK Home Office regulations, under valid personal and project licenses. All mice were maintained on an outbred background and housed using standard facilities. They had access to water *ad libitum*, were fed the Harlan standard diet (Special Diets Service UK, expanded diet) and were maintained on a 12:12 hour light-dark schedule.

3.1.2 Mouse Model and transgenes used in this project

A number of different mouse models, and cell lines derived from the mouse were used in this study (all shown in Table 3-1). These included *loxP* targeted alleles and reporter constructs, as well as various transgenes driving *Cre* recombinase expression. Three different Cre recombinase transgenes were used, Ah-Cre, TTR-CreER^{T}, and CMV-Cre. Additionally, we used a Lentiviral Cre delivery system in some cultures (Lenti-CMV-ER^{T2}CreER^{T2}). These transgenes are expressed in various tissues (Ah: gastrointestinal tract, TTR: liver, CMV: ubiquitous in the early embryo) and can be activated by different inducers (i.e. β-Naphthoflavone or Tamoxifen). The Ah transgene allows the β-Naphthoflavone (β-NF) inducible transcription of Cre recombinase through the xenobiotic activation of a CYP1A1 promoter. Some of the transgenes express Cre recombinase fused to a mutated estrogen receptor (ER$^{T(2)}$), which allows the nuclear translocation of Cre recombinase in the presence of Tamoxifen. Mice carrying alleles encoding Cre recombinases were crossed to different combinations of conditional transgenes, bearing *loxP* target sequences, and reporter alleles. For a more detailed explanation of the Cre/*loxP* system see Section 1.4.1.1 of the Introduction.

Table 3-1. Outline of the transgenic mice used.

TRANGENE	DESCRIPTION		REFERENCES
Cre recombinases		**Inducer**	
Ah-Cre (Tg(Cyp1a1-Cre)1Dwi)	*Cre* recombinase expression under the CYP1A1 promoter. *Cre* expression can be induced through β-Naphthoflavone in the epithelia of the gastrointestinal tract.	β-NF	(Ireland et al. 2004)
CMV-Cre (Tg(CMV-Cre)1Cgn)	*Cre* recombinase expressed during early embryogenesis under the control of the human cytomegalovirus minimal promoter.	Not inducible	(Schwenk et al. 1995)
TTR-CreER^{T} (Tg(Ttr-Cre/Esr1*)1Vco)	Tamoxifen inducible Cre recombinase under the control of the transthyretin promoter.	Tam	(Tannour-Louet et al. 2002)
Cre reporters			
ROSA-lacZ (Gt(ROSA)26Sor^{tm1Sor})	A floxed stop cassette is inserted between a *lacZ* gene and the ubiquitous ROSA26 promoter. In the presence of Cre recombinase the stop cassette is removed and the lacZ reporter is expressed.		(Soriano 1999)
ROSA-RFP (Gt(ROSA)26Sor$^{tm1.1Hjf}$)	A floxed stop cassette is inserted between a *tandem-dimer red fluorescent protein* (*tdRFP*) gene and the ubiquitous ROSA26 promoter. In the presence of Cre recombinase the stop cassette is removed and the tdRFP reporter is expressed.		(Luche et al. 2007)
Other transgenes			
Axin1^{fl}	Endogens *Axin1* allele baring *loxP* sites flanking exon 2 that allow excision of the start codon.		(Feng et al. 2012)
Axin2^{fl} (Conductin^{fl})	Endogens *Axin2* allele baring *loxP* sites flanking exon 2 that allow excision of the start codon.		(Feng, unpublished)
Axin2^{lacZ} (Conductin^{lacZ}, Axin2^{tm1Wbm})	Nuclear-localization β-Galactosidase (NLS-lacZ) inserted into of *Axin2.*		(Lustig et al. 2002)
GSK3α^{fl}, GSK3β^{Neo} (Gsk3a^{tm1Jrw}, Gsk3b^{tm1Jrw})	Endogens *GSK3α* allele baring *loxP* sites that allow excision of the start codon, of the endogens *GSK3β* allele replaced my a Neomycin selection cassette		(Doble et al. 2007)

3.1.3 Colony Maintenance

Adult animals (above 6 weeks of age) were bred in pairs or trios of one male and two females. Pups remained with their mothers until approximately 4 weeks of age and were weaned off, when feeding independently. Pups were separated and sexed at time of weaning.

3.1.3.1 Timed mating

When the exact developmental stage of the mouse embryos was important, mice were bred by timed mating. Timed mating was performed by setting up young females (6 to 10 weeks of age) with older males in the evening and checked for vaginal plugs the next morning. If plugs were present (E 0.5), females were sacrificed and embryos extracted at the appropriate age. If no plug was found, females were separated from males during the day and put together again in the evening for up to three consecutive days. Embryos from timed mating were analysed to study the embryonic effects of Axin loss (see Section 3.1.5) or to generate embryonic stem cell lines (see Section 3.2.1).

3.1.4 Experimental Procedure

3.1.4.1 Ear biopsies

In order to identify individual mice in a cage and to assess their genotype (see Section 3.6.5.1) ear biopsies were performed. One week after weaning, ear biopsies were taken using a 2 mm ear punch (K.L. Giddings Ltd) with the kind assistance of Patrick Mason, Helen Read, and Elaine Taylor.

3.1.4.2 Dissection of mice

Mice were culled following a schedule 1 approved method of culling (i.e. cervical dislocation) and dissected using a microdissection kit after confirmed permanent cessation of circulation. Mice were sprayed with 70 % EtOH, pinned to a Styrofoam dissection board,

and opened along the midline of the abdomen by cutting through both the skin and the peritoneal wall. Mouse embryos or livers were then carefully removed and processed immediately depending on further need.

3.1.5 Embryonic deletion of Axin1 and Axin2

To study the embryonic phenotype of Axin1 and Axin2 loss, $Axin1^{fl/fl}$ and $Axin2^{fl/fl}$ mice were mated with CMV-Cre mice (Schwenk et al. 1995). The offspring were genotyped and mice heterozygote for the deleted allele (*$Axin1^{wt/\Delta}$* or *$Axin2^{wt/\Delta}$)* were incrossed by timed mating (see Section 3.1.3.1).

On E 9.5 or 10.5 pregnant mice were sacrificed and dissected as described above (see Section 3.1.4.2). The uterine horns were dissected out into PBS and placed on ice. Embryos were separated by cutting between each implantation site along the uterine horn under a dissection microscope. Each embryo was then carefully isolated from the uterus and the decidua and peeled out of the yolk sac and the amnion with forceps. Embryos were imaged using a Zeiss Stemi SVII stereomicroscope. Following imaging, a piece of the tail was removed for genotyping and embryos were fixed in 4 % Paraformaldehyde (PFA, Sigma-Aldrich) and processed for paraffin embedding and sectioning (see Section 3.5).

3.1.6 Tissue fixation for histology

Mouse tissues or whole embryos designated for histological analysis were immersed in ice-cold formalin (4 % neutral buffered formaldehyde in saline, Sigma-Aldrich) immediately following dissection. After the tissue was fixed at 4 °C over night it was washed 2 x for 5 min in PBS and then transferred to 70 % EtOH and stored at 4 °C until processing.

For whole mount β- Galactosidase staining, tissue was fixed in 2 % formaldehyde (Sigma-Aldrich), 0.1 % glutaraldehyde ([v/v], Sigma-Aldrich) in PBS and further processed following the method described in Section 3.5.7.

3.2 2D culture and manipulations

3.2.1 Generation of parental ES cell lines

In this study conditional and constitutive mutant Axin1 and Axin2 lines were used as well as a GSK3-double knockout line as a control. Conditional Axin1 or Axin2 ES cell lines were derived as described below form $Axin1^{fl/fl}$ and/or $Axin2^{fl/fl}$ mice. These mice were generated by Feng and colleges in two independent experiments, in which exon 2 of each of the genes was targeted by homologue recombination with a construct containing the *loxP*-flanked exon 2 (Feng et al 2012, Feng, unpublished). Constitutive mutant $Axin2^{lacZ/lacZ}$ ES cells were derived from $Axin2^{lacZ/lacZ}$ mice (Lustig et al. 2002) and the GSK3 double knockout line ($GSK3^{\Delta/\Delta}$) and control cells ($GSK3^{fl/fl}$) were a kind gift from Bradley Doble and James Woodgett (Doble et al. 2007).

To generate the parental Axin lines $Axin1^{fl/fl}$ ($A1^{fl/fl}$); $Axin2^{fl/fl}$ ($A2^{fl/fl}$); $Axin2^{lacZ/lacZ}$ ($A2^{lacZ/lacZ}$); $Axin1^{fl/fl}$, $Axin2^{fl/fl}$ ($A1^{fl/fl}$, $A2^{fl/fl}$); and $Axin1^{fl/fl}$, $Axin2^{lacZ/lacZ}$ ($A1^{fl/fl}$, $A2^{lacZ/lacZ}$) young females (6-9 weeks) of the appropriate genotypes were set up by timed mating (see Section 3.1.3.1) with older males of the same genotype. Pregnant females were sacrificed by cervical dislocation 3 days after detection of a vaginal plug (E 3.5), uteri were dissected, and blastocysts were flushed out with Hank's Balanced Salt solution (HBSS, Gibco). Blastocysts were cultured singly in drops (approx. 5 µl) of KSOM medium (EmbryoMax, Millipore) under mineral oil (Sigma-Aldrich) until hatching. Medium was then changed twice to 2i medium plus Pen and Strep (see Table 3-3) to completely remove KSOM medium. The medium was changed every other day until prominent outgrowth of the inner cell mass was observed. Outgrowths were then washed 3 x in PBS and disaggregated by trypsinising and trituration though a finely drawn Pasteur pipette. Cell suspensions were then seeded in 100 µl 2i medium on gelatine-coated 96 well dishes (see Section 3.2.3). Cells were maintained using normal ES cell culturing conditions, until the third passage Pen and Strep medium was used.

"After successfully deriving cell lines much beer and chocolate were consumed" (Dr Nick Allen, personal communication).

The parental Axin ES cell lines were kindly generated by Prof. Nick Allen and Dr. Susie Hunter.

Table 3-2. ES cell lines.

CELL LINE		ALLELES				PHENOTYPE
Parental line	**Knockout**	**Axin1**	**Axin2**	**GSK-3α**	**GSK-3β**	
$A1^{fl/fl}$		fl/fl	wt	wt	wt	wt
	$A1^{\Delta/\Delta}$	Δ/Δ	wt	wt	wt	A1 loss
$A2^{fl/fl}$		wt	fl/fl	wt	wt	wt
	$A2^{\Delta/\Delta}$	wt	Δ/Δ	wt	wt	A2 loss
$A2^{lacZ/lacZ}$		wt	lacZ/lacZ	wt	wt	Ax2 loss
$A1^{fl/fl}$, $A2^{fl/fl}$		fl/fl	fl/fl	wt	wt	wt
	$A1^{\Delta/\Delta}$, $A2^{\Delta/\Delta}$	Δ/Δ	Δ/Δ	wt	wt	A1 and A2 loss
$A1^{fl/fl}$, $A2^{lacZ/lacZ}$		fl/fl	lacZ/lacZ	wt	wt	A2 loss
	$A1^{\Delta/\Delta}$, $A2^{lacZ/lacZ}$	Δ/Δ	lacZ/lacZ	wt	wt	A1 and A2 loss
$GSK3^{fl/fl}$		wt	wt	fl/fl	wt	wt
	$GSK3^{\Delta/\Delta}$	wt	wt	Δ/Δ	Neo/Neo	GSK3 loss

An allelic series of ES cell lines was used in this study. Lines carried combination of the following alleles: wild type *Axin1* or *Axin2* (wt), a β-Galactosidase insert (*lacZ*), conditional alleles with *loxP* sites finking exon 2 (fl) of *Axin1* (A1) or *Axin2* (A2). *LoxP*-flanked exons were deleted by transient transfection of Cre recombinase (Δ). A GSK3 double knout line $GSK3^{\Delta/\Delta}$ was also used (Doble et al. 2007).

Parental ES cell lines were transfected with Cre recombinase to generate Axin mutant ES cell lines, missing exon 2 (see Section 3.2.5).

3.2.2 ES culture conditions

All embryonic stem cell lines were maintained at 37 °C and 5 % CO_2 in a humidified incubator (Binder). For splitting, cells were aspirated, washed with warm PBS (Gibco) and incubated with a minimal amount of 0.05 % trypsin/EDTA (Gibco) for 5 min at 37 °C or until cells detached. The reaction was stopped by adding 5 to 10 trypsin volumes of ES base medium and cells were counted with a haemocytometer. An appropriate number of cells was

pelleted at 200 x g for 5 min and then plated at 30,000 cells/cm^2 in prewarmed medium on gelatine-coated tissue culture flasks unless otherwise stated. Cells were fed every one- to-two days and passed every two –to- three days, when they had reached about 70 % to 80 % confluency.

Cells were routinely maintained in 2i medium and changed to 1i medium when plating to perform an experiment unless otherwise stated. The passage number of each cell line was routinely recorded. Cells were used no longer than passage 30. Table 3-3 shows all the different ES media compositions used in this project.

Table 3-3. ES cell media composition.

MEDIUM	PURPOSE
ES base medium (EB medium)	
DMEM/F12 L-Glutamine (2 mM) β- Mercaptoethanol (10^{-4} M) Fetal Bovine Serum, ES qualified (FBS, 10 %)	Washing Generation of embryoid bodies
ES medium	
ES base medium LIF (10^6 U/l, ESGRO)	Experimental procedures
1i medium	
ES medium PD0325901 (0.5 µM, Stemgent) DMSO (0.1 µl/ml)	Experimental procedures
2i medium (1i + CHIR)	
ES medium PD0325901 (0.5 µM, Stemgent) CHIR99021 (3 µM, Stemgent)	Maintenance and ES cells and GSK3 inhibitor treatment during experiments
ES freezing medium	
ES base medium (50 %) Fetal Bovine Serum, ES qualified (FBS, 40 %) DMSO (10 %, Sigma-Aldrich)	Freezing
Conditioned medium	
ES cell conditioning medium (50 %, 3.2.8.1) 2i medium (50 %)	Maintenance at low cell number
Selection medium	
2i medium Puromycin (1 µg/ml, Sigma-Aldrich)	Selection of Antibiotic resistant cells

Table 3-3. (Continued) ES cell media composition.

MEDIUM	PURPOSE
Pen Strep medium	
2i medium Penicillin (50 U/ml) Streptomycin (50 µg/ml)	New ES cell lines up to passage 3
+ Wnt3a medium	
1i medium Wnt conditioning medium (10%, see 3.2.8.3)	Treatment with Wnt3A during experiments
- Wnt medium	
1i medium L-cell conditioning medium (10%, see 3.2.8.3)	No Wnt3a treatment during experiments

All components were purchased from Gibco, Invitrogen unless otherwise stated and were used prewarmed.

3.2.3 Gelatine coating of ES culture flasks and plates

For gelatine coating; tissue culture plates or flasks (Nunc, Thermo-Fisher) were covered in 0.1 % gelatine (ESGRO), for a minimum of 20 min in the incubator. Gelatine was aspirated immediately before cells were added.

3.2.4 Freezing cells and thawing of ES cell lines

For long-term storage, ES cell lines were frozen and stored in liquid nitrogen until further use. To this end, cells were harvested, as for passaging (see Section 3.2.2), resuspended at 1 - 2 x 10^6 cells in 0.5 ml ES freezing medium in cryo vials (Nunc, Thermo-Fisher) and placed in a freezing container (Nalgene) in a -80 °C freezer. The freezing container provided a 1 °C/min cooling rate and thus allowed slow and gentle freezing of cells overnight. Cell vials were then transferred to liquid nitrogen for long-term storage.

If frozen cells were needed, vials were quickly thawed in the water bath at 37 °C. Cells were then washed with pre-warmed ES base medium and pelleted at 200 x g for 5 min. 1 x 10^6 cells were then plated on gelatine coated T25 flasks (Nunc, Thermo-Fisher) and maintained as usual.

3.2.5 Transfection of ES cells (Lipofection)

The parental ES cell lines $A1^{fl/fl}$; $A2^{fl/fl}$; $A1^{fl/fl}$, $A2^{fl/fl}$; and $A1^{fl/fl}$, $A2^{lacZ/lacZ}$ contained exons that are flanked by *loxP* sites. Using Lipofection, ES cell lines were transfected with Cre recombinase expressing construct. For Lipofection, ES cell lines were plated at 30,000 cells/cm^2 on gelatine coated 6-well tissue culture plates (Nunc) in 2 ml 2i medium. The next day cells were fed with fresh medium 4 h prior to transfection. The lipofection was performed using Lipofectamin2000 (Invitrogen). To this end, 25 µl/ml lipofectamine and 3 µg/well of pCAGGS-Cre-IRESpuro plasmid DNA were diluted separately in OPTIMEM (Gibco). Both dilutions were incubated for 5 min before they were mixed together, incubated for a further 20 min, and added onto the cells. 4 h later the transfection mix was replaced by fresh 2i medium. The following day cells were split at least 1: 5 x in selection medium (2i medium supplemented with 1 µg/ml Puromycin, Sigma-Aldrich). After two days of selection cells were maintained in antibiotic free 2i medium until colonies had formed (9 to 15 days). Colonies were then picked and analysed by PCR (see Section 3.2.6 and 3.6.5).

3.2.6 Picking of ES cell colonies

Single colonies were picked into 96 well plates, 9 to 15 days after lipofection. Cells were washed twice with PBS and then covered with PBS. Using a P20 pipet, set to 10 µl, single colonies were picked into v-bottomed-96 well plates containing 10 µl PBS per well. Cells were incubated for 10 min at 37 °C after an addition of 30 µl trypsin per well. Then 100 µl conditioned medium were added to stop the reaction and cells were transferred to gelatine coated flat-bottomed-96-well plates. After 3 to 4 days cells were replica plated into two fresh 96 well plates. Cells of one plate where frozen down in freezing medium, the other plate was used to obtain DNA for genotyping PCR (see Section 3.6.5). Desired ES cell clones were then thawed and expanded as usual.

3.2.7 Generation of embryoid bodies and cardiomyocyte assay

To differentiate ES cells *in vitro*, aggregates of ES cells were incubated without LIF in „hanging drop" culture to generate embryoid bodies (EBs) (Doetschman et al. 1985; Keller 1995).

Single ES cells were re-suspended at 0.3 x 10^5 cells/ml in EB medium. 27 µl drops of cell suspension, containing 1350 cells each, were then pipetted on the lid of a 10 cm^2 bacterial dishes and carefully turned upside down. The bottom of the dish was filled with PBS to prevent the drops from drying out. Cells were incubated for 3 days in the drops before they were carefully re-suspended in EB medium and transferred to a fresh 10 cm^2 bacterial dishes. Medium was change every other day. All media changes were performed after allowing the organoid to settle to the bottom of a 15 ml tube by gravity.

After 8 days, EBs showing spontaneously contracting cells were counted to score the development of cardiomyocytes. On day 14, embryoid bodies were labelled with BrdU (see Section 3.4.5), harvested, and processed for mRNA extraction (see Section 3.6.7.2) or prepared for paraffin embedding, sectioning, and staining. EBs dedicated for staining were washed 2 x in PBS and then fixed for 30 min in 4 % PFA (Sigma-Aldrich) at room temperature or with 100 % ice cold Methanol (Sigma-Aldrich) for 20 min depending on the antibodies to be used (see Table 3-9 for details) and processed according to Section 3.5.1.

3.2.8 Production of conditioning media

3.2.8.1 ES cell conditioning medium

Wild type ES cell lines were grown to 50 – 70 % confluency in 2i medium. Cells were then carefully washed 2 x with DMEM/F12 and covered with fresh 2i medium. Medium was left on the cell for several hours (up to 12 h) while the pH was monitored. Medium was then collected, spun at 300 x g for 5 min to remove debris and filtered through a 0.22 µl low-protein-binding filter. Conditioning medium was stored at 4 °C for up to 2 weeks.

3.2.8.2 R-Spondin conditioning medium

R-Spondin conditioning medium was produced in the 293T-HA-RSpo1-Fc cell line that was a kind gift from Calvin Kuo (Ootani et al. 2009).

293T-HA-RSpo1-Fc cells were thawed using the normal protocol (see Section 3.2.4) and plated on a T75 tissue culture flask in growth medium (see Table 3-4 for medium composition). They were split every three-to-four days at a ratio between 1:5 and 1:10 and maintained in growth medium supplemented with Zeocin (300 μg/ml, Invitrogen).

To generate conditioning medium, cells were split once in growth medium without Zeocin. At the next split cells were seeded at 8,500 cells/cm^2 in a triple flask in R-Spondin production medium. The supernatant was removed after 4 days and replaced with fresh R-Spondin production medium, which was left a further 3 days before removal. Both supernatants harvested at day 4 and day 7 were pooled, spun at 300 x g for 5 min to remove any remaining cells, and filtered through a 0.22 μl low-protein-binding filter (Millipore). The activity of the R-Spondin conditioning medium was tested as described in Section 3.2.8.4 and stored at 4 °C until needed.

Simultaneously, medium from HEK293T cells without an *R-Spondin1* expression construct was harvested to provide no R-Spondin control medium.

Table 3-4. Media to generate of R-Spondin and Wnt conditioning medium.

MEDIUM		PURPOSE
Growth medium		
	DMEM, GlutaMAX FBS (10 %) Penicillin (50 U/ml) Streptomycin (50 μg/ml)	Maintenance of 293T-HA-RSpo1-Fc cells, T-Rex ΔN-β-Catenin and Wnt3A cells as well as production of Wnt3a conditioning medium
R-Spondin production medium		
	Advanced DMEM/F12 GlutaMAX (2 mM) HEPES (10 mM) Penicillin (50 U/ml) Streptomycin (50 μg/ml)	R-Spondin production

3.2.8.3 Wnt conditioning medium

Wnt3a conditioning medium was produced in LWnt3A cells (Shibamoto et al. 1998). These cells express non-tagged Wnt3a from a PGK promoter. Cells were grown and maintained in growth medium (see Table 3-4 for composition) supplemented with 50 µg/ml Geneticin (G418, Invitrogen)

One split before Wnt3a conditioning medium production G418 was removed from the medium. Cells were seeded at 8,500 cells/cm^2 on a triple flask and Wnt3a conditioning medium was harvested on day 4 and 7. Then medium from both harvests was filtered through a 0.22µl low-protein-binding filter. The activity of the Wnt conditioning medium was tested as described in Section 3.2.8.4 and stored at 4 °C until needed. Medium from wild type L-cells was harvested in parallel to generate no-Wnt control medium.

3.2.8.4 Activity test of Wnt and R-Spondin medium

The activity of Wnt or R-Spondin conditioning medium was determined in a TCF reporter assay. This assay relied on luciferase activity in response to TCF dependent transcription in a T-Rex ΔN-β-Catenin line (Ewan et al. 2010). This cell line contains a stabile integrated TCF-luciferase reporter as well as a Doxycycline inducible constitutively active form of β-Catenin (Tet-O-ΔN-β-Catenin).

T-Rex ΔN-β-Catenin cells were thawed and grown in growth medium (see Table 3-4 for composition) supplemented with Hygromycin B (300 µl/ml, Gibco) and Blasticidin (12 µg/ml, Gibco) for four days. The cells were then split into black, clear bottom 96-well plates (Corning) at 20,000 cells per well in 100 µl growth medium (without Hygromycin B and Blasticidin). After two days a dilution series of Wnt or R-Spondin conditioning medium (0 %, 5 %, 10 %, 20 % and 50 %) to be tested were prepared on a deep well 96-well plate. Conditioned medium from wild type cells was used to adjust the overall conditioning medium content of each treatment. If R-Spondin activity was to be determined, each well of the dilution series of R-Spondin was supplemented with 5 % Wnt3A condoning medium. If

Wnt3a conditioning medium was tested, a background concentration of 5 % R-Spondin conditioning medium was used. A dilution series of either commercial Wnt3a (R&D) or R-Spondin (Peprotech) was run alongside to compare the activity. Additionally, cells were induced to express ΔN-β-Catenin using 25 ng/ml Doxycycline (Sigma-Aldrich) as a positive control. All but 20 µl of the medium on the cells was replaced with 80 µl of the samples. Each condition was tested in triplicate. After one day of treatment a Wst1 viability assay (see 3.4.1.4) and a luciferase assay (see 3.4.2) was performed.

3.3 3D liver culture

The method outlined for liver organoid cultures was adapted from the method published by Dr Meritxell Huch (Huch et al. 2013). All media used for culturing in the following protocols are shown in Table 3-5. Organoids were routinely grown in a humidified incubator (SLS, Galaxy S) at 37 °C and 5 % CO_2.

Table 3-5. Liver organoid media and compositions.

MEDIUM	PURPOSE
2 x liver base medium	
Advanced DMEM/F12 GlutaMAX (2 mM) HEPES (10 mM) N2 (1 x) B27 supplement (1 x) N- Acetylcysteine (1.25 µM, Sigma-Aldrich)	2 x base medium to be supplemented with growth factors and diluted with advanced DMEM/F12
Expansion Medium (EM)	
2 x liver base medium (½ of final volume) EGF (50 ng/ml, Sigma-Aldrich) FGF10 (100 ng/ml, Peprotech) HGF (50 ng/ml, Peprotech) Gastrin (10 nM, Sigma-Aldrich) Nicotinamide (10 mM, Sigma-Aldrich) R-Spondin conditioning medium (5 – 10 %, see 3.2.8.2) Advanced DMEM/F12 (add up to 1 volume)	Maintenance of liver organoids (ductal cells)

Table 3-5. (Continued) Liver organoid media and compositions.

MEDIUM	PURPOSE
Differentiation medium (DM)	
2 x liver base medium (½ of final volume) EGF (50 ng/ml, Sigma-Aldrich) FGF10 (100 ng/ml, Peprotech) A8301 (50 nM, Tocris Biosciences) DAPT (10 nM, Sigma-Aldrich) Advanced DMEM/F12 (add up to 1 volume)	Differentiation of ductal cells along the hepatic lineage
Expansion medium for fresh isolations	
Expansion medium Noggin (100 ng/ml, Peprotech) Wnt3a conditioning medium (50 %, see 3.2.8.3)	Freshly isolated or thawed organoids until day 2 in culture
Fragile cell medium	
Medium for fresh isolations Y-27632 (10 µM, Sigma-Aldrich)	FACS sorting Viral transduction
Extraction medium	
DMEM, high glucose FBS (10 %) Penicillin (50 U/ml) Streptomycin (50 µg/ml)	Medium for washing during duct isolation
Digestion medium	
DMEM, high Glucose FBS, 1 % Collagenase type XI (0.0125 %, Sigma-Aldrich) Dispase (0.0125 %) DNase I (1 ng/ml, Promega)	Liver digestion for duct isolation
Organoids freezing medium	
2 x liver base medium (25 %) Advanced DMEM/F12 (25 %) FBS (40 %) DMSO (10 %)	Freezing of liver fragments or ductal cells

All media and supplements were purchased from Gibco, Invitrogen unless stated differently. Concentrations stated are final concentration in 1 x medium.

3.3.1 Primary cell isolation

Mice of the appropriate genotype were culled by cervical dislocation and livers was extracted and placed whole in cold extraction media on ice (see Section 3.1.4.2). Usually, at least three livers of the same genotype and the appropriate controls were treated at the same time. However, each liver was processed separately. Livers were transferred to a primary tissue culture hood and treated under sterile conditions from this point awards. Livers were removed to a 10 cm petri dish in 5 ml extraction medium and carefully cut into 4 pieces. During this process, care was taken, that gallbladder, extrahepatic bile ducts, diaphragms, etc. were completely removed and discarded.

Liver tissue was then placed on a tissue chopper (McIlwain) and cut into approximately 1 mm^3 pieces. These liver pieces were then transferred into a 50 ml tube containing fresh extraction medium and carefully washed by pipetting up and down three times with a 10 ml stripette while avoiding touching the tissue.

At this point tissue was either frozen in freezing medium for future extraction (see Section 3.3.3) or processed straight away. To this end, Liver pieces were immersed in 20 ml digestion medium and incubated at 37°C in a water bath. Tissue was swirled every 5 min. Every 30 min digestion solution was replaced and checked for bile ducts over the course of 4 to 5 h. To this end, tissue was vigorously pipetted up and down 5 x using a 10 ml stripette, then left to settle. The supernatant was removed to a 10 cm petri dish and examined under a tissue culture microscope. Supernatant containing mainly hepatocytes was discarded (usually during the 1^{st} h of incubation). If big cell clumps were present, they were pelleted at 100 x g for 5 min and added back to the digesting liver tissue to free enclosed bile ducts. Free bile ducts were picked out of the supernatant with a P 100 set to 50 µl into fresh extraction medium. Supernatant mainly containing clean bile ducts was collected as a whole, pelleted at 100 x g for 5 min, resuspended in 10 ml extraction buffer, and kept on ice until the tissue was completely digested and all the bile ducts harvested. Pooled bile ducts were then washed in extraction medium followed by one wash in 10 ml advanced DMEM/F12 and pelleted at 100

x g for 5 min. Clean bile ducts were mixed with the appropriate amount of ice-cold, liquid Matrigel (Corning) and seeded in six 50 µl Matrigel domes per well in prewarmed 6 well tissue culture plates. Each dome contained approximately 50 to 100 bile ducts. Once the Matrigel had completely polymerised, 2 ml expansion medium for fresh isolations was added to each well. Medium was changed on day 2 to expansion medium (EM) and organoids were passaged and maintained according to Section 3.3.2.

3.3.2 Passage and expansion of liver organoids

Organoids were routinely grown in Matrigel (Corning) and expansion medium EM (see Table 3-5 for medium composition), fed every 2 to 3 days and passaged once a week. For passage, medium was removed from the well and Matrigel was carefully washed with cold PBS. Prewarmed TrypLE (Gibco) was then added to each well and incubated at 37 °C for 2 min in the incubator. Organoids and TrypLE were then removed to a 15 ml tube and incubated for a further 5 to 10 min at 37 °C in the water bath. When the organoids were digested to single cells, they were washed twice with 5 ml of advanced DMEM/F12 and pelleted at 200 x g for 5 min. Cells were then re-suspended in the appropriate amount of Matrigel and seeded as a dome on pre-warmed tissue culture plates. If 384 well plates were used, cells were plated on cold plates and the Matrigel was allowed to cover the whole well. Table 3-6 shows the amount of Matrigel and medium used for different plate types.

Table 3-6. Volume of Matrigel and medium used in different plates.

PLATE	MATRIGEL	MEDIUM
6-well plate	6 x 50 µl	2 ml
24-well plate	50 µl	500 µl
U-bottom 96 well plate	15 µl	70 µl
Flat bottom 96 well plate	10 µl	50 µl
384 well plate	8 µl	30 µl

3.3.3 Freezing and thawing of liver pieces or organoids

For long-term storage liver organoids or pieces of liver directly after the dissection of a mouse, were frozen and stored in liquid nitrogen until further use.

Organoids were harvested as for passaging (see Section 3.3.2), and re-suspended in 0.5 ml per 50 µl Matrigel in organoid freezing medium in cry vials (Nunc, Thermo-Fisher) and placed in a freezing container (Nalgene) in a -80 °C freezer. The freezing container provided a 1 °C/min cooling rate and thus allowed slow and gentle freezing of cells overnight. Cell vials were then transferred to liquid nitrogen for long-term storage.

If frozen cells were needed, vials were quickly thawed in the water bath at 37 °C. Organoids were washed with pre-warmed advanced DMEM/F12 and pellet at 200 x g for 5 min. Cells were then re-suspended in Matrigel and plated at the appropriate density in organoid medium for fresh isolation.

Liver pieces were washed ones in advanced DMEM/F12 and then frozen in organoid medium as described above. Pieces from one mouse liver were divided into 4 vials containing freezing medium. Liver pieces were thawed as described for the organoids and processed as for fresh isolation.

3.3.4 Differentiation of liver organoids

If liver organoids needed to be differentiated into hepatocytes, organoids were passaged as described above and left in EM for 2 days. Then the medium was changed to differentiation medium (DM, see Table 3-5 for composition), cells were fed every three to 4 days and analysed on day 10 to 16 as indicated in the results chapter. Usually half of the wells were kept in EM while the other half was put into DM. Figure 5-3 A shows a scheme of a the differentiation protocol.

3.3.5 Adeno- and lentiviral transduction of liver organoids

Liver organoids were transduced with adenovirus (Ad5-GFP, a kind gift of A. Parker) or lentivirus (Lenti-GFP, a kind gift from R. Clarkson, or Lenti-CMV-ER^{T2}CreER^{T2}, NBS Biologicals Ltd.). The viral transduction protocol was adapted from Koo et al. (2011) and Onuma et al. (2013). Briefly, two days before the transduction organoids were plated in 50 µl of Matrigel on a 24 well plate in expansion medium for fresh isolation (EM supplemented with Wnt and Noggin). On the day of transduction, Matrigel was removed as for passaging. To assure the digestion into single cell organoids were pipetted up and down with a pulled gals Pasteur pipette during the TrypLE digestion. Cells were then washed in liver base medium and re-suspended in 10 µl medium for fragile cells (EM supplemented with Wnt, Noggin, and Y27632). The virus (MOI 10 or 50) was diluted in 1 x organoid base medium supplemented with Y27632 and polybrene (8 µg/ml, Sigma). 10 µl of cells suspension were mixed carefully with 250 µl of viral suspension and plated on top of a layer of Matrigel in a 48 well plates. Cells were incubate over night at 37 °C 5 % CO_2. Cells were then collected in a 1.5 ml tube and span at 250 x g for 5 min in a microcentrifuge. The infection medium was discarded; cells were re-suspended with 120 µl of Matrigel and plated in 50 µl domes on a 24 well plate in medium for fragile cells. The medium was changed every other day. When the sphere regrew, they were split and cultured as usual. Normal budding organoids appeared after 1 weeks. Organoids transduced with Lenti-CMV-ER^{T2}CreER^{T2} were selected in 1 µg/ml Puromycin (Sigma-Aldrich) for 2 days following transduction.

3.3.6 Induction of Cre expression in organoid culture

The Cre recombinases used in this study were either induced by β-Naphthoflavone (β-NF, for Ah-Cre), Tamoxifen (Tam), or its active metabolite 4-Hydroxytamoxifen (4-OHT, for TTR-CreER^{T} and Lenti-CMV-ER^{T2}CreER^{T2}). For the use in tissue culture, Tam and β-NF (both Sigma-Aldrich) were made up in DMSO to generate a stock concentration of 4 mM each. 4-

OHT (Sigma-Aldrich) was diluted in EtOH generate a 10 mM stock. Unless otherwise stated, experiments were performed using a final concentration of 1 µM 4-OHT.

The induction of Cre recombinase was usually done simultaneously with the start of the differentiation procedure. Figure 5-3 A shows the protocol used to induce and differentiate liver organoids cultures carrying the Ah-Cre transgene.

3.4 Cell and culture analysis

3.4.1 Viability assays and growth analysis

3.4.1.1 CellTiterGlo® cell viability assay

A CellTiterGlo® (Promega) luminescent cell viability assay, for ES cells, was performed as an endpoint assay to determine the number of viable cells in a sample. The assays relied on ATP as an indicator for metabolically active cells.

Cells grown in 2D were lysed at the required time points by the addition of a volume of CellTiterGlo® Reagent equal to the cell culture medium already present in each well. Lysis was performed at room temperature for 15 min on an orbital shaker prior to assaying luminesces using a FluoStar optima plate reader (BMG Labtech).

The CellTiterGlo viability assay was used to generate growth curves of embryonic stem cell lines. To this end, cells of each line were seeded ay 10,000 cell/cm^2 on gelatine coated, black, clear-bottom 96 well plates (Thermo Fisher) in 100 µl medium. Every day 50 µl of ES cell medium was replaced. Cell viability of 3 cell lines for each genotype was measured in triplicate every day over the course of 6 days.

3.4.1.2 Simultaneous viability and toxicity assay

We simultaneously performed a Real Time-Glo™ MT and CellTox™ Green assay (both Promega) on continuously growing ES cell cultures to assesse the proportion of dead and live

cells in each culture. The viability assay depended on the reduction of a NanoLuc substrate in metabolically active cells. The cytotoxicity assay is based on the change in membrane integrity as the result of cell death.

ES cell lines were seeded at 20.000 cells/ cm^2 on gelatine coated, black, clear-bottom 96 well plates (Thermo Fisher) in 100 µl medium containing the CellTox™ Green and a Real Time-Glo™ MT reagents according to manufacturer's instructions. After two days, fluorescence levels (indicating dead cells) and luciferase activity (indicating metabolically active cells) were measured in each well using a FluoStar optima plate reader (BMG Labtech).

3.4.1.3 PrestoBlue assay

A PrestoBlue viability assay was performed on continuously growing organoids. 10 % PrestoBlue (Invitrogen) were added to each well and incubated for 4 to 6 h in the incubator. Then 50 µl supernatant were removed and the fluorescence at 560 nm measured using a FluoStar optima plate reader (BMG Labtech).

3.4.1.4 Wst1 assay

A Wst1 viability assay was performed as an endpoint assay. 10 % Wst1 (Roche) was added to each well and incubated for 1 h in the incubator. Then 50 µl supernatant were removed and transferred onto a clear 96-well plate. A culture reader was then used to measure the absorbance at 450 nm and at 590 nm (background). Depending on the volume in each well, three aliquots of supernatant were removed and measured.

3.4.1.5 Organoid growth analysis

To identify changes in growth and morphology liver organoids were imaged and analysed for changes in various parameters. Liver organoids were passaged, plated, and then imaged every 2 days on a GelCount™ (Oxford Optronix) and software for 16 days. CHARM settings, a script of defined parameters, were established, with threshold values for specific parameters

such as optical density, size, circularity and quality of edge of objects detected within the well. The CHARM settings were optimized to accurately pick up the outlines of different sized organoids. Figure A-2 in the Appendix shows an example of liver organoids being analysed using GelCount Full information on the CHARM settings used is shown in Appendix Table A-1.

3.4.2 Bright glow luciferase assay

Luciferase assay was performed using the Bright glow products from Promega. Before the assay, all the necessary reagents were thawed and equilibrated to room temperature in a water bath at room temperature. The assay plate was carefully tipped out to remove culture medium and then washed with prewarmed PBS and tipped out again. Each well was the filled with 50 µl PBS and 50 µl Bright glow. Following 5 min incubation in the dark, while rigorously shaking luminescence was measured using a FluoStar optima plate reader (BMG Labtech).

3.4.3 TCF reporter assay in ES cells

To assess TCF dependent transcription in Axin mutant ES cell lines, cells were seeded at 25,000 cells/cm^2 in 2i medium on a 96-well plate. The next day, cells were transfected using FuGENE 6 (Promega) according to manufacturer's instruction. Cells were transfected with 100 ng/well Super8xTOP-flash TCF reporter construct, which expresses firefly luciferase under the control of a minimal TA viral promoter and 7 TCF/LEF binding sites (Veeman et al. 2003). As a background control, cells were transfected with a Super8xFop-flash construct containing 6 mutant TCF/LEF binding sites (Veeman et al. 2003). All wells were additionally transfected with 10 ng/well pRL- TK Renilla luciferase vector (Promega) as a transfection control. 4 h past transfection, transfection medium was replaced and cells were treated with 1i medium, with or without Wnt3a conditioning medium for 24 h. The next day, renilla, and firefly luciferase activity was assayed using the Dual-Luciferase Assay System (Promega) according to manufacturer's instruction.

3.4.4 Alkaline phosphatase detection

Undifferentiated ES cells can be characterised by high levels of alkaline phosphatase. In this study, alkaline phosphatase expression was measured qualitatively and quantitatively. Methods to perform both of these assays are described in the following sections.

3.4.4.1 Alkaline phosphatase staining

ES cells seeded at 10,000 cells/cm^2 were grown for 5 days before they were washed twice with PBS. Then cells were fixed in 4 % PFA in PBS for 5 min and rinsed twice with PBT (PBS containing 0.5 % Triton X-100). To stain the cells they were covered with staining solution (One Fast Red TR/Naphthol AS-MX tablet, 1 Tris buffer tablet, dissolved in 6 ml ddH_2O, Sigma-Aldrich) and incubated in the dark for 20 min. Rinsing twice with PBT stopped the reaction. Alkaline phosphatase positive, undifferentiated cells were stained red while differentiated cells remained unstained. The amount of stained to unstained colonies was analysed.

3.4.4.2 Quantification of alkaline phosphatase

ES cells were grown in triplicate on 96 well plates at 30,000 cells/cm^2. On day 3 cell viability was analysed using PrestoBlue assay (see Section 3.4.1.3). Then cells were washed 2 x in ice cold PBS and lysed using 50 µl ice-cold lysis buffer (20 mM TBS pH 7.4 (Fisher Scientific), 1% Triton X-100 (Sigma-Aldrich)). Cells were removed to a microcentrifuge tube and incubated for 30 min while shaking at 4 °C. Lysates were then spun at 15,000 x g at 4 °C for 30 min and the alkaline phosphatase activity of the supernatant was measured using the alkaline phosphatase Diethanolamine Activity Kit (Sigma-Aldrich). 50 µl of samples were mixed with an equal volume of alkaline phosphatase reaction buffer including the substrate (pNPP, p-nitrophenyl phosphate, at 13.4 mM final) in a clear 96 well plate. After 10 min incubation, the reaction was stopped by adding 0.5 N NaOH and the absorbance at A_{405nm} was measured using a FluoStar optima plate reader (BMG Labtech).

3.4.5 Labelling of proliferating cells

Cultured cells were incubated with 10 µM BrdU (Sigma-Aldrich) for 1 h prior to cell harvest to label cells in S phase. Subsequently, cells were fixed in 4% PFA and embedded in paraffin to perform immunohistochemistry (see Section 3.5.1). Alternatively, cells in S-phase were incubated with 10 µM EdU (5-ethynyl-2'-deoxyuridine, Invitrogen) for 1 h to perform subsequent immune fluorescent staining (see Section 3.5.9) or FACS (Fluorescence activated cell sorting, see below)

3.4.6 CARS microscopy

Coherent anti-Stokes Raman scattering (CARS) microscopy is a label-free imaging technique that allows the examination of living biological samples in real time with a high three-dimensional spatial resolution and chemical specificity (Evans and Xie 2008; Pope et al. 2013). CARS is a third-order nonlinear process (four wave mixing) where the interference between two optical fields (pump and Stokes) drives molecular bonds to coherently vibrate. A third field is then used to generate a strong anti-Stokes Raman scattering signal as the result of the coherent vibrations. The difference between the pump and Stokes fields used to drive coherent vibrations can be tuned to match specific molecular bonds.

CARS microscopy is especially useful to image concentrated unstained lipids found in the plasma membrane or in lipid droplets. The large number of C-H bonds in the lipid acyl chain have a characteristic CARS resonance peak at 2850 cm^{-1}.

Liver organoids both in expansion and differentiation conditions were imaged live using a home-built set-up based on a single Ti:Sapphire 5 fs broadband (660-970 nm) laser system as described in detail in (Pope et al. 2013). Hyperspectral images were acquired over the spectral range 2600 to 3300 cm^{-1}, with 5 cm^{-1} steps. Z-stacks were taken at the lipid peak (2850cm^{-1}), in 0.5 µm steps. In both cases the laser powers at the sample were 60%. CARS images were taken with the help of Iestyn Pope and analysed by Arnica Kuruna and Francesco Masia (all members of the Borri and Langbein labs).

3.4.7 OcellO 3D culture morphometric assay

Organoids were analysed in a high throughput and multi-dimensional screening platform and underwent principle component analysis in collaboration with Leo Prize and his company OcellO. To this end, organoids were plated at 20 000 cells/ml in a volume of 14.5 µl Matrigel per well on a 384-well plates in 15 µl EM on day 0. On day 2 organoids were either kept in EM or changed to DM. At the same time β-NF was added to induce the expression of Ah-Cre, or DMSO as a control. In the 384-well format fresh medium was usually added to the medium already in the well every 2nd day. Medium was removed from the plate by tipping the plate out on day 2 and day 12. Each condition was plated in 12 replicates.

On day 16 organoids were fixed in 1x OcellO fix and stain, sealed with an adhesive seal, wrapped in aluminium foil, and incubated over night at room temperature while gently shaking. The next day, wells were filled up completely with PBS, resealed, and shipped to OcellO. At OcellO fixed organoids were washed and prepared for imaging. The 384-well plate was imaged using a 4x lens, covering the whole well, as a z-stack in 15 µm steps. 30 images were taken per well. Organoids were analysed by Bram Herpers using OcellO's proprietary software that exports dimensions, counts and relative measurements for: number of organoids, organoid size, wall thickness, organoid shape, number of lumens, lumen size, lumen shape, lumen filling, cell number, cell shape, number of nuclei, nucleus shape, cell/nucleus alignment, apical/basal nucleus position, and cells per organoid.

3.5 Staining methods

3.5.1 Paraffin embedding of fixed samples

Fixed tissues, EBs, and organoids were embedded in paraffin and sectioned to perform immunohistochemical staining on slides. For easier handling of organoids, the Matrigel was

removed directly following fixation by washing 3 x in ice cold PBS. They were then embedded in 1 % low melting Agarose (Sigma-Aldrich), as were EBs.

Fixed tissues, EBs, and organoids were processed using an automatic processor (Leica TP1050) in a cassette (Fisher). Samples were dehydrated in an increasing concentration of EtOH (70 %, 1 h; 95 %, 1 h; 100 %, 2 x 1 h 30 min; 100 %, 2 h) and then transferred to xylene and incubated twice for 2 h. Afterwards samples were washed in liquid paraffin for 1 h followed by 2 x 2 h and then embedded in paraffin wax for sectioning.

3.5.2 Sectioning of fixed samples

Samples embedded in a paraffin block were cut into 5 µm sections using a microtome (Leica RM2135). Sections were then mounted onto slides coated with poly-L-lysin and baked at 58 °C for 24 h. Paraffin embedding and sectioning was kindly performed by Derek Scarborough and Mark Isaac.

3.5.3 Dewaxing and rehydration of tissue sections

Tissue sections were dewaxed by three 5 min washes in xylene (Fisher Scientific) followed by a rehydration series in decreasing concentrations of EtOH (100 %, 2 x 5 min; 95 %, 2 x 5 min; 70 %, 5 min). Slides were then transferred into dH_2O for 1 min. For tissue that had been stained by β-Galactosidase staining (see Section 3.5.7) prior to embedding, Histo-Clear (National Diagnostics) was used instead of xylene to maintain the blue staining.

Following dewaxing and rehydration, samples were either stained with H&E (see Section 3.5.4) or used for immunohistochemical analysis (IHC, see Section 3.5.5).

3.5.4 Haematoxylin and Eosin (H&E) staining of tissue sections

H&E staining allows the visualisation of nuclei (Haematoxylin, blue) and proteins (Eosin, red). Sections were dewaxed and rehydrated as described in 3.5.3. Afterwards, they were immersed in Mayer's Haemalum (R.A. Lamb) for 5 min. Then slides were washed carefully

under running tap water and then submerged in 1% aqueous Eosin (R.A. Lamb) for 5 min, before they were dehydrated and mounted as described in Section 3.5.

3.5.5 Immunohistochemistry (IHC)

IHC was performed to visualise the presence and locations of specific antigens in paraffin embedded tissue sections. All samples were first dewaxed and rehydrated following the method described in 3.5.3. The following Section describes a generic protocol for IHC, which was followed throughout the project. Special conditions and modifications for certain antibodies are shown in Table 3-7. For example, mouse secondary antibodies, the M.O.M. kit (Vector labs) was used, while for rabbit secondary antibodies the Vectastain ABC kit (Vector labs) was utilised. In general, PBS was used, but for certain antibodies PBS was replaced by washing buffer (1 x TBS (Fisher Scientific), 0.1 % (v/v) Tween-20 (Sigma-Aldrich))

I Antigen retrieval and unmasking

Cross-linking bonds formed during fixations were broken to unmask the antigens. To this end, slides were boiled in preheated citrate buffer (Dako, 1:10 in dH_2O) for 20 min, followed by a 5 min wash in hot PBS. Slides were then transferred to PBS at room temperature for a further 5 min.

Table 3-7. Conditions and antibodies used for IHC.

PRIMARY AB	MANUFACTURER	STAINING KIT USED	WASHING BUFFER	CONCENTRATION	SECONDARY ANTIBIOTIC	OTHER COMMENTS
Anti-β-Catenin (total)	BD Transduction labs, #610154	M.O.M kit	TBS/T	1/300	Biotinylated anti-mouse (Vector Labs)	
Anti-BrdU	Sigma-Aldrich, #BBU-33	M.O.M kit	PBS	1/1000	Biotinylated anti-mouse (Vector Labs)	Denaturation of DNA in 2 N HCl at 37°C for 30 min after peroxidase treatment needed
Anti-Ki67	Millipore, #ab9260	Vectastain ABC kit	TBS/T	1/500	Biotinylated anti-rabbit (Vector Labs	
Anti-AFP	R&D, #MAB1368	M.O.M kit	PBS	1/150	Biotinylated anti-mouse (Vector Labs)	
Anti-p53	Santa Cruz, #Sc-6243	Vectastain ABC kit	TBS/T	1/50	Biotinylated anti-rabbit (Vector Labs)	
Anti-Cyclin B1	Cell signaling technology, #4135S	M.O.M kit	TBS/T	1/500	Biotinylated anti-mouse (Vector Labs)	
Anti-Oct 4	Abcam, #ab19857	Vectastain ABC kit	TBS/T	1/250	Biotinylated anti-rabbit (Vector Labs)	
Anti-SMA	Abcam, #ab5694	Vectastain ABC kit	TBS/T	1/200	Biotinylated anti-rabbit (Vector Labs)	
Anti-βIII-tubulin	Sigma, T4026	M.O.M kit	TBS/T	1/150	Biotinylated anti-mouse (Vector Labs)	

II Blocking of endogenous peroxidases

Endogenous peroxidases were blocked by incubation of sections for 5 to 30 min (depending on antibody used, see Table 3-7) in 0.75 % H_2O_2 (diluted from a 30% solution, Sigma-Aldrich) in PBS, followed by a brief rinse with dH_2O and two 5 min washes in PBS.

III Blocking of non-specific antibody binding

Non-specific binding of antibody was prevented by blocking with serum. The serum used for blocking depended on the species in which the secondary antibody was raised. For rabbit antibodies normal goat serum was used (Vectastain ABC kit, Vector labs), for mouse antibodies Mouse Ig Blocking Reagent (M.O.M kit, Vector labs) was used. To this end, either 1 drop of goat serum was mixed with 3.3 ml PBS or 2 drops of Mouse Ig Blocking Reagent was added to 2.5 ml PBS.

Slides were carefully dried and the area containing the sample was circled with a hydrophobic pen (Fisher Scientific) and covered with 150 to 300 µl blocking solution. Slides were kept in a humidified chamber during 1 h incubation.

IV Primary Antibody Treatment

Primary antibodies were diluted to the appropriate working concentration in either PBS, 1% bovine serum albumin (BSA, Sigma-Aldrich) for use with rabbit secondary antibodies, or M.O.M dilution (80 µl/ml M.O.M in PBS) for mouse secondary. Primary antibody treatment was done with 100 to 200 µl drops of antibody solution on the slide in a humidified chamber, overnight at 4 °C, while gently shaking. The next day, slides were washed three times for 5 min in PBS.

V Secondary Antibody Treatment

Biotinylated secondary antibody was diluted in 2.5 ml M.O.M. dilution (mouse antibodies) or in PBS, 1 % BSA (all other antibodies) and incubated for 30 min (mouse) or 1 h (other).

VI HRP Conjugation to secondary antibodies

Horseradish peroxidase (HRP) was linked to the biotin of the secondary antibody to amplify the signal. To this end Avidin-Biotin Complex (ABC) was prepared by adding solution A and solution B (Vectastain ABC kit or M.O.M kit, Vector labs) to PBS according to manufacturer instructions 30 min before use. ABC solution was then applied to the slides and incubated for 15 (ABC kit) to 30 min (M.O.M. kit) in the dark, followed by three 5 min washes in PBS.

VII Visualisation of antibody binding and counterstaining

The HRP substrate diaminobenzine (DAB) was used to visualize antibody binding. To this end, DAB (Sigma-Aldrich) was prepared following manufacturer instructions and applied to the sections for 5 -10 min, until brown stain could be detected. Samples were then washed in dH_2O and counterstained in Mayer's Haematoxylin solution (Sigma-Aldrich) for 45 - 90 s and washed in a bath under running tap water to remove excess stain.

3.5.6 Dehydration and Mounting of slides

Slides were dehydrated by incubating in a series of washes of increasing concentrations of EtOH (70 %, 1 min; 95 %, 2 x 1 min; 10 0%, 2 x 1 min) followed by three 3 min washes in xylene. Slides were then mounted in DPX mounting medium (Sigma-Aldrich), covered with a glass coverslip and dried under the fume hood. For sections previously stained by β-Galactosidase staining (see Section 3.5.7) Histo-Clear and Histo-Mount (both National Diagnostics) were used instead of xylene and DPX.

3.5.7 Whole mount β-Galactosidase (lacZ) staining

Activity of the $Axin2^{lacZ}$ allele, that expresses β-Galactosidase whenever the Axin2 promoter is activated, and the ROSA-lacZ allele, a reporter for Cre mediated recombination, were visualised using this whole mount staining protocol. The tissues, including liver organoids were fixed for 1 hour in lacZ fixative solution at room temperature. Cells cultured

by conventional 2D culture were only fixed for 15 min in the same solution. Tissue and cells were then washed in lacZ washing buffer and stained overnight at 37 °C in lacZ staining solution. Tissue or cells were then washed with PBS and imaged or postfixed in 10 % formalin and processed for sectioning (see Section 3.5.1).

Table 3-8. Solutions for lacZ staining.

LacZ fixative
PBS (Formedium)
Glutaraldehyde, 0.2 % (Sigma-Aldrich)
EGTA, 5 mM (Sigma-Aldrich),
$MgCl_2$, 2 mM (Fisher Scientific)
NP40, 0.02 % (Sigma-Aldrich)
LacZ washing buffer
PBS (Formedium)
$MgCl_2$, 2 mM (Fisher Scientific)
NP40, 0.02 % (Sigma-Aldrich)
NaDeoxycholate 0.01 % (Sigma-Aldrich)
LacZ staining buffer
LacZ washing buffer
$K_4Fe(CN)_6\,3H_2O$, 5 mM (Sigma-Aldrich)
$K_3Fe(CN)_6$, 5 mM (Sigma-Aldrich)
keep in the dark
X-Gal solution, 2 mg/ml (Promega) added directly before staining

3.5.8 Whole mount immune fluorescent staining

I Staining of cells grown in 2D

Embryonic stem cells were grown on black, clear bottom 96-well imagine plates. At the desired time point, cells were fixed *in situ* for 15 min in 4 % PFA (Sigma-Aldrich) at room temperature or with 100 % ice cold Methanol (Sigma-Aldrich) depending on the antibodies to be used (see Table 3-9 for details). Cells were then washed 2 x in 3 % BSA/PBS and permeabilised with 0.2 % Triton X-100 in PBS for 20 min. After three washes with PBS and blocking with 10 % horse serum (Gibco) for 1 h cells were incubated with primary antibodies

in 0.1 % BSA/PBS at the appropriate concentration (see Table 3-9 for details) over night at 4 °C. The next day, cells were incubated for 1 h with a suitable fluorescent secondary antibody in 0.1 % BSA/PBS in the dark. When necessary, cells were incubated with 5 µg/ml Hoechst 33342 (Invitrogen) to stain nuclei. Cells were washed 3 x in PBS and imaged using the Olympus IX 71 inverted fluorescent microscope or the Leica DMIRE2 inverted confocal microscope.

II Staining of cells grown in 3D

Organoids were grown on black, clear bottom 96-well imagine plates in 14 µl domes of Matrigel. At the desired time point, cells were fixed for 30 min in 4 % PFA (Sigma-Aldrich) at room temperature or with 100 % ice cold Methanol (Sigma-Aldrich) depending on the antibodies to be used (see Table 3-9 for details). Cells were then washed 3 x in PBS-Glycine (100 mM Glycine (Sigma-Aldrich) in PBS) and incubated in IF blocking solution (10 % horse serum, 0.1 % BSA, 0.2 X Triton X-100, 0.05% Tween 20 in PBS) over night. The next day primary antibodies were added in IF buffer (0.1 % BSA, 0.2 X Triton X-100, 0.05% Tween 20 in PBS) and left on for 24 h, followed by 3 washes in IF buffer of which the last one was performed overnight. Then organoids were incubated for further 24 h with a suitable fluorescent secondary antibody in IF buffer. This was again followed by 3 washes in IF buffer of which the last one was performed overnight. Organoids were incubated with 5 µg/ml Hoechst 33342 (Invitrogen) for 60 min to stain nuclei. Cells were washed 3 x in PBS and imaged using the Olympus IX 71 inverted fluorescent microscope or the Leica DMIRE2 inverted confocal microscope.

Table 3-9. Conditions and antibodies used for whole mount fluorescence staining.

SPECIFICITY	SOURCE	MANUFACTURER	FIXTIVE	CONCENTRATION
Anti-APC	Rabbit	Abcam, #ab15270	Methanol or 4%PFA	1/100
Anti-AFP	Mouse	R&D, #MAB1368	Methanol or 4%PFA	1/100
Anti-Alb	Goat	Santa Cruz, #sc 46291	Methanol or 4%PFA	1/50
Anti-Caspase 3	Rabbit	R&D Transduction, #AF835	4% PFA	1/200
Anti-CD44 (all isotopes)	Rat	Abcam, #ab95518	4% PFA	1/100
Anti-CD44 (v 10 specific)	Rabbit	Millipore, #ab2082	4% PFA	1/100
Anti-Cdc2	Rabbit	Cell signalling, #9112S	4% PFA	1/100
Anti-Krt19	Rat	DSHB, Troma III	Methanol	1/500
Anti-Cyclin B1	Rabbit	Thermo Fisher, #PA1-37524	4% PFA	1/200
Anti-Cyclin B2	Goat	Santa Cruz, #sc-5235	4% PFA	1/100
Anti-FoxM1	Rabbit	Santa Cruz, #sc-502	4% PFA	1/100
Anti-Histone H3	Rabbit	Abcam, #ab4729	Methanol or 4% PFA	1/500
Anti-Hnf 4α	Rabbit	Santa Cruz, #sc-8987	Methanol	1/100
Anti-Ki67	Mouse	Vector Labs, #vp-K452	4% PFA	1/100
Anti-Pericentrin	Rabbit	Abcam, #ab4448	Methanol	1/1000
Anti-β-Catenin (total)	Mouse	BD Transduction #610154	4% PFA	1/100
Anti-β-Catenin (active)	Mouse	Millipore, #05-665	4% PFA or Methanol	1/100
Anti-β-tubulin	Rabbit	Cell signalling, #2146	4% PFA	1/50
Anti-γ-tubulin	Mouse	Abcam, #ab27074	Methanol or 4% PFA	1/500

Table 3-10. Fluorescent secondary antibodies and conditions.

SPECIFICITY	FLUOROPHORE	SOURCE	MANUFACTURE	CONCENTRATION
Anti-mouse	Alexa Fluor 488	goat	Invitrogen	1/500
Anti-mouse	Alexa Fluor 568	goat	Invitrogen	1/500
Anti-rabbit	Alexa Fluor 488	goat	Invitrogen	1/500
Anti-rabbit	Alexa Fluor 568	goat	Invitrogen	1/500
Anti-goat	Cy 5	donkey	Abcam	1/500
Anti-rat	Texas Red	goat	Vectorlabs	1/500

3.5.9 Whole mount EdU detection

Cells and cultures previously incubated with EdU (see Section 3.4.5) were fixed and processed as for whole mount antibodies staining. Before the blocking with horse serum, cells on a plate or organoids in Matrigel domes were permeabilised with 0.5 % Triton X-100 in PBS for 20 min and treated using the Click-iT® EdU Alexa Fluor® 488 Imaging Kit (Invitrogen) following manufacturer's instructions. Then normal whole mount immune fluorescent staining procedure was continued.

3.6 Molecular Biology techniques

3.6.1 Transformation of Bacterial Cells

Plasmids were transformed into Xl1-Blue Competent E. coli. cells (Agilent Technologies) for amplification. To this end, 0.5 ng to 2 ng plasmid DNA was added to 15 µl Competent cells and incubated on ice for 30 min. After a heat- shock for 45 s at 42 °C, Xl1-Blue E. coli, were incubated on ice for 2 min. Then 100 µl pre-heated SOC (Super Optimal Broth with Catabolite repression, SOB, Formedium, with 20 mM glucose, Sigma-Aldrich) medium was added and the reaction was incubated at 37 °C for 1 h while shaking at 200 rpm. Following transformation, bacteria were plated out on LB-Agar plates containing the appropriate selection antibiotic and incubated over night at 37 °C. See Table 3-11 for a brief description of each plasmid used in this study and Appendix 1 for plasmid maps.

Table 3-11. Plasmids used in this study

PLASMID	DESCRIPTION	BACTERIAL SELECTION	MAMMALIAN SELECTION	REFERENCES
pCAGGS-Cre-IRESpuro	Expression of Cre recombinase under the control of the chicken-beta-actin promoter and an hCMV immediate early enhancer. The recombinase is linked to a puromycin resistance gene by an internal ribosomal entry site (IRES). This vector was used to achieve Cre recombination in culture.	Ampicillin	Puromycin	(Schnuetgen et al. 2006)
Super8xTOP-flash	A TCF reporter construct, which expresses firefly luciferase under the control of a minimal TA viral promoter and 7 TCF/LEF binding sites. This vector is used as a Wnt signalling reporter.	Ampicillin	-	(Veeman et al. 2003)
Super8xFop-flash	The Super8xFop-flash construct contains 6 mutant TCF/LEF binding sites. This plasmid provides a control Wnt reporter.	Ampicillin	-	(Veeman et al. 2003)
pRL- TK Renilla	This vector provides constitute expression of renilla luciferase. It is used to provide a transfection control in TCF reporter assays.	Ampicillin	-	(Promega)

3.6.2 Plasmid preparation (Miniprep and Maxiprep)

A 5 ml bacterial culture was prepared by picking single bacterial colonies from the LB-Agar plate into LB broth supplemented with the appropriate selection antibiotic over night at 37 ˚C at 200 rpm. Plasmids were then purified using the QIAprep Spin Miniprep Kit (Qiagen) following manufactures instructions.

For Maxiprep 5 ml start up cultures were incubated for 6 h, then diluted 1/100 in selection LB broth, incubated over night at 37 ˚C, 200 rpm and purified with PureLink™ HiPure Plasmid Maxiprep Kit (Invitrogen).

Plasmids that were needed sterile for transfection of cultured cells (see Section 3.2.5) were further cleaned up by adding 2 volumes of EtOH and 1/10 volumes Sodium acetate (Sigma-Aldrich). The mix was incubated on ice for 5 min and pelleted at 18,000 x g for 5 min. The DNA pellet was then carefully washed 3 x with 70 % EtOH. From this point onwards, all the following steps were performed under a tissue culture hood. The EtOH was drained off as well as possible and the DNA pellet was left to dry for approximately 1 h. The pellet was then resuspended in filter sterilized elution buffer (5 mM Tris in ddH_2O). Plasmids were stored at -20 °C until further use.

3.6.3 Quantification and qualification of nucleic acids

Concentration and purity of plasmids, genomic DNA, and total RNA were determined by using a NanoDrop2000 (Thermo Scientific). RNA concentrations were measured in triplicate.

3.6.4 Sequencing

Plasmid DNA samples and purified PCR products were submitted for automated sequence analysis to DNA Sequencing & Services (MRCPPU, College of Life Sciences, University of Dundee, Scotland, www.dnaseq.co.uk). Sequencing reactions were carried out using Applied Biosystems Big-Dye Ver 3.1 chemistry on an Applied Biosystems model 3730 automated capillary DNA sequencer.

3.6.5 Polymerase chain reaction (PCR)

3.6.5.1 DNA extraction for genotyping

DNA was extracted from ear biopsies (see Section 3.1.4.1) taken shortly after weaning and again at death from tailpieces to assess the genotyping of mice by PCR. Other sources of mouse tissue for genotyping were mouse liver fragments and tail tips of E 9.5 or E 10.5 embryos. Mouse tissue was placed in a 1.5 ml tube and stored at -20 °C until further use. The biopsies were then lysed in 150 µl DirectPCR Lysis Reagent (Viagen Biotech, Inc.) supplemented with 0.5 mg/ml Proteinase K (Promega) over night at 55 °C. The next day, the solution was incubated at 85 C for 1 h to inactivate Proteinase K. Hairs and un-lysed cell clumps were precipitate by centrifugation at 16,000 x g for 10 s. Supernatant was stored at -20 °C until further use.

DNA was also extracted from organoids. Organoids grown in Matrigel were washed once in PBS and then processed, following the method described for ear biopsies and mouse tails.

To extract genomic DNA from ES cells grown on a 96 well plate, cells were washed with 100 µl PBS and then incubated in 100 µl ES cell lysis buffer (10 mM Tris pH 7.5, 10 mM EDTA, 10 mM NaCl, 0.5 % (w/v) Sarkosyl, 500 µg/ml Proteinase K) in a humid container at 55 °C overnight. The following day, the DNA was removed to a 1.5 ml tube with 400 µl EtOH and spun for 30 min at 16,000 x g. The pellet was then washed three times with 70 % EtOH,

drained and air dried before it was resuspended in 50 µl ddH_2O and stored at -20 °C until further use.

ES cells grown on bigger dishes were harvested by trypsinising; approximately 0.5 x 10^6 cells were removed to a 1.5 ml tube, washed with PBS, and then treaded as described above.

If pure DNA was needed to perform qPCR the method described in Section 3.6.7.1 was followed.

3.6.5.2 PCR protocol

PCR assays were performed in 8-well PCR SnapStrip tubes (Anachem). Prior to the PCR reaction an aliquot of gDNA was heated to 95 °C for 10 min and then quickly placed on ice. Afterwards, 0.75 µl gDNA was added to 24.25 µl PCR mix (see Table 3-12 for exact composition). For each primer set a negative control using ddH_2O instead of gDNA was run alongside the sample PCRs. Primers were either used as described in previous publications, as found on JAX[e].

PCR reactions were performed in a Thermal Cycler T3000 (Biometra). Exact primer sequences and specific cycling conditions can be found in Table 3-13.

Table 3-12. Constituents of PCR mix.

COMPONENT	VOLUME
2 x GoTaq Green Master Mix (Promega) dNTP (400 µM)* $MgCl_2$ (3 mM)* GoTaq DNA Polymerase* Gel leading dye*	12.5 µl
Primer 1 (5 µM)	1.5 µl
Primer 2 (5 µM)	1.5 µl
Primer 3 (optional, 5 µM)	(1.5 µl)
ddH_2O	Add up to 24.25 µl

*Already included in in the 2 x GoTaq Green Master Mix (Promega)

[e] (http://jaxmice.jax.org/support/genotyping/).

Table 3-13. Genotyping PCR primer sequences and cycling conditions.

GENE	PRIMER (5'-3')	PCR CONDITIONS	PRODUCTS	SOURCE
AHR	F: AGGTTCCCTGGGACTTGTTT R: TCACCAAACCCTCCATCAGT	95 °C, 5 min; (94 °C, 20 s; 57 °C, 20 s; 72 °C, 1 min)$_{30}$; 72°C, 10 min	Responder: 196 bp non-responder: 178 bp	(Marsh 2008)
Axin1$^{\Delta}$ and Axin1^{fl} (Type B)	F: CTCTGAATGTGGACTGTGTCCTTCCATCAC R: GCTGTGCAGGAGCTCTACTAAGCCTCTA	95 °C, 5 min; (95°C, 1 min; 58 °C, 2 min; 72°C, 3 min)$_{30;}$ 72°C, 10 min	wt: 2042 bp, fl: 2190 bp, KO: 402 bp	(Feng, unpublished)
Axin1^{fl} (Type A)	F: CCTCAAGTAGACGGTACAACGAAGGCAGAG R: CTGTGCAGGAGCTCTACTAAGCCTCTACAC	95 °C, 5 min; (95°C, 1 min; 60 °C, 1 min; 72 °C, 3 min)$_{35;}$ 72 °C, 10 min	wt: 383 bp mutant: 531 bp	(Feng et al. 2012)
Axin2$^{\Delta}$ and Axin2^{fl} (Type B)	F: CTTGCGTGTTCTGGTTGTCGTGGGAGT R: TAGCAGTGGAATGACCTCTTCCCAAACTGG	95 °C, 5 min; (95 °C, 1 min; 62 °C, 2 min; 72 °C, 3 min)$_{30;}$ 72 °C, 10 min	wt: 1854 bp, fl: 1995 bp KO: 504 bp	(Feng, unpublished)
Axin2^{fl} (Type A)	F: CCTGGAAGATGAGCTAGCTTTGCAGATGTC R: CAAAACTCAGTTGCAGTCGCTAGCAGTTCC	95 °C, 5 min; (95 °C, 30 s; 57 °C, 30 s; 72 °C, 1 min)$_{30}$; 72 °C, 10 min	wt: 505 bp mutant: 643 bp	(Feng, unpublished)
Axin2^{lacZ} (Type C)	F: AAGCTGCGTCGGATACTTGAGA R1: AGTCCATCTTCATTCCGCCTAGC R2: TGGTAATGCTGCAGTGGCTTG	95 °C, 5 min; (95 °C, 1 min; 52 °C, 1 min; 72 °C, 2 min)$_{35;}$ 72 °C, 10 min	wt: 497 bp mutant: 400 bp	(Lustig et al. 2002)
Cre	F: TGACCGTACACCAAAATTTG R: ATTGCCCCTGTTTCACTATC	95 °C, 3 min; (95 °C, 30 s; 62 °C, 30 s; 72 °C, 1 min)$_{30}$; 72 °C, 10 min	wt: none mutant: 1000 bp	(Ireland et al. 2004)
ROSA-lacZ	F: CTGGCGTTACCCAACTTAAT R: ATAACTGCCGTCACTCCAAC	95 °C, 3 min; (95 °C, 30 s; 62 °C, 30 s; 72 °C, 1 min)$_{30}$; 72 °C, 10 min	wt: none mutant: 512 bp	(Soriano 1999)
GSK3α	F: CCCCCACCAAGTGATTTCACTGCTA R: AACATGAAATTCCGGGCTCCAACTCTAT	95 °C, 5 min; (95 °C, 30 s; 56 °C, 30 s; 72 °C, 30 s)$_{35}$; 72 °C, 10 min	wt: 750 bp mutant: 250 bp	(Doble et al. 2007)
GSK3β	F1: AACCACAGTAGTGGCAACTC F2: CGTGCTACTTCCATTTGTCACG R: CCAGTCACAAATCGTACTGC	95 °C, 5 min; (95 °C, 30 s; 56 °C, 30 s; 72 °C, 30 s)$_{35}$; 72 °C, 10 min	wt: 506 bp mutant: 4790 bp	(Doble et al. 2007)
Y-chromosome	F: TCTTAAACTCTGAAGAAGAGAC R: GTCTTGCCTGTATGTGATGG	95 °C, 5 min; (95 °C, 1 min; 50 °C, 2 min; 72 °C, 3 min)$_{30,}$ 72 °C, 10 min	male: 404 bp	(Kunieda et al. 1992)
β-Catenin^{fl}, (and β-Catenin$^{\Delta}$)	F: AAGGTAGAGTGATGAAAGTTGTT R1: CACCATGTCCTCTGTCTATTC (R2: TACACTATTGAATCACAGGGACTT)	95 °C, 5 min; (95 °C, 1 min; 60 °C, 2 min; 72 °C, 3 min)$_{30,}$ 72 °C, 10 min	wt: 221 bp, fl: 324 bp (KO: 500 bp)	(Brault et al. 2001)

3.6.6 Agarose gel electrophoresis

Agarose gel electrophoresis was used to separate DNA fragments from restriction digests or PCR and to visualize them. Agarose gels at the desired density (4 % for AhR, 1.5 % rest) were produced by dissolving Agarose (Bioline) in Tris-acetate – EDTA buffer (TAE, Geneflow) in a conical flask in the microwave. After cooling the solution down evenly through constant swirling, 1 drop of ethidum bromide was added per 50 ml gel. Gels were then poured into appropriate sized moulds and combs were inserted to create wells. Once the gels were properly set, they were placed in gel electrophoresis tanks surrounded by TAE buffer. 20 µl of each PCR sample was loaded per well. If the PCR buffer did not contain leading dye (i.e. from qPCR and qRT-PCR reactions) samples were diluted in 1 x gel loading solution (NEB) prior to loading. Samples were run alongside a molecular ladder (NEB) of appropriate size at 110 V until the desired bands were sufficiently separated. DNA bands on the gel were visualised using a GelDoc UV transilluminator (Bio-Rad).

3.6.7 Genomic qPCR and qRT-PCR

3.6.7.1 DNA extraction for genomic qPCR

DNA extraction for pure DNA used in genomic qPCR experiments was extracted using the Gentra Puregene kit (Qiagen) according to manufacturer's instruction.

3.6.7.2 RNA extraction for qRT-PCR

Total RNA was isolated from the organoids, mouse livers or ES cells using the RNeasy series from Qiagen following manufacturer's instruction. Samples were lysed and homogenised in RTL buffer supplemented with 10 µl/ml β-Mercaptoethanol. QIAshredder spin columns (Qiagen) were used to homogenize ES cells and organoids. An on-column DNase I treatment was always performed during extraction.

3.6.7.3 Reverse transcription of RNA

Reverse transcriptions of RNA into cDNA were carried out using the ImProm-II™ Reverse Transcription System (Promega, Southampton, UK) according to manufacturer's instructions. For each 5 µl reaction 1 µg RNA was added to 1 µg random hexamer primers in nuclease-free H_2O. Sample mixes were heated at 70 °C before being chilled at 4 °C for 5 min each. Spinning for 10 s collected condensate. Sample mixes were kept on ice.

Reaction mix comprising 1 x ImProm-II reaction buffer, 3 mM $MgCl_2$, dNTP mix (0.5 mM each), and 20 u recombinant RNasin Ribonuclease inhibitor was made up in nuclease-free H_2O, with 1 µl ImProm-II reverse transcriptase or 1 µl nuclease-free H2O added to RT reaction mix and No RT control reaction mix respectively. 15 µl reaction mix was added to 5 µl sample mix for a final volume of 20 µl per reaction. RT reaction temperatures were as follows; 25 °C for 5 min, 42 °C for 60 min, and 70 °C for 15 min. RT products were stored at -20 °C until required.

3.6.7.4 Quantification of DNA or cDNA

qRT-PCR or genomic qPCR was run in triplicates on a DNA thermal cycler (StepOne Real-Time PCR Systems, Applied Biosystems) using SYBR Green (Bioline, London, UK). Each well was made up of 1 x SYBR green fast mix (Bioline) 2 µl of cDNA, 0.5 µl of each primer (10 mM) and 8 µl nuclease free H_2O (Sigma-Aldrich). The plate was sealed and centrifuged for 1 min at 8,000 rpm. Full qRT-PCR primer sequences are listed in Table 3-14. Thermocycler conditions were set to 95 °C for 20 s followed by 40 cycles of 95 °C denaturation for 3 s and 60 °C annealing for 30 s. The data were collected automatically using the StepOne Software.

A qRT-PCR reaction for all cDNA samples was also run with primers for the housekeeping gene *β-actin, GAPDH, or β2-microglobulin* (*B2M*) in order to normalize the expression levels of target genes. Genomic DNA samples were normalized to the single copy gene ApoB.

Following PCR amplification SYBR green melt curves were examined to ensure the absence of primer dimers, unspecific products or contamination. Amplification products were also routinely analysed by gel electrophoreses to verify the production of a single product of appropriate length.

Table 3-14. Primers for qRT-PCR.

GENE	FORWARD PRIMER (5' to 3')	REVERSE PRIMER (5' to 3')	SOURCE
Ax1 KO*	GGCGTTTGGAAGAAGAAGAAAAGAGAGC	CCCACAGAAATAGTAGCCCACAACAATG	Feng et al, 2012
Ax2 Full**	ATAACTCGCTGTCGTTGGCG	GGCTACCTCCCCACCTTGAATG	Feng et al, 2012
Ax2 KO*	GCAGCTCAGCAAAAAGGGAAAT	TACATGGGGAGCACTGTCTCGT	Feng et al, 2012
β-Actin	TGTTACCAACTGGGACGACA	GGGGTGTTGAAGGTCTCAAA	Feng et al, 2012
β-Catenin	TGAATGGGAGCAAGGCTTTTC	TGGGATGAGCAGCGTCAAAC	Feng et al, 2012
B2M	CTTTCTGGTGCTTGTCTCACTG	AGCATTTGGATTTCAATGTGAG	Feng et al, 2012
c-Jun	CTTCTACGACGATGCCCTCAAC	AGTGGTGATGTGCCCATTGC	Feng et al, 2012
c-Myc	CCTTTGGGCGTTGGAAACC	TCCTCGTCGCAGATGAAATAGG	Feng et al, 2012
CD44 (v 10)	CCATCCAACAACTTCTATTCTGCC	TGTCTGGGTATTGAAAGGTGTAGCC	Feng et al, 2012
cdc20	AATGACTACTACCTGAATCTTGT	GGATGTCACCAGAACCAG	Feng et al, 2012
cdc25	ACAAAGAGGAGGAAGAGTGTGCC	GGAAGACATCAGGGATAGAGACTGG	Feng et al, 2012
cdc25a	ACAAAGAGGAGGAAGAGTGTGCC	GGAAGACATCAGGGATAGAGACTGG	Feng et al, 2012
Cdx1	ACGCCTACGAATGCATG	CTTGGTTCGGGTCTTACCG	Primer Bank***
Cyclin B2	TCTTGCCTGTCTCAGAAG	CTCCATGTAGCCTGTGTAA	Feng et al, 2012
Cyclin D1	TGCCATCCATGCGGAAA	AGCGGGAAGAACTCCTCTTC	Feng et al, 2012
Foxa2	GGGAGCGGTGAAGATGGA	TCATGTTGCTCACGGAGGAGTA	Feng et al, 2012
FoxM1	TGGCTTGGAAAGATGAGT	GCTCCAGGTGACAATTCT	Feng et al, 2012

Table 3-14. (Continued) Primers for qRT-PCR.

GENE	FORWARD PRIMER (5' to 3')	REVERSE PRIMER (5' to 3')	SOURCE
Gata4	GGAAGACACCCCAATCTCG	CATGGCCCCACAATTGAC	Primer Bank***
Hnf1α	CTGGCAACTTGCATCCACTA	AGTTCTGCAGGTCTCCCTCA	Feng et al, 2012
Hnf4α	ACAACTCCTGCCTCCAGCACTA	TCGCCTCTTTCTCGATGCTT	Feng et al, 2012
Ki67	AGAAGTCCAGGTCTACAG	TCGTTGCTATTGCTAAGG	Feng et al, 2012
Krt19	CCTCCCGAGATTACAACCACTA	AATCTTGGAGTTGTCAATGGTG	Primer Bank***
Lgr5	GACAATGCTCTCACAGAC	GGAGTGGATTCTATTATTATGG	Primer Bank***
Nanog	AACCAAAGGATGAAGTGCAAGCGG	TCCAAGTTGGGTTGGTCCAAGTCT	Primer Bank***
Nestin	CCCTGAAGTCGAGGAGCTG	CTGCTGCACCTCTAAGCGA	Primer Bank***
NeuroD1	ATGACCAAATCATACAGCGAGAG	TCTGCCTCGTGTTCCTCGT	Primer Bank***
Oct-4	AGCTGCTGAAGCAGAAGAGGATCA	TCTCATTGTTGTCGGCTTCCTCCA	Primer Bank***
p53	CAGGGCTGAGACACAATCCTCC	GTGCCAGGGTCCAACAACTG	Feng et al, 2012
Pax6	CCATCTTTGCTTGGGAAATC	GCTTCATCCGAGTCTTCTCC	Primer Bank***
Rex1	AGGAAATAGGTAGAGCGCATCGCA	AGGCGATCCTGCTTTCTTCTGTGT	Feng et al, 2012
Runx2	GCCGGGAATGATGAGAACTA	GGTGAAACTCTTGCCTCGTC	Feng et al, 2012
Sox17	CGAGCCAAAGCGGAGTCTC	TGCCAAGGTCAACGCCTTC	Feng et al, 2012
Tiam1	CTTTCTGAGTCTGTGCATTCG	AATCGATGGTAAACCTGTTTCG	Feng et al, 2012
TTR	GGCTCACCACAGATGAGAAGTTC	ACAAATGGGAGCTACTGCTTTGGC	Primer Bank***

*KO primers detect the presence of exon 2 only in wt and fl Axin mRNA. **Full Primer detects a C terminal region of Axin mRNA independent of recombination. ***Harvard primer bank available at: http://pga.mgh.harvard.edu/primerbank/

For qRT-PCR expression levels of target genes were normalized to the housekeeping gene and calculated using the $2^{-\Delta\Delta Ct}$ method (Livak and Schmittgen, 2001). When analysing gDNA recombination levels of the single copy gene *ApoB* were recorded as reference. In this instance data were normalized to ApoB and calculated using the $2^{-\Delta\Delta Ct}$ method (Livak and Schmittgen, 2001). Samples were only analysed further if they had a single peak in the melting curve and the technical repeats were within 1 C_t value of each other.

To analyse the difference between the mean of two biological groups a Mann-Whitney U test was performed using GraphPad Prism 5 for Mac OS X. One-Way ANOVA test was used to analyse the difference across several biological groups, followed by a post-Hoc Tukey's test to perform pair-wise comparisons between groups using GraphPad Prism 5 for Mac OS X. A significant difference between means was accepted, when p value was equal or less than 0.05.

3.6.7.5 RT2 Profiler PCR assay

To perform the embryonic stem cell RT^2 Profiler assay (Qiagen, PAMM-081Z) RNA was extracted as described in Section 3.6.7.2). But cDNA synthesis was performed using the RT^2 Fist strand kit (Qiagen). For each 96-well assay plate 2700 µl qPCR master mix was made up of 1350 µl 2 x RT^2 SYBR green master mix, 1248 µl nuclease-free H_2O, and 102 µl RT product. 25 µl PCR components mix was added to each well of the RT^2 profiler PCR arrays on ice and the plates were spun at 1,000 x g at room temperature for 1 min to ensure removal of air bubbles. The cycling conditions of the Applied Biosystems StepOne Plus qRT-PCR system and melting curve analysis was identical to that described in before. A C_t threshold of 2 was set for all wells and the $\Delta\Delta C_t$ method of analysis was used to determine fold changes using RT^2 Profiler PCR Array Data Analysis version 3.5 [f]. Reference genes used were glyceraldehyde-3 phosphate, β-2 microglobulin, β-glucouronidase and 90 kDa heat shock protein-β.

[f] Available by accessing http://pcrdataanalysis.sabiosciences.com/pcr/arrayanalysis.php?target=upload

3.6.8 Protein Analysis

3.6.8.1 Protein extraction ES cells for western blot for an sandwich immunoassays

ES cells grown on a 6 well plate (Nunc, Thermo-Fisher) were lysed to extract protein for a multiplex sandwich immune assay (Luckert et al. 2011). Cells were washed with PBS and lysed directly on the plate using 200 µl lysis buffer (see Table 3-15). Cells were scraped off the plate and lysed for 45 min at 4 °C under shaking. Insoluble material was pelleted at 15,000 x g at 4 °C for 30 min. Lysates were snap frozen in LN_2 and stored at -80 °C until further use.

Table 3-15. Lysis buffer for protein extractions.

Sandwich immunoassays lysis buffer
Triton X-100 (0.5 % [v/v])
NaCl (150 mM)
Tris-HCl pH 8 (20 mM, Ambion)
Complete protease inhibitor (1 x Roche Applied Science)
Phosphatase inhibitor cocktail (1 x Roche Applied Science)

All components were purchased from all Sigma-Aldrich unless otherwise stated.

3.6.8.2 Protein quantification

Quantification of protein concentrations of protein lysates were performed in a 96-well assay following the Bradford method (Bradford 1976). 80 µl of diluted samples were (1: 100 in ddH_2O) were incubated for 5 min with 20 µl of pure Bradford reagent (Sigma-Aldrich). Afterwards the extinction at 595 nm was measured using a FluoStar optima plate reader (BMG Labtech). A BSA (Pierce) standard curve was also generated (40, 20, 10, 5, 2.5, 1.25 µg/ml). Then the protein concentration of the samples was determined using GraphPad Prism using Boltzman sigmoidal equation.

3.6.9 Multiplex sandwich assays to detect β-Catenin levels/phosphor forms

A multiplex sandwich assay to detect cellular β-Catenin levels was performed in the lab of Prof Oliver Poetz. To this end protein extracts obtained as described in 3.6.8.1 were sent to Reutlingen, Germany on dry ice

The bead-based assay allowed the quantification of multiple post-translational modifications of β-Catenin in the same sample without competition. It was used to detect total amounts of β-Catenin and different phosphorylation forms in a sandwich immunoassay, β-Catenin in complex with E-Cadherin in a co-immunoprecipitation, and transcriptionally active β-Catenin in a GST pull-down assay with TCF4, ECT (E-cadherin cytosolic tail) and ICAT (Inhibitor of β-Catenin and TCF-4). The procedure was first described in Luckert et al. 2011 and was the further developed as described in Groll et al. 2015. Briefly, antibodies for β-Catenin (R&D), E-Cadherin (R&D), GST (GE Healthcare) and anti-rabbit antibodies (Jackson ImmunoResearch Inc.) were covalently coupled to different carboxylated fluorescent microspheres (Luminex). Phospho-specific β-Catenin antibodies (anti – PS33, anti - PS45, anti- PS552 and anti- PS675, Cell Signaling Technology) were incubated for 4 h at room temperature with anti-rabbited coated microspheres. Beads coated with anti-GFP antibodies were additionally incubated with GFP-tagged bait proteins (TCF4, ECT and ICAT, 1 µg for 100,000 bead) for 6 h at room temperature. Coated microsphere were stored at 4 °C in the dark in ELISA blocking reagent (Roche) supplemented with 0.05 % NaN_3 until further use.

20 µg protein lysate was diluted to 40 µl in lysis buffer (see Table 3-15) and mixed with 20 µl microspheres (2,000 beads per set and well in ELISA blocking reagent, Roche). Lysates and beads were incubated overnight at 4 °C in a 96-well plate (nonbinding surface, Corning) in a thermo mixer (Eppendorf AG) at 750 rpm. The samples were then transferred to a PCR plate (Brand) and processed on a semi-automated platform (KingFisher 96, Thermo Fisher Scientific) that allows the movement of the magnetic beads with magnetic rods. The beads were first washed in PBS, 0.1% Tween (Sigma-Aldrich), then they were incubated for 1 h

with anti β-Catenin detection antibody (1 µg/ml, BD Biosciences), followed by 2 washes in PBS, 0.1% Tween. Next, the microspheres were transferred to the secondary phycoerythrin-conjugated antibody, (2.5 µg/ml, goat anti-mouse phycoerythrin-conjugated antibody, Jackson ImmunoResearch Inc.) in 1 % donkey serum (Sigma-Aldrich) for 45 min. After two more washes in PBS, 0.1% Tween beads were analysed using a Luminex 100 IS system (Luminex) in 100 µl ELISA blocking reagent (Roche) containing 0.1% Tween. For each sample, the mean fluorescence intensities of at least 100 microsphere was analysed. The standard deviation was calculated based on biological triplicates.

3.7 Data acquisition and analysis

3.7.1 Technical repeats and biological groups

Unless stated differently, experiments were performed using biological and technical triplicates.

I Organoids

Experiments in organoids were performed using organoids derived from three individual mice of the same genotype at the same time. When organoids of different genotypes were analysed they were all handled in parallel. In all experiments, 3 technical repeats were performed for each of the individual organoids lines.

II ES cells

Table 3-16 summarizes the available ES cell cones for each genotype. If possible, we used different ES cell clones from several mothers as parental ES cell lines. These underwent Cre recombination to generate Knockout lines. Three different ES cell lines were used in each experiment to form biological triplicates; additionally each individual cell line was use in technical triplicates.

Table 3-16. Biological repeats of ES cell lines available

CELL LINE	AVAILABLE CLONES	GENOTYPE GROUPES
Parental line		
A1$^{fl/fl}$	Several ES cell clones from different mothers	Cell lines from A1$^{fl/fl}$; A2$^{fl/fl}$; and A1$^{fl/fl}$, A2$^{fl/fl}$ were used to from the **wt** control group (and **wt + CHIR99021**)
A2$^{fl/fl}$	Only one parental clone	
A1$^{fl/fl}$, A2$^{fl/fl}$	Only one parental clone	
A1$^{fl/fl}$, A2$^{lacZ/lacZ}$	Several ES cell clones from different mothers	
Knockout cell lines		
A1$^{\Delta/\Delta}$	Several clones from different parental lines	Cell lines derived from different parental lines were used in the **A1$^{\Delta/\Delta}$** group
A2$^{\Delta/\Delta}$	Several clones from one parental line	Cell lines from one parental line were used in the **A2$^{\Delta/\Delta}$** group
A2$^{lacZ/lacZ}$	Several ES cell clones from different mothers	Cell lines from A2$^{lacZ/lacZ}$ and A1$^{fl/fl}$, A2$^{lacZ/lacZ}$ were used in the **A2$^{lacZ/lacZ}$** group
A1$^{\Delta/\Delta}$, A2$^{\Delta/\Delta}$	Several clones from one parental line	Cell lines from one parental line were used in the **A1$^{\Delta/\Delta}$, A2$^{\Delta/\Delta}$** group
A1$^{\Delta/\Delta}$, A2$^{lacZ/lacZ}$	Several clones from different parental lines	Cell lines from derived from different parental lines were used in the **A1$^{\Delta/\Delta}$, A2$^{lacZ/lacZ}$** group
GSK3$^{\Delta/\Delta}$	One cell line only	ES cells from one cell line were used in 3 x 3 replicates in the **GSK3$^{\Delta/\Delta}$** controls

3.7.2 Image creation and analysis

Images of chromogenic immunohistochemistry were taken with a Leica DMRB microscope or an Axio Scan.Z1 Slide scanning microscope (Zeiss). Fluorescent microscopy was performed using the Olympus IX 71 inverted fluorescent microscope or the Leica DMIRE2 inverted confocal microscope. Fiji (Fiji is just Image) and ZEN 2 (Zeiss) was used for quantitative analysis of staining.

Cell counting was performed as following:

I EdU staining of ES cells

We counted the percentage of EdU positive nuclei out of 250 cells for 3 cell lines per genotype in triplicate.

II Different immunohistochemical stains in EBs:

In embryoid bodies, the total number of cells, and the number of positively stained cells were counted in cross-sections of individual EB's. Mean numbers of stained cells were then generated as the percentage of total cells per EB cross-section of 10 EBs. We used three different cell lines of each genotype to make EBs (with the exception of $GSK3^{\Delta/\Delta}$, were we performed technical triplicates from the same cell line). Cell scoring was performed blind to avoid possible bias

3.7.3 Comparison of means

Quantitative data generated in experiments were entered into Excel (Microsoft) spread sheets. If appropriate data were normalized and mean values of technical triplicates were calculated. All mean values for each biological group were then entered into GraphPad Prism 5 for Mac OS X. Data from each biological group were then tested for significant difference between means using One-Way ANOVA. If data from more than two groups were compared, One-Way ANOVA test was used to establish the difference across all the groups, followed by a Post-Hoc Tukey's post-hoc test. We also used GraphPad Prism 5 for Mac OS X. software or Excel to plot the data as mean standard deviation within each group. Unless specifically stated, only significant differences compared to wt cells were shown.

4 Effects of Axin loss in embryonic development

4.1 Introduction

A study by Gui-Jie Feng and her colleagues, investigating the effects of Axin1 loss in the mouse liver, challenged the understanding of Axin function and its role in Wnt regulation (Feng et a. 2012). Axin1 loss led to an acute increase in proliferation and the late onset of HCC in the absence of a clear Wnt-activated phenotype (see Section 1.3.6 for details).

We believe that, to properly understand the link between Axin mutations and tumourigenesis it is vital to take a step back, from the pathological situation, and re-evaluate Axin function in general. The mechanism of Axin-dependent tumourigenesis in the liver is likely due to fundamental processes; important in many physiological situations.

To test this hypothesis, we examined the role of Axin1 and its homologue Axin2 in embryonic development. In addition to furthering the understating of general Axin function, we also aim to add to the knowledge about how the Wnt signalling pathway mediates its effect on maintaining self-renewal, and governing lineage commitment and differentiation. The Wnt signalling pathway has been shown to play a major role in regulating embryonic development, although the mechanism through which these functions are governed is not yet understood (see 1.3.5).

The focus of this chapter is the analysis of the effects of conditional Axin1 and Axin2 loss on embryonic stem cell (ES cell) properties, embryonic development, and Wnt regulation in ES cells and the mouse embryo.

4.2 Generation of an allelic series of Axin mutant ES cell lines

4.2.1 Derivation of parental Axin mutant ES cell lines

In order to study the role of Axin1 and its homologue Axin2 in embryonic development we generated a series of Axin mutant mouse embryonic stem cell (ES cell) lines that carry different combinations of the Axin1^{fl} (A1^{fl}), Axin2^{fl} (A2^{fl}), and Axin2^{lacZ} (A2^{lacZ}) alleles (see Table 4-1 and Figure 4-1). The analysis of ES cell lines with different combination of Axin alleles should give insight into their redundancy and the effect of gene dosage on stem cell properties and Wnt signalling pathway regulation.

Table 4-1. Generated ES cell lines.

CELL LINE		ALLELES	
Parental line	**Knockout**	**Axin1**	**Axin2**
A1$^{fl/fl}$		fl/fl	wt
	A1$^{\Delta/\Delta}$	Δ/Δ	wt
A2$^{fl/fl}$		wt	fl/fl
	A2$^{\Delta/\Delta}$	wt	Δ/Δ
A2$^{lacZ/lacZ}$		wt	lacZ/lacZ
A1$^{fl/fl}$, A2$^{fl/fl}$		fl/fl	fl/fl
	A1$^{\Delta/\Delta}$, A2$^{\Delta/\Delta}$	Δ/Δ	Δ/Δ
A1$^{fl/fl}$, A2$^{lacZ/lacZ}$		fl/fl	lacZ/lacZ
	A1$^{\Delta/\Delta}$, A2$^{lacZ/lacZ}$	Δ/Δ	lacZ/lacZ

Lines carried combination of the following alleles: wild type (wt) Axin1 or Axin2, a β-Galactosidase insert (lacZ) into Axin2 (A2) and/or a conditional allele (fl) Axin1 (A1) or Axin2 (A2) hat was then deleted by transient transfection of Cre recombinase (Δ).

The first step in this process was to generate cohorts of male and female mice of the appropriate genotype and to set them up for timed mating. Preimplantation blastocysts were harvested from pregnant mice and the cells of the inner cell mass were isolated, with the help of Dr. Susi Hunter and Prof. Nick Alan. Several clones of parental ES lines of 5 different genotypes (Table 4-1) were isolated and genotyped by PCR (data not shown).

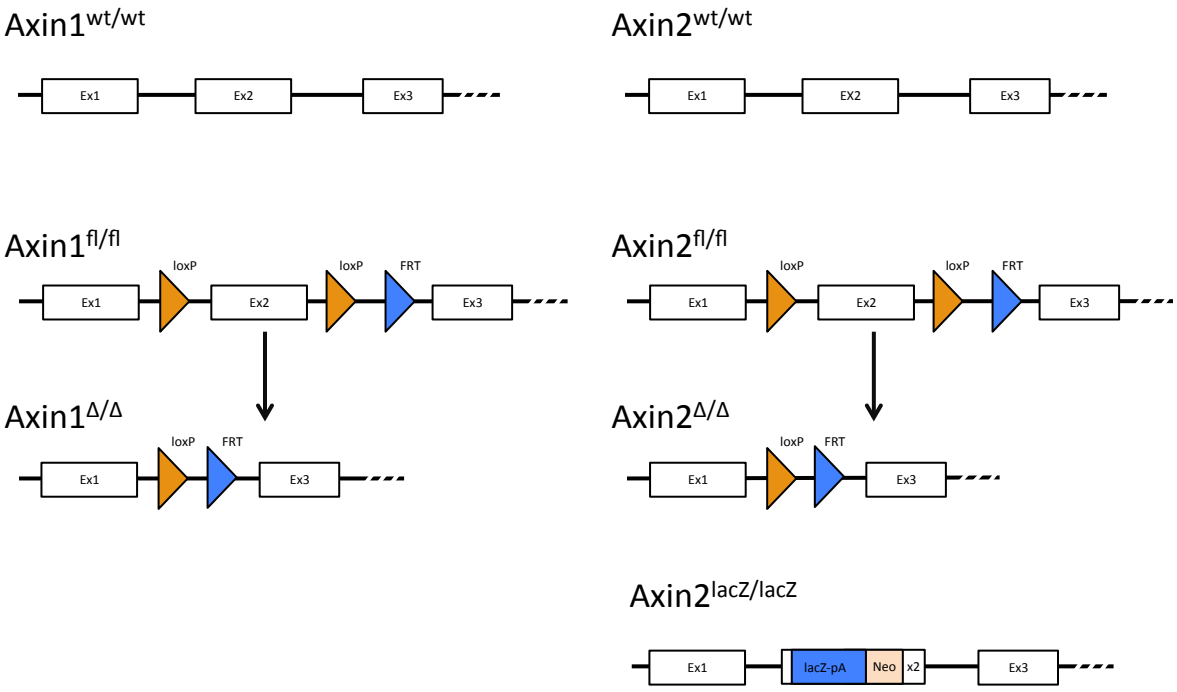

Figure 4-1. Gene structures of Axin1 and 2 alleles.
In this study we used Axin1 and 2 wt alleles, alleles carrying loxP sites flanking Exon 2 (Axin$^{fl/fl}$, that could be deleted by Cre recombinase to generate Axin$^{\Delta/\Delta}$ alleles, as well as the Axin2^{lacZ} allele contains a *lacZ* gene in frame with the endogens start codon of *Axin2*, replacing exon 2. Figures adapted from Feng et al. (2012), Feng, unpublished, and Lustig et al. (2002).

For the generation, growth, and expansion of our ES cell lines, we maintained them in 2i medium (see Table 3-3 in material and methods for the exact composition) under feeder-free conditions. The basis of this medium is the use of a GSK3 (i.e. CHIR99021) and a MEK/Erk inhibitor (i.e. PD0325901) to maintain stem cell pluripotency. During subsequent experiments examining the effects of Axin loss in ES cells, we grew cells in 1i (medium without CHIR99021) to remove the 'Wnt stimulation' from the medium.

In addition to the allelic series of Axin mutant ES cells we also analysed a GSK3 double mutant ES cell lines (Doble et al. 2007), which served as control for Wnt activation in ES cells. Additionally, we maintained wild type cells in 2i medium (wt +CHIR) as a second Wnt activated control. Details of these experiments follow later.

4.2.2 Selection of parental ES cell lines

We then selected 3 to 5 cell lines of each genotype for continued analysis to ensure that the biology observed was less likely to be due to clonal variation as opposed to Axin-dependent biology. The selection process included determination of the ES cell character of the cell lines by alkaline phosphatase staining, in addition to genotyping and sex determination. Only male ES cell lines, as determined by PCR for the X and Y Chromosomes (data not shown), were selected for continued analysis. Because female ES cells lines are considered to have a very high risk of X-Chromosome instability (Robertson et al. 1983).

During the long process to generate embryonic stem cell lines, cells underwent a lot of stress, which could lead to the loss of pluripotency in some cell lines. Alkaline phosphatase is expressed in pluripotent embryonic stem cells. While the cells undergo differentiation they lose their stem cell character, and thus the expression of *alkaline phosphatase*. Figure 4-2 shows a range of different parental ES cell lines grown in 2i medium stained by alkaline phosphatase staining independent of their genotype. Under normal culturing conditions (2i), ES cells form round colonies of pluripotent cells.

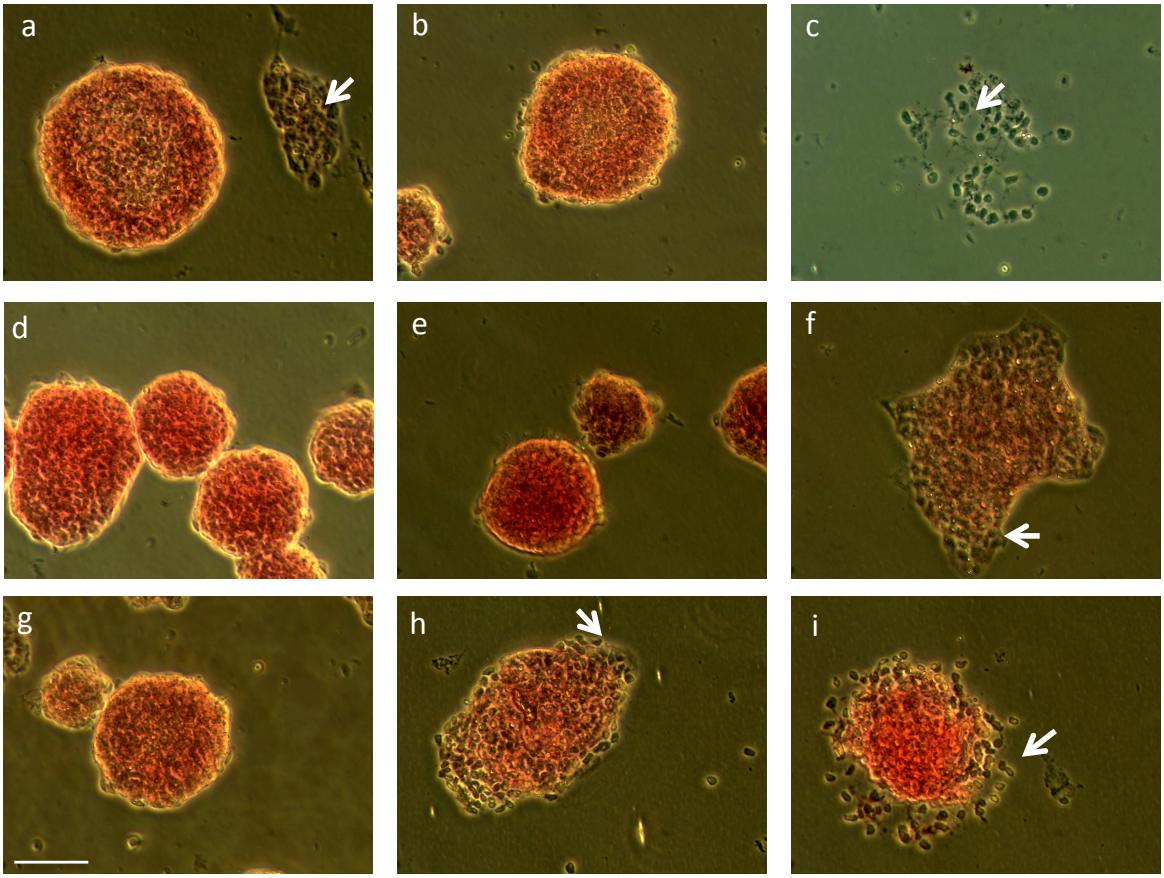

Figure 4-2. Alkaline phosphatase staining of parental ES cell lines.
A selection of different parental ES cell clones (including loxP flanked exons). Embryonic stem cells grown in full medium (2i) formed round colonies that stained positive for alkaline phosphatase (red) when they were undifferentiated. Differentiated cells were found at the edge of the colonies (white arrows) and formed feeder like layer around the ES colonies. Stem cells lines with strongly stained round colonies and few differentiated cells at the colonies' edges (i.e. **a, b, d, e,** and **g**) were selected for further analysis. If the parental cell line lost most of the stem cell potential, shown by unstained cell colonies (i.e. **c, f, h,** and **i**), they were rejected. Scale bar represents 100 µm.

Only at the edge of the colonies, do some cells start to differentiate and spread out at the bottom of the culture dish, forming an almost feeder-like cell layer. We only selected cell lines that formed well-defined, round ES cell clones, with strong alkaline phosphatase staining when grown in full 2i medium (see i.e. Figure 4-2 a, b, d, e, and g). Lines that mainly produced weakly, or unstained cells were neglected (see i.e. Figure 4-2 c, f, h, and i).

4.2.3 Generation and selection of Axin mutant ES cell lines through Cre recombination

Selected parental ES cell lines carrying conditional alleles (i.e. $A1^{fl}$ and/or $A2^{fl}$), were then transiently transfected with the Cre-expressing pCAGGS-Cre-puro-IRES plasmid (Schnuetgen et al. 2006) to remove the *loxP*-flanked exon 2 by Cre mediated recombination. Figure 1-10 in the introduction shows a schema of the different Axin alleles used in this study before and after Cre mediated recombination.

Following the lipofection with Cre-carrying plasmid as described in Section 3.2.5 a range of different clones were picked for further analysis. The mouse ES cell lines generated were all analysed by PCR to confirm the successful removal of exon 2 in both Axins. Polymerase chain reaction (PCR) followed by Agarose gel electroporation was performed to determine the genotype of each cell line. Figure 4-3 shows the results of the genotyping PCR reactions. The status of the Axin1 allele was determined using two different primer sets (type A and B), Axin2 was tested using three different primer sets (type A, B and C) (see Figure 4-3 F for a schema). Primer set type A amplified a genomic region including parts of Exon 2. This primer set amplified the wild type and lacZ alleles (indistinguishable), as well as the slightly longer fl allele. To detect the knockout alleles, primer sets type B were used. These primers bound on either side of Exon 2 of Axin1 or 2. In case of a knockout, Exon 2 was removed so that a short PCR product was amplified using those primers. Unrecombined (fl) and wild type alleles produce much larger PCR products that did not always get amplified faithfully. To detect the $Axin2^{lacZ}$ allele primer set type C was used. A combination of one forward and two reverse primers amplified either the wild type and fl alleles (undistinguishable), or the lacZ alleles.

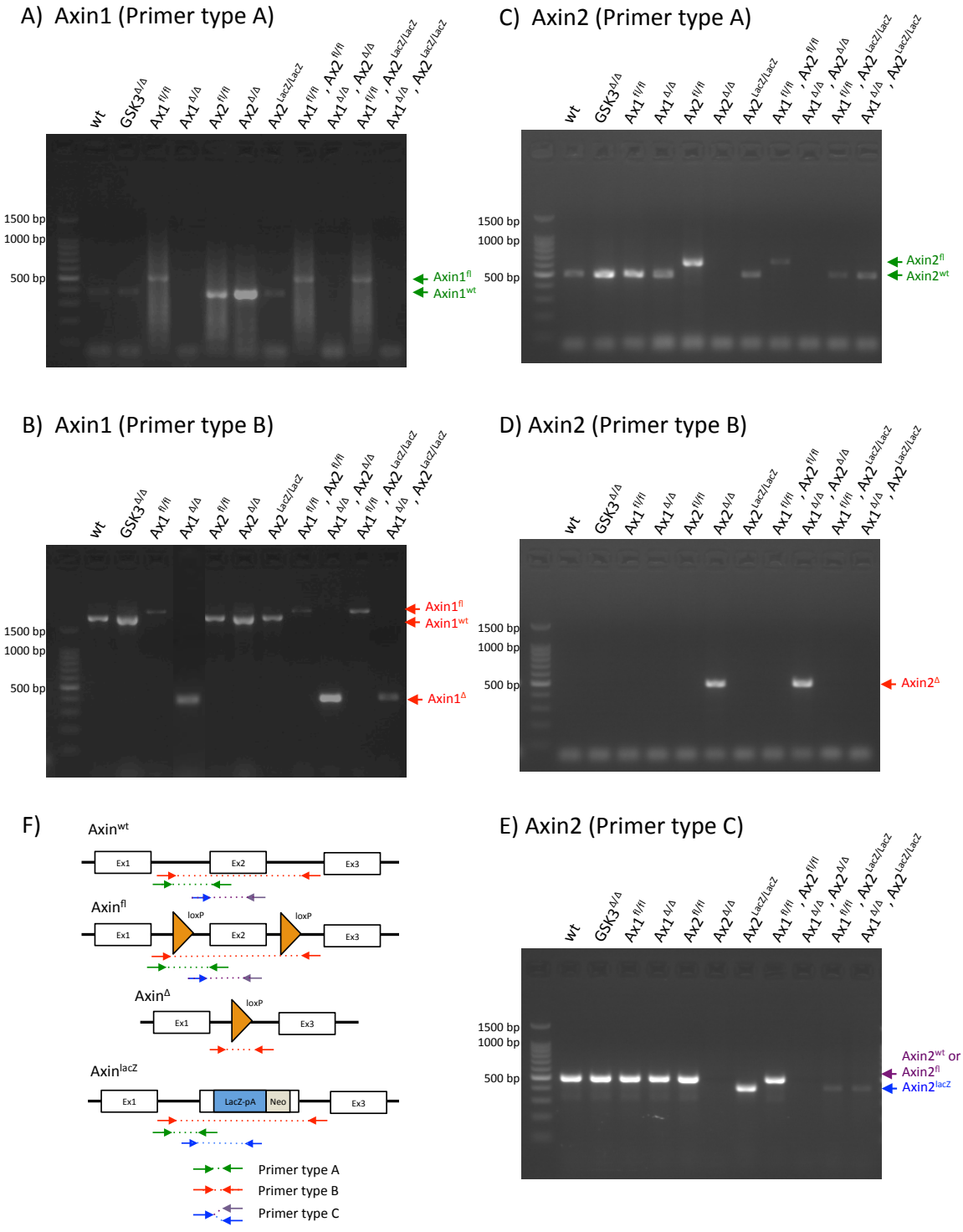
A) Axin1 (Primer type A)
wt
GSK3Δ/Δ
Ax1 fl/fl
Ax1 Δ/Δ
Ax2 fl/fl
Ax2 Δ/Δ
Ax2 LacZ/LacZ
Ax1 fl/fl , Ax2 fl/fl
Ax1 Δ/Δ , Ax2 Δ/Δ
Ax1 fl/fl , Ax2 LacZ/LacZ
Ax1 Δ/Δ , Ax2 LacZ/LacZ
1500 bp
1000 bp
500 bp
Axin1fl
Axin1wt
C) Axin2 (Primer type A)
Axin2fl
Axin2wt
B) Axin1 (Primer type B)
Axin1fl
Axin1wt
Axin1Δ
D) Axin2 (Primer type B)
Axin2Δ
F)
Axinwt
Ex1
Ex2
Ex3
Axinfl
loxP
AxinΔ
AxinlacZ
LacZ-pA
Neo
Primer type A
Primer type B
Primer type C
E) Axin2 (Primer type C)
Axin2wt or
Axin2fl
Axin2lacZ

Figure 4-3. Genotype of selected ES cell clones.
Five different PCR reactions were performed to test for the presence of wild type (wt), $Axin^{fl}$ ($Ax1^{fl/fl}$ or $Ax2^{fl/fl}$), $Axin^{\Delta/\Delta}$ ($Ax1^{\Delta/\Delta}$ or $Ax2^{\Delta/\Delta}$) and $Axin2^{lacZ}$ ($Ax2^{lacZ}$) alleles in the ES cell lines. The arrows indicate positive bands. **F)** The approximate position of the different primer sets used. Primer set type A (green, used in **A** and **B**) sits in Exon2 and upstream of the location of the first loxP site. This primer set nicely amplifies the wild type ($Axin1^{wt}$: 383 bp, $Axin2^{wt}$: 505 bp) or gene targeted allele ($Axin1^{fl}$: 531 bp, $Axin2^{fl}$: 643 bp) but has no product in case of the mutant ($Axin1^{\Delta}$ or $Axin1^{\Delta}$). The $Axin2^{lacZ}$ allele produces the same band as $Axin2^{wt}$. Primer set type B (red, used in **C** and **D**) sits right and left of the position of the *loxP* sites in each of the alleles and is very efficient in generating a PCR product for the mutant allele ($Axin1^{\Delta}$: 402 bp, $Axin2^{\Delta}$: 504 bp), but rarely amplifies the wild type ($Axin1^{wt}$: 2042 bp, $Axin2^{wt}$: 1854 bp), lacZ ($Axin2^{lacZ}$: 1854 bp), or gene targeted allele ($Axin1^{fl}$: 2190 bp, $Axin2^{fl}$: 1995 bp). Primer set type C (blue/purple used in **E**) consist of one forward, and two reverse primers that can either amplify the wild type ($Axin2^{wt}$: 497 bp) or lacZ ($Axin2^{lacZ}$: 400 bp) allele. The gene targeted allele $Axin2^{fl}$ produces the same band as the wild type allele using this primer set. PCR products were run alongside a 100 bp marker (Promega).

Using all five different primer sets the genotype of each cell line was determined (Figure 4-3).

In addition to the genotyping experiments cell lines grown in full medium (2i) were also analysed for alkaline phosphatase expression, as described in Section 4.2.2 (data not shown). We then selected 3 to 5 clones of each genotype for further analysis. Table 4-1 shows the genotype of the different parental, and Axin mutant, cell lines generated for this study.

In addition to the different Axin mutant ES cell lines we also analysed a GSK3 double mutant ES cell lines (Doble et al. 2007), which served as control for Wnt activation in ES cells.

4.3 Compensatory regulation of Axin

Since Axin1 and Axin2 are 44% identical and have been shown to be functionally equivalent in mouse development (Chia and Costantini 2005; Behrens et al. 1998) it might have been expected that Axin2 expression would have been upregulated following Axin1 loss since Axin2 has β-Catenin /TCF binding sites in its promoter region and loss of Axin1 would be expected to result in the induction of Wnt/β-Catenin signalling. Vice-versa, the constitutive expression of Axin1 might be expected to functionally compensate for Axin2 in contexts where Axin2 is expressed. To investigate the compensatory upregulation of a functional Axin, we performed gene expression analysis with primers that include parts of Exon 2 of either Axin1 or Axin2.

These experiments were also used to further confirm the loss of Exon 2 of both Axins, following Cre mediate recombination, because the primers could not detect any mRNA lacking this exon. As expected, qRT-PCR against exon 2 of *Axin1* mRNA could not detect Axin1 in $A1^{\Delta/\Delta}$; $A1^{\Delta/\Delta}$, $A2^{\Delta/\Delta}$; or $A1^{\Delta/\Delta}$ $A2^{lacZ/lacZ}$ ES cell lines grown in 1i medium (Figure 4-4 A), confirming successful knockout of Axin1 in all of those samples.

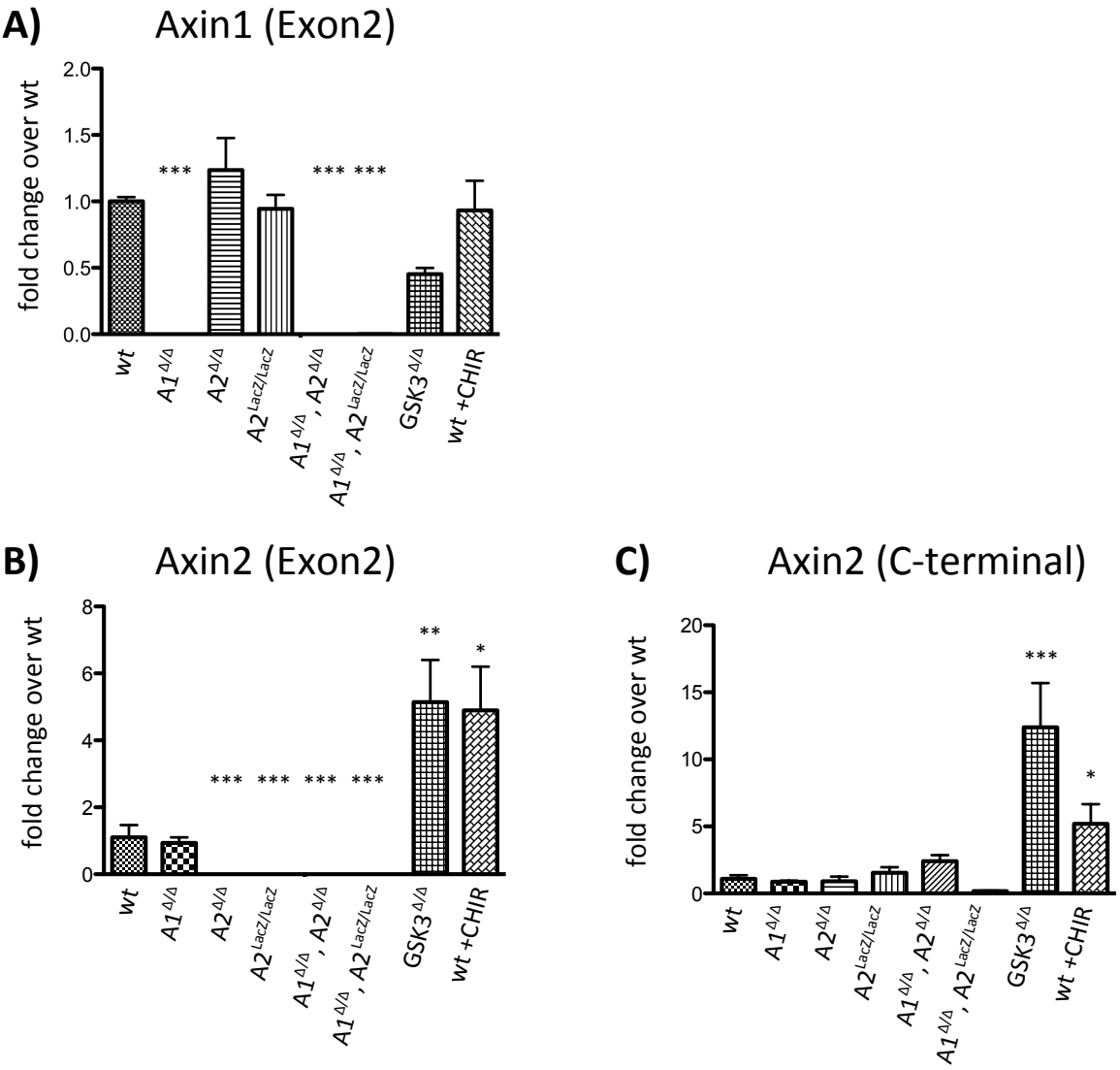

Figure 4-4. Expression of *Axin1* and *Axin2* mRNA in Axin mutant mouse ES cell lines.
A) Gene expression of *Axin1* with primers against a region including Exon 2. **B)** Gene expression of *Axin2* with primers against a region including Exon 2. **C)** Gene expression of Axin2 with primers against a C-terminal mRNA region. Data are presented as the mean fold change of wt ES cells relative to β-Actin. N=3, error bars: SEM, Significance levels are only shown compared to wt and were determined using one-way ANOVA and a post-hoc Tukey's test to compare between groups *: p<0.05, **: p<0.01, ***: p<0.001.

However, in the Axin2 mutant ES cells ($A2^{\Delta/\Delta}$ and $A2^{lacZ/lacZ}$), as well as the $GSK3^{\Delta/\Delta}$ and wild type cells treated with the GSK3 inhibitor CHIR9021 (wt + CHIR), *Axin1* mRNA levels were not significantly changed compared to wt cells grown in 1i. qRT-PCR against Exon 2 of *Axin2* mRNA did also not show any remaining exon 2 in both single Axin2 mutants ($A2^{\Delta/\Delta}$ and $A2^{lacZ/lacZ}$) as well as the Axin double mutants ($A1^{\Delta/\Delta}$, $A2^{\Delta/\Delta}$ and $A1^{\Delta/\Delta}$, $A2^{lacZ/lacZ}$) (Figure 4-4 B). In $A1^{\Delta/\Delta}$ ES cells *Axin2* expression did not change.

The effect of the loss of Axin1 on Axin2 expression was a little surprising, since *Axin2* expression is usually upregulated as a consequence of high Wnt signalling (Jho et al. 2002; Lustig et al. 2002). Due to the important role in β-Catenin degradation, the loss of both Axins should increase Wnt signalling and activate the negative feedback loop that promotes *Axin2* expression. Indeed, *Axin2* mRNA levels were significantly increased in the $GSK3^{\Delta/\Delta}$ and wt+ CHIR control ES cells compared to wt cells (Figure 4-4 B). Gui-Jie Feng detected a slight compensatory upregulation of *Axin2* expression in the liver following Axin1 loss (Feng et al. 2012) this could not be seen in the ES cells.

To enable a further investigation into a compensatory upregulation of *Axin2,* we decided to utilise a different primer set that detects a C-terminal region of *Axin2* mRNA independent of the recombination event. Data from this qRT-PCR reaction confirmed the overexpression of *Axin2* in $GSK3^{\Delta/\Delta}$ and wt + CHIR control lines. But again, *Axin2* gene expression was not significantly altered in any of the Axin single or double mutant ES cells (Figure 4-4 C).

Here, we could show that *Axin1* and *Axin2* expression were not increased following loss of the complementary allele. However, we are not in a position to comment on the relative levels of *Axin1* in comparison to *Axin2* mRNA or on the protein levels. Overall Axin2 protein levels are believed to be lower than Axin1, even upon Wnt stimulation (Bernkopf et al. 2015).

4.4 Effects of Axin loss on Wnt signalling

The results shown above indicate that neither the loss of Axin1, nor the loss of Axin2, led to a compensatory upregulation of mRNA of the other homologue. Given the importance of *Axin2* expression, as a negative feedback loop of Wnt activation (Lammi et al. 2004; Lustig et al. 2002), and the lack thereof in Axin mutant ES cells, we decided to further analyse the influence of Axin loss on the Wnt signalling pathway.

Both Axins are scaffolds for the formation of the β-Catenin destruction complex, which directly marks β-Catenin for proteasomal degradation. Loss of Axin protein should prevent the efficient formation of the destruction complex and inhibit the proteasomal degradation of β-Catenin.

Doble and his colleagues investigated the effect of loss of other members of the destruction complex, namely *GSK3α* and *GSK3β,* and found that the loss of both *GSK3s* led to the hyperactivation of Wnt signalling in mouse ES cells (Doble et al. 2007). Following complete loss of GSK3 protein, cytosolic and nuclear levels of β-Catenin and TCF dependent transcription drastically increased. Similar effects were seen in APC mutant ES cells lines, which like Axin serves as a scaffold for the β-Catenin destruction complex (Kielman et al. 2002). In Axin mutant ES cell lines, β-Catenin would be expected to accumulate, translocate into the nucleus, and activate downstream target gene expression.

4.4.1 β-Catenin localisation following Axin loss

We performed immunofluorescence analysis on the Axin mutant mouse line in 1i conditions to investigate if Axin loss indeed causes nuclear translocalisation of β-Catenin in the absence of ectopic Wnt stimulation. In wild type ES cells in 1i, β-Catenin was detected at the cell membrane and diffusely in the cytosol (Figure 4-5, wt). Interestingly, we observed no clear changes in β-Catenin localization in either of the single-mutant lines (Figure 4-5, $A1^{\Delta/\Delta}$; $A2^{\Delta/\Delta}$; and $A2^{lacZ/lacZ}$).

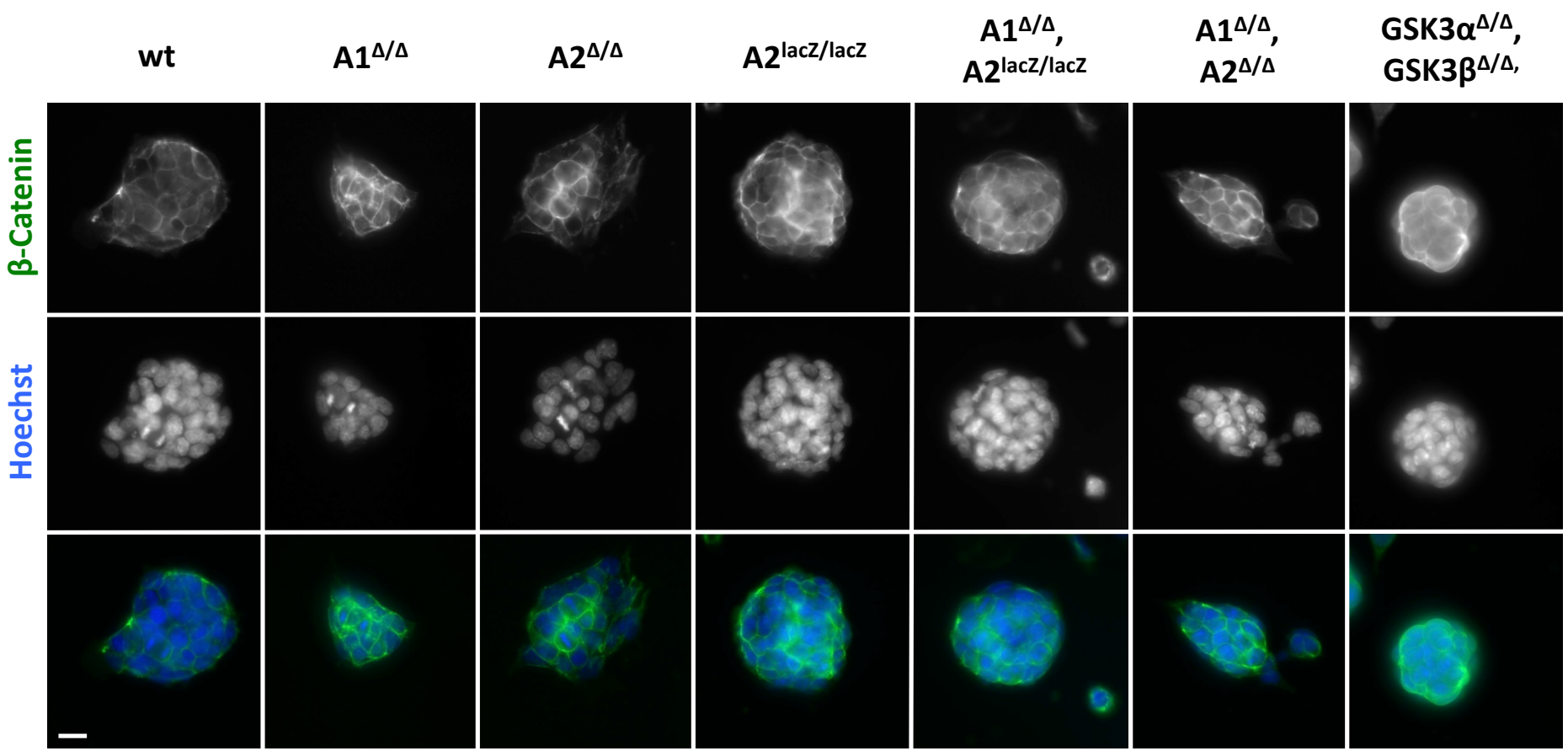

Figure 4-5. β-Catenin localisation in Axin mutant ES cells.
ES cells of the indicated genotype were grown in 1i medium, fixed, and stained for total β-Catenin (Alexa488, top) and nuclei (Hoechst 33342, middle). A merge of both channels is shown at the bottom. Scale bar: 20 µm.

Surprisingly, the loss of both Axin alleles ($A1^{\Delta/\Delta}$, $A2^{\Delta/\Delta}$ or $A1^{\Delta/\Delta}$, $A2^{lacZ/lacZ}$) did not seem to result in a strong nuclear β-Catenin signal (Figure 4-5 $A1^{\Delta/\Delta}$, $A2^{\Delta/\Delta}$; and $A1^{\Delta/\Delta}$, $A2^{lacZ/lacZ}$).

However, there was an increase in β-Catenin staining intensity, in $GSK3^{\Delta/\Delta}$ cells (Figure 4-5 $GSK3\alpha^{\Delta/\Delta}$, $GSK3\beta^{\Delta/\Delta}$) although the change in intensity was not simple to assess based on immunocytochemistry. When taken across the allelic series, there was some visual indication of a general increase in β-Catenin staining intensity although this could not be quantified in this assay format. A second factor making it hard to assess the staining intensity was the observation that ES cells lacking a greater number of Axin alleles (or GSK3 mutant alleles) had a different 'rounder' colony morphology that was characteristic of undifferentiated colonies, even when grown in 1i.

4.4.2 TCF dependent transcription

To assess whether the increases in β-Catenin staining intensity correlated with its activity in the nucleus, we used a luciferase-based reporter system to measure TCF-mediated transcription. ES cells were transiently transfected with a super8xTOPFlash plasmid containing 7 TCF/LEF binding sites upstream of a luciferase reporter (Veeman et al. 2003). Control cells were transfected with a super8xFOPFlash plasmid, which carries 6 mutant TCF/LEF binding sites. Luciferase activity was measured for each cell line and normalised for unspecific binding (super8xFOPFlash control) and transfection efficiency (co-transfected pRL- TK Renilla - plasmid). TCF-reporter activity was assessed after treatments with or without Wnt-3a-conditioned medium for 24 h. Wt cells and Axin single mutants exhibited the same basal levels of TCF-reporter activity in Wnt untreated conditions (Figure 4-6). Furthermore, they all responded to the Wnt3a treatment in a similar fashion. While the $A1^{\Delta/\Delta}$, $A2^{\Delta/\Delta}$ double mutant cells showed an equivalent TCF reporter activity pattern as observed in the wt and the single mutants, the $A1^{\Delta/\Delta}$, $A2^{lacZ/lacZ}$ cells exhibited an overall increased level of luciferase activity. However, this was not statistically significant using one-way ANOVA and post-hoc Tukey's test.

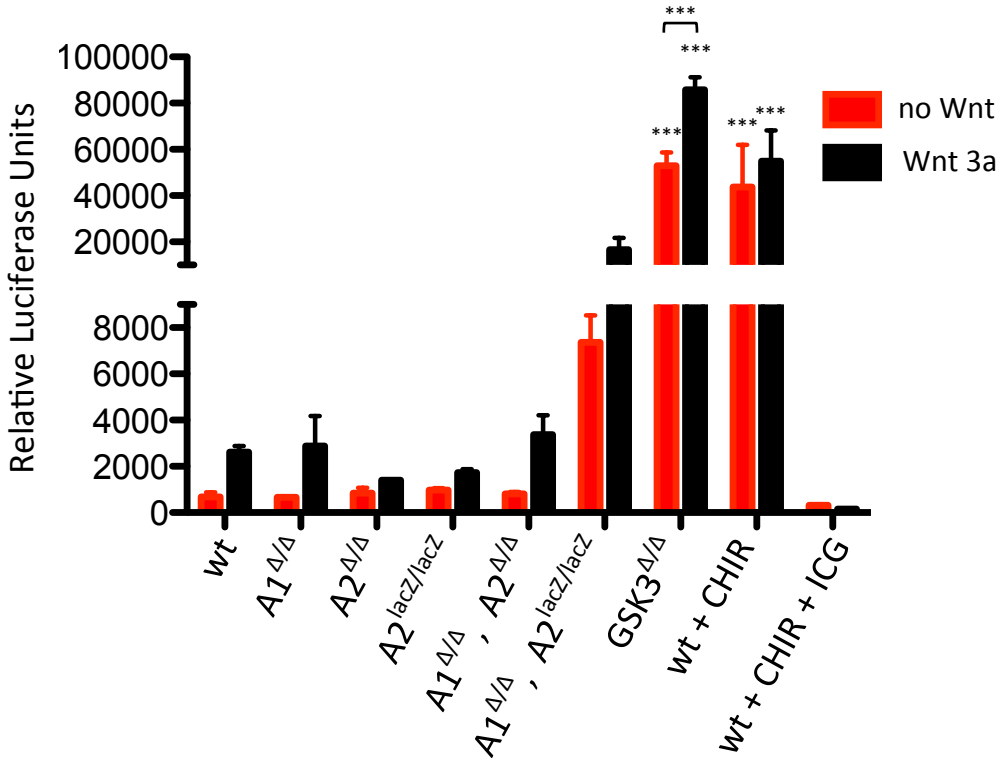

Figure 4-6. TCF dependent transcription and gene expression changes in Axin mutant ES cells.
TCF reporter assay on ES cell lines transient transfection of super8xTOPFlash plasmid treated for 24h with Wnt 3a conditioning (black bars) or control medium (red bars) both in 1i medium. Control ES cells were treated with CHIR99021 (GSK3 inhibitor) or CHIR + ICG001 (β-Catenin/TCF binding inhibitor). Each bar represents the average from three independent samples; data were normalized to non-specific super8xFOPFlash and constitutive Renilla controls. Significance levels are shown compared to wt without Wnt or between Wnt treated and untreated samples of the same genotype. Error bars: SEM, ***: $p<0.001$. Determined using one-way ANOVA and post-hoc Tukey's test to compare between groups.

GSK3 double mutant, as well as the wt + CHIR99021 treated control cells showed a drastic and highly significant ($p<0.001$) increase in TCF reporter activity with and without Wnt 3a treatment. In wt+ CHIR cells additionally exposed to ICG001, an inhibitor of TCF-β-Catenin interaction, TCF activity was almost abolished.

4.4.3 Wnt target gene expression

We wanted to test the expression of endogenous Wnt/β-Catenin target genes in our ES cells. Usually, *Axin2* is the gene of choice to determine Wnt signalling activity by q-RT PCR. In Section 4.3 we have already shown, that even the loss of both Axin homologues had no effects on *Axin2* expression (Figure 4-4 B, C). Since *Axin2* itself was mutated in some of our ES cells, we also examined the expression of the Wnt target gene c-Myc (He et al. 1998). Interestingly, none of the ES cell samples analysed in this study, showed any effect on *c-Myc* expression, including those ES cells that had been treated with GSK3 inhibitor, or those that lacked both GSK3 homologues (Figure 4-7 A). However, since *c-Myc* is also a target of STAT3, which is activated through LIF in the culture medium (Kidder et al. 2008; Cartwright 2005), *c-Myc* expression might be uncoupled from Wnt activation in this context.

To study an alternative well-characterised Wnt target, we analysed *Cdx1* expression in Axin mutant ES cells. In mouse embryonic stem cells, the expression of the homeobox gene *Cdx1* can be induced by Wnt stimulation (Lickert et al. 2000). In contrast to *Axin2* and *c-Myc* expression, *Cdx1* showed a strong response to Axin deletion. qRT-PCR data showed no changes in *Cdx1* expression as the result of the loss of one of the Axin genes (Figure 4-7 B). In both Axin double mutants, however, *Cdx1* expression levels were drastically increased. This increase was highly significant ($P<0.01$) and occurred to a similar extent to that observed in $GSK3^{\Delta/\Delta}$ and wt + CHIR control cells.

We also tested the expression levels of *β-Catenin,* in order to assess the involvement of translation on the abundance of β-Catenin protein, which is available to take part in any Wnt signalling activity.

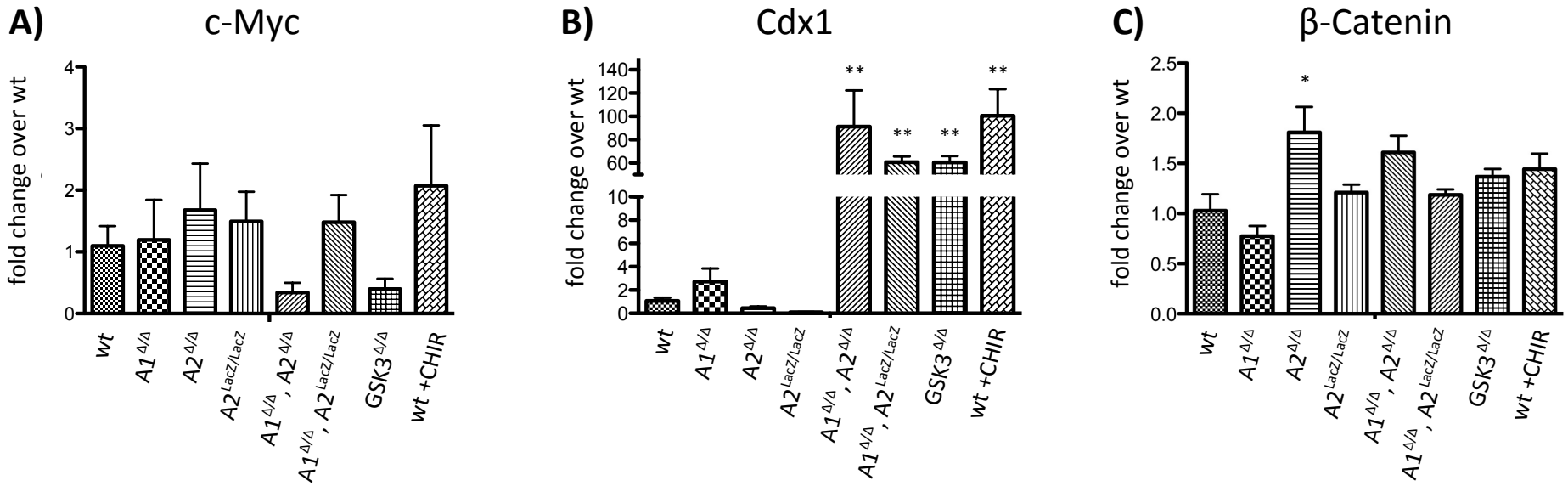

Figure 4-7. Expression of β-Catenin and Wnt target genes in Axin mutant mouse ES cell lines.
Axin mutant ES cells grown in 1i medium were tested for their expression levels of the Wnt target genes *c-Myc* **(A)** and *Cdx1* **(B),** and *β-Catenin* itself **(C).** Data are presented as the mean fold change of wt ES cells relative to β-Actin. N=3, error bars: SEM, Significance levels are only shown compared to wt and were determined using one-way ANOVA and a post-hoc Tukey's test to compare between groups *: p<0.05, **: p<0.01.

This data only showed slight fluctuations in *β-Catenin* mRNA levels in response to Axin loss (Figure 4-7 C). In Axin2$^{\Delta/\Delta}$ ES cells a marginally significant increase was found ($p< 0.05$). Since none of the other experiments examining Wnt response found any significant increase, we assumed this fluctuation not to be of physiological importance.

4.4.4 β-Catenin protein levels

The data shown in the previous experiments, with the exception of *Cdx1* expression, failed to show an influence of Axin loss on Wnt signalling in embryonic stem cells, similar to the one found in GSK3 or APC mutant ES cells (Doble et al. 2007; Kielman et al. 2002). Since β-Catenin is the main player in canonical Wnt signalling (see Section 1.3.1), we continued by quantifying the levels of β-Catenin protein and pools of β-Catenin with selected post-translational modifications. Table 4-2 provides a summary of β-Catenin phosphorylation sites together with the corresponding Kinases and suggested functions.

Post-translational modifications of β-Catenin, including phosphorylation, influence its ability to interact with other proteins (Kikuchi et al. 2006; Harris and Peifer 2005). Together with total protein levels, binding partner influence the subcellular localisation and activity of β-Catenin. Axin, as a member of the β-Catenin destruction complex (see Section1.3.1), as well as scaffold protein for many cellular kinases (see Section 1.3.3), could be involved in the regulation of a wide variety of post-translational modifications of β-Catenin.

Table 4-2. β-Catenin phosphorylation sites and effects.

SITE	KINASE	FUNCTION
β-Catenin in the destruction complex		
S45	CK1 CDK6	Initial phosphorylation of β-Catenin in the destruction complex priming for subsequent GSK3 mediated phosphorylation of Serine 33, 37, and T41 (Amit et al. 2002; C. Liu et al. 2002; Park et al. 2007).
T41	GSK3, CDK2	First phosphorylation site for GSK3 following priming at S45 by CK1 (Hagen et al. 2002; C. Liu et al. 2002; Park et al. 2004).
S33	GSK3, CDK2	Subsequent phosphorylation by GSK3. Phospho Ser33 together with P-Ser37 allows the interaction of β-Catenin with the β-Propeller domain of β-TrCP for subsequent ubiquitination and proteasomal degradation (Orford et al. 1997; Wu et al. 2003; Park et al. 2004).
S37	GSK3, CDK2	See S33.
Influencing E-Cadherin binding		
Y142	Fyn, Fer, Met	Reduced of β-Catenin/E-Cadherin binding and increased nuclear translocation and transcription (Piedra et al. 2003)
Y654	Scr 186, ErbB2, Met	P-Y654 inhibits β-Catenin/E-cadherin interaction leading to the dissociation of the complex and E-Cadherin degradation resulting in β-Catenin translocation into the nucleus and target activation (Roura et al. 1999; Papkoff and Aikawa 1998; Zeng et al. 2006).
Other		
S33/S37/T41	PKCα	Non canonical inhibition of Wnt/ β-Catenin signalling (Gwak et al. 2006).
S552	AKT PKA	Increased nuclear translocation and transcription and preventing ubiquitination (Taurin et al. 2006; Fang et al. 2007; Taurin et al. 2008).
S675	AKT PKA	see S552

Table was adapted from Lloyd-Lewis (2011)

Using a bead-based multiplex array for different β-Catenin pools (Luckert et al. 2011; Groll et al. 2015), we quantified β-Catenin levels in lysates of Axin mutant ES cell lines with the help of Oliver Poetz. In an immuno-sandwich assay, a panel of antibodies against different post-translationally modified pools of β-Catenin were bound to different micro beads to pull-down β-Catenin from ES cell lysates. A pan- β-Catenin antibody was then used to quantify β-Catenin levels in each pool. Figure 4-8 A provides a schematic of the assay setup. A panel of antibody-coated beads could then be used to detect different β-Catenin pools from the same sample.

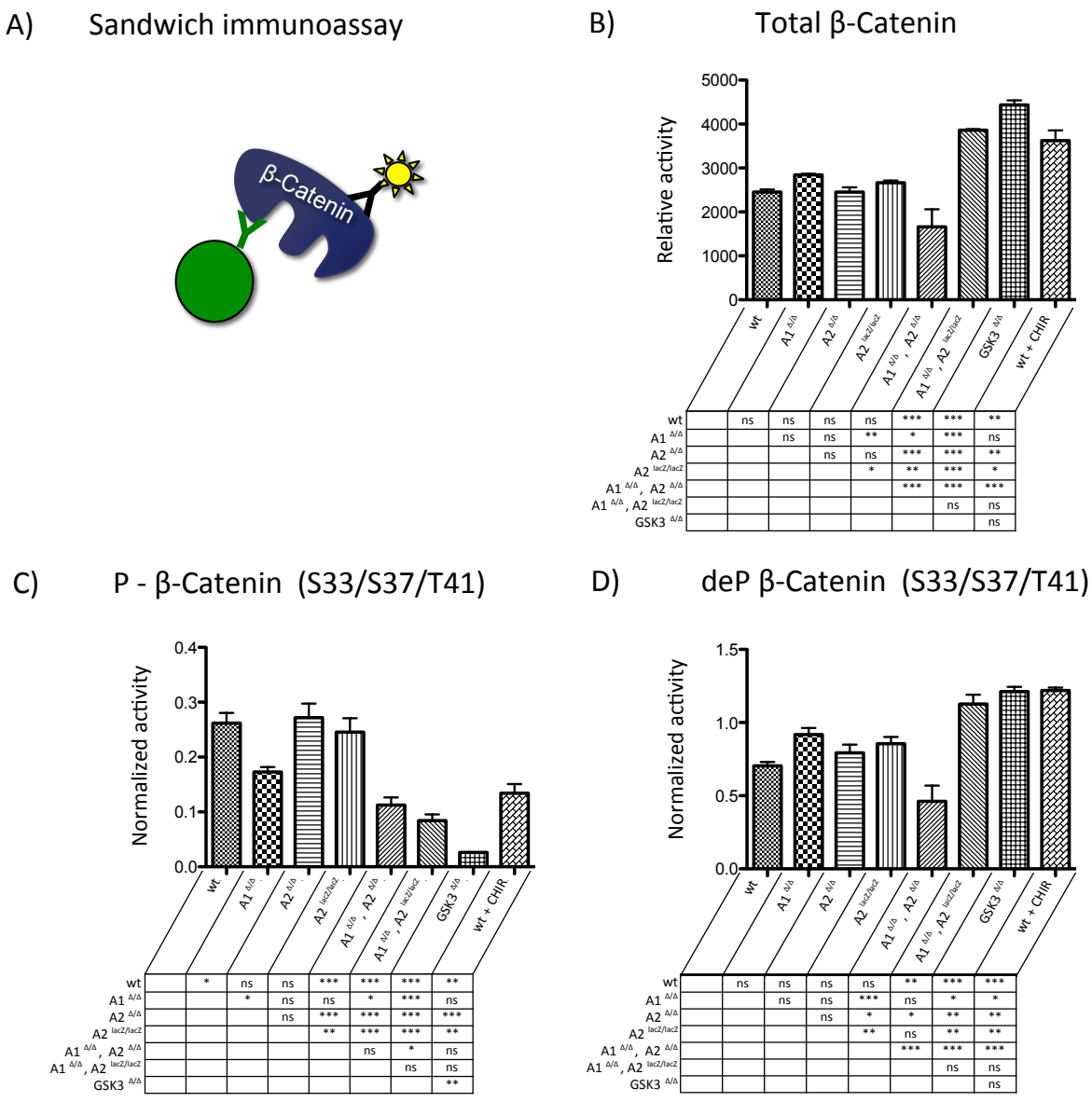

Figure 4-8. Phospo-, dePhospo S33/S37/T41 and total β-Catenin levels in Axin mutant ES cell lines.

Protein lysates from ES cell lines grown in 1i medium were analysed for different β-Catenin pools in a bead-based multiplex sandwich immunoassay. **A)** Schematic representation of the assay. Antibodies against differently post-translational modified β-Catenin were bound to fluorescent beads. Captured pan β-Catenin was then detected with a labelled antibody for total β-Catenin. **B)** Total β-Catenin levels found in the cell lysates. All following pools were then normalized to total levels. **C)** All β-Catenin phosphorylated at Serine 33 and 37 and Threonine 41. **D)** Pool of β-Catenin not phosphorylated at Serine 33 and 37 and Threonine 41. Data were obtained from 3 biological samples from 10 µg cell lysates. Error bars: SEM. Data were analysed using a one-way ANOVA and a post-hoc Tukey's test to compare between groups *: p<0.05, **: p<0.01, ***: p<0.001.

Fist, we analysed the levels of total β-Catenin in the samples. As expected, $GSK3^{\Delta/\Delta}$ and wt + CHIR control ES cells had significantly increased levels of β-Catenin (Figure 4-8 B). The loss of one of the Axin homologues in $Axin1^{\Delta/\Delta}$; $Axin2^{\Delta/\Delta}$; or $Axin2^{lacZ/lacZ}$, did not change total β-Catenin levels compared to wt cells. The same was true for $Axin1^{\Delta/\Delta}$, $Axin2^{\Delta/\Delta}$ double mutants. In $Axin1^{\Delta/\Delta}$, $Axin2^{lacZ/lacZ}$ cell lines, however, total β-Catenin was significantly increased ($p<0.001$). The signal detected for total β-Catenin was used to normalise all subsequent β-Catenin pools.

Next, we analysed the β-Catenin pools phosphorylated at S33, S37, and T41. These phosphorylation sites are usually phosphorylated by GSK3 within the destruction complex to mark β-Catenin for ubiquitination and degradation (Hagen et al. 2002; C. Liu et al. 2002; Park et al. 2004). Indeed, loss of GSK3, as well as treatment of wt cells with a GSK3 inhibitor (CHIR99021), decreased $P^{S33/S37/T41}$- β-Catenin levels drastically.

Interestingly, the loss of Axin2 alone, did not change the pool of β-Catenin phosphorylated at S33/S37/T41, compared to wt cells; while this pool was significantly reduced in $Axin1^{\Delta/\Delta}$ ES cells lines ($p<0.05$, Figure 4-8 C). Compared to $Axin1^{\Delta/\Delta}$, the loss of the second Axin allele further decreased $P^{S33/S37/T41}$-β-Catenin (not significantly for $Axin1^{\Delta/\Delta}$, $Axin2^{\Delta/\Delta}$, but significantly for $Axin1^{\Delta/\Delta}$, $Axin2^{lacZ/lacZ}$ ($p<0.05$)).

The pool of active β-Catenin, without a phosphorylation at S33, S37, and T41, was also analysed. Here, only $Axin1^{\Delta/\Delta}$, $Axin2^{lacZ/lacZ}$ and control cell lines were increased in comparison to the wild type Figure 4-8 D). Single Axin mutants, as well as $Axin1^{\Delta/\Delta}$, $Axin2^{\Delta/\Delta}$ cell lines, did not have altered levels of dephosphospho- Serine 33, 37 and Threonine 41.

In the destruction complex, β-Catenin is phosphorylated by CK1 at Serine 45 to prime for subsequent phosphorylations by GSK3. According to research conducted in the group of Irit Alkalay, this phosphorylation is Axin dependent (Amit et al. 2002). Nonetheless, loss of Axin1 or Axin2 did not lead to a significant change of P^{S45}- β-Catenin levels in the immune-sandwich assay (Figure 4-9 A). The only significant reduction was found in $Axin1^{\Delta/\Delta}$, $Axin2^{\Delta/\Delta}$ ES cell lines ($p<0.01$).

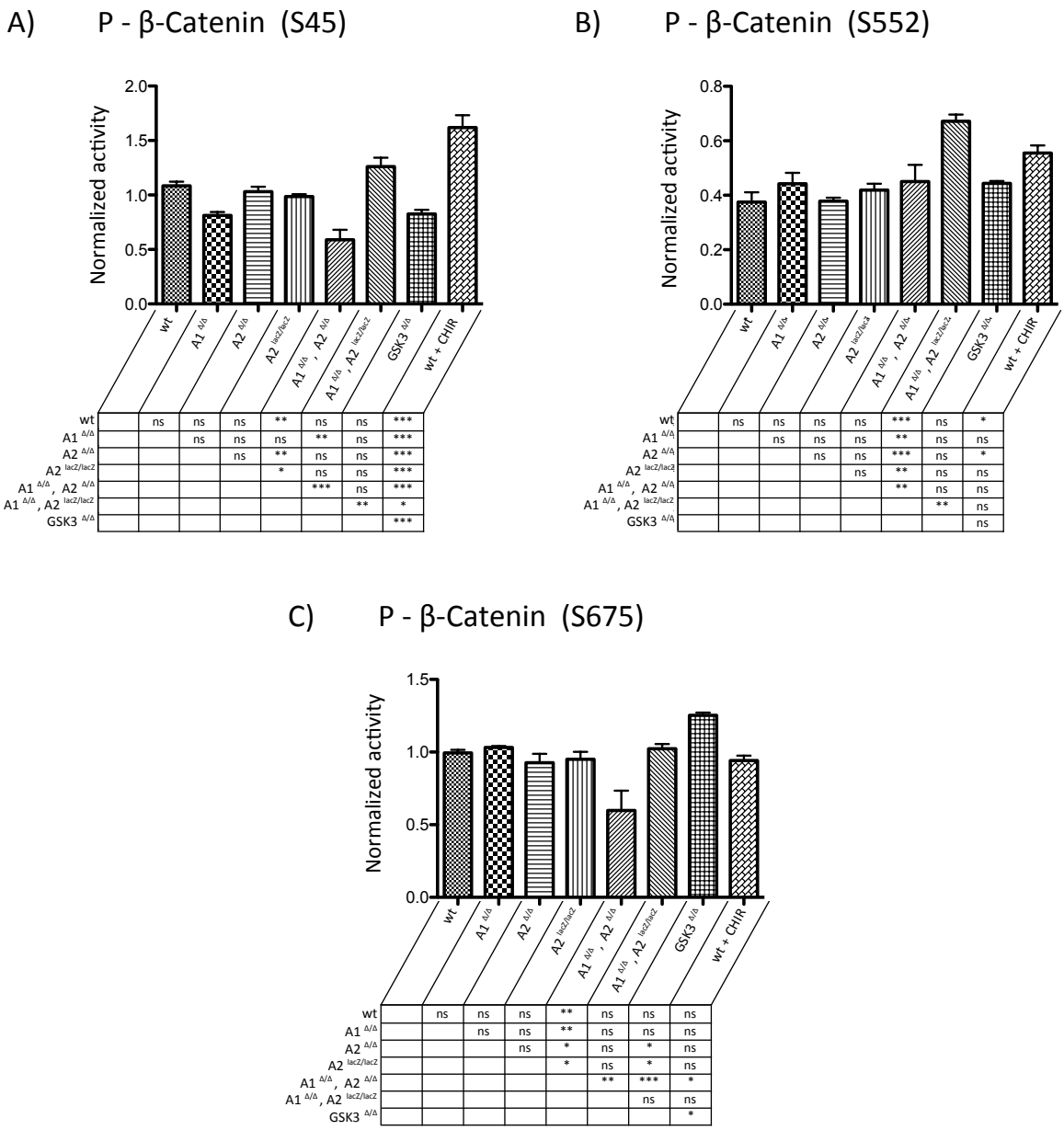

Figure 4-9. Phosphorylated pools of β-Catenin found in lysates of Axin mutant ES cell lines.
A) Pool of β-Catenin phosphorylated at Serine 45. **B)** β-Catenin phosphorylated at Serine 552. **C)** β-Catenin pool phosphorylated at Serine 675. **D)** Schematic representation of the assay. Antibodies against differently post-translational modified β-Catenin were bound to fluorescent beads. Capture β-Catenin was then detected with a labelled antibody for total β-Catenin. Data were obtained from 3 biological samples from 10 µg cell lysates. Error bars: SEM. Data were analysed using a one-way ANOVA and a post-hoc Tukey's test to compare between groups *: p<0.05, **: p<0.01, ***: p<0.001.

Interestingly, while GSK3 double knockouts did not have any effect on PS45 levels, treatments of wt ES cells with a GSK3 inhibitor actually increased P^{S45}- β-Catenin levels.

In addition to the N-terminal phosphorylations of β-Catenin, we also quantified C-terminal phosphorylation at Serine 552 and 675. β-Catenin phosphorylation at these sites, by PKA (Protein kinase A) and Akt (Protein kinase B), have been linked to the inhibition of ubiquitination and increased TCF-4 dependent transcription (Taurin et al. 2006; Fang et al. 2007; Taurin et al. 2008). In Axin single mutant ES cells lines, neither the pool of P^{S552} - β-Catenin nor P^{S675}- β-Catenin was significantly changed (Figure 4-9 B, C). The data for Axin double mutant cells was more complex. While P^{S552} was increased in $Axin1^{\Delta/\Delta}$, $Axin2^{lacZ/lacZ}$ but stayed at wt levels in $Axin1^{\Delta/\Delta}$, $Axin2^{\Delta/\Delta}$ (Figure 4-9 B), P^{S675} was decreased in $Axin1^{\Delta/\Delta}$, $Axin2^{\Delta/\Delta}$ but was unchanged in $Axin1^{\Delta/\Delta}$, $Axin2^{lacZ/lacZ}$ (Figure 4-9 C). GSK3 double knockout and CHIR treatment had no strong effects on those phosphorylation sites.

Next, we tested the abundance of 'free' β-Catenin; the endogenous pool of β-Catenin that has been suggested to be 'available' (i.e. not in a complex) to drive transcription of target genes. The assays for 'free' β-Catenin was performed as part of the multiplex system using bait-proteins in a miniaturized pull-down assay of β-Catenin with GFP-tagged-fusion proteins (Groll et al. 2015). The bait-proteins contained the β-Catenin binding sequences of E-Cadherin (ECT, E-Cadherin cytosolic tail), TCF4, or ICAT (inhibitor of β-Catenin). Figure 4-10 E shows a schematic of the GFP-pull-down assays.

In all three assays detecting cellular β-Catenin, the $GSK3^{\Delta/\Delta}$ and wt + CHIR99021 control cell lines showed significantly increased β-Catenin pools (Figure 4-10 A, B, C). Among the Axin mutant ES cells lines, the same trend was observed in both of the Axin double mutant ES cell lines, as well as in Axin1 single mutants, although this was not always statistically significant in a one-way ANOVA and post-hoc Tukey's test. Axin2 single mutants ($Axin2^{\Delta/\Delta}$ and $Axin2^{lacZ/lacZ}$) always stayed at wt levels. In $Axin1^{\Delta/\Delta}$ cells, pull-down with GFP-ECT revealed a significant increase of cellular β-Catenin ($p<0.01$).

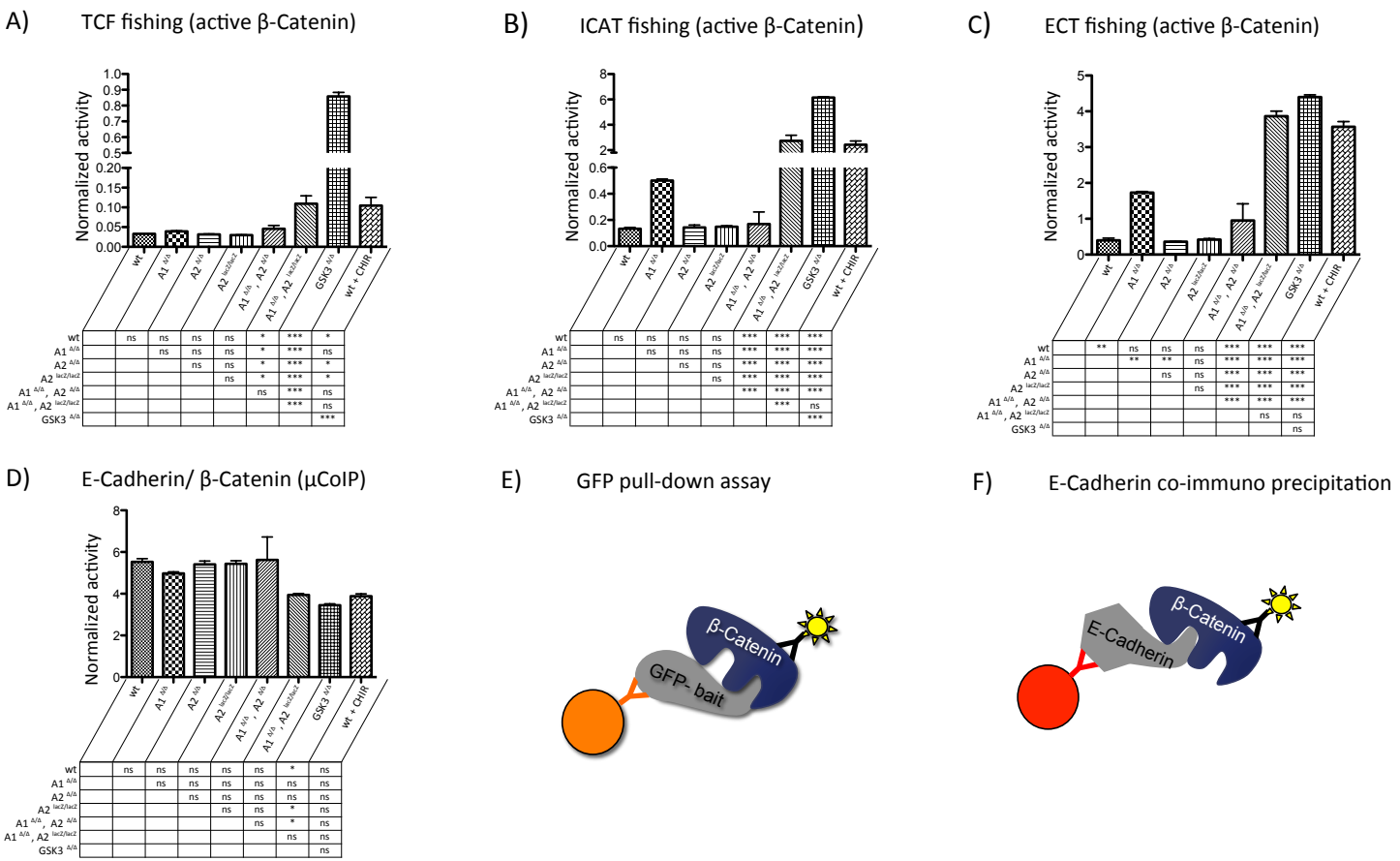

Figure 4-10. Protein-protein interaction and co-immunoprecipitation assays.
Protein lysates from ES cell lines grown in 1i medium were analysed for different β-Catenin pools in a bead-based multiplex sandwich immunoassay. **A-C)** Protein-protein interaction assay to detected 'active' pools of β-Catenin levels found in the cell lysates. **E)** GFP-tagged bait proteins (TCF4 **(A)**, ICAT **(B)** and ECT **(C)**) were captured on fluorescent beads with anti-GPF antibodies and used to pull down 'active' β-Catenin pools from the samples. **D)** Co-immunoprecipitation to detect E-Cadherin bound β-Catenin in the ES cell lysates. **F)** Anti-E-Catherin antibody on a bead was used for the co-immunoprecipitation assay. Data were obtained from 3 biological samples from 10 µg cell lysates and was normalized to total β-Catenin levels. Error bars: SEM. Data were analysed using a one-way ANOVA and a post-hoc Tukey's test to compare between groups. *: p<0.05, **: p<0.01, ***: p<0.001.

'Free' β-Catenin pools in Axin1$^{\Delta/\Delta}$, Axin2$^{lacZ/lacZ}$ lysates were significantly increased in all three pull-down assay to varying degrees. Overall, the increase in 'free' β-Catenin levels was most pronounced when ICAT (Figure 4-10 B) served as the bait-protein, and to a lesser extent, when ECT (Figure 4-10 C) or TCF4 (Figure 4-10) were used (see also Table 4-3). An interesting observation was the comparison between the β-Catenin levels in Axin1$^{\Delta/\Delta}$, Axin2$^{lacZ/lacZ}$ lysates, compared to both of the control groups (GSK3$^{\Delta/\Delta}$ and wt +CHIR). In all three experiments, CHIR treated cells showed the same level of 'free' β-Catenin as observed in the Axin1$^{\Delta/\Delta}$, Axin2$^{lacZ/lacZ}$, while the levels GSK3$^{\Delta/\Delta}$ were usually higher. TCF-pull-down showed the most striking difference between the samples (Figure 4-10 A). The level of β-Catenin in GSK3$^{\Delta/\Delta}$ lysates was increased by approximately 8 fold over wt + CHIR and Axin1$^{\Delta/\Delta}$, Axin2$^{lacZ/lacZ}$ cells (Table 4-3).

Table 4-3. Fold changes in GFP-pull-down assays

	TCF	ICAT	ECT
GSK3$^{\Delta/\Delta}$ / wt	25.89 ± 1.17	46.79 ± 4.88	11.53 ± 2.33
A1$^{\Delta/\Delta}$, A2$^{lacZ/lacZ}$ / wt	3.30 ± 0.91	20.75 ± 5.53	10.14 ± 2.10
GSK3$^{\Delta/\Delta}$ / A1$^{\Delta/\Delta}$, A2$^{lacZ/lacZ}$	8.21 ± 2.17	2.39 ±0.53	1.16 ± 0.06

Taken together, the results of the assays for 'free' β-Catenin suggested that levels of 'free' β-Catenin can be induced following Axin, or GSK3 loss and via GSK3 inhibition. However the different formats of the binding assays showed quantitatively (and possibly qualitatively) different outputs suggesting that the concept of 'free' β-Catenin may not be as simple as initially proposed and that 'free' β-Catenin may comprise a set of protein complexes that have different subsets of 'free' sites for binding to experimental ligands. This hypothesis is being explored by ongoing experiments. Furthermore, the results show significant differences between different Axin allele combinations. Loss of Axin1 alone did in some assay formats resulted in increased 'free β-Catenin ', while loss of Axin2 did not. However, only combinations of Axin1 with the Axin2^{lacZ} allele resulted in changes to 'free' β-Catenin levels in

all assay formats. It should be noted, that the allelic response pattern observed in the TCF-pull-down (presumably representing β-Catenin that is free to bind TCF4; although not already bound) matched the pattern of data obtained in the TCF reporter assay described earlier (see Section 4.4.2).

Finally, we analysed the pool of β-Catenin in complex with endogenous E-Cadherin. In this assay an E-Cadherin antibody, as well as a pan β-Catenin antibody, were used in a co-immuno-precipitation experiment (Figure 4-10 F). The amounts of E-Cadherin/ β-Catenin complexes not significantly altered between the different lysates (Figure 4-10 D).

4.4.5 Summary of the effects of Axin loss on Wnt signalling activity

Taken together, the data obtained from β-Catenin immunocytochemistry, TCF-reporter activity, gene expression, and protein analysis showed the following effects of Axin loss on Wnt/ β-Catenin signalling

I Axin1$^{\Delta/\Delta}$

In Axin1$^{\Delta/\Delta}$ ES cell lines, TCF reporter activity and Wnt target gene expression analysis did not show any changes compared to wt ES cells. However, the pool of $P^{S33/S37/T41}$ was slightly decreased together with a small increase in 'free' β-Catenin, measured in an ECT pull-down assay.

This data suggests, that Axin1 loss in ES cells disturbs the activity of the β-Catenin destruction complex slightly.

II Axin2$^{\Delta/\Delta}$

Wnt/β-Catenin signalling activity was unchanged in single Axin2$^{\Delta/\Delta}$ ES cell lines in all the assays performed here.

III Axin2$^{lacZ/lacZ}$

Similar to Axin2$^{\Delta/\Delta}$, the Axin2$^{lacZ/lacZ}$ variant had no detected effects on Wnt/β-Catenin signalling on its own.

IV Axin$^{\Delta/\Delta}$, Axin2$^{\Delta/\Delta}$

The loss of both conditional Axin homologue alleles in Axin1$^{\Delta/\Delta}$, Axin2$^{\Delta/\Delta}$ ES cell lines, showed some Wnt/β-Catenin signalling related effects. *Cdx1* expression levels were upregulated, and P$^{S33/S37/T41}$-as well as P^{S45}- β-Catenin levels were decreased. Simultaneously, P^{S675}- β-Catenin levels were also reduced.

V Axin$^{\Delta/\Delta}$, Axin2$^{lacZ/lacZ}$

Loss of both Axin genes in Axin1$^{\Delta/\Delta}$, Axin2$^{lacZ/lacZ}$ ES cell lines showed the strongest effect in regard to Wnt/β-Catenin signalling deregulation. *Cdx1* expression, total, deP$^{S33/S37/T41}$-, and P^{S552}- β-Catenin levels, and 'free' β-Catenin (in TCF, ICAT, and ECT pull-downs) were upregulated compared to wt cells. TCF reporter activity was also increased, although not significantly. Simultaneously, the pool of β-Catenin marked for degradation by phosphorylation at S33, S37, and T41 in the destruction complex was decreased.

Importantly, the effects of Axin double mutants were much stronger in cells carrying the Axin2$^{lacZ/lacZ}$ allele, suggesting that both versions of Axin2 mutations were not equivalent (see also Section 4.8.4).

4.5 Effects of Axin mutations on cell cycle regulation and proliferation

While on the one hand, overexpression of β-Catenin was reported to reduce cell viability in fibroblast and epithelial cell lines (Kim et al. 2000), on the other hand, Axin1 deletion in mouse livers was linked to increased proliferation and the upregulation of cell cycle related gene expression (Feng et al. 2012). Furthermore, Axin1 and Axin2 function have been linked to actions at the MTOC and G2/M cell cycle progression while β-Catenin /TCF target genes (e.g. c-Myc) have been linked to G1/S cell cycle progression. Therefore, we decided to assess proliferation, cell viability, and apoptosis levels in Axin mutant ES cells.

4.5.1 S-phase cell cycle progression in ES cells

First, we incubated ES cells grown in 1i medium with 10 μM EdU for 1 h to label cells in S-Phase. EdU incorporation was the visualized using the Click-iT® EdU Alexa Fluor® 488 Imaging Kit (Invitrogen), cells were counter staining with Hoechst 33342 and imaged on a fluorescent microscope (Figure 4-11 A).

The proportion of EdU positive cells was then scored for each ES cell line. We found a trend towards a stepwise increase in EdU positive cells following the loss of Axin alleles (Figure 4-11 B). This indicated that Axin mutant ES cells might proceed faster through the cell cycle than the Axin wt parental control cells. However, the increase in S-phase labelled cells was not statistically significant.

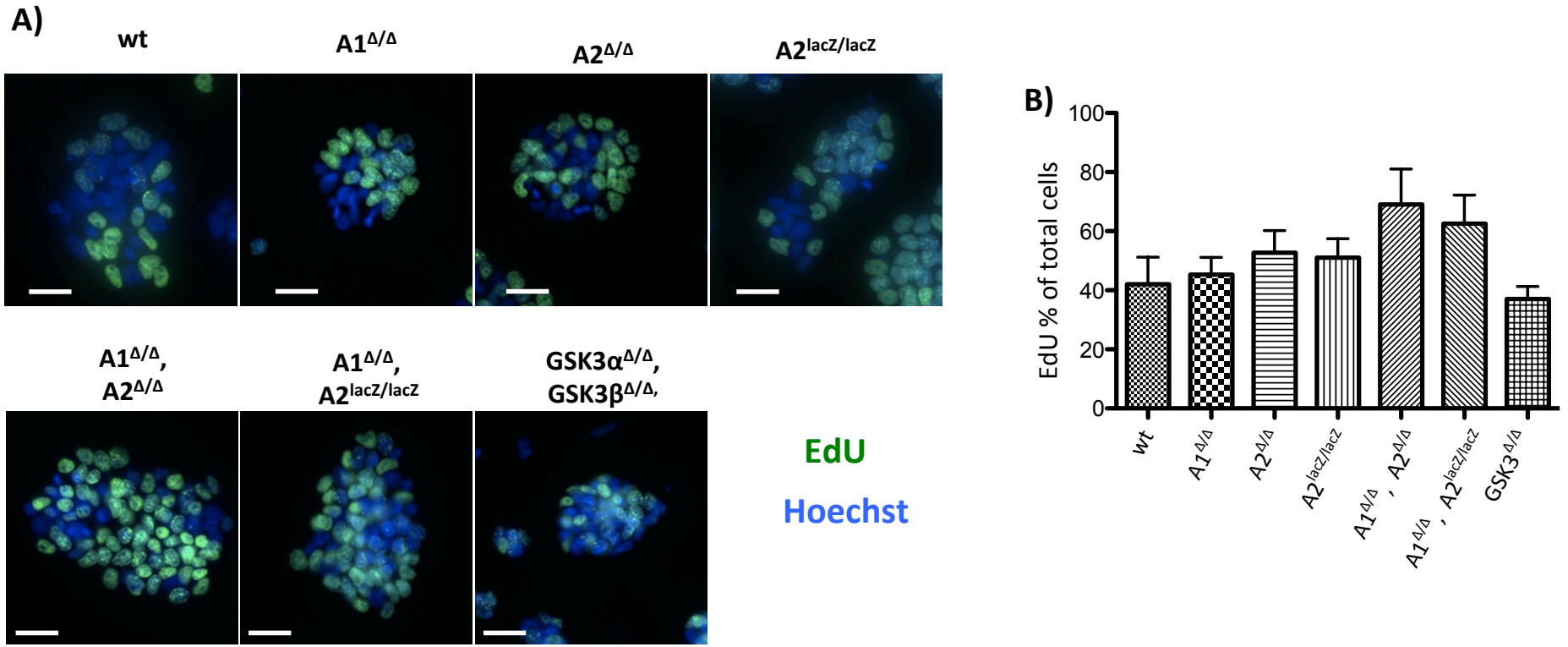

Figure 4-11. EdU incorporation in Axin mutant ES cell lines

A) ES cells of the indicated genotype were grown in 1i medium, incubated with EdU to label cells in s-phase fixed, and stained using a Click-it-EdU detection kit. Nuclei were stained using Hoechst 33342. A merge of both channels is shown. Scale bars indicates 20 µm. **B)** The number of EdU positive cells within a 100 total cells were counted in triplicate per cell line. Three cell lines were counted for each genotype. Error bars: SEM. No significant changes were found using a one way ANOVA and a Tukey's post-hoc test.

4.5.2 Growth and viability of Axin mutant ES cell lines

To further investigate whether the Axin mutant cell lines indeed proliferated faster, we decided to analyse their growth dynamics. Axin mutant and control cell lines were plated at the same density, then cell viability was measured every 24h using a CellTiter-Glo luminescence cell viability assay and the growth rate was determined. In this assay, we found no evidence of an increase or decrease of cell viability in any of the cell lines tested (Figure 4-12 A). These data were consistent with those found in $APC^{Min/Min}$ and GSK3 mutant ES cell lines (Doble et al. 2007; Kielman et al. 2002)

We then hypothesised that an increase in cell proliferation as the result of Axin loss, could be masked by an increase in apoptosis level. The CellTiter-Glo assay measures the metabolic activity of cultured cells, based on cellular ATP levels, which is used as a proxy for the total number of viable cells in a culture. High levels of apoptosis on a background of high proliferation could result in unchanged viability readouts.

Thus, we performed a CellTox-Green Cytotoxicity assay simultaneously with a RealTime-Glo™ MT cell viability assay on ES cells grown in 1i for 2 days without change of culture medium. These assays allow the simultaneous measurement of live and dead cells in growing cultures. The cytotoxicity assay is based on the change in membrane integrity as the result of cell death. The data obtained in both assays is shown in (Figure 4-12 B). We found, that cell viability, again, was not significantly changed (Figure 4-12 B, clear bars), while the level of apoptosis was also not significantly altered in all the cell lines tested (Figure 4-12 B, red bars).

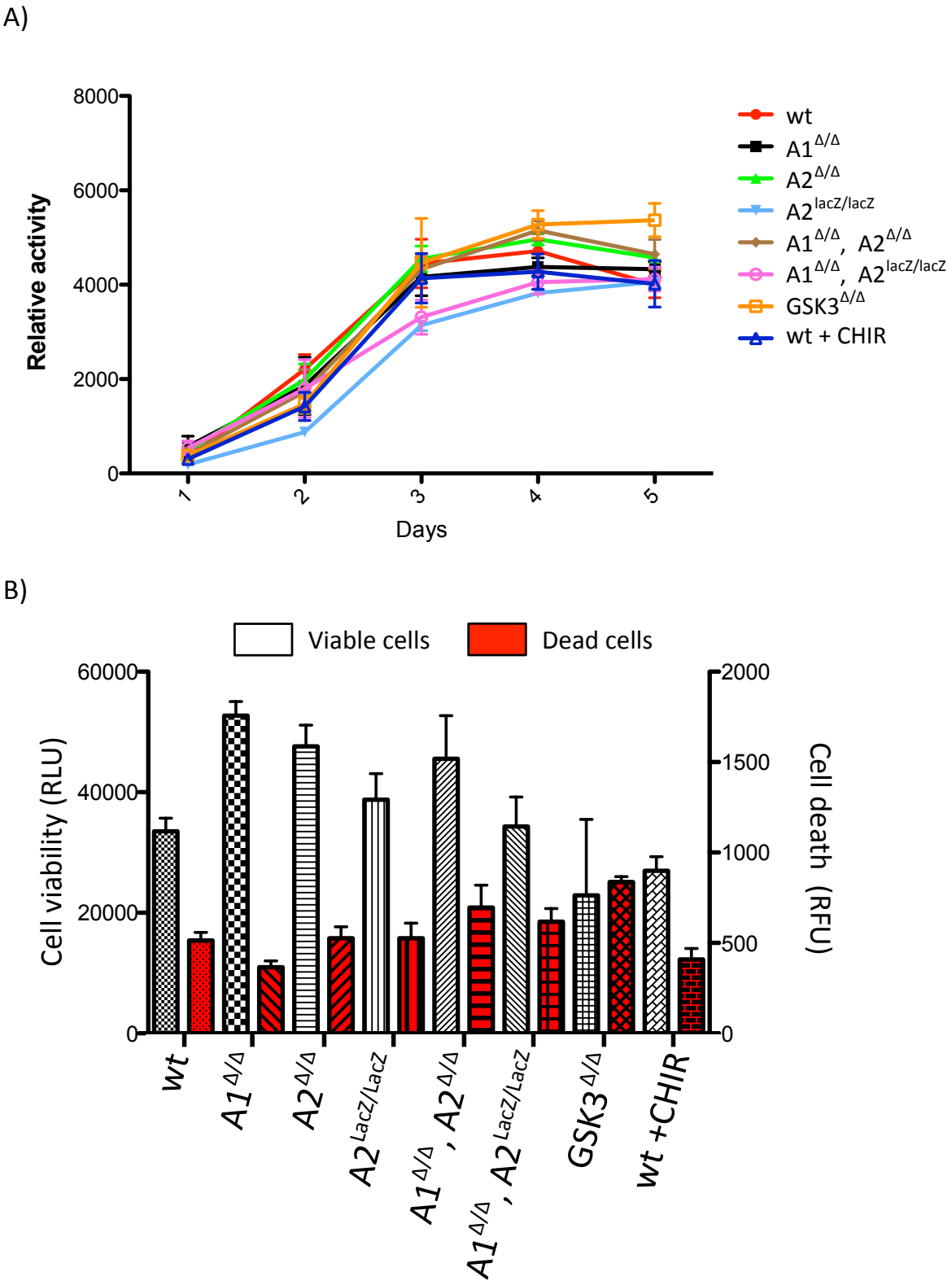

Figure 4-12. Growth curves, cell viability, and toxicity of Axin mutant ES cells.
A) ES cells grown in 1i medium were plated simultaneously at 10 000 cell/cm^2. At each time point 3 wells per cell line were harvested to perform a cell titre glow assay (Promega). Error bars: SEM **B)** ES cells lines were grown for 2 days in 1i medium without change of medium. Then a Real Time-Glo^{TM} assay (Promega) to measure cell viability (clear bars) and a CellTox^{TM} Green assay (Promega) to measure cell toxicity (red bars) were performed simultaneously on the same sample. N=3. Error bars: SEM. Data were analysed using a one-way ANOVA and a post-hoc Tukey's test to compare between groups. No significant differences between cell viability and toxicity was detected.

4.5.3 Expression of cell cycle related genes in Axin mutant ES cells

Cell viability and growth was not found to be affected in Axin mutant ES cell lines. In Axin1 mutant livers, however, a G2/M and cell cycle related gene expression profile was found (Feng et al. 2012). Based on this, we performed qRT-PCR against *Ki-67* and *Cyclin B1* expression as the last confirmation of an unchanged cell cycle profile in Axin mutant ES cells.

In keeping with the previous results, neither Ki-67 nor Cyclin B1 expression levels were significantly changed in any of the Axin mutant ES cell lines (Figure 4-13).

Taken together, the analysis of gene expression, growth, and apoptosis showed that the cell cycle is not affected by the mutation of one or two Axin genes. The data were consistent with the loss of GSK3 or mutations of ACP in ES cell lines, in which ES cell grows was also found to be unaffected (Doble et al. 2007; Kielman et al. 2002).

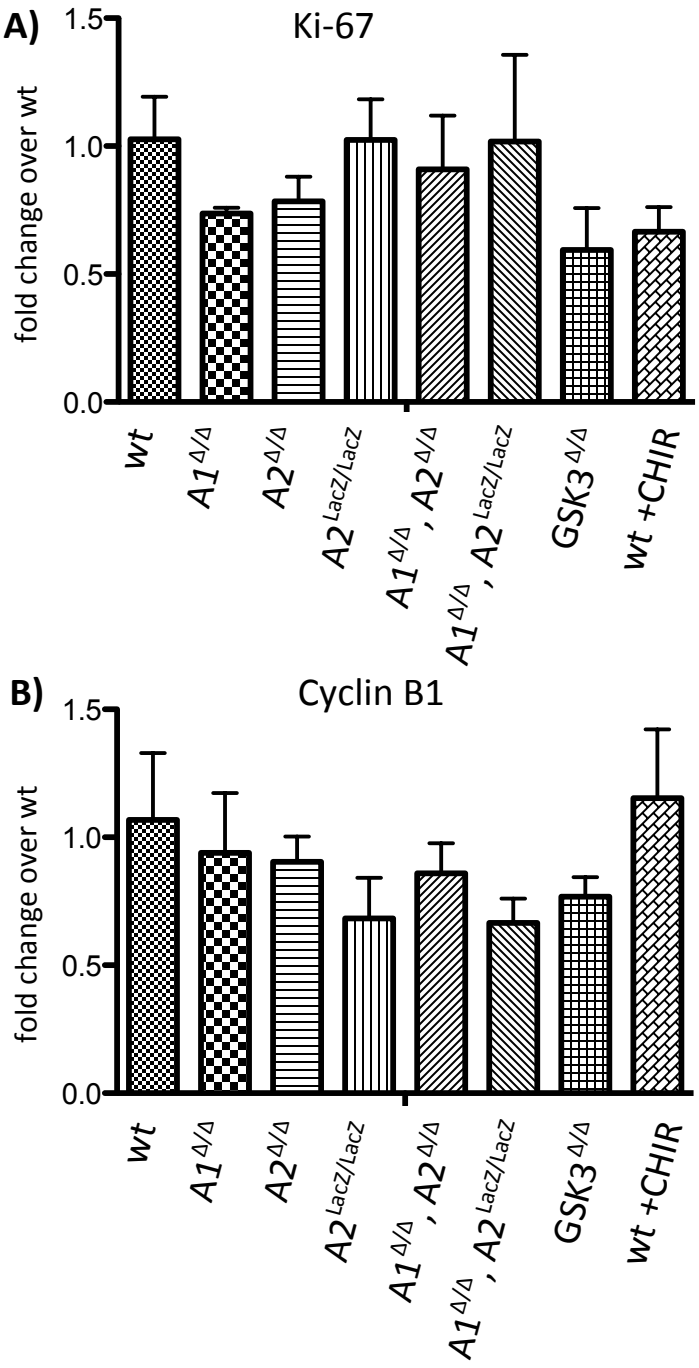

Figure 4-13. Expression of *Ki 67* and *Cyclin B1* in Axin mutant mouse ES cell lines.
Axin mutant ES cells grown in 1i medium were tested for their expression levels of *Ki-67* **(A)** and *Cyclin B1* **(B).** Data are presented as the mean fold change of wt ES cells relative to β-Actin. N=3, error bars: SEM, No significant changes were detected between the wt and the other cell lines using one-way ANOVA and a post-hoc Tukey's test to compare between groups.

4.6 Maintenance of pluripotency in Axin mutant ES cells

Most studies of Wnt signalling in embryonic stem cells find a strong connection between Wnt activity and stem cell self-renewal (Nusse et al. 2008; Wend et al. 2010). GSK3 double knockout in ES cells for example led to a strong reduction in their differentiation potential, through the activation of Wnt signalling (Doble wt al. 2007). Other publications suggest that Wnt signalling promotes mesoderm differentiation, while suppressing the development of neuroectoderm in mouse ES cells (Aubert et al. 2002; Haegele et al. 2003; Sato et al. 2004; Bakre et al. 2007).

A notable feature of both Axin double mutant ES cells that we observed while working with them, was that they maintained very round and highly refractive colony morphology even under conditions where wild type ES cell lines started to differentiate. This was especially visible in immunocytochemistry assays, like the β-Catenin staining shown earlier (see Section 4.4.1 and Figure 4-5).

We therefore hypothesised that Axin mutant ES cells may be impaired in their differentiation capacity, similar to GSK3 knockout and APC ES cells (Doble et al. 2007; Kielman et al. 2002; Atlasi et al. 2013).

4.6.1 Alkaline phosphatase levels in Axin mutant ES cells

First, we analysed alkaline phosphatase expression (AP) in ES cells grown in 1i conditions for 3 days. As explained previously, pluripotent stem cells express high levels of AP, while differentiated cells lose their expression.

In an AP staining experiment, we could show that wt cells grown in 2i conditions (wt+ CHIR) maintain strong levels of AP staining after 3 days in culture (Figure 4-14 A, top left). wt cells grown in 1i condition (without the GSK3 inhibitor) for this amount of time did lose much of the staining (Figure 4-14 A, second from left).

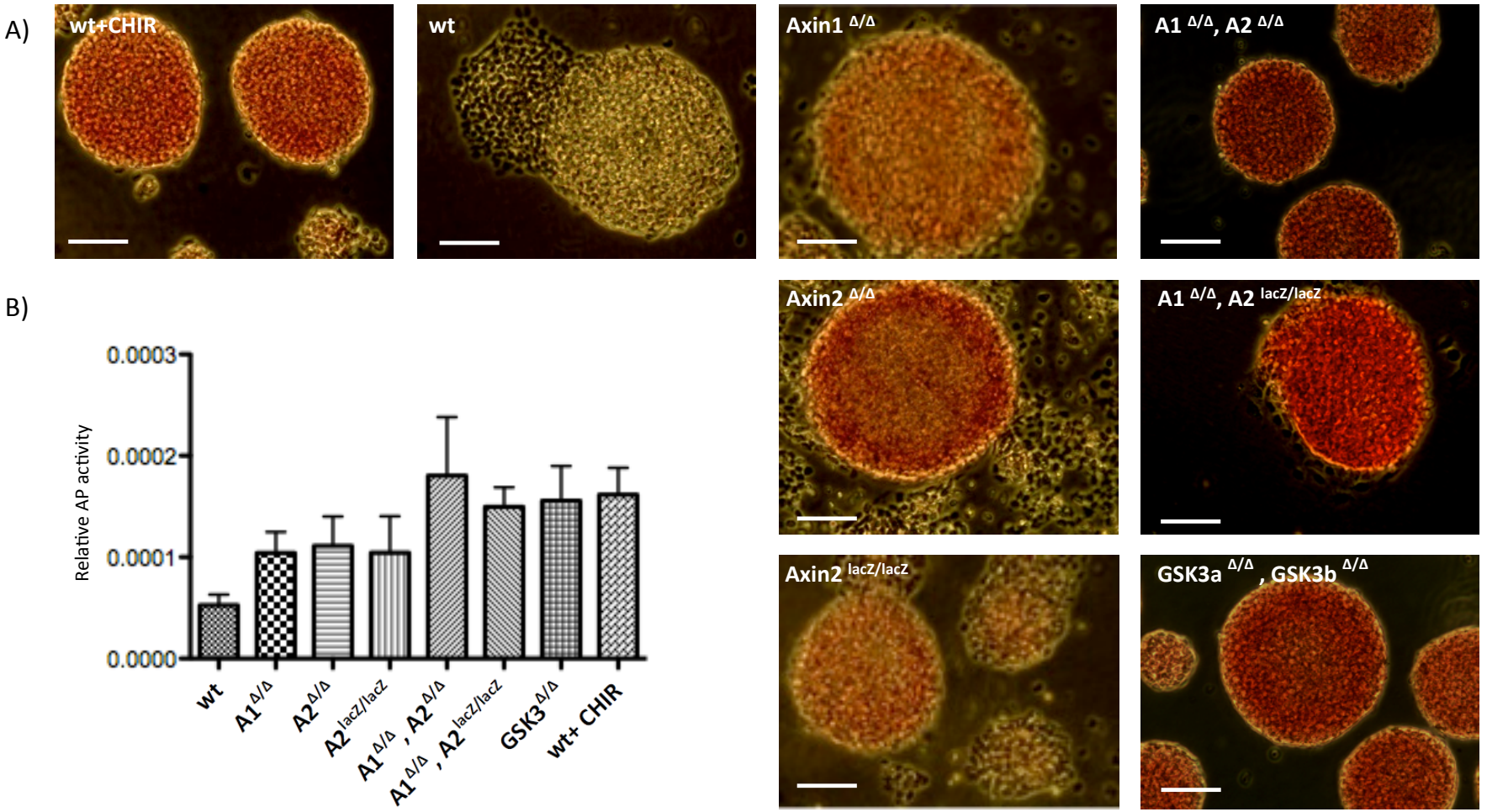

Figure 4-14. Alkaline phosphatase expression in Axin mutant ES cells.

A) Alkaline phosphatase staining was performed on ES cells grown in 1i medium. Cells expressing high levels of alkaline phosphatase stain bright red, cells expressing low levels remain unstained. Scale bars represent 100 µm. **B)** Quantification of alkaline phosphatase level in ES cell lysates using the alkaline phosphatase Diethanolamine Activity Kit (Sigma-Aldrich). Data are shown normalized to cell viability measures in a Presto blue assay. N=3. Error bars: SEM. Data were analysed using a one-way ANOVA and a post-hoc Tukey's test to compare between groups. No significant differences were detected.

Single loss of either of the Axin genes, resulted in colonies that maintained a high degree of AP positive cells (Figure 4-14 A, second row from the right). The colonies in those cell lines formed round colonies of pluripotent cells, stained red for AP, surrounded by a feeder-like layer of unstained, differentiated cells.

Axin double mutant ES cell lines with either the $Axin2^{\Delta/\Delta}$ or the $Axin2^{lacZ/lacZ}$ allele mainly showed tightly packed, strongly AP positive ES cell clones. Unstained cells were observed very rarely (Figure 4-14 A, top and middle on the right). The same was true for GSK3 double knockout control cells.

The data observed in the AP staining experiment were also confirmed in an independent quantification of AP activity in a quantitative assay. Here the stepwise increase of AP activity with the loss of each Axin gene was observed Figure 4-14 B). However, the trend observed in activity levels was not statistically different, possibly due to the size of the enzymatic assay window.

4.6.2 Oct4 protein levels in ES cells

A second marker for stem cell pluripotency is the transcription factor Oct4 (Pou5f1). Similar to the expression of AP, shown above, staining for Oct4 protein was stronger following the loss of each additional Axin allele (Figure 4-15). Wt ES cells grown in 1i medium for an extended period had low levels of Oct4 protein. In $Axin1^{\Delta/\Delta}$ the amount of Oct4 was very similar to the wt. Loss of Axin2 slightly raised staining intensity in both $Axin2^{\Delta/\Delta}$ and $Axin2^{lacZ/lacZ}$ cells. In double mutants for Axin and GSK3, the strongest Oct4 staining intensity was found.

Higher levels of Oct4 protein as the result of Axin loss could have two different causes. Firstly, Axin loss could lead to the stabilisation of Oct4 protein. Secondly, *Oct4* mRNA levels could be raised following Axin loss.

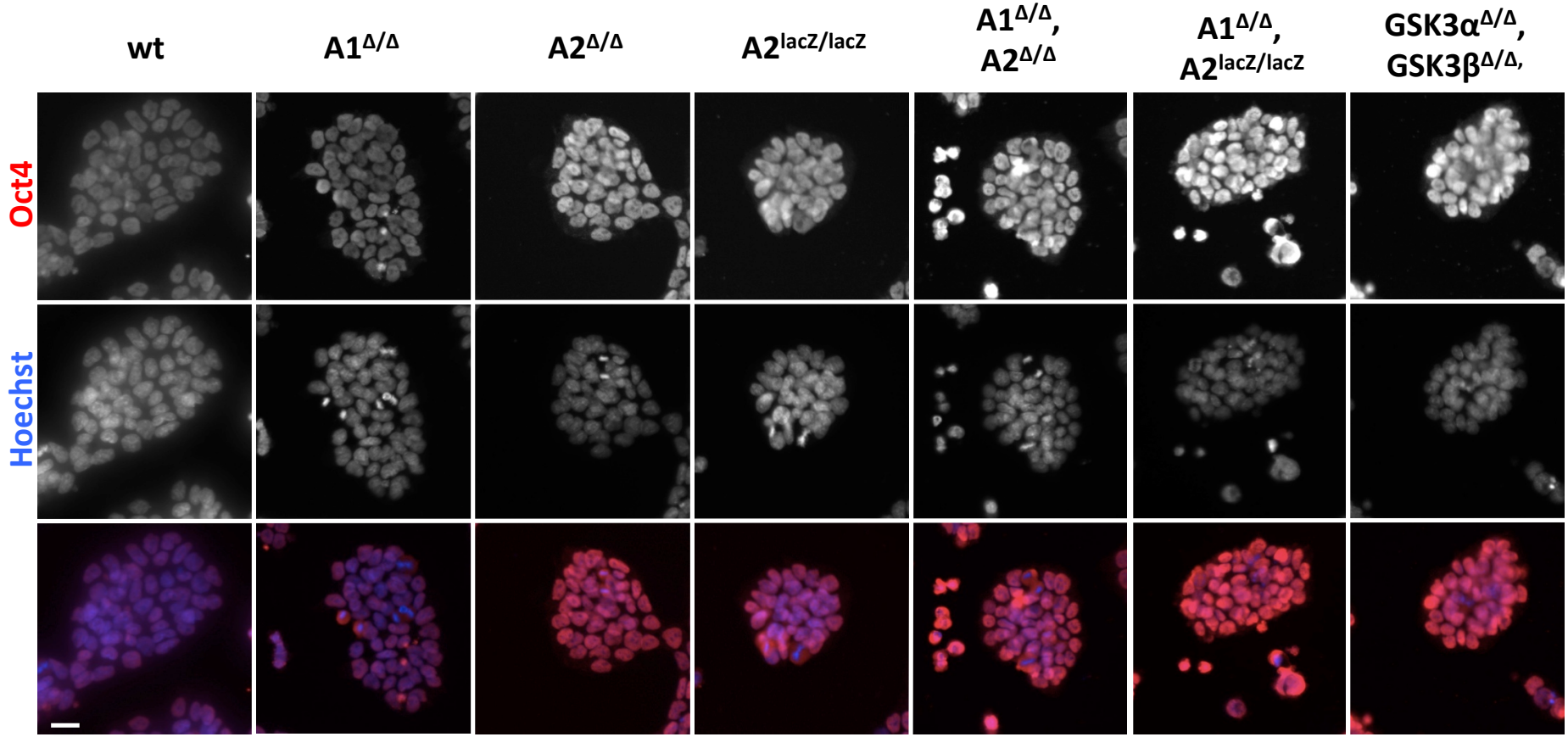

Figure 4-15. Oct4 staining of Axin mutant ES cells

ES cells of the indicated genotype were grown in 1i medium, fixed, and stained for Oct4 (Alexa568, top) and nuclei (Hoechst 33342, middle). A merge of both channels is shown at the bottom. Scale bar indicates 20 µm.

4.6.3 Expression of pluripotency markers in ES cells

To test whether *Oct4* expression levels increase in response to Axin loss in embryonic stem cells, we performed qRT-PCR analysis. The data obtained, showed no significant changes in any of the Axin mutant ES cells lines (Figure 4-16 A).

These results suggested that Oct4 protein levels, but not mRNA expression levels, were altered in response to the mutation of Axin and GSK3.

Next, we tested the expression of *Nanog* and *Rex1*, both of which are also considered to be markers of pluripotency as well. While *Oct4* expression is usually found in ES cells, 'naïve' epiblast and post implantation epiblast, *Rex1* and *Nanog* expression is more restricted to ES cells and preimplantation embryos (Kalkan and Smith 2014).

Data from qRT-PCR for both of these markers also did not change significantly in any of the ES cells lines examined (Figure 4-16 B, C)

It is also of interest that GSK3 knockout, as well as treatment of wt cells with a GSK3 inhibitor (wt + CHIR), did not alter Nanog, Oct4 and Rex1 expression levels in cells grown in 1i medium for 3 days.

To summarize, Axin loss did stabilize Oct4 protein levels and increased alkaline phosphatase staining when cells were grow in 1i medium indicating increased levels of pluripotency as compared to wt cells. However, gene expression levels of the three pluripotency markers *Oct4, Nanog* and *Rex1* were unchanged.

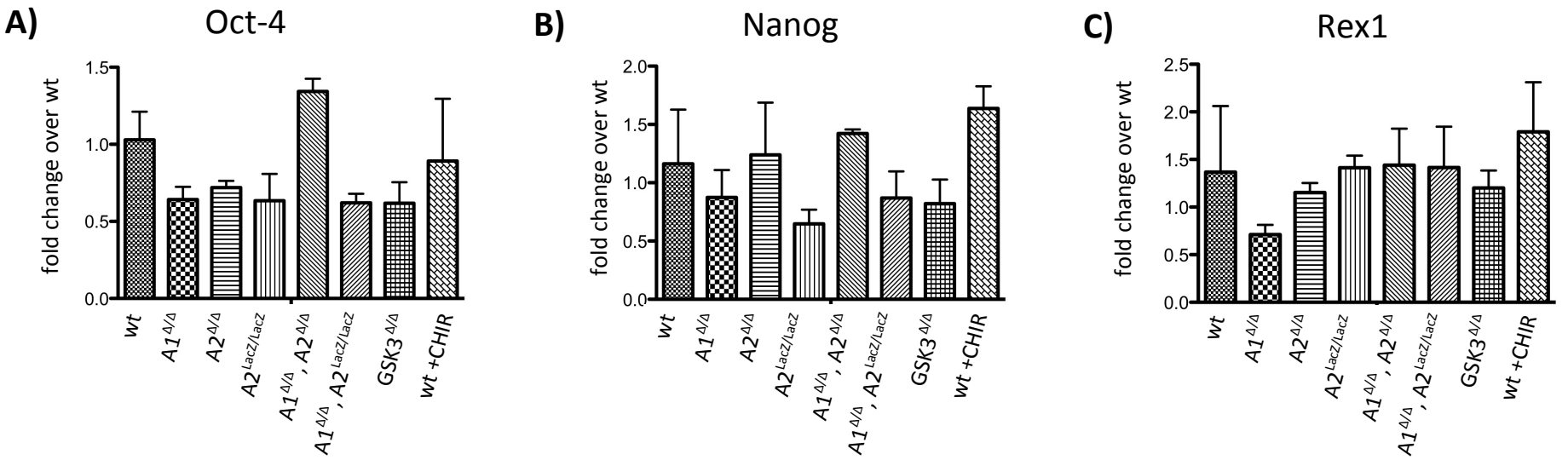

Figure 4-16. Expression of pluripotency markers *in* Axin mutant mouse ES cell lines.
Axin mutant ES cells grown in 1i medium were tested for their expression levels of *Oct4* **(A),** *Nanog* **(B),** and *Rex1* **(C).** Data are presented as the mean fold change of wt ES cells relative to β-Actin. N=3, error bars: SEM, Significance levels are only shown compared to wt and were determined using one-way ANOVA and a post-hoc Tukey's test to compare between groups. No significant changes were detected.

4.7 Differentiation of Axin mutant ES cell lines

Higher AP and Oct4 protein levels suggested that Axin mutant ES cell lines retained higher self-renewal capacity than wt in extended cultures without GSK3 inhibitor. This led us to further investigate the differentiation potential of Axin mutant ES cell lines.

The differentiation of ES cell lines can be achieved *in vitro* by generating so-called embryoid bodies (EBs) (Doetschman et al. 1985; Keller 1995). Wild type ES cell lines grown under non-attachment conditions can form three-dimensional aggregates, which differentiate into the three germ layers if left undisturbed. Using the hanging drop method, we generated EBs from all different ES cell lines.

4.7.1 Lineage differentiation in Axin mutant EBs

The wt cell line developed normally into EBs with transparent cystic structures, reminiscent of the embryonic yolk sac in EB medium (medium without LIF, PD0325901 and CHIR99021). In Axin1 and Axin2 single mutant EBs, some cystic structures could be found, while $Axin1^{\Delta/\Delta}$, $Axin2^{\Delta/\Delta}$ double mutant EBs never formed these transparent cysts under identical conditions. $Axin1^{\Delta/\Delta}$, $Axin2^{lacZ/lacZ}$ EBs also formed aggregates void of cystic structures, however the morphology of some of the EBs was cauliflower-like; others formed round balls. Overall, Axin double mutants formed much tighter packed aggregates than wt and single Axin mutants. Cells treated with GSK3 inhibitor for the duration of the EB formation, as well as GSK3 double knockout cells, also formed aggregates that were cauliflower-like in shape. (Figure 4-17 A and Figure A-3 in Appendix 3, as well as Movie A- 1, show examples of EBs of all the different genotypes.)

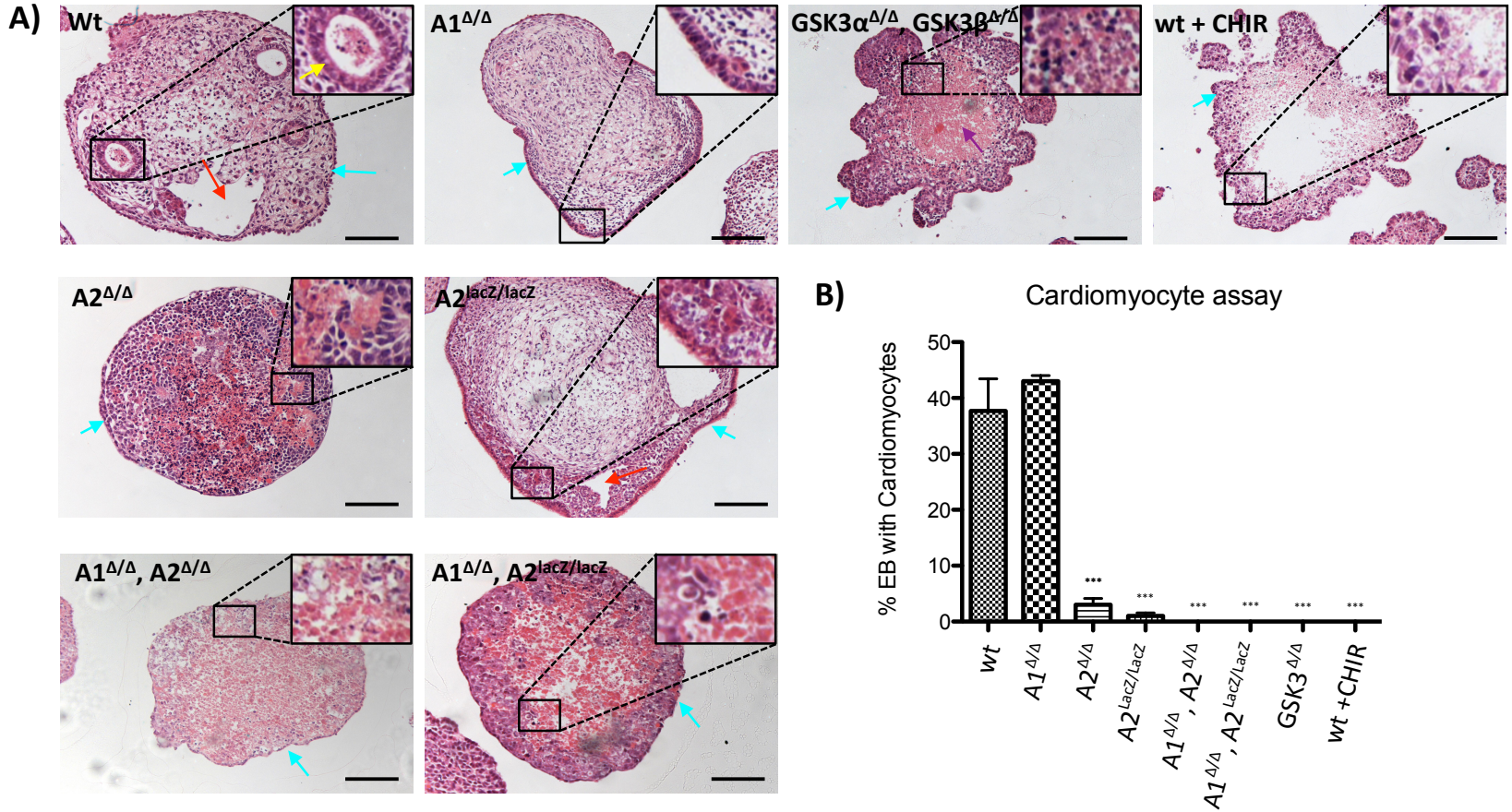

Figure 4-17. H&E staining of Axin mutant embryoid bodies.

A) Embryoid bodies derived from Axin mutant ES cell lines fixed and stained with Haematoxylin and Eosin on day 14 of development. Differentiation into different germ layers is indicated by arrows: Parietal endoderm (blue,→); mesoderm/internal epithelia (yellow, →); ectoderm/columnar epithelia (possibly neural tubes) (green,→); internal cyst structures red,→); collagen and laminin matrix deposition (purple,→). Scale bars: 50 µm. Pictures were taken with the help of Kyle Hawker. **B)** Embryoid bodies derived from Axin mutant ES cell were scored for spontaneously beating cardiomyocytes on day 8 of development. At least 200 embryoid bodies were scored for each genotype. Embryoid bodies from 3 cell lines of each genotype were scored. Error bars: SEM. Data were analysed using a one-way ANOVA and a post-hoc Tukey's test to compare between groups. Significant differences are only shown compared to wt. ***: p<0.001.

I Development of cardiomyocytes in EBs

Over the course of 8 days in culture, approximately 40% of the EBs (n > 200) of wt ES cells formed spontaneously contracting cardiomyocytes that were visible microscopically (Figure 4-17 B and Movie A- 1 in the Appendix). These contractile cells were also found in a similar amount of EBs derived from $Axin1^{\Delta/\Delta}$ cell lines.

Mutations of Axin2, in either $Axin2^{\Delta/\Delta}$, or $Axin2^{lacZ/lacZ}$ EBs, rarely formed any EBs containing cardiomyocytes, while the Axin double mutant EBs never displayed these contractile cells. The observation of that $Axin2^{lacZ/lacZ}$ ES cells failed to differentiate was surprising since $Axin2^{lacZ/lacZ}$ mice have been described as viable (Lustig et al. 2002; Yu et al. 2005). Further considerations of this apparent paradox are made in the Discussion section.

II Evidence for lineage differentiation in H&E stains of EBs

The defect in differentiation was then further analysed in H&E stains of EBs, cultured for 14 days in differentiation conditions. EBs derived from wt cells showed signs of differentiation into all three different germ layers (Figure 4-17 A and Figure A-3 A in Appendix 3). In addition to mesodermal muscle tissue, they contained internal cavities surrounded by endothelial structures, also indicating mesoderm differentiation. Parietal endoderm was present as a cell layer around the EBs. EBs also showed indications of ectodermal differentiation in the form of columnar epithelia, which might be precursors of neural tube structures (neuroepithelia). Examples of the different structures are indicated in Figure 4-17 A and Figure A-3, Appendix 3 for all genotypes they were found in.

EBs generated from cell lines lacking a single Axin gene, also show indications of differentiation into the different germ layers (Figure 4-17 A and Figure A-3 B-D, Appendix 3).

By contrast, loss of both Axin genes in $Axin1^{\Delta/\Delta}$, $Axin2^{\Delta/\Delta}$ and $Axin1^{\Delta/\Delta}$, $Axin2^{lacZ/lacZ}$ resulted in EBs with a thin parietal endoderm layer, but without any other obvious structures indicative of differentiation. There was, however, a build-up of matrix deposition,

probably composed of collagen and laminin (Figure 4-17 A and Figure A-3 E, F in Appendix 3).

EBs from GSK3$^{\Delta/\Delta}$ and wt cells treated with CHIR had parietal ectoderm structures and matrix deposits, similar to Axin double mutants (Figure 4-17 A and Figure A-3 G, H in Appendix 3). However, the overall EB morphology was cauliflower-like rather than ball shaped. The core of EBs of cells treated with CHIR99021 often showed high levels of dead cells, which might be the result of inhibitor toxicity or oxygen deprivation.

III The pluripotency marker Oct4 in EBs

The cardiomyocyte assay, as well as the analysis of H&E stained sections of EBs, was suggestive of impaired differentiation in Axin double mutant ES cells. Since Axin mutant ES cell lines maintained high levels of Oct4 protein when cultured in 1i medium for 3 days (see Section 4.6.2), we also analysed EBs for Oct4 staining patterns using immunohistochemistry (Figure 4-18 A).

Wnt upregulation in EBs is known to maintain high levels of pluripotency and to cause strong Oct4 staining levels in GSK3$^{\Delta/\Delta}$ (Doble et al. 2007) and wt cells treated with the GSK3 inhibitor BIO (Sato et al. 2004).

These findings were confirmed in our EBs. While wt EBs lost most of the Oct4 staining 14 days into the differentiation process, GSK3$^{\Delta/\Delta}$ and wt + CHIR treated EBs retained many patches with high levels of Oct4 staining (Figure 4-18 A). In all Axin single mutant EBs Oct4 staining was very rare, but some Oct4 positive cell patches still remained. Both Axin double mutant ES cell lines generated EBs with strong Oct4 staining. In those, approximately 60% of all cells stained positive for Oct4, which was the same the in GSK3$^{\Delta/\Delta}$ and wt + CHIR EBs (Figure 4-18 B).

These results imply that loss of both Axins (either allelic combination), but not the loss of single alleles, led to a strong maintenance of ‘stemness’ similar to GSK3 knockout or inhibition.

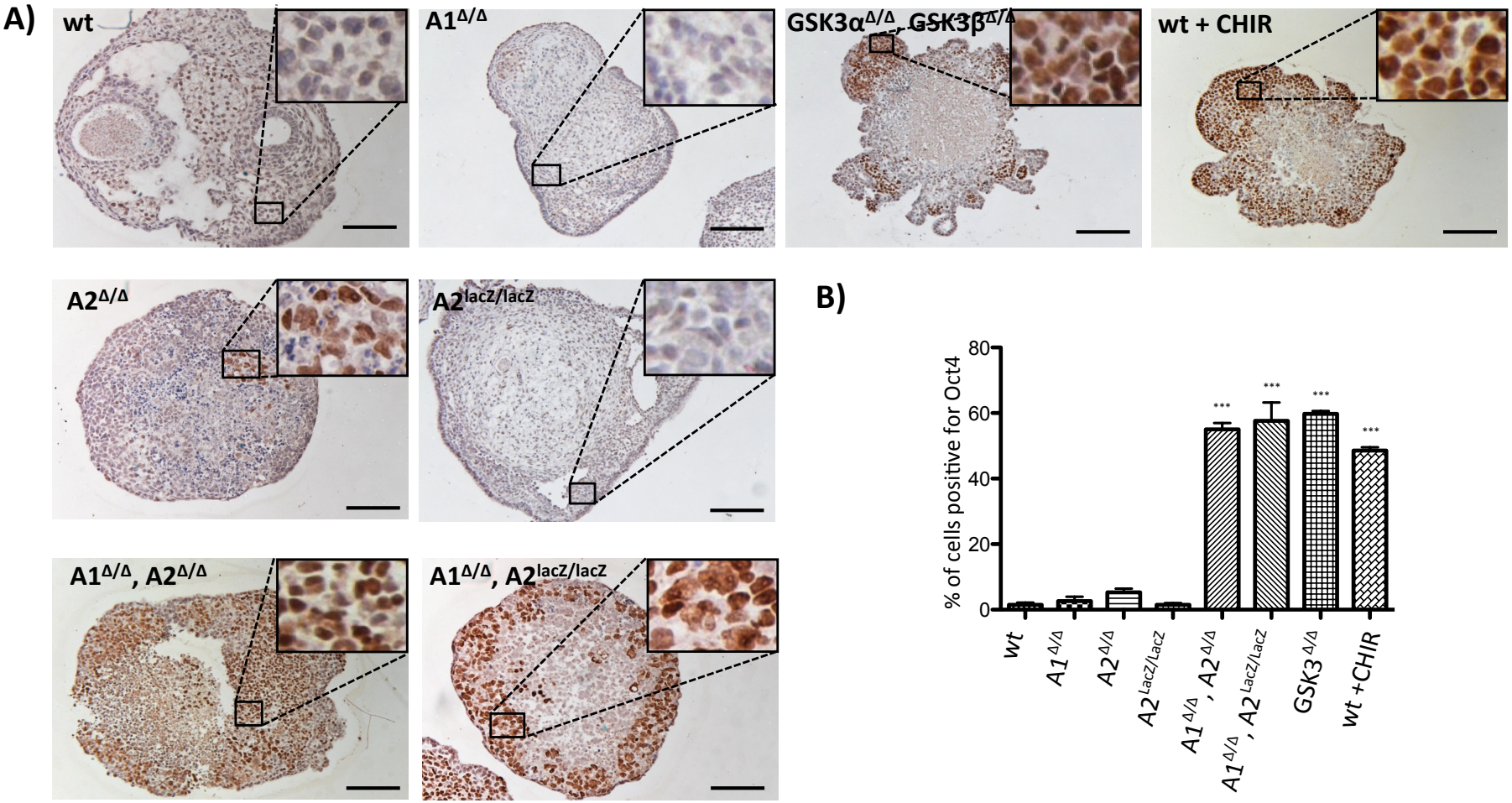

Figure 4-18. Oct4 staining of embryoid bodies.

A) Embryoid bodies derived from Axin mutant ES cell lines fixed and stained for Oct4 on day 14 of development. Sections were counterstained with Haematoxylin. Scale bars: 50 µm. **B)** Numbers of Oct4 positive cells per embryoid body were counted for at least 30 embryoid bodies. Embryoid bodies from 3 cell lines of each genotype were scored. Data are shown as % of total cells. Data were analysed using a one-way ANOVA and a post-hoc Bonferroni test to compare between groups. Significant differences are only shown compared to wt. ***: $p<0.001$. Staining and analysis were performed by the PTY student Kyle Hawker under my supervision.

IV Differentiation into endodermal, mesodermal, and ectodermal lineage

We next analysed whether the Axin mutant ES cells had differentiated into EBs comprising all three different germ layers in more detail. We used one differentiation marker for each germ layer in an immunohistochemical analysis: α-smooth muscle actin (SMA) for mesodermal differentiation; α-fetoprotein (AFP) for endoderm differentiation and β-III-tubulin as an ectodermal marker.

Patches of cells stained for SMA indicted that wt, $Axin1^{\Delta/\Delta}$; $Axin2^{\Delta/\Delta}$; and $Axin2^{lacZ/lacZ}$ EBs had undergone mesodermal differentiation (Figure 4-19 A). Interestingly, the number of SMA stained cells per embryoid body in $Axin1^{\Delta/\Delta}$ was significantly reduced compared to wt cells ($p<0.001$) (Figure 4-19 B), even though cardiomyocyte differentiation (mesoderm lineage) was shown to be unimpaired (Figure 4-17 B). $Axin2^{\Delta/\Delta}$, and $Axin2^{lacZ/lacZ}$ EBs showed a strong reduction in spontaneously beating cardiomyocytes at day 8, but SMA staining levels were not significantly different to the wt 14 days into the culturing process. *In vivo*, SMA marks the beginning of cardiomyocyte differentiation; its expression, however, is downregulated at E9.5 in mouse development (Clement et al. 2007). These results suggested that EBs of all Axin single mutant ES cells were able to undergo initial mesodermal differentiation. However, loss of Axin1 and Axin2 seem to affect further lineage commitment differentially. While Axin1 loss enabled the cells to form functional cardiomyocytes, Axin2 loss in $Axin2^{\Delta/\Delta}$, or $Axin2^{lacZ/lacZ}$ EBs, arrested the development early or pushed the cells along a different branch of the mesodermal lineage.

EBs from Axin double mutants, as well as wt + CHIR and $GSK3^{\Delta/\Delta}$, had highly reduced SMA staining (Figure 4-19 A, B). These data were a further indication of the reduction of the differentiation potential in following Axin mutation.

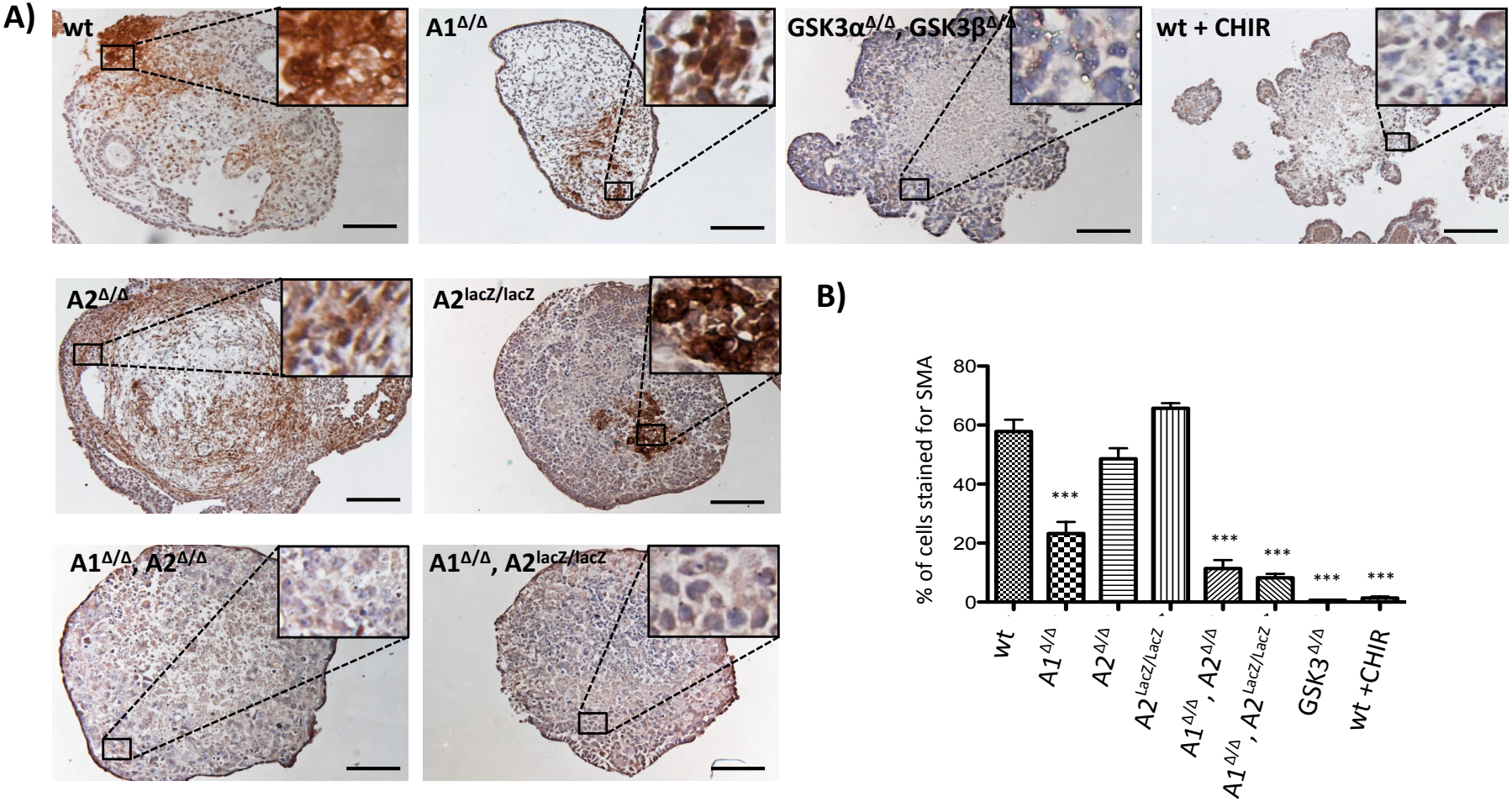

Figure 4-19. SMA staining of embryoid bodies.

A) Embryoid bodies derived from Axin mutant ES cell lines fixed and stained for α-smooth muscle actin (SMA) on day 14 of development. Sections were counterstained with Haematoxylin. Scale bars: 50 µm. **B)** Numbers of SMA positive cells per embryoid body were counted for at least 30 embryoid bodies. Embryoid bodies from 3 cell lines of each genotype were scored. Data are shown as % of total cells. Data were analysed using a one-way ANOVA and a post-hoc Bonferroni test to compare between groups. ***: $p<0.001$. Staining and analysis were performed by the PTY student Kyle Hawker under my supervision.

Staining for AFP (α-fetoprotein), an endodermal marker, was also consistent with the idea that Axin mutations had the potential to impair stem cell differentiation. EBs derived from $Axin2^{\Delta/\Delta}$ ES cells had a slightly reduced percentage of AFP positive cells, compared to wt (Figure 4-20 A, B). However, this was not statistically significant. In $Axin2^{lacZ/lacZ}$ EBs, no changes were observed. Regions of positive staining were also found in $Axin1^{\Delta/\Delta}$ EBs, but at lower levels than in the wt ($p<0.01$). In Axin wt, as well as single Axin mutant EBs, the cells staining positive for AFP were predominately found at the outermost layer, suggesting differentiation of cells into parietal endoderm. The staining pattern found in Axin double mutant EBs was very similar, although AFP positive cells were rarer (both allelic combinations had fewer AFP positive cells; $p< 0.001$). The same was true for GSK3 and wt +CHIR derived EBs ($p<0.001$ and $p<0.01$ respectively).

Finally, β-III-tubulin staining was performed, to indicate ectodermal differentiation. Unfortunately, the staining had a high level of background, so that the results cannot be regarded as highly reliable. Nevertheless, we found a reduction in β-III-tubulin staining in Axin double mutant EBs, compared with all other cell lines (Figure 4-21 A, B). This effect was most pronounced in EBs derived from $Axin1^{\Delta/\Delta}$, $Axin2^{\Delta/\Delta}$ cells ($p<0001$). Staining for different ectodermal marked (e.g. GFAP, Nestin, Pax6, or Sox1), will have to be performed to confirm these data.

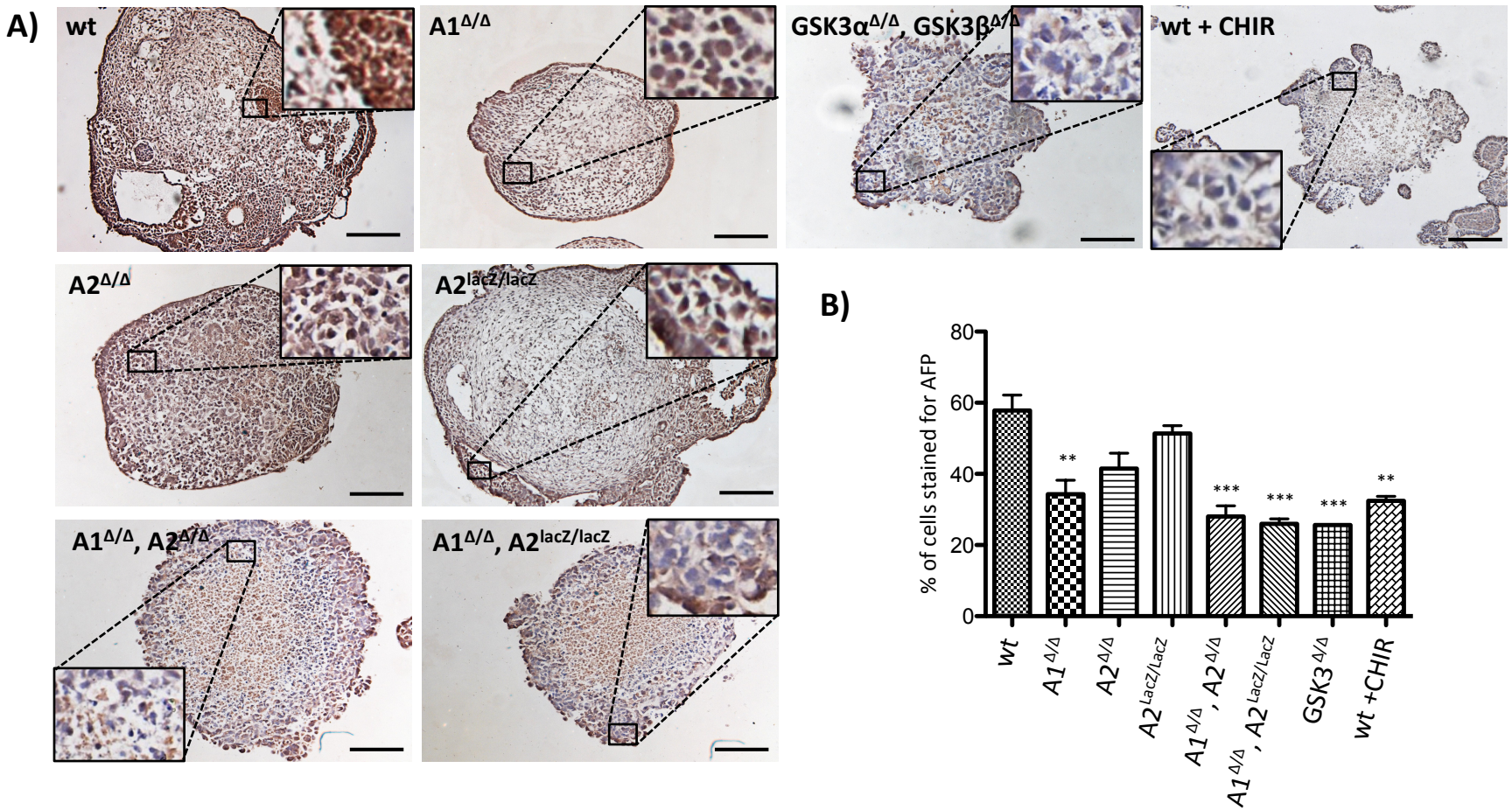

Figure 4-20. AFP staining of embryoid bodies.

A) Embryoid bodies derived from Axin mutant ES cell lines fixed and stained for α-fetoprotein (AFP) on day 14 of development. Sections were counterstained with Haematoxylin. Scale bars: 50 µm. **B)** Numbers of AFP positive cells per embryoid body were counted for at least 30 embryoid bodies. Embryoid bodies from 3 cell lines of each genotype were scored. Data are shown as % of total cells. Data were analysed using a one-way ANOVA and a post-hoc Bonferroni test to compare between groups. Significant differences are only shown compared to wt. **: $p<0.01$, ***: $p<0.001$. Staining and analysis were performed by the PTY student Kyle Hawker under my supervision.

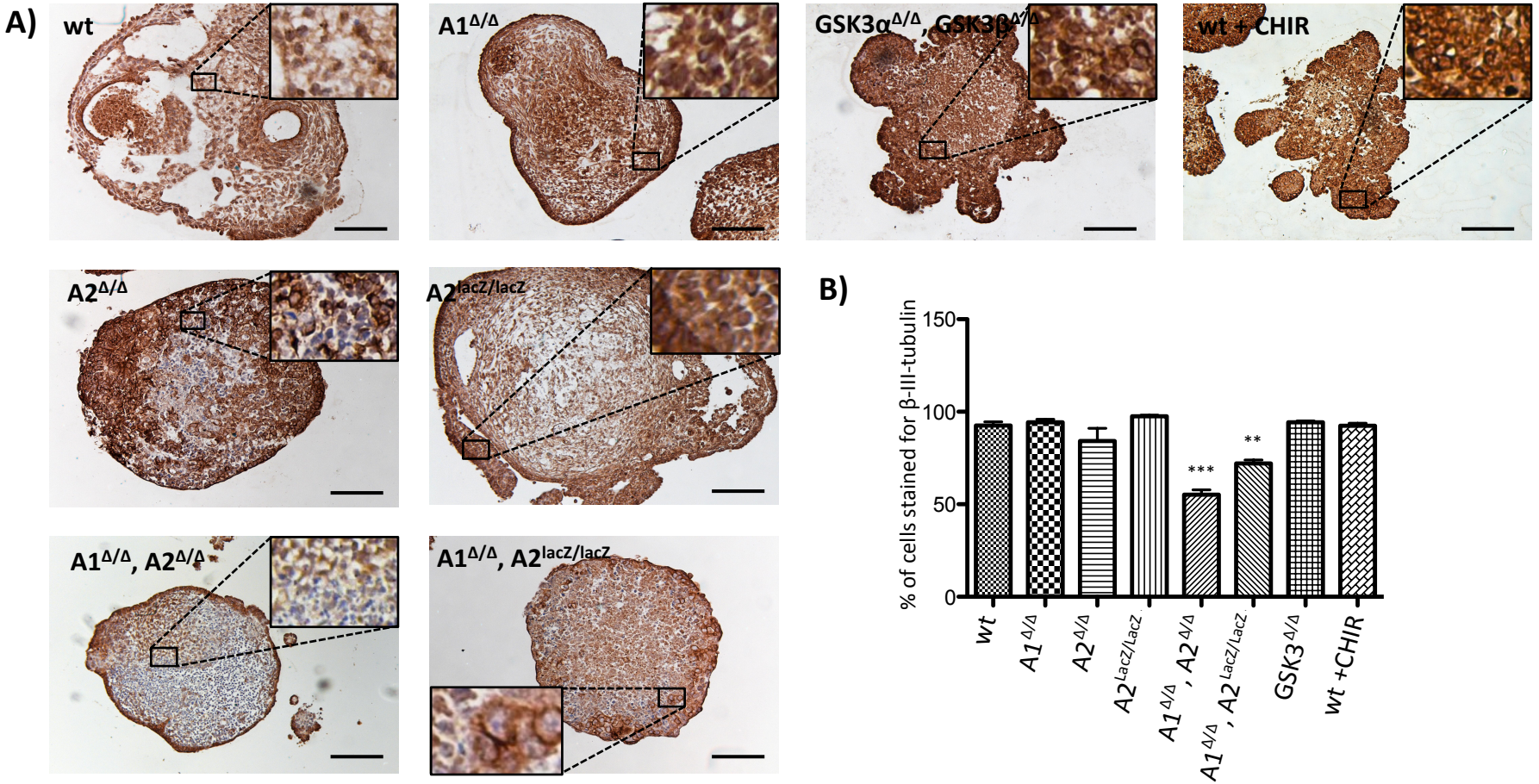

Figure 4-21. β-III-tubulin staining of embryoid bodies.

A) Embryoid bodies derived from Axin mutant ES cell lines fixed and stained for β-III-tubulin on day 14 of development. Sections were counterstained with Haematoxylin. Scale bars: 50 μm. **B)** Numbers of β-III-tubulin positive cells per embryoid body were counted for at least 30 embryoid bodies. Embryoid bodies from 3 cell lines of each genotype were scored. Data are shown as % of total cells. Data were analysed using a one-way ANOVA and a post-hoc Bonferroni test to compare between groups. Significant differences are only shown compared to wt. **: $p<0.01$, ***: $p<0.001$. Staining and analysis were performed by the PTY student Kyle Hawker under my supervision.

In the experiments shown above, we found strongly impaired differentiation in ES cells lacking both Axin genes. Therefore, we further analysed the expression of a whole panel of stem cell and differentiation markers in Axin1$^{\Delta/\Delta}$, Axin2$^{\Delta/\Delta}$ EBs. A RT^2 PCR profiler array designed for stem cell differentiation was performed. It contained a range of 84 pluripotency and differentiation markers. The results were analysed using the $\Delta\Delta C_T$ method to create a scatter graph demonstrating the overall effect of Axin double mutant on embryoid bodies (Figure 4-22). A large number of genes were significantly up- or downregulated, as a result of Axin loss in Axin1$^{\Delta/\Delta}$, Axin2$^{\Delta/\Delta}$ EBs. In order to better interpret the data, the 84 genes were categorised into groups corresponding to their roles in embryogenesis, a full list can be found in (Table A-2 of Appendix 3). After careful analysis of the gene groups, patterns began to emerge from the data collected. Our expectations were largely matched; pluripotency markers were upregulated, whilst certain groups of differentiation markers were down regulated. The most prominent gene groups that underwent comprehensive expression changes are outlined in Table 4-4

Table 4-4. Gene expression changes of the thee most changed gene group in the RT^2 PCR profiler array.

GROUP	GENE	EXPRESSION CHANGE	OVERALL CHANGE
Pluripotency	Nanog	+127.62	Upregulation
	Oct4	+1.85	
	Rex1	+2.8	
Neural	NeuroD1	-18.4	Down regulation
	Nestin	-8.13	
	Pax6	-14.31	
Endoderm	Foxa2	-4.38	Down regulation
	Gata4	+2.78	
	AFP	-133.4	

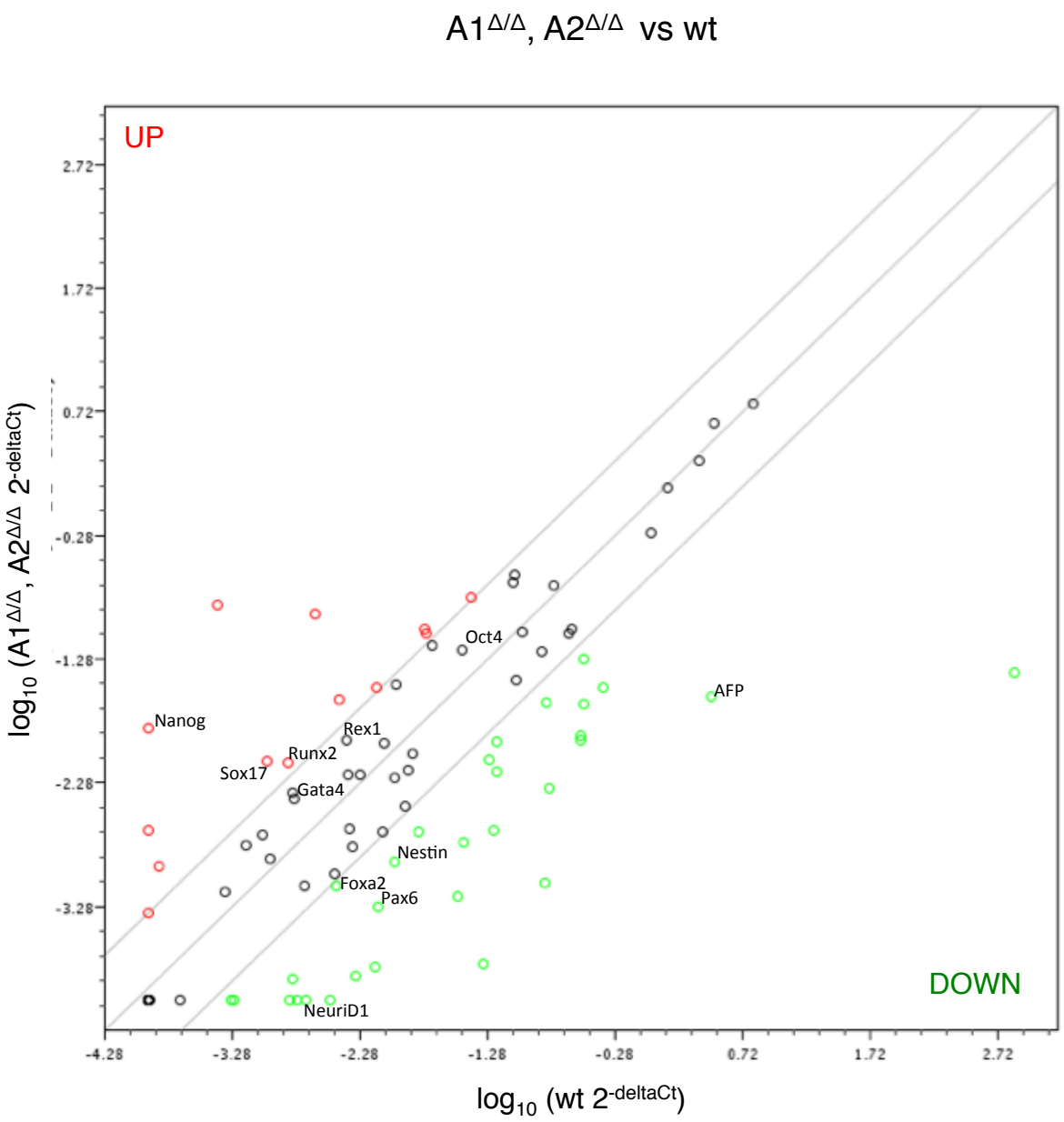

Figure 4-22. RT^2 PCR profiler array to detect gene expression changes in Axin double mutant EBs. A1$^{\Delta/\Delta}$, A2$^{\Delta/\Delta}$ embryoid bodies were compared to embryoid bodies from parental line A1$^{fl/fl}$, A2$^{fl/fl}$ (wt) in a qRT-PCR-based profiler array for 84 lineage and ES cell specific genes. Outer lines indicate a ±4-fold gene expression change. Red dots indicate up-regulation, whereas green dots indicate down-regulation. Black dots indicate genes that were within the ±4-fold margin. *GAPDH, B2M, GusB* and *Hsp90ab1* were used as reference genes. N=1. This experiment was performed by Ian Blackburn under my supervision.

The Pluripotency marker *Nanog* had the most striking upregulation, but also Oct4 and Rex1 were increased in embryoid bodies. Neural differentiation (part of the ectodermal lineage) appeared strongly down regulated as *NeuroD1, Nestin, and Pax6* all exhibited large decreases in their expression levels in $Axin1^{\Delta/\Delta}$, $Axin2^{\Delta/\Delta}$ EBs compared to their parental EBs. The endoderm markers were down-regulated; with *AFP* exhibiting the largest change. *FoxA2* was also down regulated in the PCR profiler array, while *Sox17* was increased. We also observed an increase in the endoderm marker *Gata4* and the oestrogenic marker *Runx2* (mesoderm) similar to the one observed after GSK3 knockout by Doble, et al (2007).

The data from the RT^2 PCR profiler array, were only generated from EBs generated from a single $Axin1^{\Delta/\Delta}$, $Axin2^{\Delta/\Delta}$ ES cell line, and one wt control line ($Axin1^{fl/fl}$, $Axin2^{fl/fl}$) without technical replicates. The data will be verified in normal qRT-PCR assay on all different Axin mutant EBs in future. However, the results so far support the idea that combined mutation of Axin1 and Axin2 (likely either allelic combination) in embryoid bodies impairs differentiation.

The data from immunohistochemical analysis, together with the array data, showed that Axin double mutant EBs retained a high level of pluripotency and were impaired in their differentiation potential. Ectodermal differentiation; especially neuroectoderm development, was reduced in Axin double mutant EBs. The inhibition of neuroectoderm differentiation was also found inhibited in other Wnt activation studies in mouse ES cells (Aubert et al. 2002; Haegele et al. 2003; Sato et al. 2004; Bakre et al. 2007). Mesodermal differentiation was affected in two ways. While SMA, and thus muscle development, was down regulated, the oestrogenic marker *Runx2* was induced. Endoderm differentiation was also widely reduced. However, the parietal endoderm lineage, represented by Sox17, was upregulated. In all of the EB assays shown above, Axin double mutants from both genotypes, closely resembled EBs with impaired GSK3 function ($GSK3^{\Delta/\Delta}$ or wt + CHIR).

Single Axin mutants showed substantially less effects. Axin2$^{\Delta/\Delta}$ and Axin2$^{lacZ/lacZ}$ had the same staining patterns as wt EBs, but formed cardiomyocytes at a much lower rate. Axin1$^{\Delta/\Delta}$ EBs had reduced SMA and AFP levels, while they resembled wt EBs in the other assays.

4.7.2 Wnt signalling in EBs

The data obtained in the lineage analysis revealed that both Axin double mutant EBs showed a very similar phenotype as GSK3$^{\Delta/\Delta}$ EBs. This led us to examine whether Axin loss in the differentiation condition influenced Wnt/β-Catenin signalling directly.

We stained Embryoid bodies generated from all different ES cell lines for total β-Catenin and scored for cells with high level of nuclear or cytosolic β-Catenin (Figure 4-23 A, B). In EBs derived from wt and Axin1$^{\Delta/\Delta}$ ES cells, strong, mostly membrane bound β-Catenin was observed in structures identified as parietal endoderm or mesodermal internal epithelia in H&E stains (see inserts in Figure 4-17). In Axin2$^{lacZ/lacZ}$ EBs, a very similar staining pattern was observed, while Axin2$^{\Delta/\Delta}$ showed some patches of β-Catenin all over the EBs, leading to a significantly increased score ($p<0.01$) (Figure 4-23 A, B).

In both Axin double mutants, as well as GSK3$^{\Delta/\Delta}$ and wt + CHIR treated EBs; β-Catenin levels were hugely increased ($p<0.001$). In those genotypes, much of the β-Catenin staining was found in the nucleus (see inserts in Figure 4-17).

These results were a strong indication that the loss of both Axin genes, in the differentiation conditions, did interfere with the function of the destruction complex. In Axin double mutant EBs, we observed similar β-Catenin staining patterns to APC (Kielman et al. 2002; Atlasi et al. 2013) and GSK3 mutants (Doble et al. 2007).

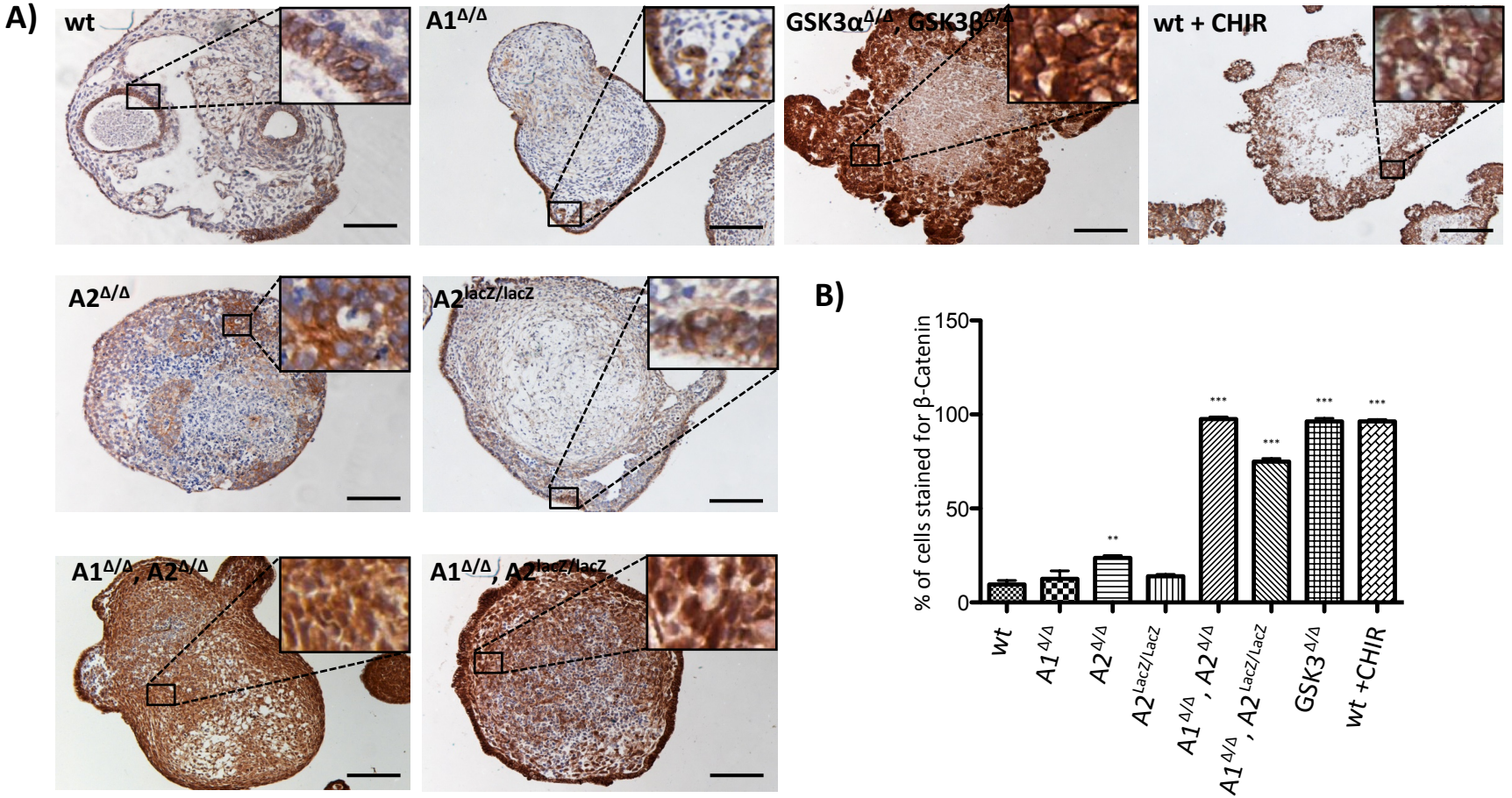

Figure 4-23. β-Catenin staining of embryoid bodies.

A) Embryoid bodies derived from Axin mutant ES cell lines fixed and stained for β-Catenin on day 14 of development. Sections were counterstained with Haematoxylin. Scale bars: 50 µm. **B)** Numbers of β-Catenin positive cells per embryoid body were counted for at least 30 embryoid bodies. Embryoid bodies from 3 cell lines of each genotype were scored. Data are shown as % of total cells. Data were analysed using a one-way ANOVA and a post-hoc Bonferroni test to compare between groups. Significant differences are only shown compared to wt. **: $p<0.01$, ***: $p<0.001$. Staining and analysis were performed by the PTY student Kyle Hawker under my supervision.

Additionally, we tested for expression of the Wnt target genes *Axin2, c-Myc* and *CD44* in the embryoid bodies by qRT-PCR. Consistent with the staining for cellular β-Catenin levels, Wnt target genes were upregulated in EB samples derived from ES cell lines containing Axin or GSK3 mutations. Expression levels of *Axin2* (with primers within the floxed Exon 2) confirmed Axin2 loss in Axin2 single and double mutant ES cells (Figure 4-24 B, C, D & E). Axin2 levels were slightly increased compared to wt in $Axin1^{\Delta/\Delta}$ EBs (Figure 4-24 A) suggesting that the 'text-book' prediction of a compensatory upregulation of Axin2 following loss of Axin1 in a (Wnt activated) negative feedback loop does occur in this context as expected (Lammi et al. 2004; Lustig et al. 2002). As previously reported, GSK3 inhibition and knockout strongly increased *Axin2* levels (Figure 4-24 F, G).

C-Myc levels in EBs were only slightly increased in all different EBs (Figure 4-24). The lack of upregulation in $GSK3^{\Delta/\Delta}$ especially, suggests that *c-Myc* is not strong Wnt target during embryonic stem cell differentiation in mutant embryoid bodies. As discussed earlier *c-Myc* expression in ES cells is driven by STAT3 (Kidder et al. 2008; Cartwright 2005).

Most interesting among the Wnt target genes, was the expression of *CD44.* While *CD44* expression (v10) was unchanged in Axin single mutant EBs (Figure 4-24 A, B, C), its expression levels were increased 4 to 6 fold in $Axin1^{\Delta/\Delta}$, $Axin2^{lacZ/lacZ}$ and $Axin1^{\Delta/\Delta}$, $Axin2^{\Delta/\Delta}$ (Figure 4-24 C, D).

Hence, loss of both Axin genes in embryoid bodies did increase β-Catenin protein levels and activated some target gene expression.

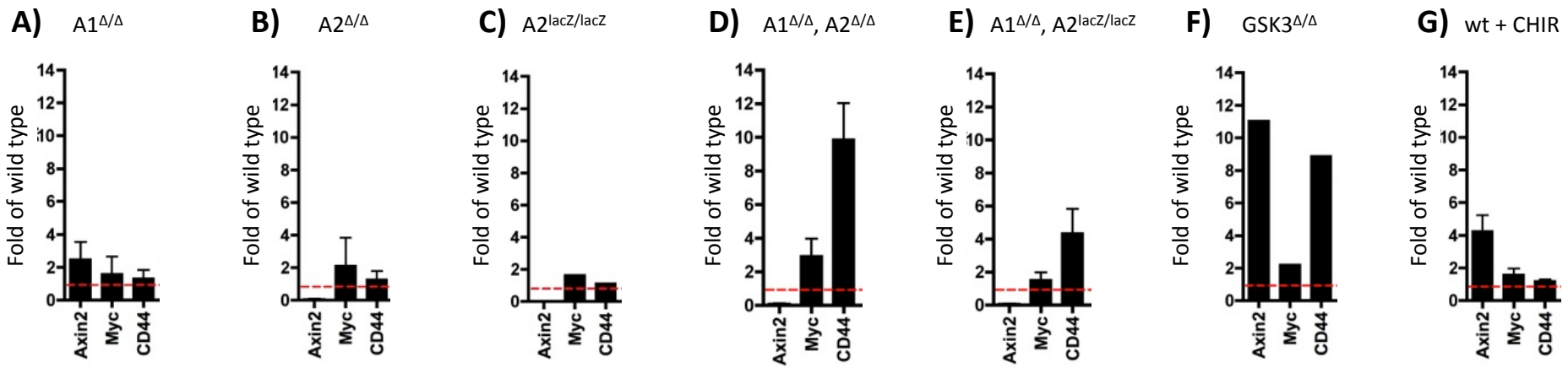

Figure 4-24. Wnt target gene expression changes in Axin mutant embryoid bodies.
EBs bodies were grown for 14 days, then mRNA was harvested and analysed for the expression of the Wnt target genes *Axin2*, c-*Myc* and *CD44*. The fold change of $A1^{\Delta/\Delta}$ **(A)**; $A2^{\Delta/\Delta}$ **(B)**; $A2^{\Delta lacZ/lacZ}$ **(C)**; $A1^{\Delta/\Delta}$, $A2^{\Delta/\Delta}$ **(D)**; $A1^{\Delta/\Delta}$, $A2^{lacZ/lacZ}$ **(E)**; $GSK3^{\Delta/\Delta}$ **(F)** EBs; and wt EBs treated with CHIR99021 **(G)** compared to wt EBs are shown. Wt expression levels are indicated with a red line. Data were normalized to β-Actin expression. N=3 for all, but $A2^{\Delta lacZ/lacZ}$ and $GSK3^{\Delta/\Delta}$ (both N=1). EBs were grown, harvested, and lysed by me. Ken Ewan helped with the performance of the qRT-PCR assay under my supervision.

4.7.3 Proliferation levels in Axin mutant EBs

While scoring the embryoid bodies for the different stains, we detected a trend towards an increase in total cell number per EB in Axin1$^{\Delta/\Delta}$ (Table 4-5). EBs treated with the GSK3 inhibitor CHIR99021 always resulted in EBs with low cell numbers.

Table 4-5. Mean number of cells per Embryoid body

	wt	Ax1$^{\Delta/\Delta}$	Ax2$^{\Delta/\Delta}$	Ax2$^{LacZ/LacZ}$	Ax1$^{\Delta/\Delta}$ Ax2$^{\Delta/\Delta}$	Ax1$^{\Delta/\Delta}$ Ax1$^{LacZ/LacZ}$	GSK3$^{\Delta/\Delta}$	wt + CHIR
Mean cell number	334 ± 71	459 ± 94	309 ± 132	311 ± 166	320 ± 19	274 ± 46	318 ± 115	155 ± 27

The numbers of total cell were counted in 30 organoids. Mean and std. derivation are given.

These results suggested that Axin1 loss in EBs, similarly to in the liver (Feng et al. 2012), caused higher proliferation levels. In contrast, CHIR99021 in the EBs compromised the cell's ability to proliferate or cause apoptosis.

This led us to perform a number of assays to detect proliferation levels in Axin mutant ES cells.

I S-phase cell cycle progression in EBs

Embryoid bodies were incubated with 10 µM BrdU (Sigma-Aldrich) for 1 h prior fixing, to label cells in S-Phase. 14-day-old EBs were then stained for BrdU incorporation.

Interestingly, in all EBs BrdU positive cells were mainly found towards the outside and only occasionally in the centre (Figure 4-25 A). Statistical analysis of the percentage of stained cells per EB only showed a significant upregulation in GSK3$^{\Delta/\Delta}$ EBs ($p<0.05$) (Figure 4-25 B). The increased number of BrdU positive cells in Axin1$^{\Delta/\Delta}$ was not found to be significant from the wt in a Bonferroni post-hoc test.

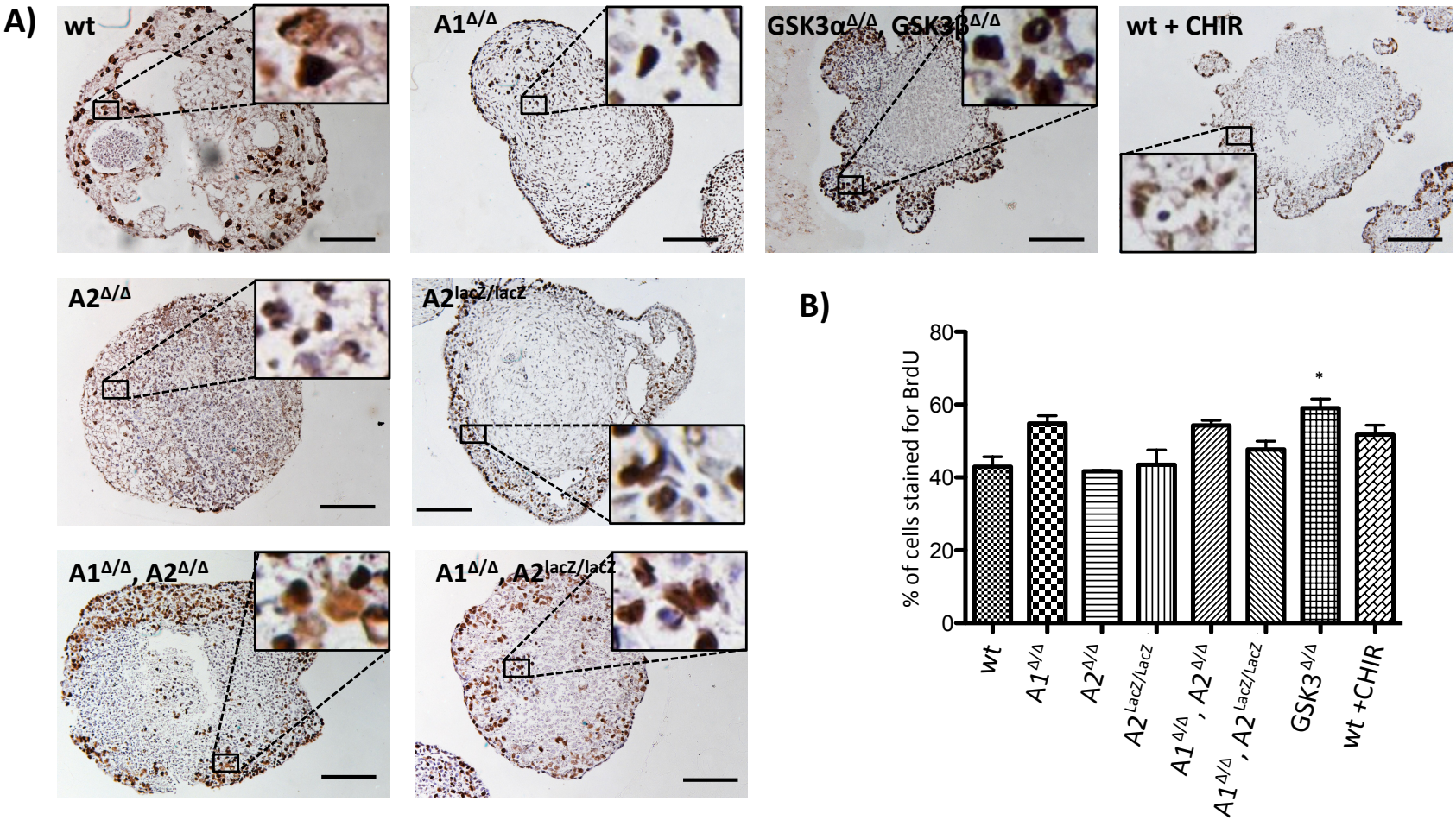

Figure 4-25. BrdU staining of embryoid bodies.
A) Embryoid bodies derived from Axin mutant ES cell lines fixed and stained for BrdU on day 14 of development. Sections were counterstained with Haematoxylin. Scale bars: 50 µm. **B)** Numbers of BrdU positive cells per embryoid body were counted for at least 30 embryoid bodies. Embryoid bodies from 3 cell lines of each genotype were scored. Data are shown as % of total cells. Data were analysed using a one-way ANOVA and a post-hoc Bonferroni test to compare between groups. *: $p<0.05$. Staining and analysis were performed by the PTY student Kyle Hawker under my supervision.

II Ki67 and Cyclinb1 staining in EBs

We also stained the EBs for Ki67, which is expressed in G1, S, G2, and M but not in G0 cells, and Cyclin B1, a marker for G2/M transition.

Ki67 positive cells were also mainly localised in the outer most cells of the EBs (Figure 4-26 A). However, the percentage of stained cells was slightly increased in Axin double mutants as well as $GSK3^{\Delta/\Delta}$ in comparison to the wt (all $p<0.05$) (Figure 4-26 B).

Cells expressing Cyclin B1 were more sparsely distributed than BrdU and Ki67 positive cells and were sometimes found at the centre of the embryoid bodies (Figure 4-27 A). Nevertheless, the proportion of stained to unstained cells per organoid was unchanged (Figure 4-27 B).

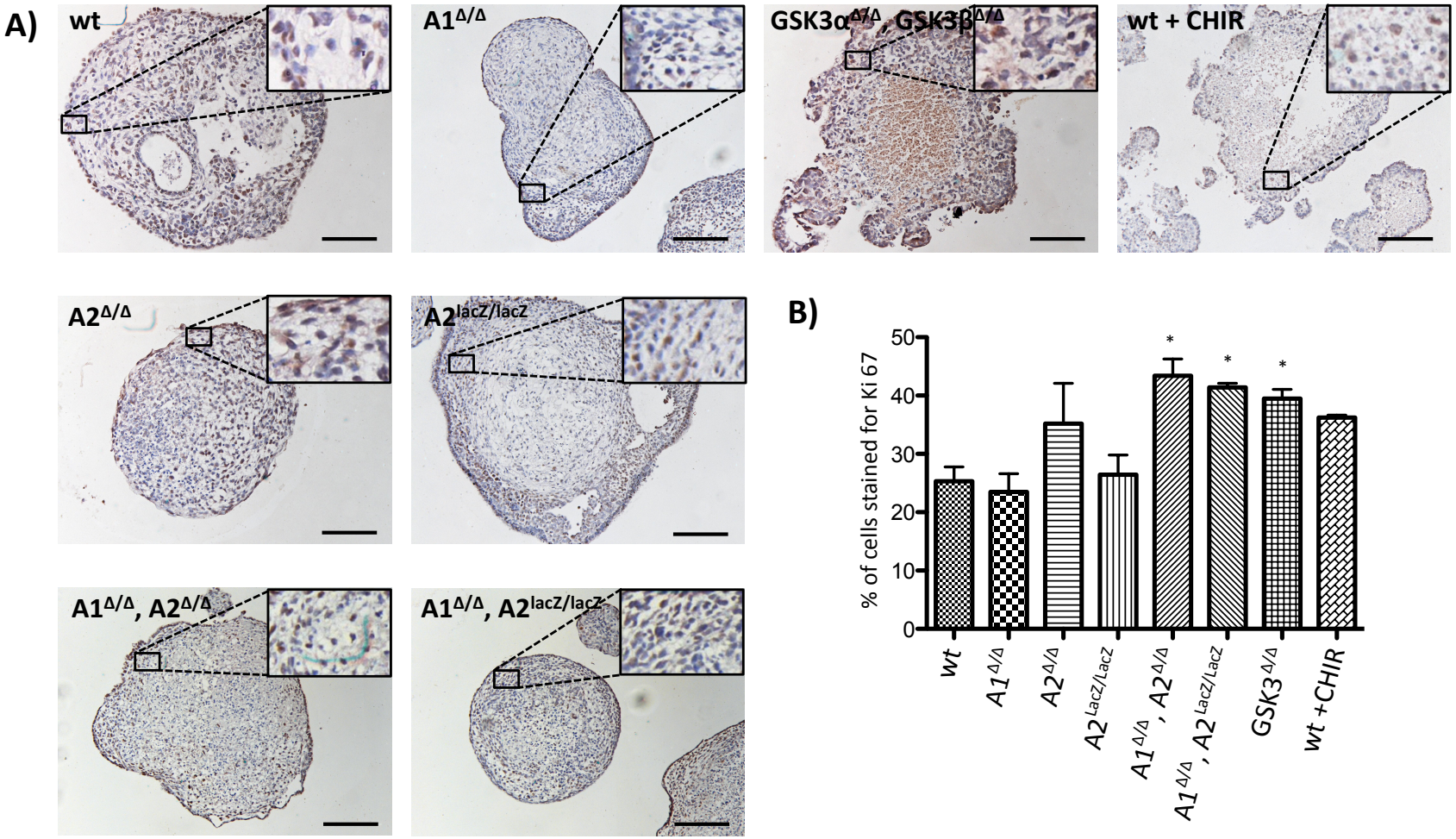

Figure 4-26. Ki 67 staining of embryoid bodies.

A) Embryoid bodies derived from Axin mutant ES cell lines fixed and stained for Ki67 on day 14 of development. Sections were counterstained with Haematoxylin. Scale bars: 50 µm. **B)** Numbers of Ki 67 positive cells per embryoid body were counted for at least 30 embryoid bodies. Embryoid bodies from 3 cell lines of each genotype were scored. Data are shown as % of total cells. Data were analysed using a one-way ANOVA and a post-hoc Bonferroni test to compare between groups. Significant differences are only shown compared to wt. *: $p<0.05$. Staining and analysis were performed by the PTY student Kyle Hawker under my supervision.

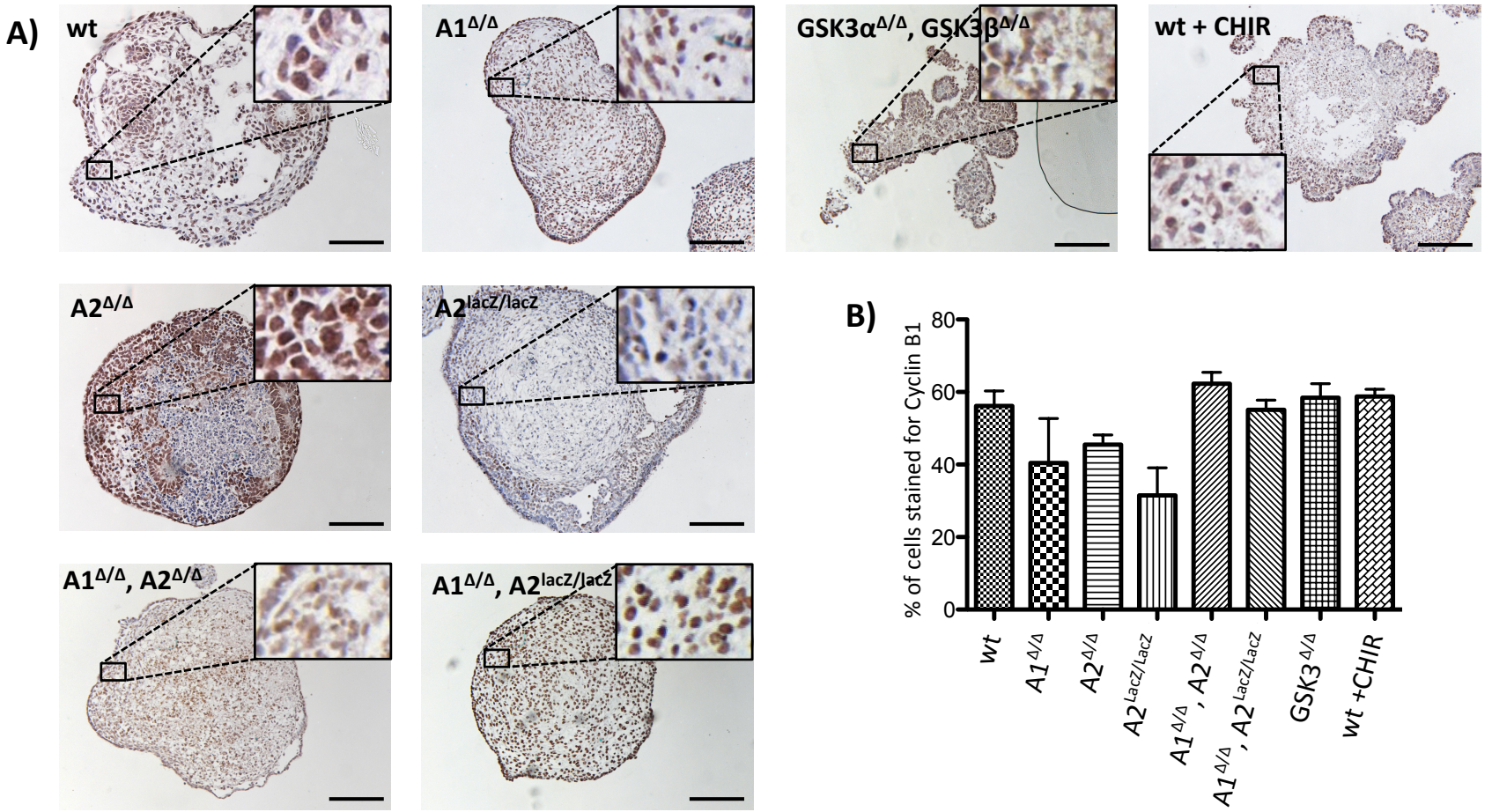

Figure 4-27. Cyclin B1 staining of embryoid bodies.

A) Embryoid bodies derived from Axin mutant ES cell lines fixed and stained for Cyclin B1 on day 14 of development. Sections were counterstained with Haematoxylin. Scale bars: 50 µm. **B)** Numbers of Cyclin B1 positive cells per embryoid body were counted for at least 30 embryoid bodies. Embryoid bodies from 3 cell lines of each genotype were scored. Data are shown as % of total cells. Data were analysed using a one-way ANOVA and a post-hoc Bonferroni test to compare between groups. No significant differences were found compared to wt. Staining and analysis were performed by the PTY student Kyle Hawker under my supervision.

III G2/M gene expression levels in EBs

Finally, we tested the expression of a panel of G2/M and cell cycle related genes. The panel was based on the one used by Gui-Jie Feng and colleagues, to asses Axin1 loss in the mouse liver (Feng et al. 2012). After performing a micro array and confirmation in a qRT-PCR assay 4 days after Axin1 deletion, they found, an enrichment of mRNAs associated with the G2/M phase of the cell cycle and cytokinesis in the liver.

In order to test the effects of Axin loss in EBs we analysed expression of a panel of mRNAs including Cdc25a, *Cyclins A2, B1, B2, Cdc20, Ki67, Mast1, and FoxM1* as markers for G2/M cell cycle progression. Mutations of single Axin genes in EBs ($Axin1^{\Delta/\Delta}$; $Axin2^{\Delta/\Delta}$; or $Axin2^{lacZ/lacZ}$) led to a slight increase in all of the G2/M signature genes tested (Figure 4-28 A, B, C). Mutations of both Axin genes ($A1^{\Delta/\Delta}$, $A2^{\Delta/\Delta}$; and $A1^{\Delta/\Delta}$ $A2^{lacZ/lacZ}$) led to a greater increase in the G2/M gene signature (Figure 4-28 D & E). Similar observations were made for GSK3 mutant EBs (Figure 4-28 F). GSK3 inhibition using the small molecule inhibitor CHIR99021, had less of an effect (similar to Axin single mutants) (Figure 4-28 G).

Taken together, immunohistochemistry and qRT-PCR data in embryoid bodies suggest that Axin mutations results in a partial increase in cell proliferation and in the numbers of cells expressing G2/M markers. This observation was similar to that observed following loss of Axin1 in the mouse liver (Feng et al. 2012), but was different from the lack of a proliferative response in ES cells. Interestingly, the G2/M signature was strongest upon mutations of both Axin genes, suggesting that similar studies should be carried out in the liver where this signature might be implicated in the mechanism of tumourigenesis. The staining pattern observed using anti-Ki67 antibody confirms this finding. However, the staining pattern for BrdU and Cyclin B1 did not show a significant effect of Axin mutations on EBs compared to wt. This difference might be the effect of long-term proliferation, apoptosis and entry of cells into G0 over the whole time of embryoid body formation.

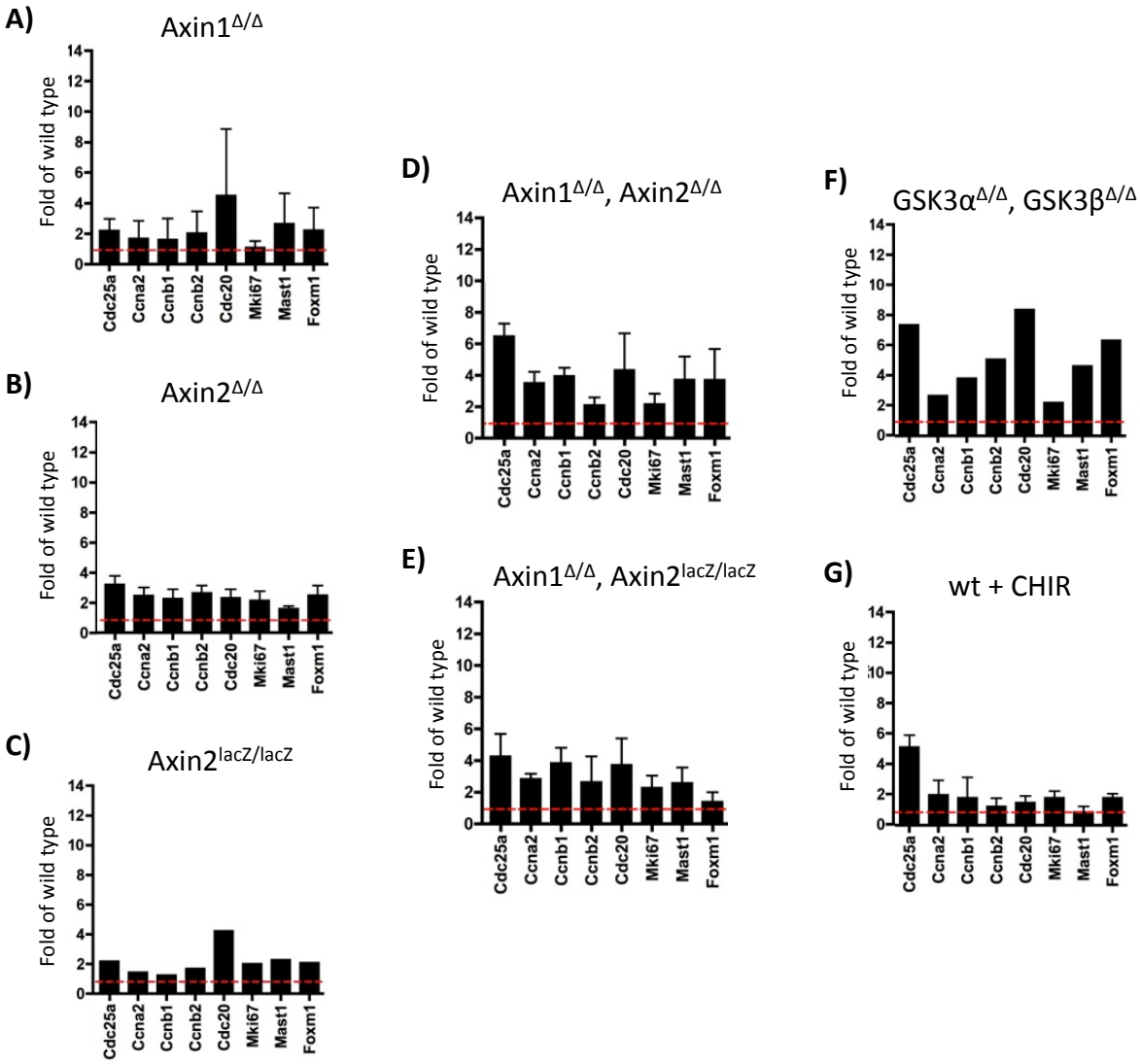

Figure 4-28. G2/M related gene expression profile in Axin mutant embryoid bodies.
EBs bodies were grown for 14 days, then mRNA was harvested and analysed for the expression of a penal of G2/M cell cycle related genes. The fold change of $A1^{\Delta/\Delta}$ **(A)**; $A2^{\Delta/\Delta}$ **(B)**; $A2^{\Delta lacZ/lacZ}$ **(C)**; $A1^{\Delta/\Delta}$, $A2^{\Delta/\Delta}$ **(D)**; $A1^{\Delta/\Delta}$, $A2^{\Delta lacZ/lacZ}$ **(E)**; $GSK3^{\Delta/\Delta}$ **(F)** EBs; and wt EBs treated with CHIR99021 **(G)** compared to wt EBs are shown. Wt expression levels are indicated with a red line. Data were normalized to β-Actin expression. N=3 for all but $A2^{\Delta lacZ/lacZ}$ and $GSK3^{\Delta/\Delta}$ (both N=1). EBs were grown and harvested by me. Ken Ewan helped with the performance of the qRT-PCR assay under my supervision.

In addition to a possible direct effect of Axin mutations, we might be looking at indirect effects of differentiation into more or less proliferative cell types. Additionally the surface area and the size of each EB could affect access to oxygen and nutrients in the core, which would explain the predominate immunohistochemical staining located on the periphery of the EBs.

4.8 Axin loss in the mouse embryo

The importance of Axin1 in embryonic development has been known since the first identification as the product of the mouse *fused* locus by Zeng and his colleagues (Zeng et al. 1997)(see also Section 1.3.5). Additionally, we found strongly impaired differentiation potential in Axin mutant ES cell lines. These findings led us to examine the embryonic phenotype of Axin loss from the alleles used in this study. In addition to giving more insight into the role of Axin in embryonic development, this chapter aims to answer the question, whether the conditional mutant alleles generate null alleles?

A simple explanation for the lack of activated β-Catenin following Axin1 loss in the liver (Feng et al 2012) as well as in the Axin1 mutant, undifferentiated ES cells, discussed earlier in this Chapter (see Section 4.4), could be due to the presence of an active β-Catenin destruction complex nucleated by Axin2. In addition to functional redundancy, the phenotype of single Axin mutants might be explained by, the incomplete loss of Axin protein following Cre mediated recombination. (For more information see Section 1.3.6 II). Lastly, and formally, the lack of upregulated Wnt signalling following Axin loss could result from the formation of an Axin-independent β-Catenin destruction complex.

4.8.1 Loss of Axin1 protein in Axin1$^{\Delta/\Delta}$

The conditional mutant strategy for Axin1 used by Feng et al. relies on the removal of exon 2 (Feng et al. 2012) (Figure 1-10 A-D). Exon 2 was flanked by *loxP* sites by homologous recombination, allowing Cre mediated recombination and thus deletion. Exon 2 contains the AUG start codon and the APC binding domain (RGS), which is important for β-Catenin regulation (Figure 1-10 A, C & D). We hypothesised that the removal of this exon should lead to the total loss of Axin protein.

To evaluate the possibility of a protein with remaining Axin1 function, we analysed Axin1$^{\Delta/\Delta}$ cDNA for alternative initiation codons and corresponding Kozak consensus sequences, using ATGpr program (Nishikawa et al. 2000)[g]. This online tool predicts translation initiation codon by combining statistical information and similarity with known protein sequences. Based on set of 660 reference sequences and a list of 133 sequences, used for assessing Kozak's rules, this software predicted and scored ORFs (open reading frame) according to their reliability. We then blasted the predicted protein sequence to find known functional protein domains using NCBI's BLASTP. (See Section 1.3 A for information about Axin domains.)

First, we tested the online tools for predication accuracy, by analysing the mouse wild type Axin1 version 1 cDNA (Vega Genome Browser[h]; Axin1 version 1 is the longest cDNA contain the alternatively spliced exon 8a; see 1.3). As expected, the most highly scored (33%) predicted ORF found, matched full length Axin1 protein and the BLASTP result indicated the presence of TNKs and β-Catenin binding sites, as well as the RGS and DIX domains (Appendix 4, Table A 3).

When Axin1$^{\Delta/\Delta}$ cDNA was used as the input sequence the 10 most reliable predicted proteins scored between 14 and 55% (Appendix 4, Table A 4). Among those, 5 predicted proteins had no known protein domains. However, the other 5 were truncated Axin proteins

[g] http://atgpr.dbcls.jp/

[h] http://vega.sanger.ac.uk/Mus_musculus/Transcript/Sequence_cDNA?db=core;g=OTTMUSG00000026498;r=17:26138688-26195811;t=OTTMUST00000065524

containing DIX domains of which 1 even had a remaining and β-Catenin binding domain. The GSK3 binding domain was only found in one of the predicted proteins. This result indicated that the Axin1$^{\Delta}$ allele might express a truncated protein with residual function from an alternative start codon, together with its Kozak sequence. However, the start codon for the predicted protein containing GSK3, β-Catenin and DIX binding domain is not in frame following a simple exon 1-3 splice of Axin1. Truncated proteins without GSK3 binding site are predicted to be non-functional or dominant negative alleles.

Immunoblotting and immunoprecipitation with antibodies that recognise different regions of the Axin1 molecule, performed by Gui-Jie Feng, failed to detect any region of remaining protein in the liver (Feng et al. 2012). However, low levels of remaining, possibly truncated Axin1 protein might have been below the levels of detection using the western blotting methods described.

4.8.2 Conditional deletion of Axin1 is embryonically lethal

To demonstrate that exon 2 is essential for Axin1 function, we investigated the effect of embryonic deletion in our Axin1$^{fl/fl}$ mice. The classic Axin1 null Axin$^{Tg1/Tg1}$ allele has been shown to be embryonically lethal at E 9.5 and was associated with a variety of defects like forebrain truncation and axis duplication (see Section 1.3.5.)(Perry et al. 1995; Zeng et al. 1997). To recreate an embryonic Axin1 exon 2$^{\Delta/\Delta}$ allele, we crossed Axin1$^{fl/fl}$ mice with the embryonically active CMV-Cre (Schwenk et al. 1995). As expected, deletion of exon 2 though CMV-Cre was observed in embryos from these crosses and these were found to have a very similar phenotype to the Axin$^{Tg1/Tg1}$ allele (see Figure 4-29 A b &c , B d-f). At E 10.5 9 Axin1$^{\Delta/\Delta}$ homozygotes out of 35 embryos were detected from crosses between Axin1$^{wt/\Delta}$ mice. This was consistent with the expected Mendelian ratio (χ^2=0.0005, df=1, p=0.47) suggesting that the phenotypes observed represented those formed following the earliest loss of function effects.

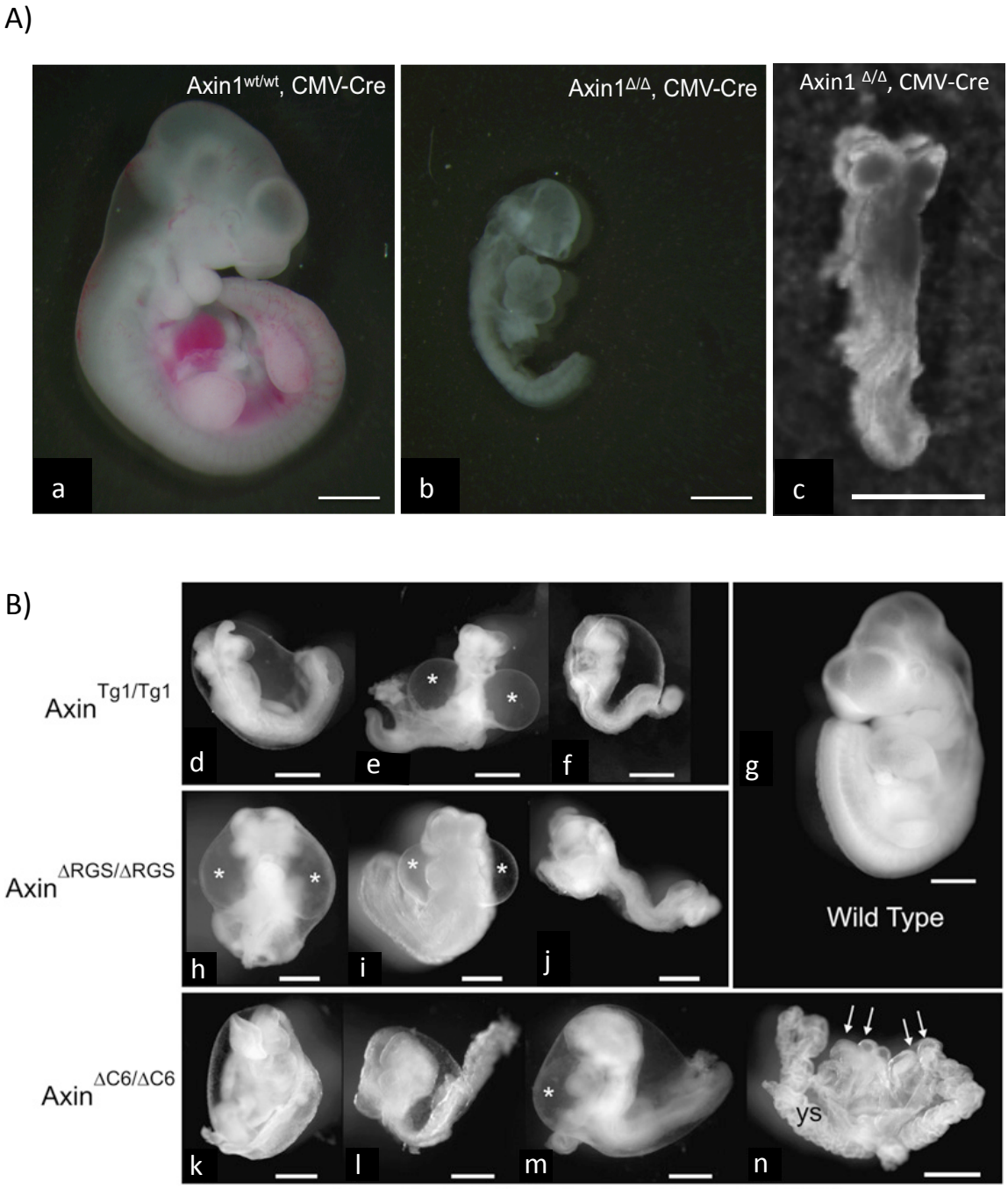

Figure 4-29. Axin1 deletion is embryonically lethal.
A) The CMV-Cre mediated recombination of the conditional Axin1 mutant ($Axin1^{fl/fl}$) shows an embryonic lethal phenotype in homozygotes ($Axin1^{\Delta/\Delta}$) **(b, c)**. **(a)** Axin1 wt embryo at E10.5. **(b, c)** $Axin1^{\Delta/\Delta}$ at the same age. All $Axin1^{\Delta/\Delta}$ the mutants show a variation of reduction in size, developmental delay, open head fold (d) and truncated heads. **B)** Pictures **d)** to **n)** were taken from Chia et al. 2009[i]. $Axin^{\Delta RGS}$ **(h-j)** or $Axin^{\Delta C6}$ **(k-n)** homozygotes display an embryonic lethal phenotype indistinguishable from that of the null allele $Axin1^{Tg1}$. (g) Wild-type embryo at E 9.5. Embryos are all shown at E9.5. Scale bars: 0.5mm

[i] Permission to reproduce this figure has been granted by the Genetics Society of America.

All Axin1$^{\Delta/\Delta}$ homozygote embryos were smaller than their Axin1$^{wt/wt}$ or Axin1$^{wt/\Delta}$ littermates and showed a variety of defects, including malformations, reduction in size, developmental delay, open head folds, and truncated heads (see Figure 4-29, A a - c). Loss of Axin1 was confirmed by PCR analysis (data not shown).

But even though the conditional Axin1 mutants resembled the embryos with full loss of the *Axin1* gene (Axin^{Tg1}, Figure 4-29 B d - f), the presence of a truncated Axin1 protein could still not be excluded completely. Chia and his colleagues generated modified Axin1 alleles with deletions in either the RGS domain (Axin $^{\Delta RGS}$, Figure 4-29 B h - j), required for APC binding, or the C-terminal region (Axin $^{\Delta C6}$, Figure 4-29 B k-n), involved in JNK activation (Chia et al. 2009). Both mutants (Axin $^{\Delta RGS}$ and Axin $^{\Delta C6}$) also displayed recessive embryonic lethality at E 9.5 with a similar range of malformations (see Figure 4-29, B h - n). Levels of protein expressed by Axin$^{\Delta C6}$ were only 25-30% of wild type levels and could be rescued by heterozygosity a the β-Catenin (null) locus, suggesting that β-Catenin upregulation was still the main cause for the mutant phenotypes (Chia et al. 2009).

Taken together, our data is consistent with the Axin1$^{\Delta/\Delta}$ allele being a functional null. However, to definitively confirm the loss of all Axin1 residual function would require the loss of all coding exons (see Section 6.7). Importantly, even if truncated Axin1 were still present at a very low level in the conditional Axin1 mutants, the definitive removal of exon 2, which contains the RGS binding site, would be predicted at a minimum to interfere with any remaining protein's ability to interact (via APC) with β-Catenin destruction complex.

4.8.3 Loss of Axin2 protein in Axin2$^{\Delta/\Delta}$

The question about remaining Axin protein in any of the mutants studied here, was especially important for Axin2. In this study we utilised two independent Axin2 alleles (Axin2$^{fl/fl}$/ Axin2$^{\Delta/\Delta}$ and Axin2$^{lacZ/lacZ}$) that differed in their phenotype when combined with the loss of Axin1 (see Section 4.4.5), suggesting that at least one of the alleles was not a full knockout.

The conditional strategy to delete Axin2 in $Axin2^{fl/fl}$ (Feng, unpublished) was based on the same strategy as the one used for Axin1 (see Figure 1-10 B - D). Again, exon 2 was flanked by *loxP* sites using homologous recombination, such that it could be removed by Cre-recombinase. Similarly to Axin1, this exon contains the start codon and the RGS domain important for β-Catenin regulation (see Section1.3).

To analyse the possibility of residual Axin2 function we also analysed the $Axin2^{\Delta}$ allele using ATGpr, a program for identifying the initiation codons in cDNA sequences, (Nishikawa et al. 2000), and NCBI's BLASTP, to identify functional domains in the predicted protein coding sequence. When wild type Axin2 cDNA (Vega Genome Browser[j]) was used as an input, the program accurately predicted the normal Axin2 protein with its TNKs and β-Catenin binding sites and the RGS and DIX domain with a reliability score of 28 % (Appendix 4 Table A 5). For $Axin2^{\Delta/\Delta}$ cDNA the 10 best predictions scored between 18 and 55%. Again, 5 predicted ORFs were for proteins without known domain structures (see Appendix 4, Table A 6). 4 predicted protein sequences included the GSK3, β-Catenin binding, and DIX domains. The last sequence contained truncated Axin2 containing the DIX domain.

The first in frame start codon following a 1-3 splice of Axin2 was found within Exon 8, thus after the GSK3 and β-Catenin binding sites. This would predict that no functional protein is made.

Sequence information for the $Axin2^{lacZ}$ allele is not publically available. However, the *lacZ* gene, with nuclear localization sequence, was reported to be inserted in the vicinity of Exon 2, in frame with the endogenous start codon (Lustig et al. 2002). In this process, most of Exon 2 was replaced. Both alleles preserve sequences outside of Exon2 and might be expected to lead to similar consequences on function.

In the case of Axin2, we have not been able to perform experiments to detect possible residual Axin2. Thus far, there are no good antibodies to detect Axin2 in the mouse. The

[j] http://vega.sanger.ac.uk/Mus_musculus/Transcript/Sequence_cDNA?db=core;g=OTTMUSG00000003199;r=11:108920349-108950783;t=OTTMUST00000006621

detection of mouse Axin2 protein at normal levels is already very challenging, the detection of a possible low-level truncated Axin2 is nearly impossible.

Given these results, it remains possible, that the Axin2$^{\Delta}$ and Axin2 ^{lacZ} allele expresses a truncated protein with residual function from an alternative pair of start codon and Kozak sequence.

4.8.4 Differential effects of Axin2^{lacZ} and embryonic deletion of Axin2^{fl} on embryonic development

Being short of a good Axin2 detection method, we decided to compare our conditional Axin2 allele with other commercially available Axin2 mouse lines in all experiments. The most commonly studied Axin2 allele in mice is Axin2$^{lacZ/lacZ,}$ in which the *lacZ* gene was inserted into exon 2 of *Axin2* (Lustig et al. 2002)(see Figure 1-10 E). In contrast to Axin1 mutants, Axin2$^{lacZ/lacZ}$ mice have been described as viable and fertile. They showed no obvious changes in embryonic patterning, with only minor defects in skull formation (Yu et al. 2005)(see Figure 4-30 B), tooth development (Lammi et al. 2004) and reduced body weight in comparison to Axin2$^{lacZ/wt}$ and wild type littermates (Dao et al. 2010).

Surprisingly, we observed that the effects of the deletion of Axin2 in the Axin2$^{fl/fl}$ mice using the embryonically active CMV-Cre allele (Schwenk et al. 1995) differed from the phenotype observed in Axin2$^{lacZ/lacZ}$ mice. Embryos homozygous for the floxed allele (Axin2$^{\Delta/\Delta}$) were embryonically lethal and showed a major reduction in body size at E.9.5 (Figure 4-30 A e, f). In heterozygotes the phenotype was more diverse. Some embryos were almost indistinguishable from the wild type littermates, whereas others showed major reduction in size and head development (Figure 4-30 A e, f shows to examples of Axin2$^{wt/\Delta}$ embryos at E.10.5). This size difference could be related to varying levels of wild type Axin2 protein in the embryos. Mosaic expression of CMV-Cre, or mosaic recombination events within one embryo, are very likely. Indeed, genotyping PCR experiments sometimes showed all three alleles (wt, fl, Δ) in one embryo (data not shown). Based on this observation, three

follow-up experiments should be considered for future studies. Genomic qPCR should be performed to be able to relate the embryo size to the recombination level in each embryo. Embryo size should also be directly related to Axin2 protein levels determined by Western blot (as soon as good Axin2 antibodies are available) and reporter constructs for Cre recombinase activity (ROSA-lacZ or ROSA-rfp (Soriano 1999; Luche et al. 2007)) can be used to correlate the embryonic phenotype with the location and quantity of recombined cells.

There is also strong evidence, that the genetic background of each mouse is important. In the first few rounds of breeding of $Axin2^{fl/wt}$ with CMV-Cre mice, no $Axin2^{wt/\Delta}$, CMV-Cre offspring were generated. Whereas the frequency of survival was increased with further rounds of breeding, suggesting a selection against the responsible loci. The heterozygous Axin2 embryos that came to full term developed into fertile adults and the deleted allele could be transmitted to the next generation. Interestingly, the phenotype observed in adult heterozygous ($Axin2^{wt/\Delta}$) animals closely resembled that of homozygous $Axin2^{lacZ/lacZ}$ mice, since affected mice displayed shorter heads, malformation of the forelimbs and kinky tails compared to wild type animals (data not shown).

In summary, our data suggests that the $Axin2^{\Delta/\Delta}$ allele is consistent with it being a more severe form of the $Axin^{lacz/lacZ}$ allele which in turn has been suggested to result from β-Catenin /TCF pathway hyperactivation.

Nevertheless, even though both constructs rely on a change of exon 2 (lacZ insertion in $Axin2^{lacZ}$ and removal of a *loxP*-flanked exon 2 in $Axin2^{\Delta}$, Figure 1-10 B to E) they showed different characteristics. In the literature, the $Axin2^{lacZ}$ allele is often referred to as an Axin2 null allele, despite the lack of published evidence to prove or disprove this theory. Until definite proof of the presence or absence of a truncated Axin2 protein is found in any of the Axin2 lines, the identity of a true null remains a mystery. A full knockout of the whole coding region of Axin2 could help to clarify the phenotype (see Section 6.7).

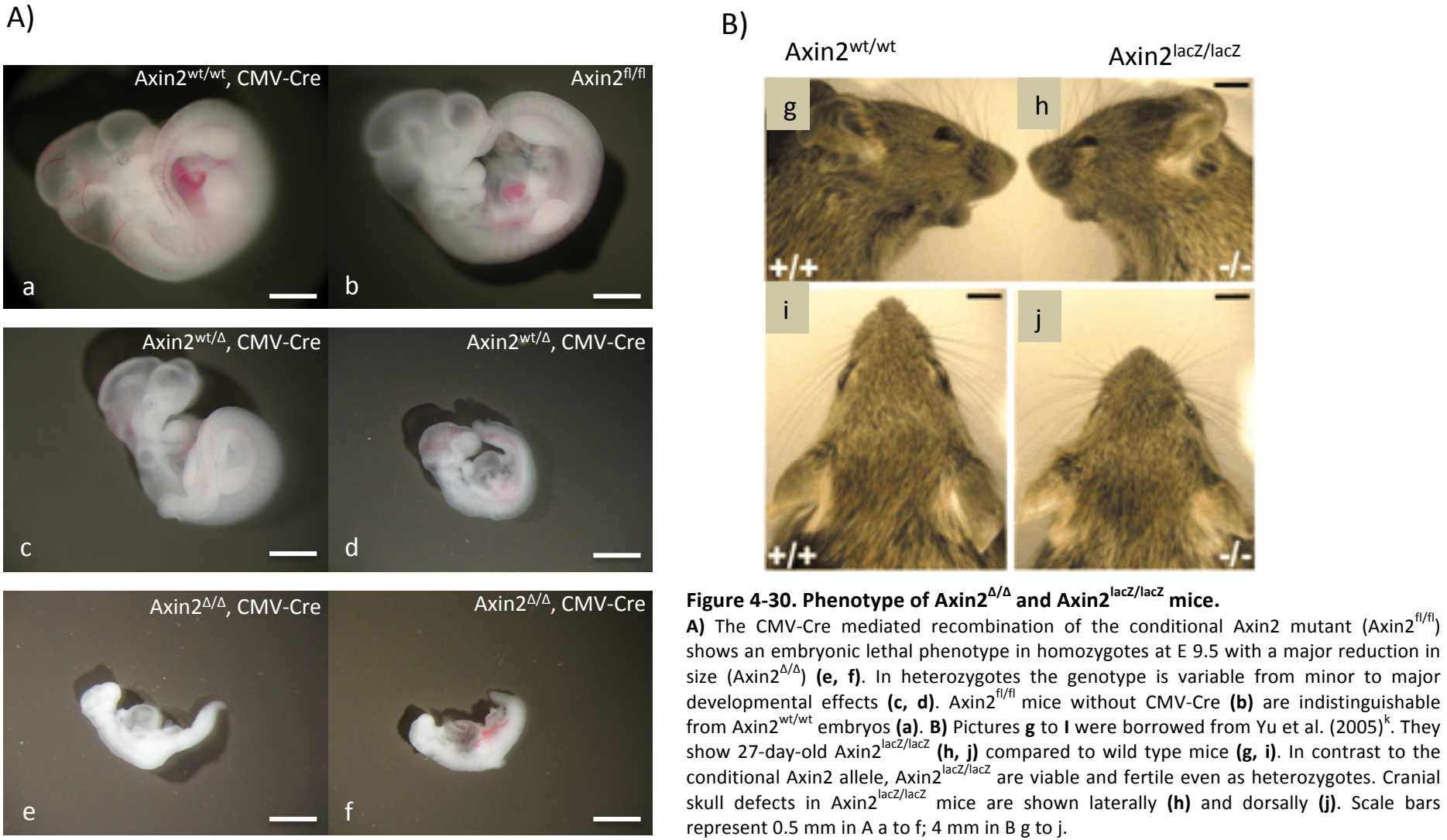

Figure 4-30. Phenotype of Axin2$^{\Delta/\Delta}$ and Axin2$^{lacZ/lacZ}$ mice.
A) The CMV-Cre mediated recombination of the conditional Axin2 mutant (Axin2$^{fl/fl}$) shows an embryonic lethal phenotype in homozygotes at E 9.5 with a major reduction in size (Axin2$^{\Delta/\Delta}$) **(e, f)**. In heterozygotes the genotype is variable from minor to major developmental effects **(c, d)**. Axin2$^{fl/fl}$ mice without CMV-Cre **(b)** are indistinguishable from Axin2$^{wt/wt}$ embryos **(a)**. **B)** Pictures **g** to **I** were borrowed from Yu et al. (2005)[k]. They show 27-day-old Axin2$^{lacZ/lacZ}$ **(h, j)** compared to wild type mice **(g, i)**. In contrast to the conditional Axin2 allele, Axin2$^{lacZ/lacZ}$ are viable and fertile even as heterozygotes. Cranial skull defects in Axin2$^{lacZ/lacZ}$ mice are shown laterally **(h)** and dorsally **(j)**. Scale bars represent 0.5 mm in A a to f; 4 mm in B g to j.

[k] Permission to reproduce this figure has been granted by the Company of Biologists.

4.9 Summary of the effects of Axin mutations in ES cells and development

In this chapter, we analysed the effects of Axin loss in embryonic stem cells and on embryonic development using a conditional allele of Axin1 ($Axin1^{fl/fl}$), and two different alleles for Axin2 ($Axin2^{fl/fl}$ and $Axin2^{lacZ/lacZ}$). In this Section, I will shortly summarize the findings. A more extended discussion of the results will be presented in Chapter 6.

After generating an allelic series of Axin mutant ES cell lines (Section 4.2), we tested if Wnt/β-Catenin was activated. We found that Wnt/β-Catenin signalling was largely unaffected in undifferentiated Axin ES cell lines (Section 4.4), but became activated when double mutant ES cells were allowed to differentiate into embryoid bodies (Section 4.7.2).

Next, we tested, whether stem cell self-renewal and differentiation was affected in a similar way to other known mutants of the Wnt signalling pathway. Wnt activation though loss of GSK3 or APC was found to cause a strong reduction in the differentiation potential of stem cells (Doble et al. 2007; Kielman et al. 2002; Atlasi et al. 2013), similar to that of other studies that have linked high Wnt activity to mesoderm differentiation, and suppression of neuroectoderm in mouse ES cells (Aubert et al. 2002; Haegele et al. 2003; Sato et al. 2004; Bakre et al. 2007). In Axin mutant ES cells we found increased levels of AP and Oct4 protein (Section 4.6) and were inhibited in their lineage potential when differentiated into EBs (Section 4.7.1) in line with the Wnt pathway mutants described above.

Cell proliferation was mostly unaffected in ES cell lines (Section 4.5) and only slightly increased in EBs following Axin1 and 2 mutation (Section 4.7.3).

Axin single mutant ES cells were mostly unaffected in any of the experiments above. Stronger effects were only observed in Axin double mutants. Interestingly, the mutation of both Axin genes using the $Axin1^{\Delta/\Delta}$, $Axin2^{lacZ/lacZ}$ genotype was often significantly different (and stronger) than $Axin1^{\Delta/\Delta}$, $Axin2^{\Delta/\Delta}$.

Lack of a strong Wnt/β-Catenin signature and the difference between the $Axin2^{\Delta/\Delta}$ and the $Axin2^{\Delta/\Delta}$ alleles led us to study full embryonic development and question the complete loss of Axin protein in the alleles studied here.

Embryonic deletion of Axin1 led to the expected effects, however the formation of a truncated Axin1 protein could not be definitively ruled out (Section 4.8.2).

The phenotype of embryonic loss of Exon 2 of $Axin2^{fl/fl}$ was very different to the one in $Axin2^{lacZ/lacZ}$ mice (Section 4.8.4), again questioning the identity of a true knockout. Detecting a truncated residual Axin protein from any of the Axin alleles is nearly impossible using current reagents and is in any case an attempt at proving a negative. Therefore a full knockout of the whole coding region may be necessary to demonstrate full loss of function (see Section 6.7).

5 Acute loss of Axin the liver leading to the development of HCC

5.1 Introduction

Hepatocellular carcinoma (HCC) is the most common form of primary liver cancer and the third most common cause of cancer death worldwide. Mutations in the canonical Wnt signalling regulator Axin1 occur in 16% of HCCs, in a subset of tumours that are poorly differentiated, chromosomally unstable, and have poor prognosis. Because Axin is a main component of the Wnt signalling pathway, tumourigenesis was traditionally believed to be due to hyperactivated Wnt signalling. Other mutations of the Wnt signalling pathway, like activating mutations of β-Catenin, can be found in many HCCs (La Coste et al. 1998; Miyoshi et al. 1998) .

To study the effect of Axin1 loss in the liver, Gui-Jie Feng et al. examined the effects of conditional deletion of Axin1 in the liver of adult mice (Feng et al. 2012). Interestingly, Axin1 loss led to an increase in cell proliferation, a G2/M cell cycle associated gene expression profile, and the development of HCC after one year. But Axin1 deletion in mouse livers was not associated with a rise in nuclear β-Catenin levels or changes in liver zonation that are found in mutants of other Wnt pathway components. However, the mouse model strikingly resembles the situation in human HCCs that have mutations in AXIN1 showing a similar gene expression signature without obvious activation of liver-specific Wnt pathway transcriptional targets (Boyault et al. 2007; Zucman-Rossi et al. 2007).

These results suggest that the conditional Axin mutant mouse line provides a good tool to study the mechanisms leading to Axin dependent tumourigenesis. However, the characterization of the effects of mutant Axin1 anti-oncogenes *in vivo* is limited to the investigation of single time points in individual mice. The use of the recently developed primary 3D culturing system can overcome these limitations and allow a closer look at the underlying mechanisms in real time (Huch et al. 2013) (see 1.4.2.2 for more information

about the liver culture system). This chapter aims to develop and validate an Axin1 deficient 3D liver organoid culture system as a model to study the acute effects following Axin1 loss in the liver, leading to the development of HCCs. The culture system should allow tightly regulated and highly efficient loss of Axin, while mimicking the *in vivo* situation as close as possible.

5.2 Development of a Axin mutant 3D liver culture system using Ah-Cre

5.2.1 Liver organoid cultures can be successfully derived and expanded *in vitro*

The first step in the analysis of Axin mutations in liver organoid culture was to establish the primary 3D culture system in the Dale lab.

Following the protocol developed by the Clevers lab (Huch et al. 2013), isolated bile duct fragments from wild type mouse livers were seeded in Matrigel, which mimics extracellular matrix, to allow three-dimensional cell growth. These fragments formed cyst-like structures overnight and kept growing into large, complex organoids in an R-Spondin1 based expansion medium (EM) in our hands (Figure 5-1 A, B). The organoids consisted mostly of single layered epithelium and some areas of pseudo-stratified epithelium and resembled ductal cells (Figure 5-1 C, left panel).

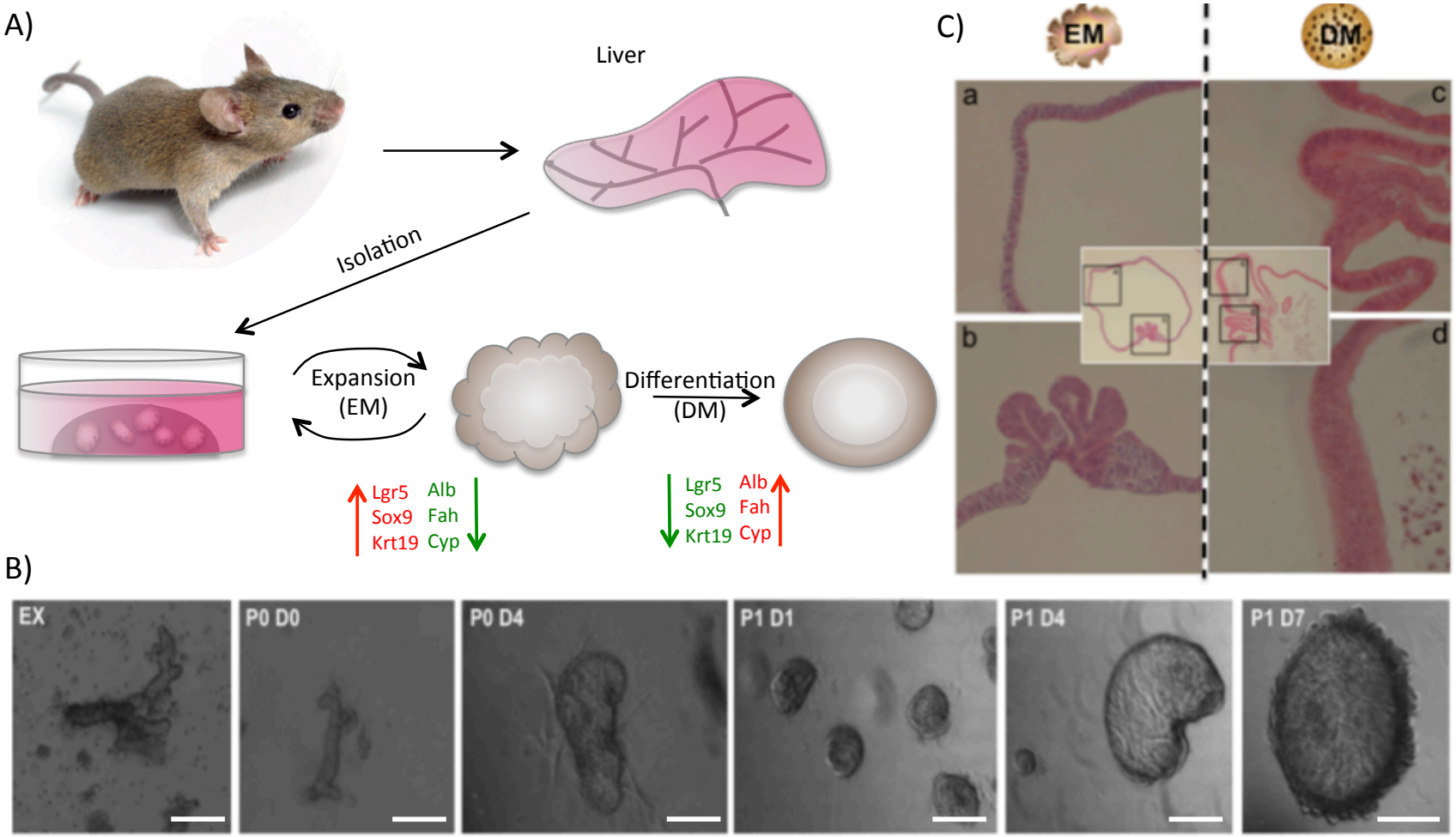

Figure 5-1. *In vitro* expansion and differentiation of ductal derived organoids.
A) Progenitor cells from intrahepatic bile ducts can be cultured and differentiated into hepatocytes *in vitro*. **B)** Biliary duct fragments during extraction (EX) and after embedding in Matrigel. Passage number (P) and Days (D) in culture are indicated. Magnification: 10x. Scale bar indicates 100 µm. **C)** H&E staining of organoids in expansion (EM) or differentiation (DM) conditions. Blow-ups show single layered epithelia **(a)** and pseudo stratified epithelia **(b, c)** in EM and DM. In DM hexagonal shaped hepatocytes are shown **(d).**

5.2.2 Differentiation of ductal derived liver organoids along the hepatic lineage

In order to induce the ductal derived organoids to undergo hepatocyte differentiation *in vitro* culture conditions are changed from EM to differentiation medium (DM) two days after passage (Figure 5-1 A). The differentiation conditions were based on the inhibition of Notch and TGF-β signalling and the removal of the Wnt signalling potentiator R-Spondin1, all of which have been linked to biliary fate determination in the liver (Tanimizu 2004; Lemaigre 2009). After 12 days in differentiation conditions the overall structure and morphology of the organoids was not visibly altered but the shape of the majority of cells within a structure changed from a spherical to a polygonal, hepatocyte-like morphology (Figure 5-1 C, right panel).

According to the experiments performed by Huch et al. *Lgr5* was actively expressed during extraction and expansion condition, similar to intrahepatic bile ducts after injury (Huch et al. 2013; Hu et al. 2007). In differentiation conditions, Wnt target gene expression was shut down, together with the loss of Lgr5 expression which is itself a Wnt pathway transcriptional target (de Lau et al. 2011; Huch et al. 2013). In our hands, q-RT-PCR for Lgr5 confirmed the significant reduction of its expression, following exposure to differentiation conditions (Figure 5-2 A).

Additionally, the down regulation of the Wnt profile after differentiation, along the hepatic lineage, was confirmed in organoids from isolated Axin2$^{lacZ/wt}$ Wnt reporter mice (Lustig et al. 2002) (Figure 1-10 E). In liver organoids grown in EM, strong *lacZ* expression could be observed throughout the whole organoid (Figure 5-2 B, top), while *Axin2-lacZ* expression in organoids grown in DM for 8 days was completely abolished (Figure 5-2 B, bottom).

Simultaneously with the loss of Wnt target gene expression the hepatocyte markers *Hnf1α, Hnf4α* and *TTR* were upregulated (Figure 5-2 A). The cholangiocyte marker *Krt19* and the hepatocyte marker *Alb* (Albumin) stayed at the same level of expression in our hands.

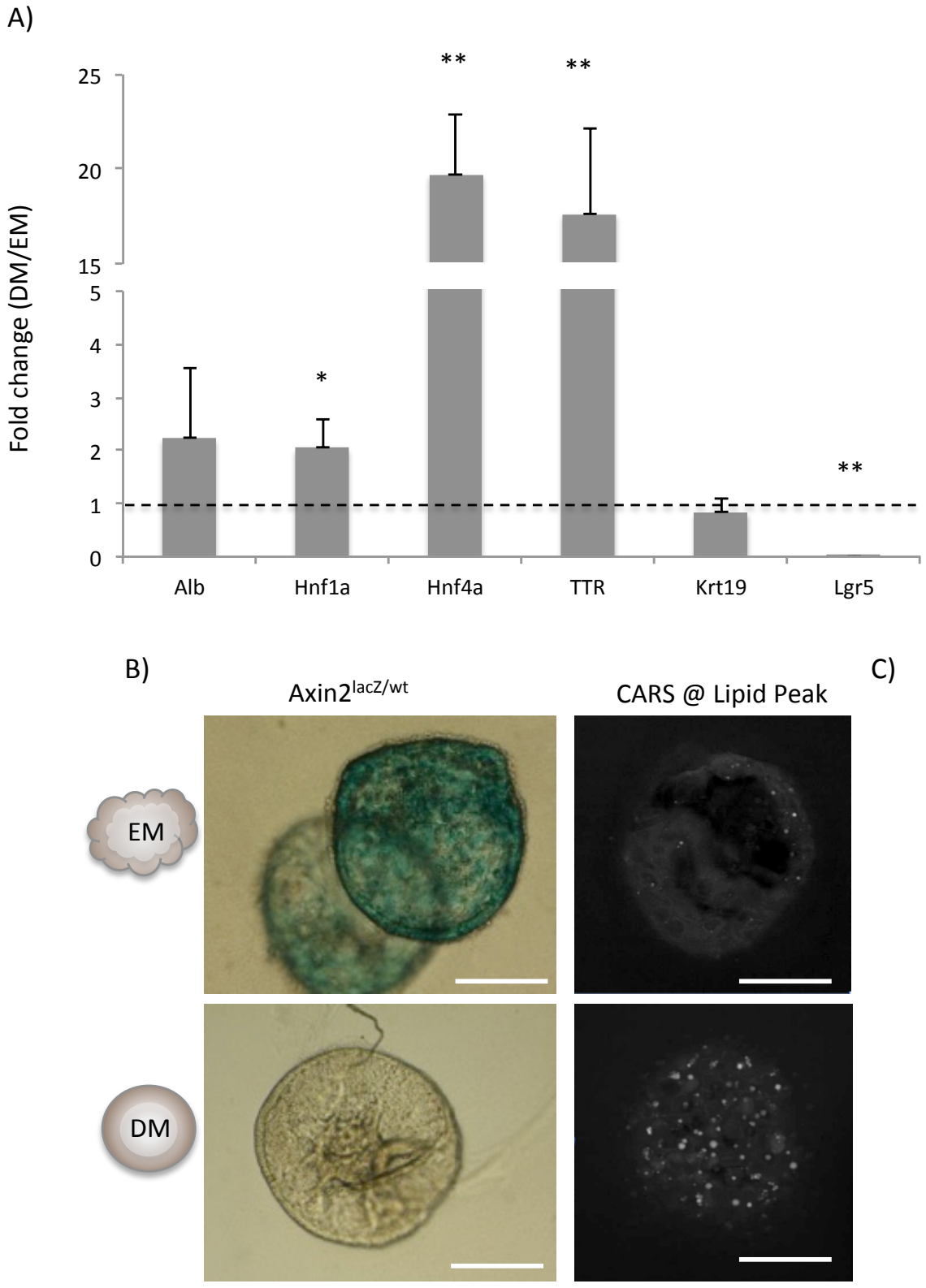

Figure 5-2. *In vitro* differentiation of liver organoids.
A) Gene expression profile of wild type liver organoids grown in differentiation medium (DM) compared to cells grown in expansion medium (EM) assessed by qRT-PCR using B2M as the reference gene. Data are presented as the mean fold change. N=3, error bars: SEM, *:P<0.05, **:P<0.001. **B)** X-gal staining of $Axin2^{lacZ/wt}$ derived livers in expansion (EM) and differentiation medium (DM). **C)** Liver organoids in EM or DM imaged using Coherent anti-Stokes Raman Scattering (CARS) microscopy at the lipid peak (2850 cm^{-1}). Scale bars indicate 50 µm.

In addition to the expression of hepatocyte-specific genes, we could also show the accumulation of lipid droplets in the cells, which had been exposed to differentiation conditions of organoids derived from wild type mice (Figure 5-2 C). The lipid content of the cells was analysed by live imaging of liver organoids, using Coherent anti-Stokes Raman Scattering (CARS) microscopy at the lipid peak (2850 cm^{-1}) with the help of Iestyn Pope, Francesco Masia and Arnica Karuna (Pope et al. 2013).

This analysis revealed that organoids grown in EM only contain a small amount of lipids (Figure 5-2 C, top), whereas organoids grown in differentiation conditions exhibit many bright puncta, characteristic for lipid droplets (Figure 5-2 C, bottom). The presence and distribution of lipid droplets could also be seen in z-stacks of liver organoids imaged by CARS at the lipid peak in Appendix 5, Movie A-2. The abundant presence of lipid droplets in DM suggested a shift in metabolic function towards lipidogenic hepatocytes following differentiation.

5.2.3 Successful Cre recombination in liver organoids though Ah-Cre

After successfully growing, expanding, and differentiating ductal-derived liver organoids in the Dale lab, the culture system needed to be further developed, to achieve tightly regulated and highly efficient deletion of Axin1. To this end, we decided to make use of the Ah-Cre transgenes (Ireland et al. 2004), which had already been used by Gui-Jie Feng and colleges in the i*n vivo* study of Axin loss (Feng et al. 2012). Using cells from Ah-Cre mice crossed with conditional Axin alleles, the addition of β-NF (β-Naphthoflavone) to the culture medium should lead to the induction Cre recombination and thus recombination of *loxP* target sites *in vitro.*

Thus, we generated organoids from $Axin1^{fl/fl}$, Ah-Cre, ROSA-lacZ and Ah-Cre, ROSA-lacZ control mice and analysed the *in vitro* recombination efficiency (see Table 3-1 for information about the alleles).

5.2.3.1 In vitro recombination of the ROSA-lacZ locus

The first step was to establish a protocol to regulate Ah-Cre mediated recombination in the primary liver organoids. Cultures derived from Axin1$^{fl/fl}$, Ah-Cre, ROSA-lacZ and control mice were maintained in EM or were differentiated into hepatocytes two days after seeding. From this time onwards, organoids were also treated with 1 µM β-NF at time of feeding to induce Cre recombination *in vitro*. Some organoids were treated with DMSO, as a negative control. On day 14 organoids were harvested and analysed. Figure 5-3 A provides a scheme, showing the induction and differentiation protocol used.

The ROSA-lacZ allele (Soriano 1999) was used as an indicator for successful Cre recombination. In the presence of active Cre recombinase a *loxP*-flanked stop codon was removed, allowing the expression of *β-Galactosidase* (*lacZ)* (see Figure 5-4 B for a schematic of the ROSA-lacZ allele). This expression could then be visualised by incubation with X-Gal (5-Brom-4-chlor-3-indoxyl-β-D-galactopyranoside), a substrate for β-Galactosidase. *LacZ* expression and thus successful recombination of the ROSA locus through β-NF induced Ah-Cre could be shown in Axin1$^{fl/fl}$ and Axin1$^{wt/wt}$ organoids both in EM (data not shown) and DM (Figure 5-3 B, bottom), whereas organoids treated with DMSO only showed some background recombinase activity (Figure 5-3 B, top). Close examination of the β-NF treated organoids revealed mosaic lacZ staining. Some organoids consisted completely of stained cells, whereas other organoids were made up of stained and unstained cell patches. This finding indicates that recombination did not occur in all cells. Recombination is a genomic event that gets passed down onto daughter cells. It can thus be assumed, that completely stained organoids were derived from a few cells that did undergo recombination very early during the treatment regime. Unstained cell patches remained because recombination of the ROSA locus was unsuccessful in those cells. However, there is a strong activation of *lacZ* expression in β-NF treated organoids compared to DMSO control in both EM and DM conditions and Axin mutant and wild type organoids.

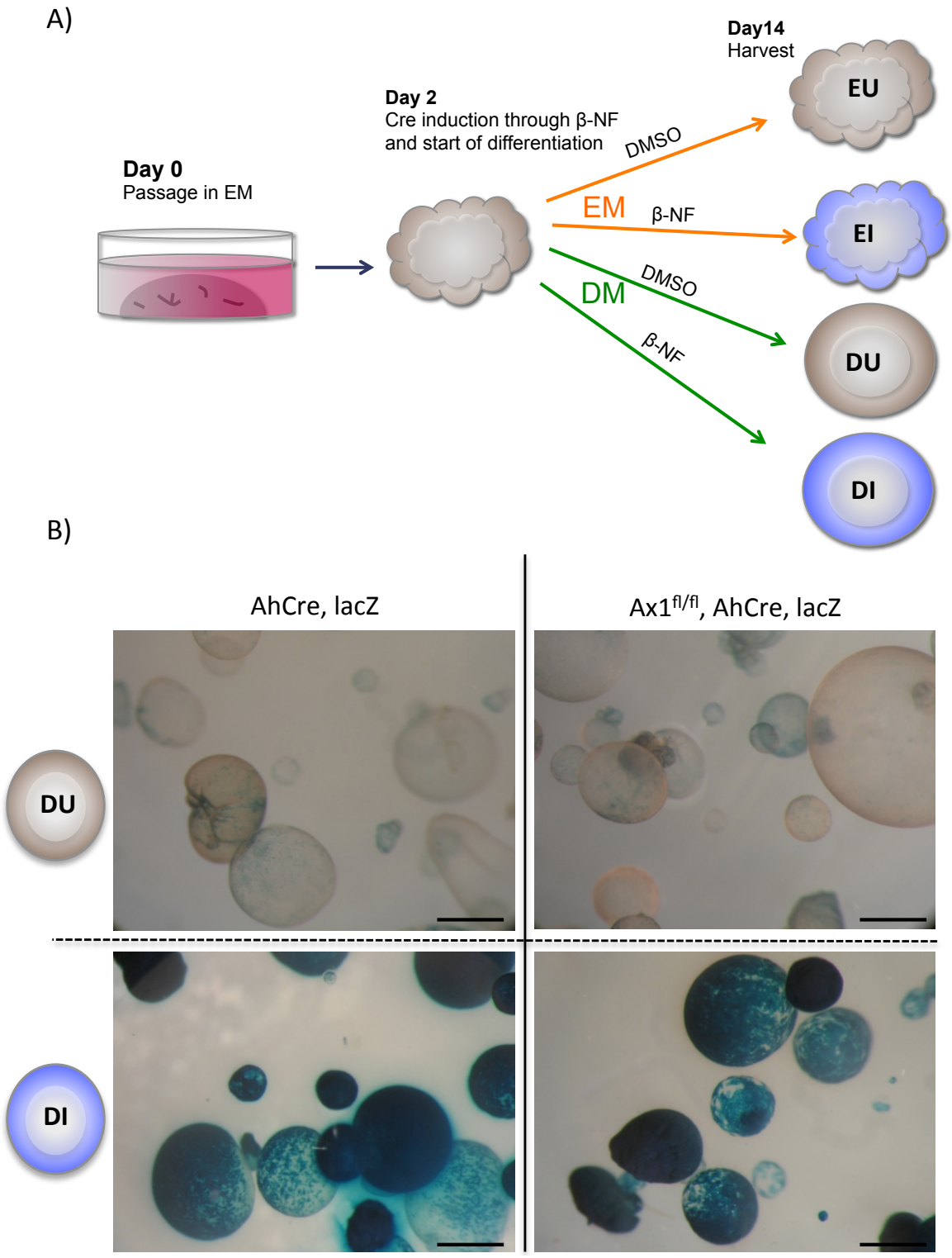

Figure 5-3. Ah-Cre mediated recombination in 3D culture.
A) Scheme showing the induction and differentiation protocol. Liver organoids were grown in expansion conditions (EM) or differentiation conditions (DM) and induced with β-Naphthoflavone (+β-NF) to induce the expression of *Cre* recombinase from the Ah-Cre transgene or DMSO as a control. **B)** X-Gal staining (blue) showed the successful recombination of the ROSA-lacZ allele in differentiation conditions treated with β-NF (DI) in comparison to control organoids (DU). Scale bars represent 100 µm. X-Gal staining shown here was performed by William Hill under my supervision.

Recombination of the ROSA-lacZ locus was also shown by genomic qPCR. For this purpose a set of primers that bound on either side of the *loxP*-flanked stop codon was used to amplify the recombined allele (Figure 5-4 B). The size of the flox-Stop-cassette in the recombined allele prevented its amplification in genomic qPCR, while the much shorter floxed out allele was amplified very efficiently.

In Axin1$^{wt/wt}$, Ah-Cre, ROSA-lacZ organoids recombination of the ROSA-locus was increased 2 to 3 fold (EM and DM respectively; in comparison to uninduced Axin1$^{fl/fl}$, Ah-Cre, ROSA-lacZ grown in EM) following Cre induction (Figure 5-4 A). In Axin1$^{fl/fl}$, Ah-Cre, ROSA-lacZ organoids, the recombination efficiency was even higher (4 to 5 fold, DM and EM respectively). This intriguing observation could be an effect of Axin1 loss through the differential expression of the *aryl-hydrocarbon receptor* (*AhR*), which mediates the response to β-NF. In the normal liver AhR is expressed perivenously, in the zone of the liver lobule that has the highest Wnt signalling activity (Sekine et al. 2007; Oinonen and Lindros 1998) and there is evidence that *AhR* itself is a Wnt target gene (reviewed by Schneider et al. 2014) (see Section 1.1.1 for more information on liver zonation).

The genomic qPCR data of the ROSA locus also suggest that some degree of recombination is occurring in all samples treated with DMSO. It is possible that this background level is a result of unspecific primer binding, or a basal level of leaky *Ah-Cre* expression in the organoids, which was seen in the lacZ staining (Figure 5-3 B, top). In the mouse liver, Ah-Cre leakiness can also be found.

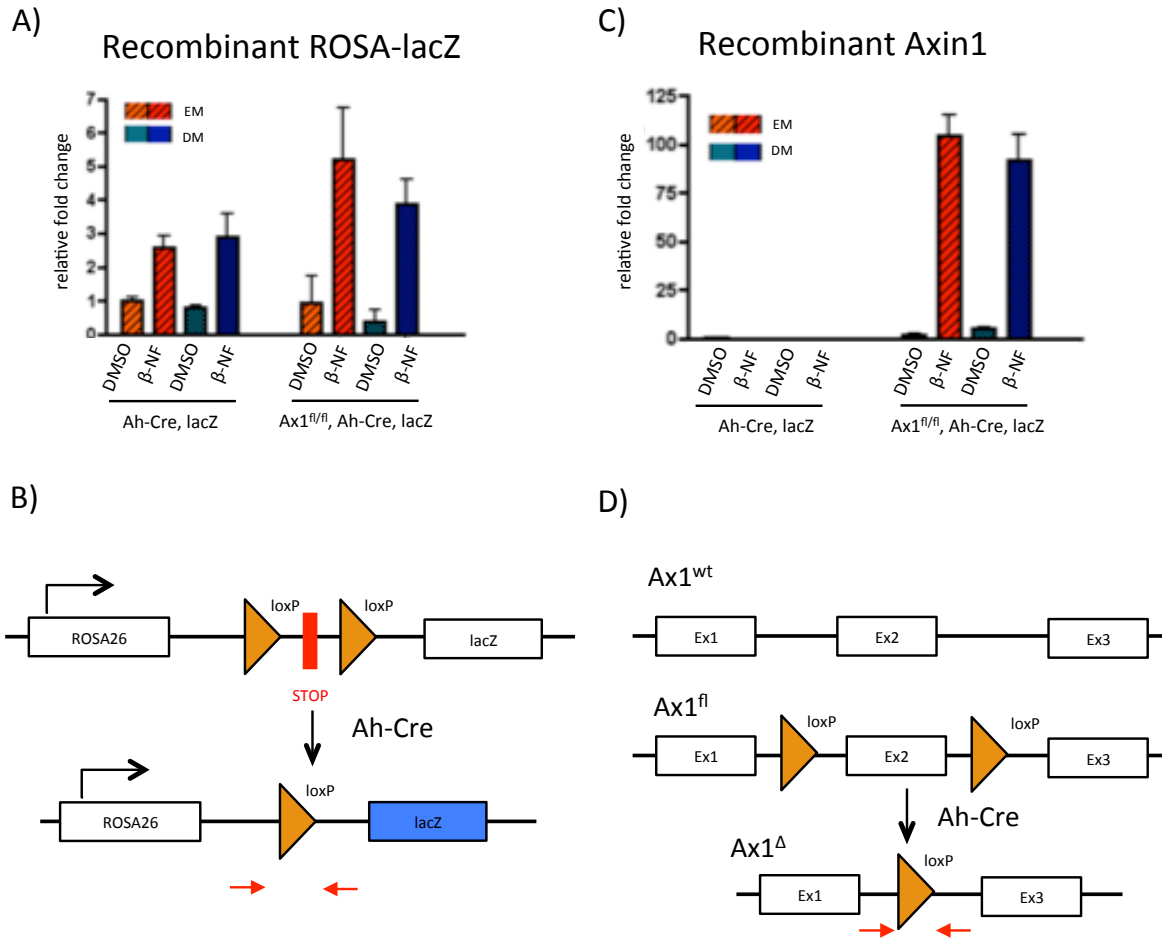

Figure 5-4. Quantification of Ah-Cre mediated recombination.
Genomic qPCR confirmed the recombinant of the *lacZ* locus **(A)** as well as of the Axin1^{fl} allele **(C)**. Data were normalised to the one copy gene *ApoB* and is shown as the relative fold change in comparison to Axin1$^{fl/fl}$, Ah-Cre, ROSA-lacZ grown in EM and treated with DMS0. N=3. **B, D)** Scheme of the ROSA-lacZ **(B)** and the Axin1^{fl} **(D)** locus before and after Cre recombination. The approximate positions of the respective primers are indicated as red arrows.

5.2.3.2 Recombination of the Axin1$^{fl/fl}$ in vitro

Genomic qPCR was also used to show recombination of the Axin1 locus in Axin1$^{fl/fl}$, Ah-Cre, ROSA-lacZ organoids. The primers used for this purpose were designed following a similar principle to the ROSA-lacZ primers. The Axin1 genomic qPCR primers only amplify the recombined Axin1$^{\Delta}$ allele efficiently and can thus be used to confirm the removal of exon 2 in Axin1$^{fl/fl}$ organoids (Figure 5-4 D). Indeed, genomic qPCR showed an almost 100-fold increase in recombined allele in β-NF treated Axin1$^{fl/fl}$ organoids in both EM and DM (Figure 5-4 C). This change was much higher than the one observed at the ROSA-locus. This difference could possibly be explained by a more efficient recombination of the Axin1^{fl} allele in comparison to the ROSA-lacZ locus. However, all samples were normalised to Axin1$^{fl/fl}$ Ah-Cre, ROSA-lacZ EU. In this sample, low background levels of recombination are present, which influenced the normalisation and thus the reliability of this experiment.

In any case, the data presented here confirms that Cre recombination of both loci was highly efficient and controllable; although a limited amount of 'leaky' recombination was detected in the DMSO control.

5.3 Effects of Ah-Cre induction on Axin$^{fl/fl}$ liver organoids

5.3.1 Gene expression profile of Axin1$^{\Delta/\Delta}$, Ah-Cre liver organoids

The next step after demonstrating the inducible deletion of Axin1 *in vitro,* was the evaluation of the 3D culture system as a model. The *in vitro* system needed to mimic the phenotype found in the *in vivo* situation closely, to serve as valuable model to study the effects of mutant Axin1 *in vitro*.

A microarray performed on Axin1 mutant mouse livers 4 days after Axin1 deletion showed an enrichment of proteins involved in the G2/M phase of the cell cycle (*Cyclins A2, B1, B2, D1, Cdk1, Cdca3, Cdc20, Ki67, Mast1, and FoxM1*) and for regulators of cytokinesis (*Aurka,*

Aurkb, Prc1, Ect2, Plk, Cyk4/RacGap1)(Feng et al. 2012). Feng et al. then went on to confirm these results by qRT-PCR. In addition, they performed qRT-PCR on known liver specific Wnt target genes. Among those, *Axin2, c-Myc,* and *Cyclin* D1 were raised 2- to 3-fold. But expression levels of *Tiam1*, *Cdc25a*, *Egfr* and *EpCAM* were not significantly altered (Figure 5-5 C).

Here we used the same set of Wnt target, G2/M, and cell cycle related genes to directly compare the *in vitro* cultures with the *in vivo* scenario. We were hoping to find a very similar expression profile in the Axin1 mutant liver organoids to demonstrate their value as a model system. To this end, mRNA was isolated from $Axin1^{fl/fl}$, Ah-Cre, ROSA-lacZ and $Axin1^{wt/wt}$, Ah-Cre, ROSA-lacZ control organoids grown in EM or DM 12 days after Cre induction through β-NF (14 day after seeding, see Figure 5-3 A for a scheme of the experimental protocol).

As expected, *Axin1* mRNA (tested with primers against exon 2) was lost from $Axin1^{fl/fl}$ organoids in both EM (Figure 5-5 A) and DM (Figure 5-5 B), reconfirming successful recombination. Interestingly, the qRT-PCR data set as a whole showed a big difference between the expansion (Figure 5-5 A) and differentiation condition (Figure 5-5 B). In the expansion condition, neither the expression of the Wnt target genes, nor the cell cycle related genes were significantly altered between the wild type and the Axin mutant organoids (Figure 5-5 A). In those conditions, the only significant change observed was a decrease in *CD44.* Overall, Axin1 loss seemed to have no effect on ductal-like organoids for the genes tested in this assay.

In contrast, the differentiation conditions showed expression changes in many genes (Figure 5-5 B). Among the Wnt target genes *Axin2* and *Tiam1* were upregulated, and *CD44* was downregulated following Axin1 loss. The rest of the Wnt target genes remained unchanged. The gene expression profile of Wnt target found in mouse livers described by Feng et al. (2012) were almost identical to the one found in differentiated Axin mutant liver organoids (Figure 5-5 B vs. C).

A) Gene expression in liver organoids grown in EM

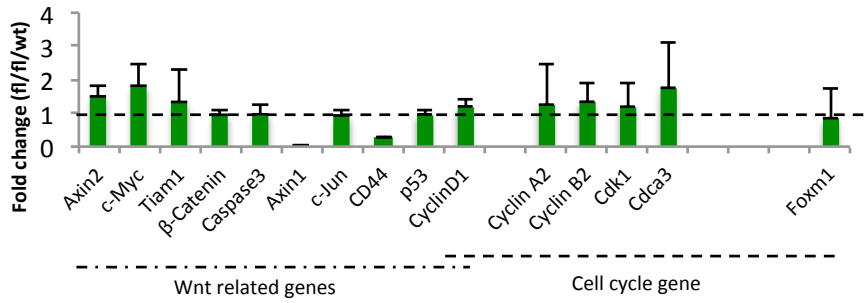

B) Gene expression in liver organoids grown in DM

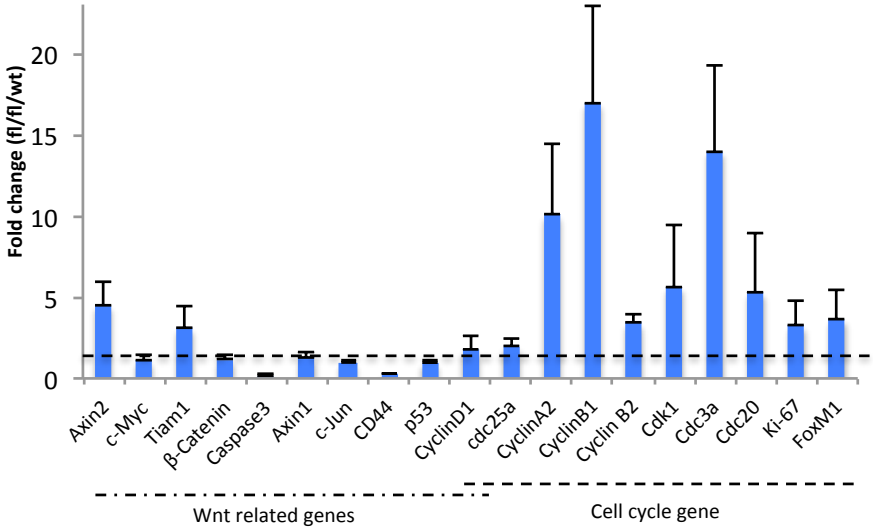

C) Gene expression in the mouse liver

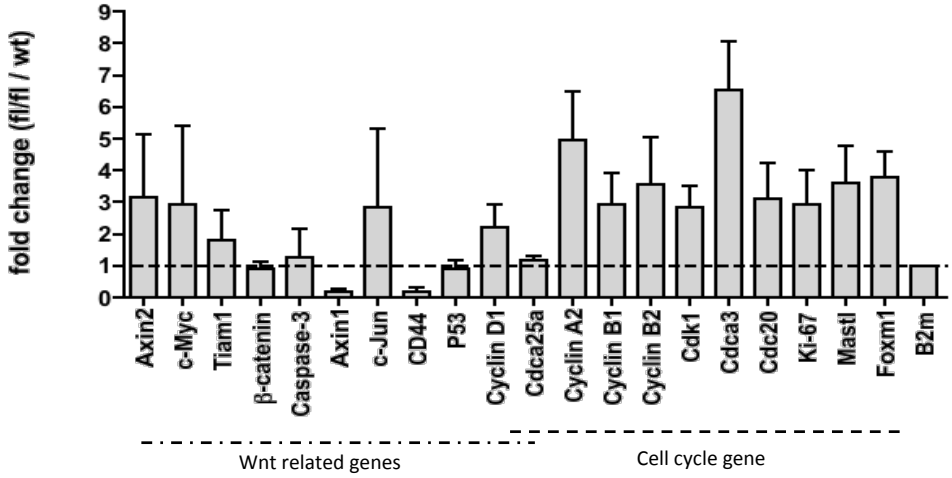

Figure 5-5. Gene expression changes in Axin1$^{\Delta/\Delta}$, Ah-Cre liver organoids.
Gene expression profiles of Axin1$^{fl/fl}$, Ah-Cre, ROSA-lacZ compared to Axin1$^{wt/wt}$, Ah-Cre, ROSA-lacZ in liver organoids **(A, B)** and the mouse liver treated with β-NF **(C)**. **A)** Gene expression profile in organoids grown in EM (mainly ductal cells). **B)** Gene expression profile in organoids grown in DM (hepatocyte like). **C)** Gene expression profile in Axin mutant mouse livers taken from Feng et al. (2012) for direct comparison. mRNA was isolated from organoids 12 days after β-NF induction. Data are expressed as fold change and mean +- SEM. N=3. Parts of the gene expression analysis were performed by William Hill under my supervision.

The cell cycle related genes in the differentiated organoids also followed the pattern observed in the mouse liver. *Cyclin A2, Cyclin B1, Cyclin B2, Cdk1, Cdc3a, Cdc20,* and *Ki67* were all upregulated following Axin1 loss in the mouse livers as well as in the liver organoids in differentiation conditions.

The most noticeable differences between the *in vivo* and *in vitro* data (in DM) were the expression changes of the Wnt target genes *c-Myc* and *c-Jun*. In the mouse liver, both of these genes were upregulated in response to Axin loss four day after induction. However, at a later time point (3-months after Cre induction), expression had retuned to normal levels (Feng et al. 2012). Here, organoids were harvested 12 days after the initial β-NF treatment. The difference between *c-Myc* and *c-Jun* in both models may thus be a feature of the different time points chosen following gene deletion and may be indirectly regulated as a consequence of Axin1 loss. In future experiments, the gene expression changes in liver organoids should be examined in a time course to detect the dynamic of these Wnt target gene over time.

The qRT-PCR data presented here shows that liver organoids in differentiation conditions exhibit similar gene expression changes due to Axin loss, as the mouse livers. In the differentiation stage the majority of cells have undergone hepatocyte differentiation and closely resemble the composition of an actual liver. In the expansion conditions, which maintain the ductal character, the gene expression profile remains unchanged.

5.3.2 Further evaluation of Axin1 loss in differentiated liver organoids

We also started to confirm the qRT-PCR results obtained for Axin1 mutant liver organoids by whole mount immunofluorescence analysis. The data shown here were obtained in differentiation conditions only.

Axin1$^{fl/fl}$, Ah-Cre, ROSA-lacZ and Ah-Cre, ROSA-lacZ organoids were both treated with β-NF and stained for FoxM1, a master regulator of cell cycle progression. In Axin1 mutant liver organoids increased levels of FoxM1 could be detected (Figure 5-6 A).

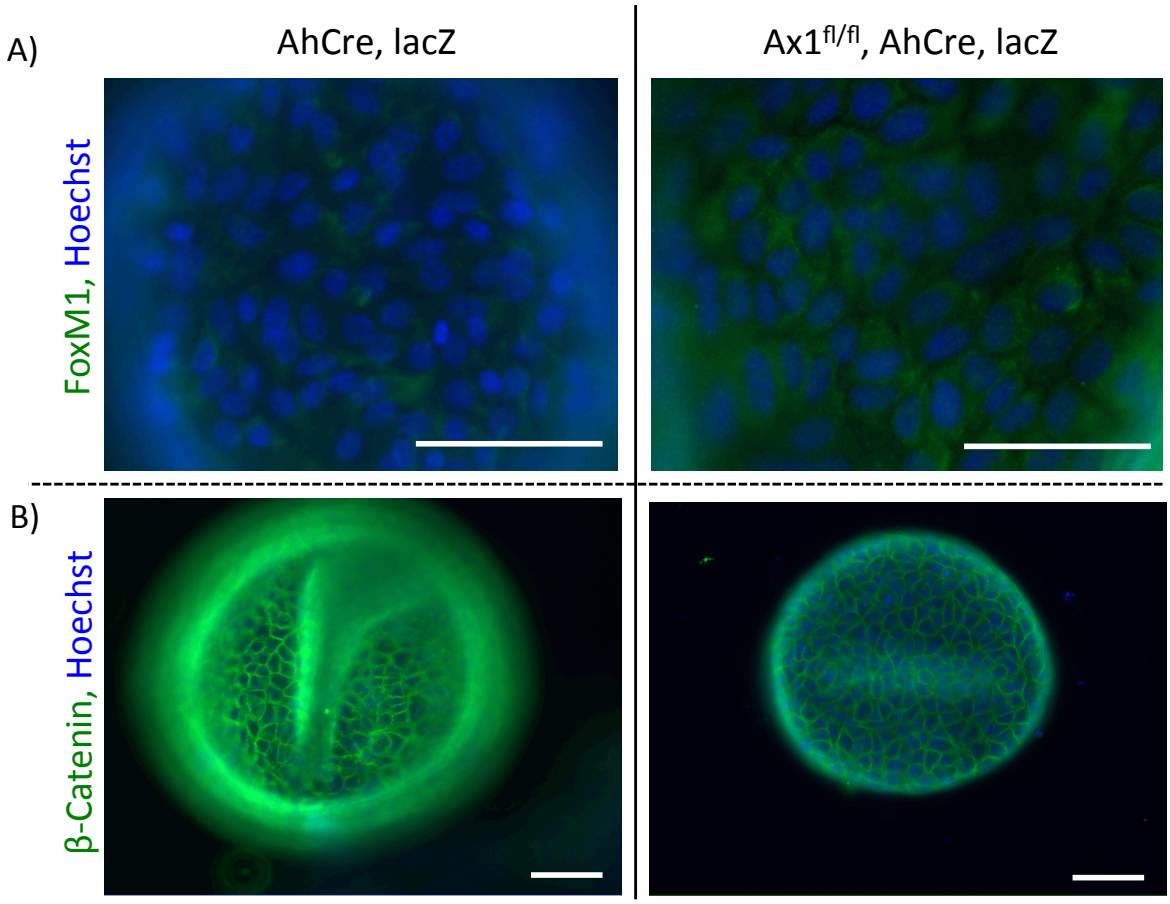

Figure 5-6. Immunofluorescence analysis for FoxM1 and β-Catenin.
Differentiated liver organoids from Axin1$^{fl/fl,}$ Ah-Cre, ROSA-lacZ and Ah-Cre, ROSA-lacZ were treated with β-NF and stained for FoxM1 **(A)** and β-Catenin **(B)** by whole mount immunofluorescence. Organoids were counterstained with Hoechst33342. Scale bars represent 20 µm.

This was consistent with the observation that Axin1 loss activated a G2/M cell cycle related gene expression signature (Figure 5-5 B). We also performed β-Catenin staining on the liver organoids. As expected there was strong membrane and only some cytosolic staining for β-Catenin in the organoids; whereas strong nuclear β-Catenin staining could not be found in any of the conditions (Figure 5-6 B). This finding again was consistent with the data obtained by Feng et al. (2012) and the gene expression profile obtained from Axin1 mutant liver organoids (Figure 5-5 B). In Axin1 mutant mouse livers, as well as differentiated Axin1$^{fl/fl}$, Ah-Cre, ROSA-lacZ organoids, no nuclear β-Catenin and no activation of Wnt target genes could be detected following the induction of Cre recombinase though β-NF.

5.3.3 Proliferation of Axin1 mutant liver organoids

To further evaluate the 3D liver culture system we examined the proliferation profile of Axin1 mutant organoids. Based on the proliferation gene expression profile observed *in vivo* and in the differentiation conditions *in vitro* (Figure 5-5 B & C), and the observed hepatomegaly following Axin1 loss in the liver (Feng et al. 2012), it was predicated that liver organoids would exhibit increased proliferation following Axin1 loss.

In the mouse liver, staining for the proliferation marker Ki67 was increased in Axin1 mutant livers compared to wild type controls (Feng et al. 2012). In liver organoids strong Ki67 staining was found in both Axin1 mutant and wild type organoids in expansion conditions (Figure 5-7 A, top). This finding indicates the highly proliferative status of the ductal-derived organoids in EM. Following the differentiation protocol, however, Ki67 staining was markedly reduced in control organoids, indicating reduced proliferation of hepatocyte-like cells (Figure 5-7 A, bottom left). By contrast Axin1 mutant liver organoids retained widespread nuclear Ki67 staining in the differentiation conditions (Figure 5-7 A, bottom right), matching the staining patterns found *in vivo*. Measuring the average diameter of the organoids on the GelCount™ enabled the assessment of the growth rate of the liver organoids in differentiation conditions.

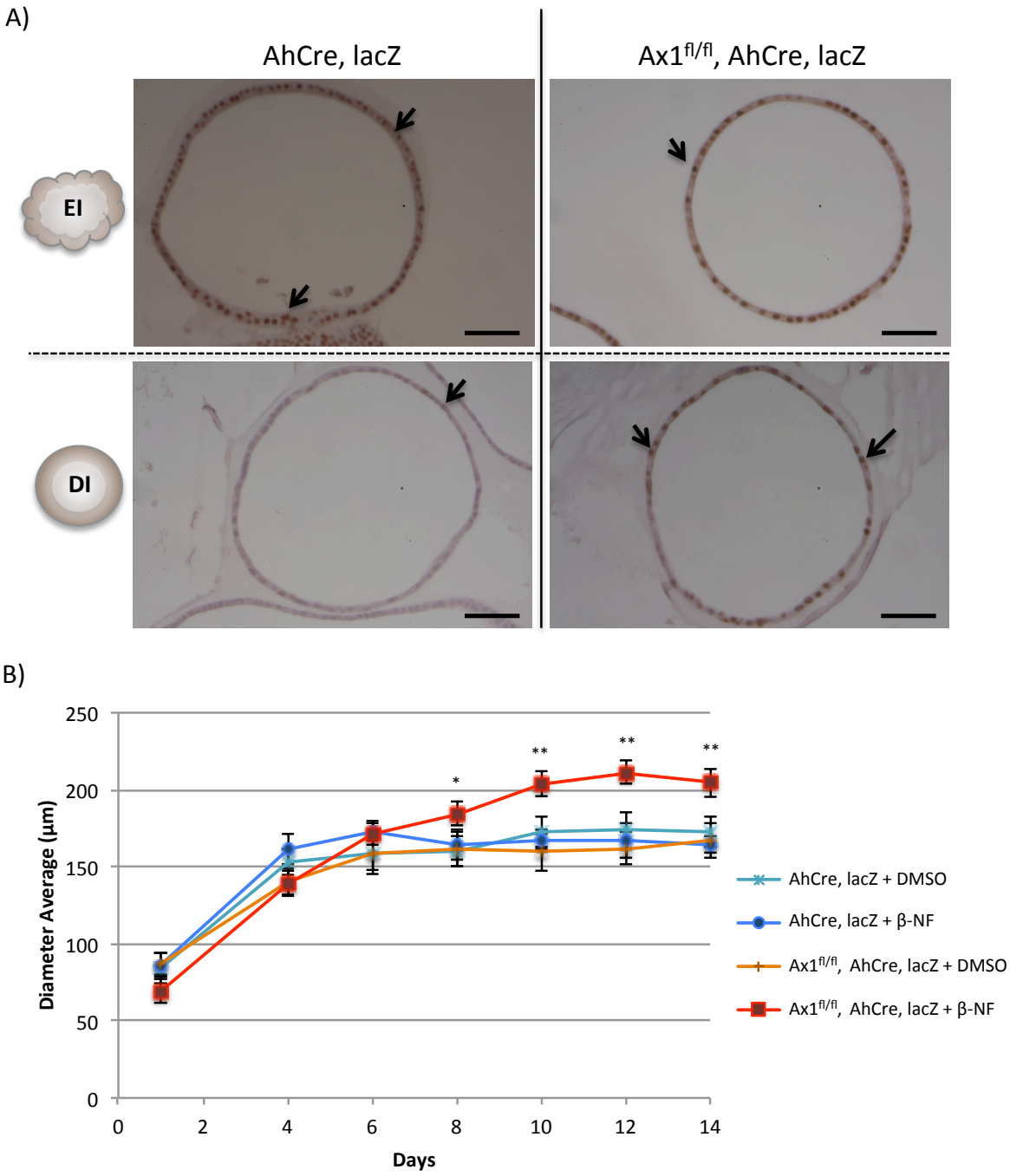

Figure 5-7. Proliferation of Axin1 mutant liver organoids.

A) Liver organoids from Axin1$^{fl/fl,}$ Ah-Cre, ROSA-lacZ and Ah-Cre, ROSA-lacZ were treated with β-NF and stained for Ki67 by immunohistochemistry in expansion (EI) or differentiation (DI) conditions. Brown cells (examples indicated with arrows) indicate Ki67 positive nuclei. Scale bars indicate 50 µm. **B)** Average organoid diameter of Axin mutant or wild type organoids in differentiation medium treated with β-NF or DMSO control was measured using the GelCount^{TM}. Error bars represent standard deviation. 4 wells were measured for each condition. Significance levels given for Ax1$^{fl/fl}$, AhCre, lacZ + β-NF compared to Ax1$^{wt/wt}$ + β-NF. *=P<0.05, **=P<0.001.

Until day 6 the growth rate of organoids derived from Cre induced (+ β-NF) $Axin1^{fl/fl}$ mice was identical to the DMSO or wild type controls (Figure 5-7 B). However, further on in the differentiation process (> 6 days) control organoids ceased to further increase in diameter, while Axin mutant organoids continued to grow further resulting in a significantly increased organoid diameter at day 14 (compared to wild type organoid treated with β-NF).

5.3.4 Changes in organoid growth following β-NF treatment

During the course of several experiments analysing the effect of Axin loss through the β-NF inducible Ah-Cre, we observed that EM organoids treated with β-NF underwent morphological changes unrelated to their phenotype. The organoids in the β-NF containing conditions grew larger and more spherical than the untreated controls in both $Axin1^{fl/fl}$ and $Axin1^{wt/wt}$ (Figure 5-8 A).

Cell viability measured in a PrestoBlue assay showed a slight increase in organoid viability in $Axin1^{fl/fl}$, Ah-Cre organoid in differentiation conditions when treated with β-NF, as compared to DMSO treated controls (Figure 5-8 C). This was consistent with the change in organoid diameter described above (Section 5.3.3). The same was true in expansion conditions (Figure 5-8 B). But surprisingly, the viability of wild type organoids treated with β-NF was also increased, which was most noticeable in EM. Therefore, we decided to further investigate the effects of β-NF treatment on wild type organoids in collaboration with the 3D culture analysis company, OcellO. Analysing liver organoids using their multi-parameter morphometric analysis workflow revealed an increase in organoid area, when cultures were grown in EM supplemented with β-NF (EI) (Figure 5-9 A). Furthermore, β-NF treatment increased the size of the nuclei of wild type organoids compared to DMSO in both EM and DM (Figure 5-9 B). Additionally, the epithelial orientation of organoids was changed after β-NF treatment. In DMSO treated organoids the apical (F-actin-rich) side was mainly facing towards the lumen (Figure 5-9 C, left); whereas wild type organoids in EI were mostly inverse, with the apical side facing towards the gel on the outside (Figure 5-9 C, right).

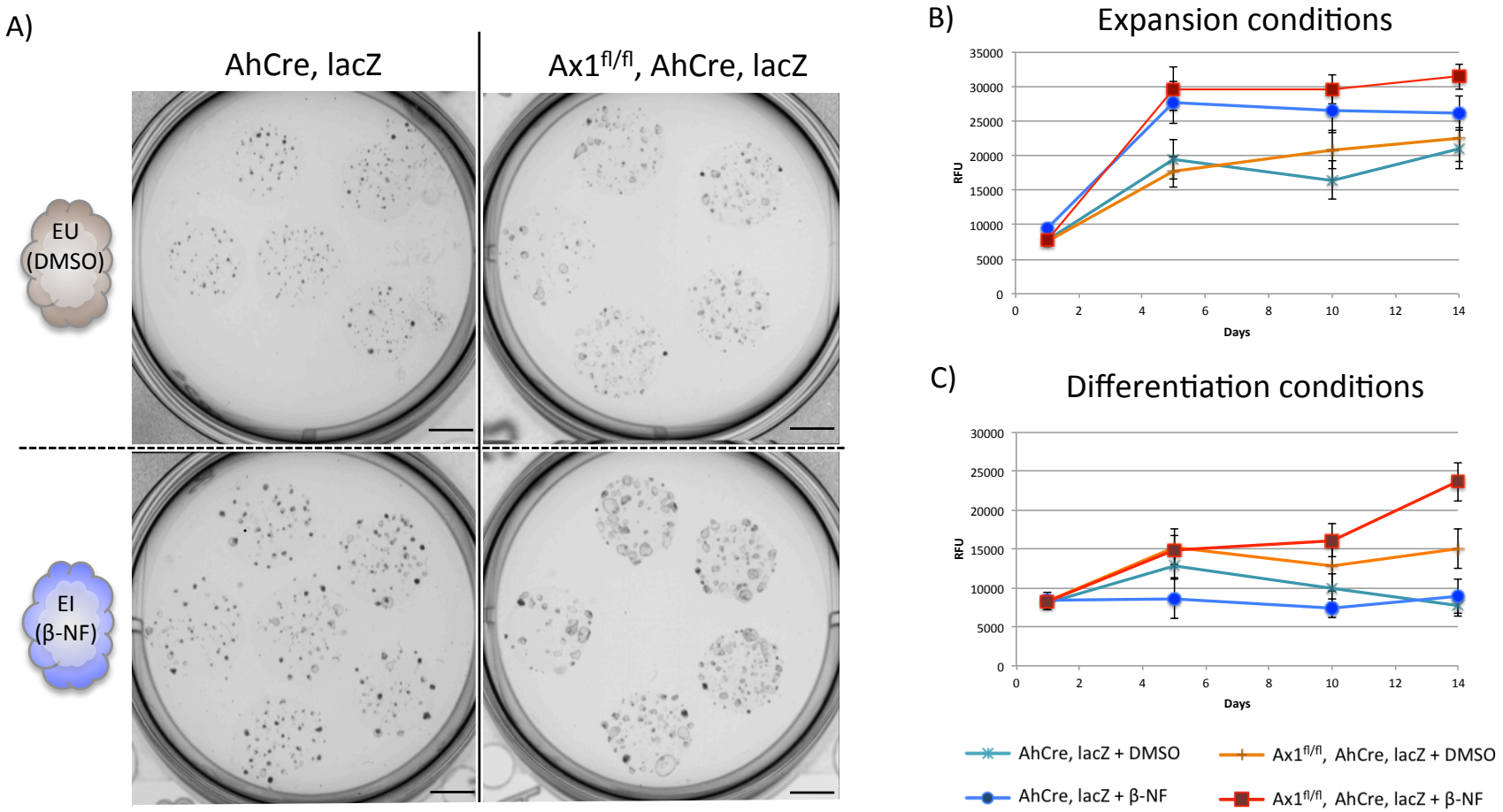

Figure 5-8. Liver organoids viability and morphology following treatment with β-NF.

A) Organoids derived from both wild type (right) and Axin1$^{fl/fl}$ (left) mice show morphological changes following in expansion conditions when treated with β-NF (EI) as compared to DMSO control (EU). Pictures were taken using the GelCount^{TM}. Scale bars indicate 2.5 mm. **B, C)** Change in liver organoids viability measured in a PrestoBlue assay over 14 days in Axin1$^{fl/fl}$, Ah-Cre, ROSA-lacZ and control organoids in expansion conditions **(B)** and differentiation conditions **(C)**. Organoids were treated with β-NF to induce Cre recombinase or DMSO as control. Data were normalised to the viability at the day of seeding. Error bars represent standard deviation. 3 24-wells were measured for each condition.

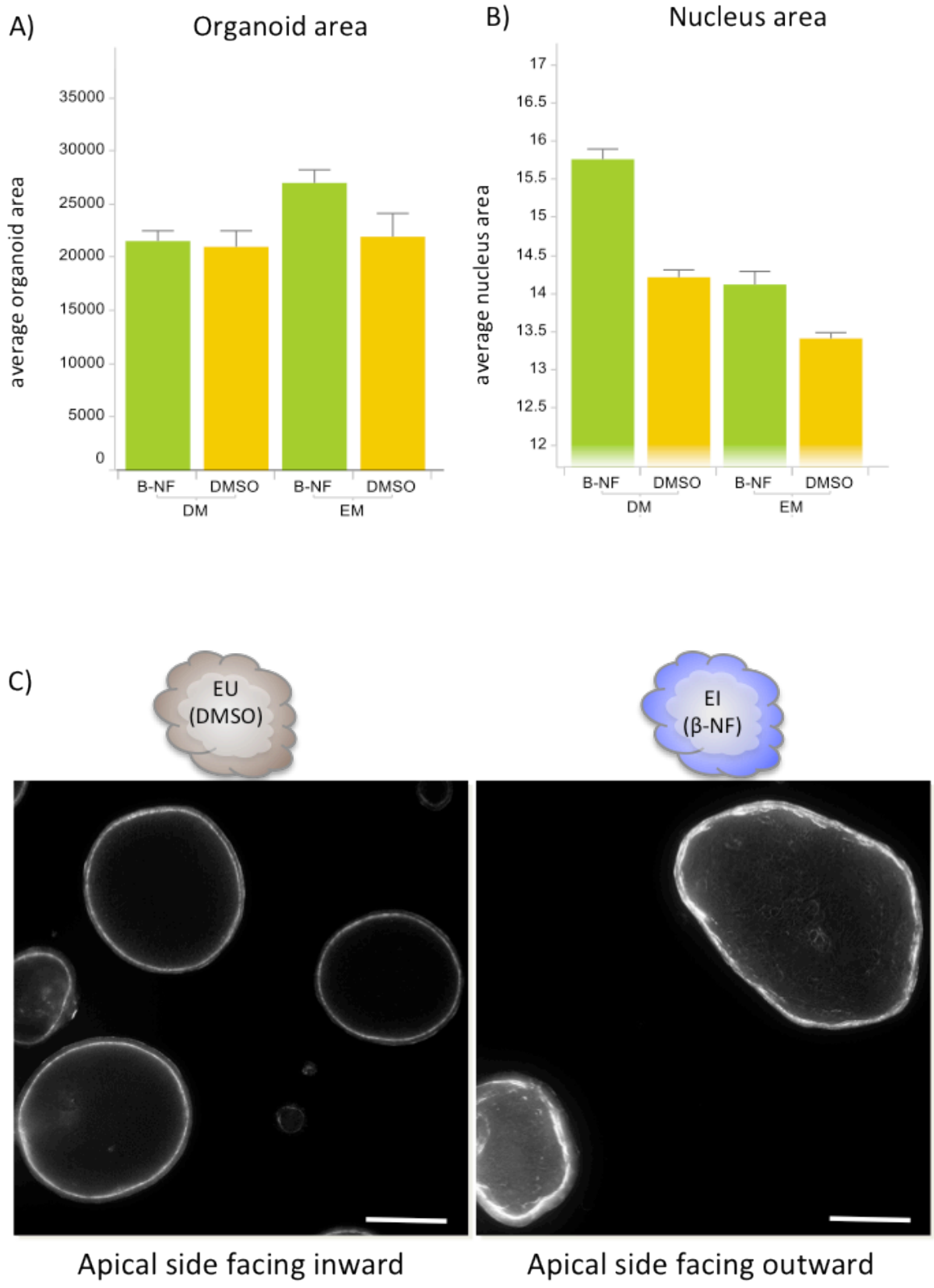

Figure 5-9. Effects of β-NF treatment on wild type liver organoids.
Wild type liver organoids were analysed using OcellO multicomponent analysis. Mean organoid area **(A)** the nucleus size (measured with DAPI, **(B)**) are show. Error bears indicate SEM. Organoids were stained for actin to show the epithelial orientation **(C)**. Scale bars indicate 200 µm.

5.4 Investigation into other Cre induction methods

The use of the Ah-Cre transgene in liver organoids provided a means to induce Cre recombination and thus Axin loss in liver organoid (5.2.3) with an increased G2/M cell cycle gene expression signature in differentiated organoids (5.3.1). However, Cre recombinase was expressed at low levels without the induction with β-NF (5.2.3). Additionally, β-NF treatment also had strong effects on the morphology and growth of wild type organoids (5.3.4). We thus decided to replace the Ah-Cre transgene in the analysis of Axin loss in liver organoids. Ideally we would like to use a system that allows very tight control of the recombination process without additional effects on the liver cultures.

5.4.1 Cre recombination though TTR-CreER^T

The first candidate to replace Ah-Cre was the Tamoxifen (Tam) inducible TTR-CreER^T transgene (Tannour-Louet et al. 2002). To test the inductility of this Cre recombinase in liver organoids, we treated TTR-CreER^T, ROSA-lacZ allele with 0.1 μM Tamoxifen (Tam) and monitored recombination through *lacZ* expression in EM and DM (data not shown). However, *lacZ* expression could only be observed in occasional cells at this low concentration.

In order to find a more efficient induction procedure, we then tested a higher concentration of Tam (1 μM) and different concentration of its active metabolite 4-Hydroxy-Tamoxifen (4-OH-Tam) (Figure 5-10). In this experiment *lacZ* expression from the ROSA-lacZ locus revealed that recombination occurred under differentiation conditions, whereas staining could only be observed very rarely in EM. The study of Axin1 loss in liver organoids through TTR-CreER^T would be limited to hepatocytes, preventing us from studying a possible involvement of ductal cells in tumourigenesis. Additionally the recombination level of TTR-CreER^T was lower than in Ah-Cre even at the highest Tamoxifen or 4-OH concentration tested.

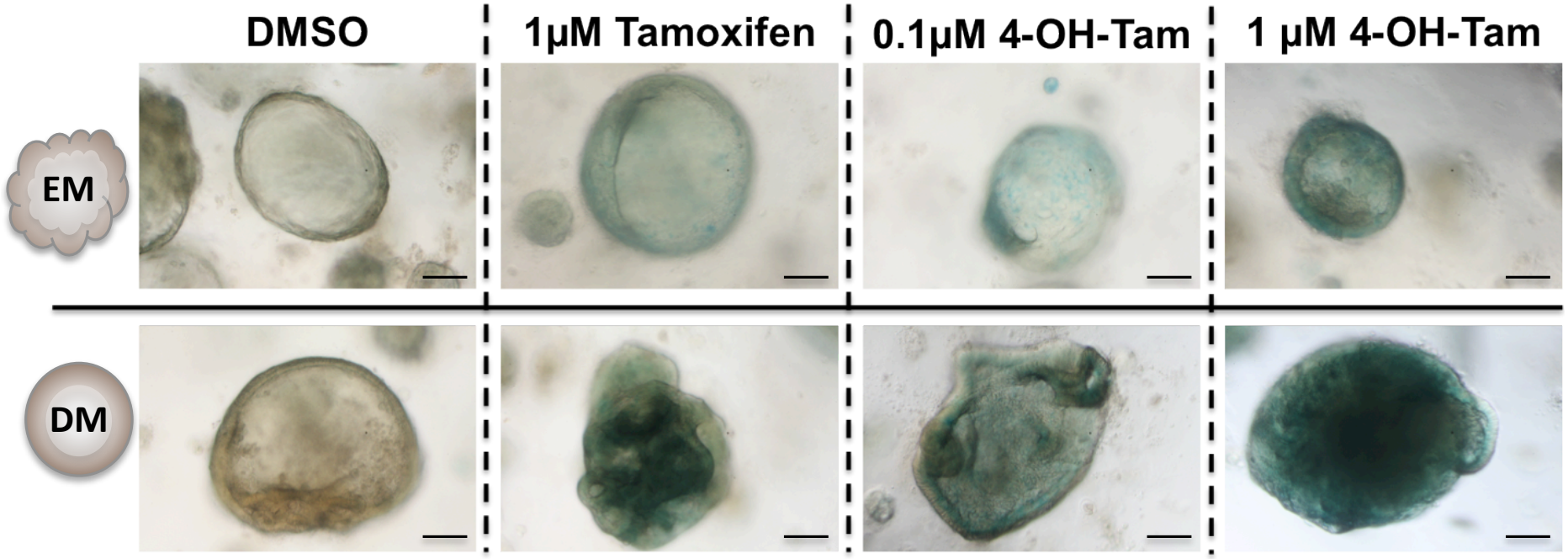

Figure 5-10. Cre induction through TTR-CreER^{T}.
Liver organoids were treated with Tamoxifen, or its active metabolite 4-OH Tamoxifen (4-OH-Tam), to induced Cre mediated recombination. *LacZ* expression from the ROSA-lacZ locus shows that the recombination is more efficient in DM then EM. Scale bars indicate 50 µm.

5.4.2 Cre delivery through viral vectors

5.4.2.1 Transduction of liver organoids with Ad5-GFP and Lenti-GFP

In an attempt to find a highly efficient, ubiquitous way to induce Cre recombination in culture, without side effects of the inducer or leakiness in the absence of inducer, we attempted to use viral mediated Cre delivery. Lenti- or adenoviral transduction could both be a viable option.

Adenovirus mediated Cre recombinase would have the advantage that the viral vector does not integrate into the host genome; whereas lentivirus does. The genomic integration of lentivirus into the genome has the disadvantage of potentially interfering with the host's genes and gene expression. However, the lentiviral construct is passed down to all the daughter cells, allowing the integration of an inducible Cre construct.

In order to decide between the different options, we attempted to transduce liver organoids with Ad5-GFP or Lenti-GFP as single cells. After 5 days, when organoid had reformed, *Gfp* expression was used as readout for transduction efficiency. Organoids transfected with Ad5-GFP contained only occasional cells expressing GFP (Figure 5-11 A); whereas lentiviral transduced cells show a higher levels of fluorescence (Figure 5-11 B). This was probably due to increased transfection efficiency as well as clonal propagation of the lentiviral construct through daughter cells. GFP expression could still be observed, 4 passages after Lentiviral transduction without any selection (Figure 5-11 C).

Since the Adeno-viral transduction efficiency was too low to assure Cre recombinase distribution and activity in all of the cells, the lentiviral approach was deemed to be more useful for our purposes. It provided the opportunity to generate organoid lines containing lentiviral Cre that can be induced at any time.

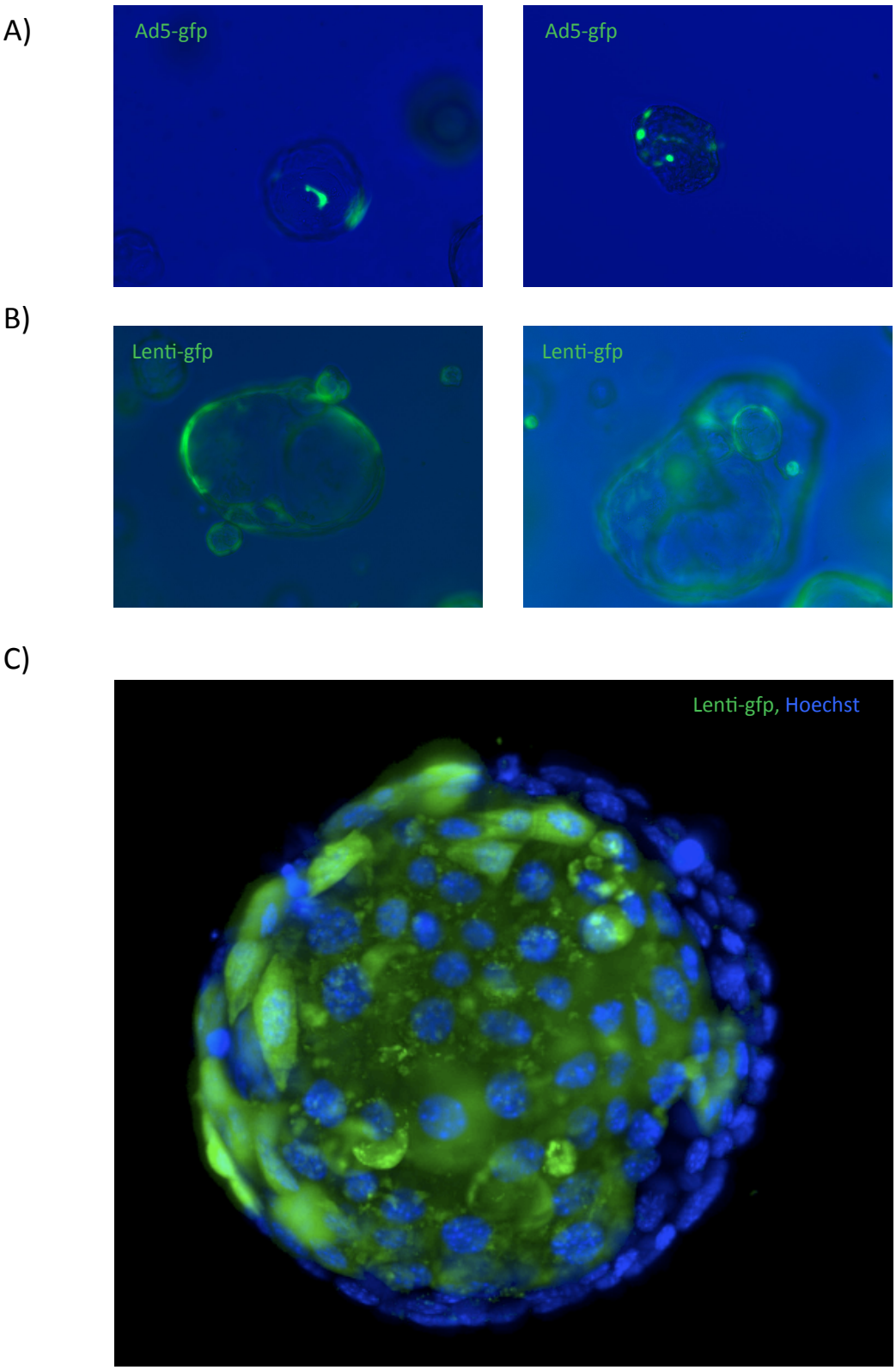

Figure 5-11. Adeno and lentiviral transduction of liver organoids.
Organoids were transduced with Ad5-GFP **(A)** or Lent-GFP **(B)** and imaged live by fluorescence microscopy to assess infection efficiency. **C)** Light sheet microscopy performed on a liver organoid infected with Lenti-GFP and passaged 4 times and counterstained using Hoechst.

5.4.2.2 Cre recombination in liver organoid using Lenti-CMV-ERT2CreERT2

Next, we used the Lenti-CMV-ER^{T2}CreER^{T2} vector in wild type and Axin1$^{fl/fl}$ organoids to achieve Cre recombination. This lentiviral vector can integrate into the host genome and express Tamoxifen inducible Cre recombinase. Successful integration of the viral vector into the genome was facilitated with 1 µg/ml Puromycin selection. Then a preliminary experiment to test the inducibility of the viral Cre-recombinase was performed. Wild type and Axin1$^{fl/fl}$ organoids with and without Lenti-CMV-ER^{T2}CreER^{T2} were treated with 1 µM 4-OHT (4-Hydroxytamoxifen) at time of feeding and DNA was extracted. In a PCR experiment, the presence of Cre recombinase as well as the Axin1^{wt}, Axin1^{fl}, and Axin1$^{\Delta}$ was examined. All organoids transduced with Lenti-CMV-ER^{T2}CreER^{T2} showed the desired band at 1000bp; indicating the presence of Cre coding DNA in the samples (Figure 5-12 A). The Cre band was absent from the untransduced controls. Genotyping for the different Axin alleles showed Axin1^{fl} and Axin1^{wt} bands at the desired size in untransduced organoids and in the no Cre controls (Figure 5-12 B). In Axin1$^{fl/fl}$, Lenti-Cre organoids treated with 1 µM 4-OHT a band for the recombined Axin1$^{\Delta}$ could be detected.

These results indicate that the transduction with Lenti-CMV-ER^{T2}CreER^{T2} and the subsequent induction of Cre recombinase was successful. However, the PCR experiments performed were not quantitative. Genomic qPCR as well as lacZ staining for the recombination of the ROSA-LacZ locus similar to those performed in organoids carrying the Ah-Cre transgene (5.2.3) need to be performed to properly validate the viral Cre delivery system.

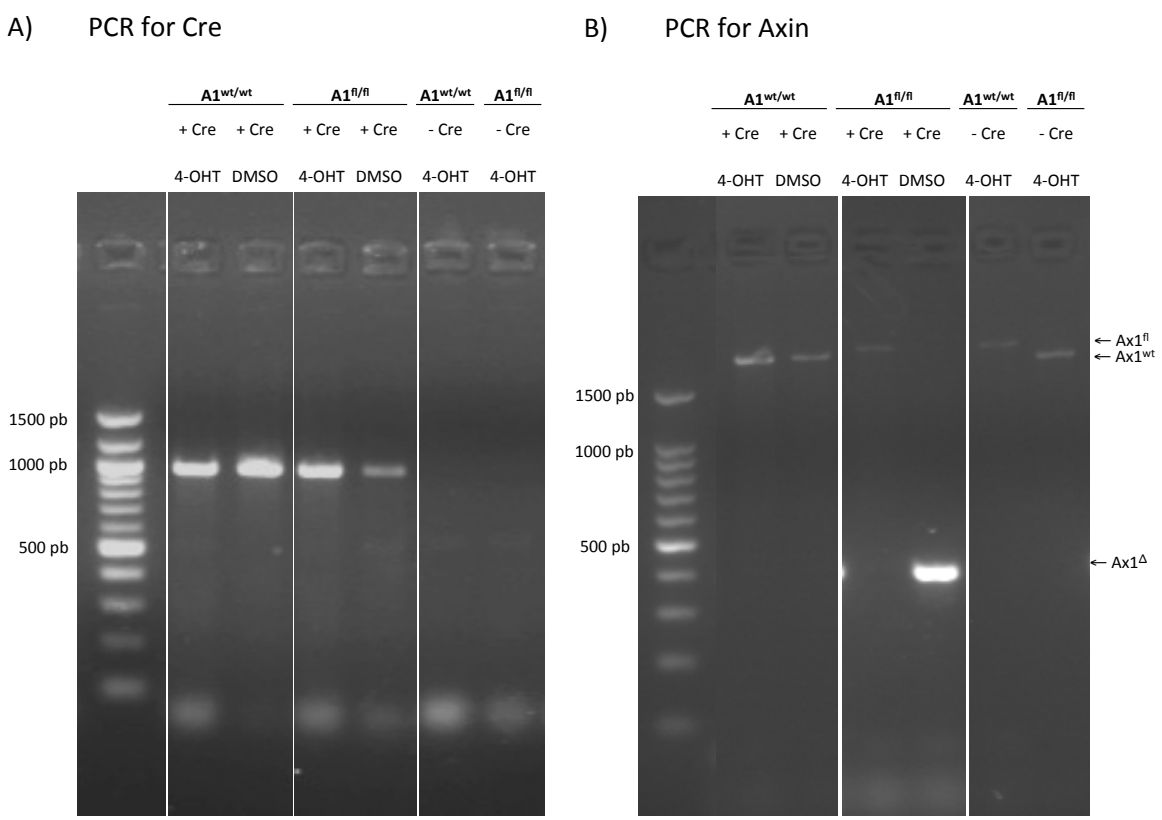

Figure 5-12. Genotyping for organoids transfected with Lenti-CMV-ER^{T2}CreER^{T2}.
Liver organoids of Axin1$^{wt/wt}$ (A1$^{wt/wt}$) or Axin1$^{fl/fl}$ (A1$^{fl/fl}$) mice, transduced with Lenti-CMV-ER^{T2}CreER^{T2} (+Cre) or without (-Cre) were treated with 1 µM 4-Hydroxytamoxife (4-OHT) or DMSO control. **A)** Organoids were subject to PCR to detect Cre-recombinase. Samples positive for Cre recombinase show a band at 1000 bp next to a 100 bp ladder (NEB). **B)** Organoids were also analysed by PCR for Axin1. Organoids with an A1^{wt} allele show a band at 2042bp, A1^{fl} at 2190pb, and A1$^{\Delta}$ at 402 bp alongside a 100 bp marker (Promega).

5.5 Summary of the investigation into Axin1 loss in liver organoids

In this chapter, the development of a 3D liver culture system is described based on the methods developed by Huch et al. (2013) to study the short-term effects of Axin loss in the liver. Here, I will summarize the results of this study. A more detailed discussion of all the results will be made in Chapter 6

Bile duct fragments isolated from the liver maintained their biliary identity in EM conditions (see Section 5.2.1). I was also able to drive them towards a hepatocyte-like fate, generating organoids that highly express the hepatocyte markers *Hnf1α, HNF4,α* and *TTR* (see Section 5.2.2). However, the differentiated organoids maintained part of their ductal identity, shown by their continuous expression of the cholangiocyte marker *Krt19*.

Axin1 deletion in the liver organoids was first performed using identical lines of mice and inducer to that used in the *in vivo* study by Feng et al. (2012) (see Section 5.2.3). Organoids carrying the Ah-Cre transgene (Ireland et al. 2004) were treated with β-NF to induce Cre mediated recombination. β-Galactosidase staining as well as genomic qPCR confirmed an efficient activation of Cre recombinase and the recombination of the ROSA-lacZ and the Axin1 locus.

The next question was, whether the Axin1 loss in the organoid model recapitulates the *in vivo* scenario. This part of the study showed that the liver organoids in the differentiation conditions closely match the situation found in the mouse livers (see Section 5.3). They exhibit a very similar gene expression profile as well as strong Ki67 staining, together with the absence of nuclear β–Catenin staining. The most noticeable differences between the culture system and the mouse livers were *c-Myc* and *c-Jun* expression (see 5.3.1). In the mouse liver both of these genes were upregulated in response to Axin loss four days after induction (Feng et al. 2012). However, three months later, the gene expression levels of both genes had returned to normal. In contrast, organoids were harvested 12 days after the initial β-NF treatment, at which point c-Myc and c-Jun were expressed at wt levels. The difference

between *c-Myc* and *c-Jun* in both models is thus most likely the result of the different time points after the initial Axin loss. The activation of Wnt targets could be a very short-lived event, immediately following the initial Axin loss. It will therefore be important to establish a timeline for the events happening within the first few days after Axin deletion.

Unfortunately, the treatment of the organoids with β-NF showed major side effects, that although they did not prevent the observation of Axin1-dependent biology, altered the functional background on which the biology could be subsequently studied (see Section 5.3.4). Independent of their genotype, organoids changed their morphology, possibly masking some of the Axin dependant effects. Another liver specific, inducible Cre recombinase tested (TTR-CreER^{T}) were only be activated in differentiation conditions and at low levels (see Section 5.4.1). The use of this CreER^{T} recombinase would thus limit the investigation to hepatocyte-like cells. In turn, this might prevent the consequences of Axin1 loss on liver stem cell function and regeneration to be studied. We therefore decided to use a viral mediated delivery process instead. After having shown that lentiviral transfection of liver organoids was feasible, we generating organoid lines caring the Tamoxifen inducible Lenti-CMV-ER^{T2}CreER^{T2} construct, and performed preliminary experiments indicating the usefulness as a Cre delivery system (see Section 5.4.2).

Given the preliminary evidence gained using the Ah-Cre transgene; that the culture system closely mimics the *in vivo* situation, together with the more suitable Lenti-viral system, we believe, we now have a valuable tool to study the cell biology and early consequences of Axin1 (and Axin2 loss leading to Axin dependent tumourigenesis.

6 Discussion

The newly developed conditional Axin1 and Axin2 knockout mouse lines (Feng et al. 2012, Feng, unpublished) are the key to examining Axin function. Recent results obtained in the Dale lab, using the conditional Axin1 mutant mouse line, challenge the idea of the role of Axin1 in the liver and in hepatocellular carcinogenesis. Traditionally, the main role of Axin1 was described through its regulatory function of β-Catenin and the Wnt signalling pathway. This link was also believed to be responsible for the development of HCC, due to Axin1 mutations. But Axin1 loss in the mouse liver led to a late onset of HCC without the rise in nuclear β-Catenin levels, or changes in liver zonation (Feng et al. 2012), that occur in mutants of other Wnt pathway components, such as β-Catenin or APC (Benhamouche et al. 2006; Tan et al. 2006). Instead, Axin1 dependent tumourigenesis in the mice, was linked to a transcriptional program associated with G2/M cell cycle and cytokinesis regulators, and increased proliferation, and hepatomegaly.

In order to understand the link between Axin mutations and the cell cycle, ultimately leading to hepatocellular carcinogenesis, we studied the effect of Axin loss in an allelic series of Axin mutant mouse embryonic stem cells (ES cells), embryonic development, and in a 3D liver culture system.

Using these systems, we aimed to assess the importance of Axin1 in the regulation of the β-Catenin destruction complex and its role in cell cycle regulation in different tissues. Furthermore, we aimed to identify redundant and non-redundant functions of Axin1 and Axin2 in those processes.

6.1 Summary of effects of Axin loss

In summary, we found some evidence of classic Wnt pathway deregulation in the allelic series of Axin mutant ES cells, but there was no G2/M related gene expression signature, which might be linked to Axin function in the cell cycle and at the mitotic spindle.

The effect of Axin mutations, on core Wnt signalling activity, got stronger when ES cells were differentiated into embryoid bodies (EBs) and during embryonic development. Interestingly, mutations in both Axin genes severely impaired the differentiation potential of the embryonic stem cells. Additionally, we found some evidence of cell cycle deregulation in response to Axin mutations in EBs.

In 3D liver cultures, where we only analysed loss of Axin1, we found no changes in Wnt/β-Catenin signalling and the cell cycle, when cells were grown in expansion conditions (EM). When Axin1 mutant cells were differentiated along the hepatic lineage (in DM), Wnt/β-Catenin signalling was still unchanged, but we found evidence of cell cycle deregulation, in the form of a G2/M related gene expression profile, similar to the effect of Axin1 loss in the mouse liver.

Overall, our study showed context-dependent effects of Axin loss on Wnt signalling activity and cell cycle deregulation. The results obtained in this thesis are shown in Table 6-1 as a simplified summary; a more detailed discussion of the results can be found in the following sections.

Table 6-1. Summary of Axin in different cell/tissue types

	$A1^{\Delta/\Delta}$	$A2^{\Delta/\Delta}$	$A2^{lacZ/lacZ}$	$A1^{\Delta/\Delta}$, $A2^{\Delta/\Delta}$	$A1^{\Delta/\Delta}$, $A2^{lacZ/lacZ}$
ES CELLS					
Classical Wnt	↑	–	–	↑	↑
G2/M signature	–	–	–	–	–
Pluripotency	–/↑	–/↑	–/↑	↑	↑
EMBRYONIC DEVELOPMENT					
Classical Wnt	–/↑	–/↑	–	↑	↑
G2/M signature	–	–	–	↑	↑
Differentiation potential	–/↓	–/↓	–/↓	↓	↓
3D LIVER CULTUR, EM					
Classical Wnt	–	**N/A**	**N/A**	**N/A**	**N/A**
G2/M signature	–	**N/A**	**N/A**	**N/A**	**N/A**
3D LIVER CULTUR, DM					
Classical Wnt	–	**N/A**	**N/A**	**N/A**	**N/A**
G2/M signature	↑	**N/A**	**N/A**	**N/A**	**N/A**

This table shows a very simplified summary of the effects of Axin loss found in this thesis.

– : normal ↑ : small up-regulation ↑ : up-regulation ↓ : small down-regulation ↓ : down-regulation

6.2 Axin loss in an allelic series of embryonic stem cells

Chapter 4 focussed on the role of Axin1 and 2 in embryonic stem cells and development. We successfully generated a range of pluripotent ES cell lines with different combinations of Axin alleles, using the $Axin1^{\Delta/\Delta}$ (Feng et al 2012), $Axin2^{\Delta/\Delta}$ (Feng, unpublished), and $Axin2^{lacZ/lacZ}$ (Lustig et al. 2002) transgenes.

We could show that Exon 2 was successfully removed from the conditional Axin1 and 2 alleles by PCR and qRT-PCR following transient transfection with a Cre expressing plasmid. Additionally, we found that neither *Axin1* nor *Axin2* gene expression was hyperactivated in response to the loss of any of the Axin genes. The expression levels stayed at the same levels as in wt ES cells, in experiments using several different primer sets. The lack of *Axin2* overexpression in response to Axin1 loss was unexpected, since *Axin2* has been found to be overexpressed following mutations of other members of the β-Catenin destruction complex,

namely GSK3 and APC, (Doble et al. 2007; Kielman et al. 2002; Atlasi et al. 2013) and in our control cells lines without GSK3 activity ($GSK3^{\Delta/\Delta}$ and wt + CHIR99021). The upregulation of *Axin2* in these papers was attributed to the negative feedback role of Axin2 following high Wnt signalling activity.

Therefore, we further analysed Wnt signalling pathway activity, by measuring the abundance of different post-translational modified pools of β-Catenin and transcriptional Wnt/β-Catenin targets.

6.2.1 Wnt signalling activation in Axin mutant ES cells

In homozygous $Axin1^{\Delta/\Delta}$ embryonic stem cells, TCF reporter activity and Wnt target gene expression analysis did not show any changes compared to wt ES cells. However, the pool of β-Catenin marked for degradation by phosphorylation at S33, S37, and T41 in the destruction complex was decreased, while 'free' β-Catenin, available to bind to ECT, was increased. These findings suggest that Axin1 does have β-Catenin regulatory function in the ES cells, but it is not as important for β-Catenin phosphorylation as GSK3 or APC (Doble et al. 2007; Kielman et al. 2002; Atlasi et al. 2013).

Mutations of Axin2 alone (in either $Axin2^{\Delta/\Delta}$, or $Axin2^{lacZ/lacZ}$ ES cells) did not have any effects on Wnt/β-Catenin signalling activity, in any of the assays performed here.

The loss of both conditional Axin homologues in $Axin1^{\Delta/\Delta}$, $Axin2^{\Delta/\Delta}$ ES cell lines, however, showed some Wnt/β-Catenin signalling related effects. *Cdx1* expression levels were upregulated, and $P^{S33/S37/T41}$-as well as P^{S45}- β-Catenin levels decreased.

Loss of both Axin genes in $Axin1^{\Delta/\Delta}$ and $Axin2^{lacZ/lacZ}$ double mutant ES cell lines, showed the strongest effect in regard to Wnt/β-Catenin signalling deregulation. *Cdx1* expression, total, $deP^{S33/S37/T41}$-, and P^{S552}- β-Catenin levels, and 'free' β-Catenin (in TCF, ICAT, and ECT pull-downs) were upregulated compared to wt cells. TCF reporter activity also increased, although not significantly. Simultaneously, the pool of $P^{S33/S37/T41}$-β-Catenin marked for degradation by the destruction complex was reduced.

Importantly, the effects of Axin double mutants were different between the $Axin2^{lacZ/lacZ}$ and the $Axin2^{\Delta/\Delta}$ allele, suggesting that both versions of Axin2 mutations were not equivalent. Since the effects of the $Axin2^{lacZ/lacZ}$ allele on Wnt signalling seemed to be stronger than the ones from the $Axin2^{\Delta/\Delta}$ allele, and were more similar to GSK3 knockout and inhibition, one could argue that $Axin2^{lacZ/lacZ}$ is a true null allele. However, I will later discuss the data obtained in mouse embryos, which strongly suggest the opposite (see Section 6.5.2).

Taken together, mutations of Axin in ES cells, especially in double mutants, did affect classical Wnt/β-Catenin signalling. However, the analysis of posttranslational modified β-Catenin, as well as transcriptional target gene expression showed a few interesting, unexpected results that are worth discussion further.

I Post-transcriptionally modified β-Catenin

In the analysis of total and post-transcriptionally modified β-Catenin, we found changes in β-Catenin levels aside from the total, phospho- and dephospho S33, S37 and T41 levels expected for a disruption of the β-Catenin destruction complex. The analysis of the different pools of β-Catenin, suggests that Axin is involved in the regulation of β-Catenin stability and activity beyond the scaffolding of GSK3.

We found very interesting differences between Axin double mutants and $GSK3^{\Delta/\Delta}$ ES cells that might give further insight into the β-Catenin regulatory role of Axin1 and/or 2. These differences between the two Axin double mutants and the $GSK3^{\Delta/\Delta}$ ES cells are summarized in Table 6-2 A and B.

Table 6-2. β-Catenin pools in Axin double mutant and GSK3 $^{\Delta/\Delta}$ ES cells.

A) Differences in β-Catenin pools in Axin double mutant and GSK3 $^{\Delta/\Delta}$ ES cells compared to wt.

β -Catenin pool	A1 $^{\Delta/\Delta}$, A2 $^{\Delta/\Delta}$	GSK3 $^{\Delta/\Delta}$	A1 $^{\Delta/\Delta}$, A2 $^{lacZ/lacZ}$
total	no change	higher	
P-S45	lower	no change	
P-S33/S37/T41	lower		
deP-S33/S37/T41	no change	higher	lower
P-S552	no change		higher
P-S675	lower	no change	
TCF binding	no change	higher	
ICAT binding	no change	higher	
ECT binding	no change	higher	
E-Cadherin bound	no change	lower	no change

B) Differences in β-Catenin pools in Axin double mutant ES cells compared to and GSK3 $^{\Delta/\Delta}$.

β -Catenin pool	A1 $^{\Delta/\Delta}$, A2 $^{\Delta/\Delta}$	A1 $^{\Delta/\Delta}$, A2 $^{lacZ/lacZ}$
total	lower	no change
P-S45	no change	higher
P-S33/S37/T41	higher	no change
deP-S33/S37/T41	lower	no change
P-S552	no change	higher
P-S675	lower	no change
TCF binding	lower	
ICAT binding	lower	
ECT binding	lower	no change
E-Cadherin bound	higher	no change

The Tables 6-2 A and B show a summary of the results obtained by statistical analysis of the normalized data in the β-Catenin protein analysis (see Section 4.4.4)

As described earlier (in Section 4.4.4 and 4.4.5), the proportion of 'free' β-Catenin that was pulled down with the different bait proteins ECT, ICAT and TCF4, differed between each of the Axin mutants, and GSK3 knockout or inhibition; suggesting the involvement of distinct molecular species of β-Catenin. In addition to the phosphorylations at S45 (see below) and S33, S37 and T41 by GSK3 and CK1, that mark β-Catenin for degradation; β-Catenin activity is regulated through many other phosphorylation sites. In the assay described here, we tested for the AKT and PKA phosphorylation sites at S552 and S667. Different phosphorylation patterns at both of these sites were found in the Axin mutant ES cell lines. A whole additional range of posttranslational modifications of β-Catenin are known, but were not tested here. They all work in concert to regulate its function in cell adhesion and transcription (reviewed by Gao et al. 2014). Axin1 and 2 could have many more functions involved in the 'fine tuning'

of β-Catenin function and binding abilities, in addition to the regulation of its stability, by interacting with a whole range of cellular kinases. The function of Axin as a scaffold protein for the Kinases involved is not yet understood (see Section 1.3) and will need to be investigated further.

One example of a cellular Kinase suggested to regulate β-Catenin function in an Axin dependent manner is CK1 (Amit et al. 2002). Under normal conditions, β – Catenin is phosphorylated at S45 by a complex comprising Axin and CK1. In our assay, this phosphorylation was reduced in $GSK3^{\Delta/\Delta}$ and in $Axin1^{\Delta/\Delta}$, $Axin2^{\Delta/\Delta}$ ES cells, while P^{S45} levels remained unchanged in $Axin1^{\Delta/\Delta}$, $Axin2^{lacZ/lacZ}$, when the data were normalized to total β-Catenin levels in each sample. The data obtained for P^{S45}- β – Catenin assay, although not conclusive, could indicate that Axin1 and 2 do have redundant CK1 scaffolding functions. Here, it would be interesting to further study the effects of Axin loss on P^{S45}- β – Catenin, other CK1 target proteins, and the influence on specific CK1 isoforms.

II Transcriptional activity

While different pools of β-Catenin were clearly affected in response to Axin loss, the data regarding Wnt target gene expression were less clear. Here, we tested for the expression of the Wnt target genes *Axin2, c-Myc* and *Cdx1* in ES cells. Of those; only *Cdx1* expression was increased in Axin double mutants. TCF reporter activity was not significantly increased in either of them. Nevertheless, there was a trend towards an increased TCF reporter activity level in $Axin1^{\Delta/\Delta}$, $Axin2^{lacZ/lacZ}$, matching the TCF/β-Catenin pull down data. Overall, the effect of Axin double mutations on target gene expression and β-Catenin pools was weaker (or detected in fewer assays) than GSK3 inhibition by CHIR99021 or complete GSK3 knockout.

A study in APC mutation ES cells lines with varying severity in regards to Wnt deregulation, also showed deferential target gene regulation (Atlasi et al. 2013). They reported, that *TCF3* expression was reduced in response to Wnt stimulation, while *Axin2* and *Cdx1* expression were increased. However, the levels of Wnt signalling activity necessary to reduce *TCF3*

expression were substantially higher than the levels needed to drive the other two genes. We think that the variation in transcriptional response in the different cell lines, is the result of a deregulation on different levels: the level of activated 'free' β–Catenin, the combination of specific (TCF/Lef) transcription factors needed for the expression of individual genes, and the expression and activity levels of the individual TCFs themselves.

In addition to explaining the variation in Wnt target gene activation in Axin and GSK3 mutant ES cell lines, different inter- and intra- cellular environments affecting each of these levels could also be contributors to the cell and tissue type specific effects of Axin mutations observed here. (Further discussions of contributing factors can be found later in the in this Chapter.)

As previously described, the combinations of different Axin mutations, and loss or inhibition of GSK3 resulted in different molecular species of β – Catenin, with distinct binding capacities. In the nucleus 'free' β – Catenin binds to members of the TCF/Lef family of transcription factors to drive target gene expression (Clevers 2006). TCF family members exhibit cell-type and promoter-specific functional differences important in selective target gene activation (Arce et al. 2006). In embryonic stem cells, TCF3 is the most abundant member. In contrast to TCF1 and 4, which usually activate Wnt target gene expression; TCF3 represses the transcription of pluripotency factors in the absence of β – Catenin in ES cells (Merrill et al. 2004; Wu et al. 2012a).

TCF reporter activity in ES cells has been shown to depend on the interaction of TCF1 or Lef1 with β – Catenin. TCF4 and TCF3 even supressed luciferase levels in a co-transfection experiment with constitutively active β – Catenin (Yi et al. 2011). In contrast, *Cdx1* is regulated by TCF4, but also retinoic acid signalling (Lickert et al. 2000). The transcriptional regulation of *c-Myc,* which is not actually a Wnt target gene in ES cells, and *Axin2* in ES cells and specifically Axin mutants have been discussed earlier.

The different levels of Wnt activation in ES cells following Axin or GSK3 mutations could thus be due to different effects of Axin or GSK3 loss of function on the transcriptional activity of β – Catenin itself; or indirect consequences of other affected cellular processes.

6.2.2 Proliferation levels in Axin mutant ES cells

Since Axin has been shown to be involved in many processes involved in cell cycle regulation (see Section 1.3.4), and Axin1 dependent development of HCC are linked to strong activation of proliferation and a G2/M cell cycle related transcriptional program (see Section 1.3.6), we decided to analyse whether Axin mutant ES cell lines also show evidence of cell cycle deregulation.

Different assays to analyse proliferation and apoptosis in Axin mutant ES cells, including growth curves and gene expression analysis, showed no changes in cell proliferation and viability. Thus the role of Axin during cell-cycle progression, possibly through interacting with the mitotic spindle, seems not to play a major role in embryonic stem cells.

6.3 Axin loss in embryonic development

6.3.1 Differentiation potential and Wnt activation during embryonic development

I Wnt signalling activity and differentiation of Axin mutant embryoid bodies

The Wnt/β –Catenin pathway is generally considered to be important for the maintenance of the pluripotency of embryonic stem cells (Nusse et al. 2008; Wend et al. 2010). Ectopic activation of β –Catenin, for example through the knockout of GSK3, has been shown to limit differentiation potential of ES cells (Doble et al. 2007). This led us to further investigate the differentiation capacity and pluripotency of Axin mutant ES cell lines.

Interestingly, while canonical Wnt signalling was not changed drastically in response to Axin mutations in embryonic stem cells, many effects on differentiation potential and

pluripotency were observed, especially in Axin1$^{\Delta/\Delta}$, Axin2$^{\Delta/\Delta}$; and Axin1$^{\Delta/\Delta}$, Axin2$^{lacZ/lacZ}$ double mutants.

Firstly, Axin double mutant ES cells lines had a very round, highly retractile colony morphology and stained strongly for Oct4 and Alkaline phosphates. However, transcription of the pluripotency markers *Oct4*, *Nanog,* and *Rex1* were unchanged in 1i conditions.

Secondly, when Axin mutant ES cells were grown in non-attachment conditions without LIF, and 2i, they developed into embryoid bodies (EBs) with different degrees of differentiation along the germ layers.

Mutations in both Axin genes resulted in EBs that were optically distinct from those without functional GSK3 (treatment with CHIR99021 or knockout of both GSK3 genes), while showing a very similar staining pattern in immunohistochemical analysis for differentiation and pluripotency markers (e.g. AFP, SMA and Oct4). According to a preliminary experiment, the gene expression profile of Axin1$^{\Delta/\Delta}$, Axin2$^{\Delta/\Delta}$ EBs was also severely changed. To test a wide panel of stem cell and differentiation markers, we performed a RT^2 PCR profiler array and found that pluripotency and some endoderm markers were upregulated, whilst expression of neural differentiation markers was decreased.

The effect on both neural and endodermal differentiation, could be linked to Wnt pathway activation. The endoderm marker Sox17 (found upregulated in of Axin1$^{\Delta/\Delta}$, Axin2$^{\Delta/\Delta}$ EBs) is known to interact with β-Catenin to up-regulate FoxA2 expression (also found to be increased) to drive endodermal differentiation (Sinner et al. 2004). Conversely, Wnt signalling is well known as an inhibitor of neural development (Aubert et al. 2002). Overexpression of a stabilized β-Catenin mutant (β-Cat^{S33A}) in embryonic stem cells failed to substantially activate TCF dependent transcription, but it inhibited neuroectoderm differentiation (Kelly et al. 2011) in line with our findings.

Another result, indicating a role of Wnt signalling regulation in embryoid bodies following Axin loss, is the finding that Runx2 expression was increased in Axin1$^{\Delta/\Delta}$, Axin2$^{\Delta/\Delta}$ EBs. Runx2 is an important mediator of bone formation and has previously been found to be

overexpressed in GSK3 double mutant EBs (Doble et al. 2007) and with Wnt activation through Simvastatin (Qiao et al. 2011).

The observation, that Axin double mutants, as well as Axin2 single mutants (both $Axin2^{\Delta/\Delta}$ and $Axin2^{lacZ/lacZ}$, did not form cardiomyocytes in our EB assay, was in agreement with the loss of pluripotency as the result of Wnt activation. Cardiac development is supposed to rely on the inhibition of canonical Wnt signalling (Eisenberg and Eisenberg 2006) and B. Doble and his colleges (2012) took the absence of cardiomyocytes in $GSK3^{\Delta/\Delta}$ as a positive read-out for Wnt hyperactivation. This would mean, that the Wnt signalling pathway could be hyperactivated in Axin2 single or Axin double mutant EBs.

Due to the strong effects of Axin loss on the differentiation potential of ES cells described above, we decided to have a closer look at β-Catenin levels and Wnt target activation during differentiation. Interestingly, the effect of Axin mutations on the Wnt signalling pathway increased when the cells were allowed to differentiate into EBs. β-Catenin levels, assessed by immunohistochemical staining, as well as *CD44 (v10)* expression, in a qRT-PCR experiment, increased in Axin double mutant EBs (both version).

The increase in β-Catenin is most likely the direct effect of destabilisation of the destruction complex in response to Axin loss. However, this could also be linked to the differentiation defects caused by other mechanisms. High β-Catenin can be found in wt EBs in the parietal endoderm or mesodermal internal epithelia. Unsurprisingly, parietal endoderm markers were among the strongest upregulated markers found in the RT^2 PCR profiler array of $Axin1^{\Delta/\Delta}$, $Axin2^{\Delta/\Delta}$ EBs (see Appendix 3, Table A-2). Thus, the identity of each cell type within the EBs and their ability to signal to each other could strongly influence Wnt signalling and β-Catenin levels in Axin mutant EBs.

A recent study by Habib and colleagues shows that activation of the Wnt signalling pathway is strongly dependent on the location of the signal during cell division (Habib et al. 2013). While ES cells grown in conditions maintaining pluripotency, daughter cells are

normally exposed to equal levels of Wnt stimulation favouring self-renewal in both cells. During differentiation, the localisation of a Wnt source determines which of the daughter cells undergoes differentiation, and which maintains the stem cell character. During this Wnt dependent process, Axin may play an important regulatory role, which makes it vital for asymmetric cell division but partly dispensable for symmetric divisions.

The effects of Axin loss on the limitation in the differentiation potential of ES cells could therefore be the effect of over activation of β-Catenin dependent transcription in asymmetric cell divisions during development.

However, more and more papers suggest, that although β-Catenin is required for the maintenance of pluripotency, its transcriptional activity is not (Faunes et al. 2013; Lyashenko et al. 2011). The group around Yehudit Bergman suggested a model in which a membrane bound complex of β-Catenin and Oct4 maintains pluripotency (Abu-Remaileh et al. 2010). They showed, that Oct4/β-Catenin interaction regulates β-Catenin protein levels in a GSK3 dependent manner. In our study, we found that while Oct4 protein levels were increased in Axin double mutants and ES cells with reduced GSK3 activity in 1i medium, *Oct4* transcription levels were unchanged. Axin1 and 2 (and other Wnt pathway components) could thus be directly involved in processes that govern Oct4 protein levels and activity.

The exact mechanisms regulating Oct4 protein levels and activity, are thus far unclear (Zeineddine et al. 2014). Its transcriptional activity is believed to be negatively regulated through PKA and ERK/MAPK, which also affects protein stabilization and localization (Brumbaugh et al. 2012; Spelat et al. 2012). Its degradation is governed through the E3 ubiquitin ligase WWP2 (Xu et al. 2009b). SUMOylation of Oct4 instead, increases its stability (Spelat et al. 2012; Gill 2004). If the idea that Axin regulates Oct4 protein stability holds true, this could mean that the β-Catenin destruction complex has a marginal role in stem cell maintenance, while the regulation of the β-Catenin/Oct4 complex becomes crucial.

Taken together, mutations of Axin1 and Axin2 decrease the potential of ES cells to differentiate, similar to GSK3 mutations. However, it is unclear if the differentiation defects are due to stabilization of transcriptionally active β-Catenin and downstream target gene expression; or if Axin (and GSK3) are involved in the regulation of pluripotency factors, independent of TCF/Lef mediated transcription.

II Wnt deregulation in Axin mutant mouse embryos

We did not directly investigate Wnt signalling activity in Axin mutant mouse embryos.

However, a very interesting study performed by N. Fossat, related different levels of malformation to the degree of Wnt activity in the mouse embryo (Fossat et al. 2011). By analysing mice with different combinations of mutants of canonical Wnt signalling components, they found that Wnt signalling strength directly correlated with the extent of head malformation in embryos.

$Axin1^{\Delta/\Delta}$ mutations, using our conditional allele, led to severe malformation of the head, similar to the ones found in a Axin null transgenes ($Axin^{Tg1}$) (Perry et al. 1995; Zeng et al. 1997). The phenotypes of the $Axin1^{\Delta/\Delta}$, CMV-Cre embryos were very similar to the ones classed in category III and higher in the severity chart put forward by Fossat et al. (2011), matching a highly Wnt active phenotype (see Figure 6-1 and Figure 4-29).

The effects of embryonic loss of Axin2 in $Axin2^{fl/fl}$ embryos were different to the ones observed in $Axin2^{lacZ/lacZ}$ mice (Yu et al. 2005). The exact phenotypes were described in Section 4.8.4. Essentially, there seemed to be a scale of malformations related to mutations of Axin2 and possibly Wnt activity. While $Axin2^{lacZ/lacZ}$ mice only showed head malformations as adults (not on the scale/category I); $Axin2^{\Delta/wt}$ embryos ranged from category I to II. Homozygous mutations in $Axin2^{\Delta/\Delta}$ showed severity levels of II and higher. The two different Axin2 alleles lay on different parts of the Wnt activity scale (see Figure 6-1).

Since the effect of the $Axin2^{\Delta}$ allele was stronger than the one observed in $Axin2^{lacZ}$, and increasing Wnt signalling activity causes increased head truncation (Fossat et al. 2011),

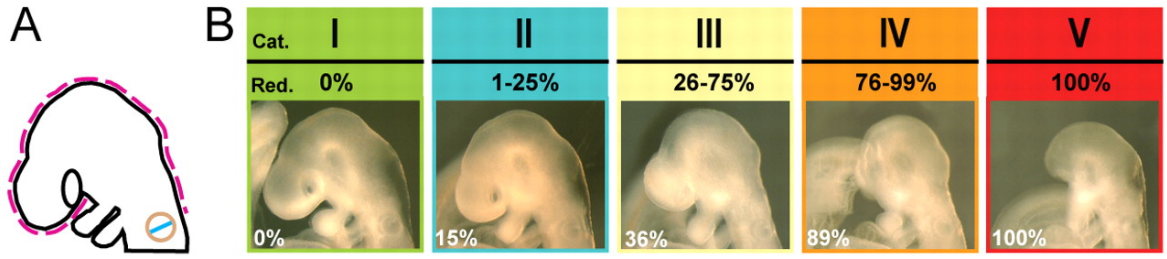

Figure 6-1. Phenotype categories of Wnt mutant embryos.
A) Morphometric analysis of head size of E9.5 embryos. The measurement is expressed as the ratio of the linear distance along the silhouette of the head from the border of the mandibular arch and maxillary prominence to the rostral margin of the otic vesicle (pink dashed line), and the diameter (blue line) of the otic vesicle (brown circle); the latter is relatively constant among embryos of the different genotypes. **B)** Phenotypic classification of the mutant embryo based on the morphology and degree of reduction of the head: Category (Cat.) I, normal; II-IV, partial truncation; V, most severe truncation. Figure taken from Fossat et al. 2011[I].

[I] Permission to reproduce this figure has been granted by the Company of Biologists.

these results suggest that Axin2^{lacZ} allele has some remaining β-Catenin regulatory function, while the Axin2$^{\Delta}$ allele could be a true null. The huge variation of malformations observed, especially in the Axin2$^{wt/\Delta}$ embryos, could be attributed to genetic background and maternal and environmental effects that, directly or indirectly, change the basic activation of β-Catenin, making Axin dependent regulation more or less crucial.

6.3.2 Effects of Axin loss on proliferation during embryonic development

Although we did not find evidence of cell cycle deregulation in the allelic series of Axin mutant ES cell lines, when they were grown in conditions maintaining pluripotency, we decided to investigate proliferation levels during embryoid body formation.

Counts of total cells, and qRT-PCR data suggested that Axin mutations lead to an increase in cell proliferation and numbers of cells expressing G2/M markers in EBs. Some data obtained by immunohistochemistry (i.e. Ki-67 staining) confirmed these findings, while the staining for BrdU and Cyclin B1 were not significantly different to wt EBs. Proliferation levels in EBs are not only influenced by direct effects of Axin mutations. Other factors, including cellular differentiation, and access to nutrients in differently sized EB, might have contributed to the cell cycle related data obtained here. Nevertheless, the pattern of G2/M related gene expression signature in EBs was very similar to the one found in Axin1 mutant mouse livers (Feng et al. 2012).

Axin1 and Axin2 have been shown to act at the MTOC and to be involved with G2/M cell cycle progression, and Wnt/β-Catenin target genes have been linked to G1/S cell cycle progression (see Section 1.3.4). It seems that none of the links between Axin function and cell cycle regulation influences proliferation levels in embryonic stem cells. During embryoid development, however, the role of Axin in the cell cycle becomes important.

The strongest effects were observed in Axin double mutants of both genotypes, indicating a redundancy of Axin1 and 2 in this process.

6.4 Axin loss in the liver organoids

In Chapter 5, we develop an Axin1 mutant 3D liver culture system derived from hepatic bile ducts to examine the acute changes following Axin1 deletion in the liver, leading to the development of HCCs in real time. We aimed to generate an organoids culture system that allowed tightly regulated and highly efficient deletion of Axin1, and closely mimicked the *in vivo* effects of Axin1 loss. In this Section, I will summarize the preliminary results of Axin function in the liver obtained from the culture system. Later (in Section 6.7.1), I will discuss the limitations of the system and describe necessary improvements to maximize its use as a tool to study Axin function in the liver.

I. Effects of Axin1 loss on Wnt signalling in Axin1 mutant liver organoids

In the previous study, conducted in the Dale lab, Axin1 loss in the liver did not activate β-Catenin and Wnt target gene transcription strongly (Feng et al. 2012). Using the newly developed 3D liver culture system, in which Axin1 loss was induced using the β-Naphthoflavone (β-NF) sensitive Ah-Cre transgene (Ireland et al 2004), we confirmed those findings. In Axin1 mutant livers and differentiated organoids *Axin2* mRNA was slightly upregulated, whereas there was no difference in expansion conditions. Expression levels of other Wnt signalling target genes (e.g. c-Myc and Tiam1) were not affected. Similarly, β-Catenin levels and localisation (assessed by immunocytochemistry) did not change in liver cultures in any of the conditions.

II. Proliferation levels in Axin1 mutant liver organoids

The Axin1 mutant 3D liver culture system used in this study also showed very similar cell cycle related phenotype as found in the mouse liver, when the cells were differentiated along the hepatic lineage. A G2/M related genes expression profile was found in $Axin1^{\Delta/\Delta}$, AhCre (+β-NF) organoids grown under differentiation conditions. Additionally, Axin1 mutant cultures grown in DM had an increased organoid diameter after 14 days in culture and the number of Ki67 positive cells was higher. Unfortunately, the study did not progress further in

the analysis of the mechanisms involved in cell cycle deregulation as a result of Axin1 loss in the liver.

Interestingly, in liver organoids in expansion conditions, no changes in cell cycle related effect were observed in response to Axin1 loss. This could either be attributed to a differential role of Axin in stem cells *versus* differentiated cells (thus a cell type and context specific effect), or the already highly proliferative state of these cells in expansion conditions is masking the effects of Axin loss on proliferation

However, the analysis was done using suboptimal culture conditions, so we are not in a position to further comment on Wnt regulation in the organoids. An improvement of the culture system (see Section 6.7.2) is needed to analyse liver cultures thoroughly. We will then also study the effects of simultaneous Axin1 and 2 loss and Axin1, Axin2, β-Catenin triple mutants, to investigate which effects are mediated through β-Catenin (see Section 6.7.4).

6.5 Axin1 and Axin2 protein from the Axin mutant alleles

An important consideration, regarding the results presented in this thesis, is to understand the nature of the Axin mutant alleles used. The vital question is whether the $Axin1^{\Delta}$ (Feng et al. 2012), $Axin2^{\Delta}$ (Feng, unpublished), and $Axin2^{lacZ}$ alleles (Lustig et al. 2002) are true nulls.

The expression of a functionally active gene product from the different Axin alleles could explain the lack of obvious Wnt/β-Catenin signalling activation in many of the experiments shown here. Additionally, the so-called Axin2 null, $Axin2^{lacZ/lacZ}$ shows a different phenotype to the one found in the conditional $Axin2^{fl/fl}$ allele. Based on both these observations, it is vital to show the complete loss of functional Axin protein.

In this Section, I will briefly summarise selected experiments, which help to clarify the functions of the different alleles.

6.5.1 Loss of Axin1 protein

Immunoblotting performed by Gui-Jie Feng and colleagues on Axin1$^{\Delta/\Delta}$ mice, showed loss of Axin1 protein and failed to detect truncated protein in the liver samples tested (Feng et al. 2012), suggesting that the knockout of Exon 2 indeed acts as a null allele. Nevertheless, it is formally impossible to rule out the expression of any functional protein, while any coding regions remain intact. (see Section 4.8.1).

The conditional deletion of Axin1 in the early embryo though, CMV-Cre (Schwenk et al. 1995) led to embryonic malformation, similar to the ones found in Axin null transgenes (Axin1^{Tg1}) (Perry et al. 1995; Zeng et al. 1997) (see Section 4.8.2). Despite the similarity to the Axin1^{Tg1} null allele, the presence of a truncated Axin1 protein in the deleted embryos (Axin1$^{\Delta/\Delta}$, CMV-Cre) could still not be excluded completely. Embryos expressing Axin1 mutations with deletions of either the RGS domain (Axin$^{\Delta RGS}$), required for APC binding, or the C-terminal region (Axin$^{\Delta C6}$), involved in JNK activation, also exhibited the same phenotypes (Chia et al. 2009).

It also needs to be mentioned, that the Axin allele, described as a true Axin1 null in the literature, actually relies on a change in Exon 2. A tandem array of the human epsilon-globin gene (~600 kb in total) was inserted between Exon 1 and Exon 3 of the *Axin1* locus. The transgene directs expression of a truncated *Axin1* mRNA product (still containing exons 3-10) which is thought to lead to a recessive loss of function allele (Perry et al. 1995; Zeng et al. 1997).

Taken together, none of the experiments described above exclude the possibility of a remaining protein from our conditional Axin1$^{\Delta/\Delta}$ allele fully. However, the similarity of the CMV-Cre Axin1$^{\Delta/\Delta}$ phenotype to that of the Tg1 allele, which is taken as a null, suggests that a null Axin1 allele was generated as expected.

Since the Axin1 mutant liver tumours, closely resemble the human tumours, we have a good model to study Axin1 dependent tumourigenesis. Mutations leading to tumourigenesis rarely rely on a full gene deletion; but rather on point mutations, or small deletions or

insertions (Vogelstein and Kinzler 2004). Loss of at least Exon 2 does definitively remove the RGS domain, thus inhibiting APC binding and normal formation of the β-Catenin destruction complex.

6.5.2 Loss of Axin2 protein

In the case of Axin2 the situation is more complicated. We used two different Axin2 alleles (see Section 1.4.1.2), which showed widely different phenotypes in embryonic stem cells biology and embryonic development.

In embryonic stem cells, the $Axin2^{lacZ/lacZ}$ and $Axin2^{fl/fl}$ alleles had similar phenotypes, although in combination with $Axin1^{\Delta/\Delta}$, $Axin2^{lacZ/lacZ}$ usually had a more severe phenotype than $Axin2^{\Delta/\Delta}$. Surprisingly, in the mouse embryo the situation seemed to be reversed. In all of the assays performed in embryoid bodies, Axin double mutants of both genotypes ($Axin1^{\Delta/\Delta}$, $Axin2^{\Delta/\Delta}$ *vs*. $Axin1^{\Delta/\Delta}$, $Axin2^{lacZ/lacZ}$) showed very similar effects.

In order to fully understand Axin2 function in the different system, it is thus important to identify the status of each of the Axin2 alleles.

An analysis of alternative start codons and matching Kozak sequences in the $Axin2^{\Delta/\Delta}$ revealed the theoretical possibility that a truncated Axin2 protein containing the β-Catenin binding site and the DIX domain (see Section 4.8.3) might be expressed from the $Axin2^{\Delta/\Delta}$ allele. However, the first in frame ATGs found following splicing within exon 1-3 were found downstream of the GSK3 and β-Catenin binding sites, which would predicate a non functional allele.

Sequence information for the $Axin2^{lacZ}$ allele is not publically available. However, the *lacZ* gene, with nuclear localization sequence, was reported to be inserted in the vicinity of Exon 2, in frame with the endogenous start codon (Lustig et al. 2002). In this process, most of Exon 2 was replaced. Both alleles preserve sequences outside of Exon2 and might be expected to lead to similar consequences on function. Importantly, neither has been proven to be a true null so far.

As a result of the definitive deletion of a subset of coding sequences, a potentially truncated Axin2 protein, if it were expressed, would not contain a RGS domain. This domain is vital for the interaction with APC and is supposed to inhibit the formation of the destruction complex (Nakamura et al. 1998). However, other important Axin domains might still be functional (see Section 1.3 for more details about these functions and the domains).

Theoretically, there is also the possibility that alterations of exon 2 (in $Axin2^{\Delta}$ and/or $Axin2^{lacZ}$), could result in the expression of new mRNA (e. g. exon 1-3 splice, alternative exon 1s or artefactual mRNAs) in a tissue and cell type specific way. In order to understand, what is expressed, when and where by any of the Axin2 alleles ($Axin2^{\Delta}$ and/or $Axin2^{lacZ}$) we would need to carefully map mRNA expression

Additionally, we are not in a position to completely exclude different genetic background. The mice used to generate ES cell lines and to breed the Axin2 mutant embryos were on an outbred background, which required a careful comparison between matched controls.

This formally leaves us with at least four different possibilities regarding the identity of Axin2 alleles used in this study:

A) $Axin2^{lacZ}$ is a true null, while $Axin2^{\Delta}$ forms a (partially) functional allele;

B) $Axin2^{\Delta}$ is a true null, while $Axin2^{lacZ}$ forms a (partially) functional allele;

C) Both alleles are true Axin2 nulls and the effects are background dependent

D) Neither $Axin2^{lacZ}$ nor $Axin2^{\Delta}$ are loss of function alleles

At this point, we are not in a position to infer the identity of any of the alleles here. Unfortunately, good Axin2 antibodies for the detection of mouse protein are, thus far, not available. Antibodies used in the literature often detect the RGS domain, which prevents us from using them on the $Axin2^{lacZ}$ and the $Axin2^{\Delta/\Delta}$ alleles. But, we are currently working on the production of new, specific antibodies in collaboration with Bruce Caterson, to enable us to detect low levels of Axin2 in the ES cells. As an additional 'in progress approach', we are

working on a CRISPR/Cas9 approach to knockout the full Axin2 coding region in ES cells to generate a definitive null allele (see Section 6.7).

6.6 Conclusions about general Axin function and its role in hepatocellular carcinogenesis

In this study, we set out to further the understanding of Axin function in general, and its involvement in hepatocellular carcinogenesis, by studying Axin1 and Axin2 loss of function mutations in embryonic stem cell, embryonic development and in the liver.

In this thesis, we found that Axin function is strongly dependent on the cell type and context.

The classic role of Axin1 and its homologue Axin2 in scaffolding the β-Catenin destruction complex (Behrens et al. 1998; Ikeda et al. 1998; Liu et al. 2002), seems to be important during embryonic development and partially in embryonic stem cells. In the liver, where we only fully analysed Axin1 function; so far, we could not find strong evidence of an inhibition of the destruction complex in the absence of Axin1.

Another role of Axin found here and in the study conducted by Feng et al. (2012), was a link between Axin function and cell cycle regulation. A mechanism, possibly involving the activation of Wnt target gene, which regulate G1/S progression, or the interaction of Axin1 and/or Axin2 and other Wnt pathway components with the MTOC in G2/M, led to increased proliferation and G2/M related gene expression in some of the systems studied here. The cell cycle regulatory function of Axin was not important in embryonic stem cells and in biliary cells in 3D culture. However, proliferation and gene expression changes were observed in Axin mutant embryoid bodies and hepatocyte-like cells in liver cultured (grown in DM).

These observations led to further questions regarding the exact mechanism(s) governing the role of Axin in different tissues. Among those are:

What mechanism(s) link Axin loss to the cell cycle regulation? Is it through the direct interaction of Axin with proteins involved in cell cycle progression or is it a β-Catenin dependent transcriptional response of a subset of Wnt target genes after all? How does the intra- and inter –cellular environment influence the specific role of Axin in different context? Are Axin 1 and Axin2 functionally redundant; in both the destruction complex and the cell cycle regulatory functions? In the following Section I will discuss theses questions further.

In HCCs with Axin1 mutations, the role of Axin in cell cycle regulation appears to be the prominent factor driving tumourigenesis. But the effect could still be linked to subtle Wnt/-β-Catenin signalling deregulation. Tumourigenesis was suggested to be dependent on a 'just right' level of canonical Wnt pathway activity (Albuquerque et al. 2002). The threshold of signalling level, necessary to induce hepatocellular carcinoma, might be very low (Buchert et al. 2010). In the liver and in 3D culture, our detection methods might not have been sensitive enough, to detect this low level of β-Catenin activation.

So far, we cannot fully exclude the possibility of β-Catenin being involved in the proliferative phenotype in the liver. Thus we will need to investigate Axin mutations on a β-Catenin loss of function background (see Section 6.7.4). However, we think it is very likely that a non-canonical mechanism drives the cell cycle phenotype in Axin mutants.

Since we have only analysed Axin1 loss in the mouse liver and in tumourigenesis (*in vivo* and *in vitro*), the effects observed could be through functional compensation by Axin2. β-Catenin levels could have remained low due to a destruction complex built around Axin2. Additionally, possible overexpression of *Axin2* (of which we found some evidence in the liver) could have been the cause of the cell cycle deregulation. Data regarding Axin double mutants in the ES cell lines and in EBs, suggest that Axin1 and Axin2 do indeed have some redundant functions in the destruction complex, which might also be found in the liver. However, Axin1 loss alone did change some pools of post-translationally modified β-Catenin that were not

found in any of the Axin2 mutant ES cell lines ($Axin2^{\Delta/\Delta}$ and $Axin2^{lacZ/lacZ}$), indicating that there are also non-redundant functions in their capacity to regulate Wnt signalling. For example, Axin1 and 2 are known to have different affinities to interact with Dvl2, which make Axin2 less responsive to upstream Wnt activation and allows strong negative-feedback function (Bernkopf et al. 2015).

In Axin1 and Axin2 double mutants ES cells and EBs, we found that the cell cycle deregulation phenotype was also still present, which suggests a partially redundant function in this process. In order to test whether Axin2 function is similar in the liver, we will analyse Axin1 and 2 double mutant organoid culture and in the mouse liver in future (see Section 6.7.3).

Interestingly, the effect of Axin loss on the Wnt signalling pathway, as well proliferation levels, were generally reduced in both embryonic stem cells and in cultured cholangiocytes (possibly adult liver stem cells), while embryonic, as well as hepatocyte, differentiation increase observed consequences of Axin loss.

As described in the Introduction (Section 1.3.5), embryonic stem cell maintenance and pluripotency can be viewed as a balancing act between rival lineage specifications and extrinsic modulators, which are constantly competing (Loh and Lim 2011; Martello and Smith 2014). The Wnt signalling pathway is one of the network nodes that can stabilize the circuit maintaining pluripotency. The effects of Axin mutations in the context of embryonic stem cells, could be balanced out by other mechanisms and pathways involved in this network, so that Axin loss does not lead to a strong phenotype. The landscape and composition of these networks change during embryonic development, resulting in the need for Axin to regulate Wnt signalling and pathway crosstalk, and asymmetric cell division.

In liver culture, cells in expansion condition could be compared to the embryonic stem cells. As potential tissue stem cells, they are likely to use similar regulatory mechanisms to the ones found in embryonic stem cells. During the differentiation in hepatocyte-like cells, Axin

mutations act in a different inter- and intra- cellular environment, leading to a prominent proliferative phenotype.

Additionally, G2/M and cell cycle related effects were mainly found in tissue and cell type that had reduced intrinsic proliferation. In highly proliferative cell types (i.e. expanding liver cultures and ES cells), possible effects of Axin loss could have been masked. Axin might even have a role in the exit of the cell from the cell cycle into G_0, which is not important in continuously growing stem cell cultures, but would have strong effects in usually non-cycling hepatocytes or in different phases of embryonic differentiation.

Overall, Axin function appears to be far more complicated than the classical theory, according to which it is only involved in the scaffolding of the β-Catenin destruction complex. In the liver, this role seems only to be a minor contributor to tumourigenesis, while other (most likely non canonical) functions involved in cell cycle regulation, take a prominent role. Further investigations into the tissue specific role of Axin1 and 2 are needed to fully understand its general function and to generate targeted HCC treatment methods.

6.7 Future directions

6.7.1 Full knockout of both Axin genes

Due to the lack of good antibodies to detect Axin protein, away from the RGS domain, we were not able to confirm the loss of Axin protein in any of the Axin1 or Axin2 knockout alleles without a doubt.

The only available way that could prove full Axin loss, is the deletion of all the coding exons, not just Exon 2. We therefore designed a CRISPR/Cas9 (clustered regularly interspaced short palindromic repeats) approach to introduce in third *loxP* site downstream of the Axin coding regions of the Axin1 and Axin2 allele of previously targeted ES cells (Marraffini and Sontheimer 2010; Ran et al. 2013b) (see Figure 6-2 A).

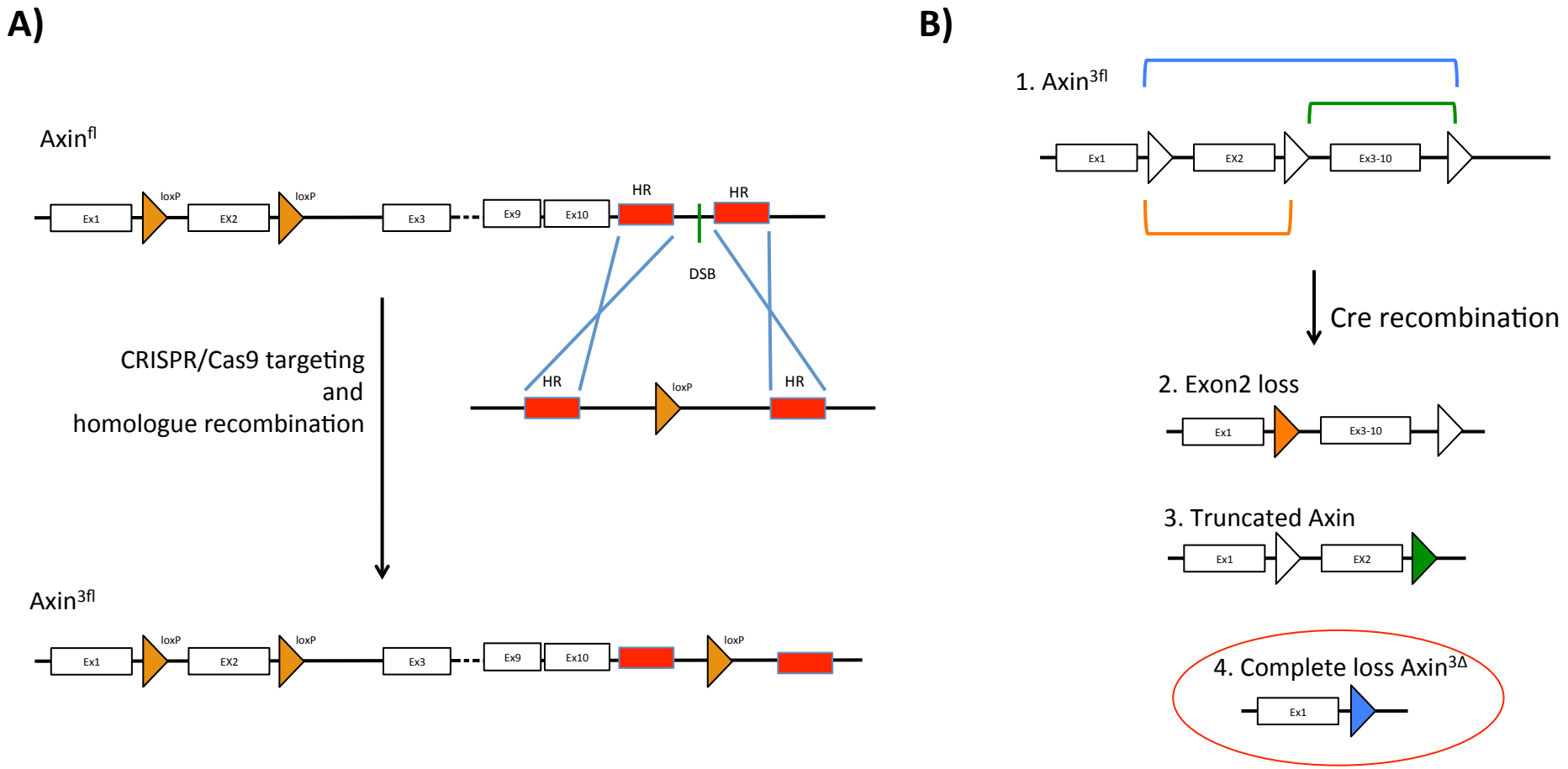

Figure 6-2. Generation of full-length Axin knockouts using CRISR/Cas9 technology, homologue, and Cre recombination.
A) The Existing Axin^{fl} alleles of Axin 1 and/or Axin2 will be targeted using CRISRP to induce a double strand break (DSB). The break will then be rescued with a donor construct containing homologue regions (HR) and a loxP site. Successful integration of the 3rd loxP site downstream of Exon 10 will generate the Axin3^{fl} alleles. **B)** Cre - mediated recombination of selected loxP sites (colour coded) will then generate alleles with different parts of the Axin allele.

The resulting alleles, that we termed Axin1^{3fl} and Axin2^{3fl} (for 3 loxP sites), can then be floxed out using Cre recombinase to generate an allele without any Axin coding sequence (see Figure 6-2 B).

We selected a suitable target site for the insertion of an additional *loxP* site, downstream of the coding regions of Axin1 and Axin2 according to the following criteria:

- Region must not have any known function that could be disturbed
- Region should not be highly conserved between species, since that points towards a not yet known function that would be disturbed
- Region should be conserved between mouse strains, since we are working on an out bred background and small differences between a target construct and the targeted region can highly reduce the targeting efficiency
- Ideally, the target site needs very few nucleotide changes to generate a *loxP* site

However, in the case of Axin1, the noncoding region between Axin1 and the next downstream gene Pdia2 (protein disulfide isomerase family A, member 2) is only 200 bp long and thus did not allow for any stringent selection of a target region. The Axin2 targeting region was chosen more stringently.

We are currently attempting to insert the 3rd loxP site using two different repair constructs: ssODN (single-stranded DNA oligonucleotide) and a donor plasmid as a template for HDR (homology-directed repair). To generate the targeting constructs, we amplified the target region of Axin1 and Axin 2 by PCR. This sequence was then cloned into a plasmid after insertion of a loxP sequence by restriction digest, or we ordered custom made ssODNs with the target sequence and loxP site.

For the CRISPR approach, we chose to use a nickase version of the Cas9 enzyme (Ran et al. 2013a). Cas9n enzyme needs small guide RNA strands to find the complementary target region in genomic DNA. There, it will induce a single strand break. If two single stranded breaks (marked by two guide RNAs) are in close proximity to each other, they can become the

integration site of our loxP site by homologue recombination. We chose this double nicking approach to reduce off- target effects of CRISPR.

Guide RNAs were designed using an online sgRNA design tool (DNA2.0 sgRNA Design Tool[m]). This tool identified Cas9 nickase target sites from the in the input sequence with an offset of 0 to 20 bp and ranked them according to computationally predicted off-target effects. Pairs of target sites were chosen for each of the Axin sequences, so that the addition of a *loxP* site destroyed at least one of the target regions, preventing targeting of the repair template and retargeting of an already engineered allele. This approach should lead to the homozygous insertion of the loxP sequence.

We are currently co-transfecting already targeted Axin^{fl} ES cell lines with pairs of sgRNAs, Cas9n and the repair constructs to insert the 3rd loxP site downstream of the Axin coding sequences. Selected cones will then undergo Cre recombination to achieve homozygous loss of Axin coding sequences.

The side-by-side comparison between the Exon2 mutant Axin ES cells and the newly targeted full Axin knockouts will hopefully show the same phenotype and we can be sure that no Axin protein is left.

6.7.2 Improvement and use of the liver organoids system

In Chapter 5, we developed a 3D liver culture system to study the loss of Axin1 in the liver. Previous work in the Dale lab, to find the mechanisms of Axin1 dependent tumourigenesis used an *in vivo* mouse liver model (Feng et al. 2012). This study showed the development of HCC with similar characteristics as in the human disease, and highlighted some short- and long-term changes following Axin1. However, the use of this *in vivo* model had its limitations. In the mouse model, we were not able to follow these changes in the mutant livers over time, in order to trace the exact development. The 3D liver culture system developed here was supposed to overcome these limitations and further elucidate the acute role of Axin1 loss.

[m] https://www.dna20.com/eCommerce/cas9/input

The culture system allows imaging of living cells for a period of time and tracing their cell fate. Additionally, it allows the comparison of normal and oncogenic cells with the same genetic background.

Here, we showed preliminary evidence that an Axin1 mutant liver culture system is a valuable tool to study Axin dependent liver tumourigenesis. However, there are still a few improvements to be made and the limitations of the culture system need to be carefully considered.

Firstly, the recombination system we were using for most of this study (AhCre) generated Axin1 liver organoids that closely mimic the effects observed in the mouse liver, but also showed major side effects. As previously described, we are now working on a Lenti virus mediated Cre delivery system to overcome these problem.

The culture system comprises cholangiocyte and hepatocytes, the two main cell types found in the liver, so that it allows the analysis of their interactions. However, other cell types found commonly in the liver, e.g. dendritic cells, Kupffer cell, stellate cells, and endothelial cells, are absent. The involvement of those cell types and for example immune responses cannot be measured in this model.

Even though cholangiocyte derived cultures can be grown and differentiated in culture, the differentiated cells express hepatocyte markers, while still retaining some ductal cell character. At this point we are not sure whether the gene expression profile of liver markers is due to individual cells expressing the whole range; or if there are different district cell types expressing only cholangiocyte or hepatocyte markers. For future experiments, it might be necessary to generate a cleaner cell population. To this end, live FACS sorting against liver or progenitor surface markers (e.g. CD24 (Qiu et al. 2011)) could be used. Additionally, the identity of each cell within an organoid could be determined by whole mount fluorescent staining for hepatocyte markers (e.g. HNF4α or Albumin) and cholangiocytes (e.g. Krt19) if needed. Co-immunofluorescence staining with hepatocyte and cholangiocyte specific markers could then show, if the differentiated organoids consist of distinct cell populations, or if there

is an intermediate cell type expressing both markers. In previous work *AXIN1* mutant HCC tumours were described as poorly differentiated (Zucman-Rossi et al. 2007). Careful analysis of the cell identity in the liver culture system could help to verify the influences of Axin 1 loss in ducal cell and hepatocytes, and its role on the differentiation process. By varying the timing of differentiation and Axin loss (the time point of exposure to differentiation medium and/or Cre recombinase) the exact time point at which Axin1 is involved in differentiation could be identified.

Now all the necessary tools, to study the mechanism(s) which results in an acute increase in hepatocyte cell volume, cell proliferation and a G2/M signature after Axin1 loss in the liver are tested and generated. Several studies have reported oscillation of Wnt signalling components like β-Catenin and Wnt target genes like Axin2 and Cyclin D1 during the cell cycle (Olmeda et al. 2003; Hadjihannas et al. 2006; Davidson et al. 2009; Tetsu and McCormick 1999). More and more Wnt signalling components were also shown to interact and regulate the centrosomes and the microtubule organising centre; among them are: Axin1, Axin2, APC, β-Catenin and GSK3 (Fumoto et al. 2009; Hadjihannas et al. 2006; Hadjihannas et al. 2010; Louie et al. 2004; Caldwell and Kaplan 2009; Kockeritz et al. 2006). Furthermore, Wnt signalling targets like Cyclin D1 and c-Myc have been associated with checkpoint control and cell cycle progression (Tetsu and McCormick 1999; Niehrs and Acebron 2012; Sheen and Dickson 2002; Sheen et al. 2003).

Cell cycle changes in the liver organoids can be investigated by live cell imaging while they happen. I will be examining, how the cells progress through the cell cycle and if there is a G2/M arrest in response to Axin loss. The liver organoids permit cell cycle analysis in mitotic arrest assays using different methods for cell cycle synchronization. Moreover, cell cycle progression can be followed using florescent tagged histones (Fraser et al. 2005), that allow the tracing of living cells undergoing mitosis, and FUCCI-probes (Fluorescent Ubiquitination-based Cell Cycle Indicator) (Sakaue-Sawano et al. 2011), a live cell cycle reporter that is based on a colour change of fluorescent probes in different phases of the cell cycle.

Additionally, we will be using the 3D liver cultures system to investigate the involvement of the newly described “Wnt-Stop” pathway in Axin dependent tumourigenesis (Acebron et al. 2014). The WNT-STOP pathway is likely to be active in multiple cancer cell lines including the breast cancer cell line MDA-MB231 and the non-small cell lung cancer line HCC15, both of which exhibit evidence of autocrine Wnt signalling (Acebron et al. 2014; Akiri et al. 2009; Bafico et al. 2004). Furthermore, the WNT-STOP pathway can help explain why multiple tumours that contain downstream mutations in β-Catenin and APC, have upregulated upstream, autocrine Wnt signalling via mechanisms such as the silencing of endogenous Wnt ligand inhibitor expression (eg. SFZD1 and DKK1). Taken together, this suggests that the ‘WNT-STOP’ pathway is a valid therapeutic target for pharmaceutical efforts.

The knowledge gained through these experiments will not only advance our understanding of the involvement of Axin1 in hepatocellular carcinogenesis and cell cycle regulation in the liver; but may also be the starting point for the development of new therapeutic strategies. The wide variety of parameters and high level of control provided by this model makes it an attractive model for drug discovery programs. Axin mutant liver organoids could be used in a medium to high-throughput study to test the efficiency and specificity of novel anti-cancer drugs. We plan to develop the response of liver organoids to the loss of Axin1 into a screen for anti-cancer agents. Especially the use of the 3D culture morphometric assay, together with the company OcellO, will allow us to generate a high throughput assay, which will quantify the key changes after Axin1 loss, including organoid morphology, an increase in G2/M cell size, protein levels and proliferation. Therapeutic compounds can be screened against Axin1 mutant organoids for their ability to reverse quantifiable phenotypes in the Axin1, but not wild-type cells. Once the primary assay has been established, a series of deconvolution assays will be performed to rank primary hits. These could include the use of a GSK-3-degradation sensitive GFP biosensor whose response is predicted to be specific to the WNT-STOP pathway (Acebron et al. 2014). Other

downstream deconvolution assays will involve the analysis of cell cycle signatures including transcriptional changes (G2/M) and cell cycle stage.

6.7.3 Axin1, Axin2 double knockout in the liver and organoids

In order to address whether a functional β-Catenin destruction complex is involved in the lack of a Wnt signature in the liver, we attempted to exclude the possibility of truncated Axin proteins from the conditional allele (see above). Another possibility for a functional destruction complex in Axin1 deficient livers, that we considered, was the constitutive upregulation of Axin2. We found that in mouse ES cells and embryoid bodies, mutations of both Axin genes indeed made the effects worse, even though *Axin2* was not upregulated in single Axin1 mutants. In contrast, in Axin1 deficient mouse livers or liver organoids *Axin2* levels were increased. This would allow the formation of the destruction complex around Axin2 and subsequent degradation of β-Catenin, resulting in normal Wnt target gene expression as seen in the gene expression profile.

However, one issue with this hypothesis, is that there is some data that suggests Axin2 is localised predominantly to the nucleus, with relative amounts present in the cytoplasm and relative amounts required in the cytoplasm to compensate for Axin1 loss not known (Salahshor and Woodgett 2005).

To test this hypothesis in the hepatic setting, we are currently generating Axin1 and Axin2 double mutant mice and liver organoids. If Axin2 in this setting is important in the destruction complex, a strong Wnt ON phenotype should be observed. Further investigations into the Axin1 and Axin2 double knockout ES cells and mouse livers will give further insight into the redundancy of Axin1 and 2.

If the Axin1 and 2 double knockouts show a strong activation of β-Catenin in the liver, this indicates that the role of both Axins in the destruction complex is similar. If the G2/M signature is abolished, the implication of Axin2 in cell cycle regulations have to be further investigated. Over-expression of Axin2 has been shown to suppress spindle checkpoint

activation and chromosomal instability (Alexandrova and Sokol 2010; Hadjihannas et al. 2010). Furthermore, Axin2 has been shown to interact with polo-like kinase 1 (PLK1) and is able to localise to the mitotic spindle and at centrosomes (Hadjihannas et al., 2010).

However, if the G2/M related gene expression profile persists in the double knockouts, Axin1 has a direct role as a tumour suppressor.

All these effects will be investigated in this *in vitro* model by live cell imaging, to observe how the cell is progressing through the cell cycle, or if the G2/M cell cycle protein up regulation is associated with a G2/M arrest. An *in vitro* model provides a much easier model to observe these mitotic events and any errors that could affect the formation of the spindle or the orientation of the spindle separation. Progression of the cell cycle is ultimately controlled by CDK activity. The 3D model could also be used for various kinase assays to determine the activity of various CDKs and provide more information about the cell cycle following Axin1 loss.

6.7.4 Axin1, Axin2 and β-Catenin triple mutants

Lastly, we have still not fully answered the question, whether β-Catenin and its transcriptional activity are involved in Axin dependent tumourigenesis.

Overall, gene expression analysis in liver organoids, the mouse liver, and in embryoid bodies did not show strong activation of Wnt target genes in response to different Axin mutations. But whole tissue/culture gene expression analysis provides only a small picture of what is occurring inside the cells. It is possible that a small population of cells have increased Wnt-target gene expression, while other cells exhibit decreased or no Wnt signalling, balancing each other out. As a result, no changes can be observed in a gene expression profile.

Additionally, below detection threshold activation of Wnt signalling, in a small subset of cells, may be enough to trigger tumourigenesis in the long run (Wend et al. 2010). A small population of cells with increased Wnt-target gene expression would not be detected if other cells exhibiting decreased or no Wnt signalling activity. The activation of β-Catenin in single

cells could drive a very strong G2/M associated gene expression profile again in just a few cells or in the whole surrounding tissue.

We will thus perform analysis of Axin1, Axin2, β-Catenin triple mutants (and all possible combinations of single and double mutants) using the β-Catenin$^{fl/fl}$ transgene (Brault et al. 2001). The analysis of this mutant in addition to the appropriate controls, could give valuable insights into the function and redundancy of Axin1 and Axin2, especially on Wnt signalling regulation. The question that will be answered is: 'does the knockout of both Axin genes lead to the development of tumours in a Wnt/β-Catenin dependent manner?'

Since Axin1 and 2 play an important role in Wnt signalling pathway regulation, we hypothesised that the acute effects of Axin1 loss in the liver are mediated by the overexpression of β-Catenin. Direct overexpression of β-Catenin has been shown to enhance liver growth and regeneration in mice. Transgenic mice overexpressing wild-type β-Catenin in the liver showed an increase in liver size and cell proliferation (Nejak-Bowen and Monga 2011; Tan et al. 2005) similar to the one described in the conditional Axin1 mutants (Feng et al. 2012). Mice expressing ΔN-β-Catenin, an oncogenic form with an increased protein stability, also exhibit increased cell proliferation leading to hyperplasia and hepatomegaly (Cadoret et al. 2001). Taken together, the effects mediated by Axin1 deletion are very similar to the ones observed in β-Catenin mutant mice, suggesting a common mechanism. It also has to be noted, that neither Axin1 loss nor the β-Catenin mutants described above develop spontaneous hepatic tumours (Nejak-Bowen and Monga 2011). β-Catenin as well as Axin1 mutations in those mice are only the first hit in a multistep process.

List of References

Aberle, H., Bauer, A., Stappert, J., Kispert, A. and Kemler, R. 1997. Beta-catenin is a target for the ubiquitin-proteasome pathway. *The EMBO journal* 16(13), pp. 3797–3804.

Abremski, K. and Hoess, R. 1984. Bacteriophage P1 site-specific recombination. Purification and properties of the Cre recombinase protein. *The Journal of biological chemistry* 259(3), pp. 1509–1514.

Abu-Remaileh, M., Gerson, A., Farago, M., Nathan, G., Alkalay, I., Zins Rousso, S., Gur, M., et al. 2010. Oct-3/4 regulates stem cell identity and cell fate decisions by modulating Wnt/β-catenin signalling. *The EMBO journal* 29(19), pp. 3236–3248.

Acebron, S.P., Karaulanov, E., Berger, B.S., Huang, Y.-L. and Niehrs, C. 2014. Mitotic Wnt signaling promotes protein stabilization and regulates cell size. *Molecular cell* 54(4), pp. 663–674.

Adams, D. 1980. *The Restaurant at the End of the Universe*. Pan Macmillan.

Adams, D.H. and Eksteen, B. 2006. Aberrant homing of mucosal T cells and extra-intestinal manifestations of inflammatory bowel disease. *Nature Reviews Immunology* 6(3), pp. 244–251.

Akiri, G., Cherian, M.M., Vijayakumar, S., Liu, G., Bafico, A. and Aaronson, S.A. 2009. Wnt pathway aberrations including autocrine Wnt activation occur at high frequency in human non-small-cell lung carcinoma. *Oncogene* 28(21), pp. 2163–2172.

Albrecht, J.H. and Hansen, L.K. 1999. Cyclin D1 promotes mitogen-independent cell cycle progression in hepatocytes. *Cell growth & differentiation : the molecular biology journal of the American Association for Cancer Research* 10(6), pp. 397–404.

Albuquerque, C., Breukel, C., van der Luijt, R., Fidalgo, P., Lage, P., Slors, F., Leitao, C., et al. 2002. The 'just-right' signaling model: APC somatic mutations are selected based on a specific level of activation of the beta-catenin signaling cascade. *Human molecular genetics* 11(13), pp. 1549–1560.

Alexandrova, E.M. and Sokol, S.Y. 2010. Xenopus axin-related protein: a link between its centrosomal localization and function in the Wnt/beta-catenin pathway. *Developmental dynamics : an official publication of the American Association of Anatomists* 239(1), pp. 261–270.

Altekruse, S.F., McGlynn, K.A. and Reichman, M.E. 2009. Hepatocellular Carcinoma Incidence, Mortality, and Survival Trends in the United States From 1975 to 2005. *Journal of Clinical Oncology* 27(9), pp. 1485–1491.

Amit, S., Hatzubai, A., Birman, Y., Andersen, J.S., Ben-Shushan, E., Mann, M., Ben-Neriah, Y., et al. 2002. Axin-mediated CKI phosphorylation of beta-catenin at Ser 45: a molecular switch for the Wnt pathway. *Genes & development* 16(9), pp. 1066–1076.

Arce, L., Yokoyama, N.N. and Waterman, M.L. 2006. Diversity of LEF/TCF action in development and disease. *Oncogene* 25(57), pp. 7492–7504.

Arendt, D. 2008. The evolution of cell types in animals: emerging principles from molecular studies. *Nature reviews. Genetics* 9(11), pp. 868–882.

Arnold, H.K., Zhang, X., Daniel, C.J., Tibbitts, D., Escamilla-Powers, J., Farrell, A., Tokarz, S., et al. 2009. The Axin1 scaffold protein promotes formation of a degradation complex for c-Myc. *The EMBO journal* 28(5), pp. 500–512.

Atlasi, Y., Noori, R., Gaspar, C., Franken, P., Sacchetti, A., Rafati, H., Mahmoudi, T., et al. 2013. Wnt Signaling Regulates the Lineage Differentiation Potential of Mouse Embryonic Stem Cells through Tcf3 Down-Regulation. *PLoS genetics* 9(5), p. e1003424.

Aubert, J., Dunstan, H., Chambers, I. and Smith, A. 2002. Functional gene screening in embryonic stem cells implicates Wnt antagonism in neural differentiation. *Nature biotechnology* 20(12), pp. 1240–1245.

Azzolin, L., Panciera, T., Soligo, S., Enzo, E., Bicciato, S., Dupont, S., Bresolin, S., et al. 2014. YAP/TAZ incorporation in the β-catenin destruction complex orchestrates the Wnt response. *Cell* 158(1), pp. 157–170.

Bafico, A., Liu, G., Goldin, L., Harris, V. and Aaronson, S.A. 2004. An autocrine mechanism for constitutive Wnt pathway activation in human cancer cells. *Cancer cell* 6(5), pp. 497–506.

Bahmanyar, S., Kaplan, D.D., Deluca, J.G., Giddings, T.H., O'Toole, E.T., Winey, M., Salmon, E.D., et al. 2008. beta-Catenin is a Nek2 substrate involved in centrosome separation. *Genes & development* 22(1), pp. 91–105.

Bakiri, L. and Wagner, E.F. 2013. Mouse models for liver cancer. *Molecular oncology* 7(2), pp. 206–223.

Bakre, M.M.M., Hoi, A.A., Mong, J.C.Y.J., Koh, Y.Y.Y., Wong, K.Y.K. and Stanton, L.W.L. 2007. Generation of multipotential mesendodermal progenitors from mouse embryonic stem cells via sustained Wnt pathway activation. *The Journal of biological chemistry* 282(43), pp. 31703–31712.

Behrens, J., Jerchow, B.A., Würtele, M., Grimm, J., Asbrand, C., Wirtz, R., Kühl, M., et al. 1998. Functional interaction of an Axin Homolog, Conductin, with beta-Catenin, APC, and GSK3beta. *Science (New York, N.Y.)* 280(5363), pp. 596–599.

Bell, D.R. and Van Zant, G. 2004. Stem cells, aging, and cancer: inevitabilities and outcomes. *Oncogene* 23(43), pp. 7290–7296.

Benhamouche, S., Decaens, T., Godard, C., Chambrey, R., Rickman, D.S., Moinard, C., Vasseur-Cognet, M., et al. 2006. Apc tumor suppressor gene is the 'zonation-keeper' of mouse liver. *Developmental cell* 10(6), pp. 759–770.

Berg, T., Rountree, C.B., Lee, L., Estrada, J., Sala, F.G., Choe, A., Veltmaat, J.M., et al. 2007. Fibroblast growth factor 10 is critical for liver growth during embryogenesis and controls hepatoblast survival via beta-catenin activation. *Hepatology (Baltimore, Md.)* 46(4), pp. 1187–1197.

Bernkopf, D.B., Hadjihannas, M.V. and Behrens, J. 2015. Negative-feedback regulation of the Wnt pathway by conductin/axin2 involves insensitivity to upstream signalling. *Journal of cell science* 128(1), pp. 33–39.

Bilic, J., Huang, Y.-L., Davidson, G., Zimmermann, T., Cruciat, C.-M., Bienz, M. and Niehrs, C. 2007. Wnt induces LRP6 signalosomes and promotes dishevelled-dependent LRP6 phosphorylation. *Science (New York, N.Y.)* 316(5831), pp. 1619–1622.

Boeuf, H., Hauss, C., Graeve, F.D., Baran, N. and Kedinger, C. 1997. Leukemia inhibitory factor-dependent transcriptional activation in embryonic stem cells. *The Journal of cell biology* 138(6), pp. 1207–1217.

Bone, H.K., Damiano, T., Bartlett, S., Perry, A., Letchford, J., Ripoll, Y.S., Nelson, A.S., et al. 2009. Involvement of GSK-3 in regulation of murine embryonic stem cell self-renewal revealed by a series of bisindolylmaleimides. *Chemistry & biology* 16(1), pp. 15–27.

Bosch, F.X., Ribes, J., Díaz, M. and Cléries, R. 2004. Primary liver cancer: Worldwide incidence and trends. *Gastroenterology* 127(5), pp. S5–S16.

Boulter, L., Govaere, O., Bird, T.G., Radulescu, S., Ramachandran, P., Pellicoro, A., Ridgway, R.A., et al. 2012. Macrophage-derived Wnt opposes Notch signaling to specify hepatic progenitor cell fate in chronic liver disease. *Nature medicine* 18(4), pp. 572–579.

Boyault, S., Rickman, D.S., de Reyniès, A., Balabaud, C., Rebouissou, S., Jeannot, E., Hérault, A., et al. 2007. Transcriptome classification of HCC is related to gene alterations and to new therapeutic targets. *Hepatology (Baltimore, Md.)* 45(1), pp. 42–52.

Bradford, M.M. 1976. A rapid and sensitive method for the quantitation of microgram quantities of protein utilizing the principle of protein-dye binding. *Analytical biochemistry* 72, pp. 248–254.

Brault, V.V., Moore, R.R., Kutsch, S.S., Ishibashi, M.M., Rowitch, D.H.D., McMahon, A.P.A., Sommer, L.L., et al. 2001. Inactivation of the beta-catenin gene by Wnt1-Cre-mediated deletion results in dramatic brain malformation and failure of craniofacial development. *Development (Cambridge, England)* 128(8), pp. 1253–1264.

Bréchot, C. 2004. Pathogenesis of hepatitis B virus—related hepatocellular carcinoma: Old and new paradigms. *Gastroenterology* 127(5), pp. S56–S61.

Brumbaugh, J., Hou, Z., Russell, J.D., Howden, S.E., Yu, P., Ledvina, A.R., Coon, J.J., et al. 2012. Phosphorylation regulates human OCT4. *PNAS* 109(19), pp. 7162–7168.

Buchert, M., Athineos, D., Abud, H.E., Burke, Z.D., Faux, M.C., Samuel, M.S., Jarnicki, A.G., et al. 2010. Genetic dissection of differential signaling threshold requirements for the Wnt/beta-catenin pathway in vivo. *PLoS genetics* 6(1), p. e1000816.

Burke, Z.D. and Tosh, D. 2006. The Wnt/β-catenin pathway: master regulator of liver zonation? *Bioessays* 28(11), pp. 1072–1077.

Cadigan, K.M. and Nusse, R. 1997. Wnt signaling: a common theme in animal development. *Genes & development* 11(24), pp. 3286–3305.

Cadoret, A., Ovejero, C., Saadi-Kheddouci, S., Souil, E., Fabre, M., Romagnolo, B., Kahn, A., et al. 2001. Hepatomegaly in transgenic mice expressing an oncogenic form of beta-catenin. *Cancer research* 61(8), pp. 3245–3249.

Caldwell, C.M. and Kaplan, K.B. 2009. The role of APC in mitosis and in chromosome instability. *Advances in experimental medicine and biology* 656, pp. 51–64.

Callow, M.G., Tran, H., Phu, L., Lau, T., Lee, J., Sandoval, W.N., Liu, P.S., et al. 2011. Ubiquitin ligase RNF146 regulates Tankyrase and Axin to promote Wnt signaling. *PloS one* 6(7), p. e22595.

Campbell, S.J., Carlotti, F., Hall, P.A., Clark, A.J. and Wolf, C.R. 1996. Regulation of the CYP1A1 promoter in transgenic mice: an exquisitely sensitive on-off system for cell specific gene regulation. *Journal of cell science* 109 (Pt 11), pp. 2619–2625.

Cartwright, P. 2005. LIF/STAT3 controls ES cell self-renewal and pluripotency by a Myc-dependent mechanism. *Development (Cambridge, England)* 132(5), pp. 885–896.

Chia, I.V. and Costantini, F. 2005. Mouse axin and axin2/conductin proteins are functionally equivalent in vivo. *Molecular and cellular biochemistry* 25(11), pp. 4371–4376.

Chia, I.V., Kim, M.J., Itoh, K., Sokol, S.Y. and Costantini, F. 2009. Both the RGS domain and the six C-terminal amino acids of mouse Axin are required for normal embryogenesis. *Genetics* 181(4), pp. 1359–1368.

Clement, S., Stouffs, M., Bettiol, E., Kampf, S., Krause, K.H., Chaponnier, C. and Jaconi, M. 2007. Expression and function of -smooth muscle actin during embryonic-stem-cell-derived cardiomyocyte differentiation. *Journal of cell science* 120(2), pp. 229–238.

Clevers, H. 2006. Wnt/beta-catenin signaling in development and disease. *Cell* 127(3), pp. 469–480.

Colnot, S. and Perret, C. 2010. Liver Zonation. In: *Molecular pathology of liver diseases*. Molecular Pathology Library. Boston, MA: Springer US, pp. 7–16.

Colnot, S., Niwa-Kawakita, M., Hamard, G., Godard, C., Le Plenier, S., Houbron, C., Romagnolo, B., et al. 2004. Colorectal cancers in a new mouse model of familial adenomatous polyposis: influence of genetic and environmental modifiers. *Laboratory investigation; a journal of technical methods and pathology* 84(12), pp. 1619–1630.

Cong, F. and Varmus, H. 2004. Nuclear-cytoplasmic shuttling of Axin regulates subcellular localization of beta-catenin. *Proceedings of the National Academy of Sciences of the United States of America* 101(9), pp. 2882–2887.

Cressman, D.E., Greenbaum, L.E., DeAngelis, R.A., Ciliberto, G., Furth, E.E., Poli, V. and Taub, R. 1996. Liver failure and defective hepatocyte regeneration in interleukin-6-deficient mice. *Science (New York, N.Y.)* 274(5291), pp. 1379–1383.

Dao, D.Y., Yang, X., Flick, L.M., Chen, D., Hilton, M.J. and O'Keefe, R.J. 2010. Axin2 regulates chondrocyte maturation and axial skeletal development. *Journal of orthopaedic research : official publication of the Orthopaedic Research Society* 28(1), pp. 89–95.

Davidson, G., Shen, J., Huang, Y.-L., Su, Y., Karaulanov, E., Bartscherer, K., Hassler, C., et al. 2009. Cell Cycle Control of Wnt Receptor Activation. *Developmental cell* 17(6), pp. 788–799.

de Lau, W., Barker, N., Low, T.Y., Koo, B.-K., Li, V.S.W., Teunissen, H., Kujala, P., et al. 2011. Lgr5 homologues associate with Wnt receptors and mediate R-spondin signalling. *Nature* 476(7360), pp. 293–297.

Diehl, J.A., Cheng, M., Roussel, M.F. and Sherr, C.J. 1998. Glycogen synthase kinase-3beta regulates cyclin D1 proteolysis and subcellular localization. *Genes & development* 12(22), pp. 3499–3511.

Doble, B.W.B., Patel, S.S., Wood, G.A.G., Kockeritz, L.K.L. and Woodgett, J.R.J. 2007. Functional redundancy of GSK-3alpha and GSK-3beta in Wnt/beta-catenin signaling shown by using an allelic series of embryonic stem cell lines. *Developmental cell* 12(6), pp. 957–971.

Doetschman, T.C., Eistetter, H., Katz, M., Schmidt, W. and Kemler, R. 1985. The in vitro development of blastocyst-derived embryonic stem cell lines: formation of visceral yolk sac, blood islands and myocardium. *Journal of embryology and experimental morphology* 87, pp. 27–45.

Dulic, V., Lees, E. and Reed, S. 1992. Association of human cyclin E with a periodic G1-S phase protein kinase. *Science (New York, N.Y.)* 257(5078), pp. 1958–1961.

Eisenberg, L.M. and Eisenberg, C.A. 2006. Wnt signal transduction and the formation of the myocardium. *Developmental biology* 293(2), pp. 305–315.

El-Serag, H.B. and Rudolph, K.L. 2007. Hepatocellular carcinoma: epidemiology and molecular carcinogenesis. *Gastroenterology* 132(7), pp. 2557–2576.

Etienne-Manneville, S. and Hall, A. 2003. Cdc42 regulates GSK-3b and adenomatous polyposis coli to control cell polarity. *Nature* 421(6924), pp. 753–756.

Evans, C.L. and Xie, X.S. 2008. Coherent anti-stokes Raman scattering microscopy: chemical imaging for biology and medicine. *Annual review of analytical chemistry (Palo Alto, Calif.)* 1, pp. 883–909.

Evans, M.J. and Kaufman, M.H. 1981. Establishment in culture of pluripotential cells from mouse embryos. *Nature* 292(5819), pp. 154–156.

Ewan, K., Pajak, B., Stubbs, M., Todd, H., Barbeau, O., Quevedo, C., Botfield, H., et al. 2010. A useful approach to identify novel small-molecule inhibitors of Wnt-dependent transcription. *Cancer research* 70(14), pp. 5963–5973.

Fagotto, F., Jho, E.H., Zeng, L., Kurth, T., Joos, T., Kaufmann, C. and Costantini, F. 1999. Domains of axin involved in protein-protein interactions, Wnt pathway inhibition, and intracellular localization. *The Journal of cell biology* 145(4), pp. 741–756.

Fang, D., Hawke, D., Zheng, Y., Xia, Y., Meisenhelder, J., Nika, H., Mills, G.B., et al. 2007. Phosphorylation of beta-catenin by AKT promotes beta-catenin transcriptional activity. *The Journal of biological chemistry* 282(15), pp. 11221–11229.

Faunes, F., Hayward, P., Descalzo, S.M., Chatterjee, S.S., Balayo, T., Trott, J., Christoforou, A., et al. 2013. A membrane-associated β-catenin/Oct4 complex correlates with ground-state pluripotency in mouse embryonic stem cells. *Development (Cambridge, England)* 140(6), pp. 1171–1183.

Fausto, N. 2004. Liver regeneration and repair: hepatocytes, progenitor cells, and stem cells. *Hepatology (Baltimore, Md.)* 39(6), pp. 1477–1487.

Fei, C., He, X., Xie, S., Miao, H., Zhou, Z. and Li, L. 2014. Smurf1-mediated Axin ubiquitination requires Smurf1 C2 domain and is cell-cycle dependent. *Journal of Biological Chemistry* 289(20), pp. 14170–14177.

Fei, C., Li, Z., Li, C., Chen, Y., Chen, Z., He, X., Mao, L., et al. 2013. Smurf1-mediated Lys29-linked nonproteolytic polyubiquitination of axin negatively regulates Wnt/β-catenin signaling. *Molecular and cellular biology* 33(20), pp. 4095–4105.

Feil, R., Brocard, J., Mascrez, B., LeMeur, M., Metzger, D. and Chambon, P. 1996. Ligand-activated site-specific recombination in mice. *Proceedings of the National Academy of Sciences of the United States of America* 93(20), pp. 10887–10890.

Feng, G.J., Cotta, W., Wei, X.Q., Poetz, O., Evans, R., Jarde, T., Reed, K., et al. 2012. Conditional disruption of Axin1 leads to development of liver tumors in mice. *Gastroenterology* 143(6), pp. 1650–1659.

Ferlay, J., Soerjomataram, I., Ervik, M., Dikshit, R., Eser, S., Mathers, C., Rebelo, M., et al. 2012. GLOBOCAN 2012 v1.0, Cancer Incidence and Mortality Worldwide: IARC CancerBase No. 11 [Online]. Available at:

http://globocan.iarc.fr/Pages/Map.aspx [Accessed: June 2015].

Fodde, R., Kuipers, J., Rosenberg, C., Smits, R., Kielman, M., Gaspar, C., van Es, J.H., et al. 2001. Mutations in the APC tumour suppressor gene cause chromosomal instability. *Nature cell biology* 3(4), pp. 433–438.

Fossat, N., Jones, V., Khoo, P.L., Bogani, D., Hardy, A., Steiner, K., Mukhopadhyay, M., et al. 2011. Stringent requirement of a proper level of canonical WNT signalling activity for head formation in mouse embryo. *Development (Cambridge, England)* 138(4), pp. 667–676.

Frame, S. and Cohen, P. 2001. GSK3 takes centre stage more than 20 years after its discovery. *Biochemical Journal* 359(Pt 1), pp. 1–16.

Fraser, S.T., Hadjantonakis, A.-K., Sahr, K.E., Willey, S., Kelly, O.G., Jones, E.A.V., Dickinson, M.E., et al. 2005. Using a histone yellow fluorescent protein fusion for tagging and tracking endothelial cells in ES cells and mice. *Genesis (New York, N.Y. : 2000)* 42(3), pp. 162–171.

Frau, M., Biasi, F., Feo, F. and Pascale, R.M. 2010. Prognostic markers and putative therapeutic targets for hepatocellular carcinoma. *Molecular aspects of medicine* 31(2), pp. 179–193.

Fuentealba, L.C., Eivers, E., Ikeda, A., Hurtado, C., Kuroda, H., Pera, E.M. and De Robertis, E.M. 2007. Integrating patterning signals: Wnt/GSK3 regulates the duration of the BMP/Smad1 signal. *Cell* 131(5), pp. 980–993.

Fumoto, K., Kadono, M., Izumi, N. and Kikuchi, A. 2009. Axin localizes to the centrosome and is involved in microtubule nucleation. *EMBO reports* 10(6), pp. 606–613.

Furuhashi, M., Yagi, K., Yamamoto, H., Furukawa, Y., Shimada, S., Nakamura, Y., Kikuchi, A., et al. 2001. Axin facilitates Smad3 activation in the transforming growth factor beta signaling pathway. *Molecular and cellular biology* 21(15), pp. 5132–5141.

Gadue, P., Huber, T.L., Paddison, P.J. and Keller, G.M. 2006. Wnt and TGF-beta signaling are required for the induction of an in vitro model of primitive streak formation using embryonic stem cells. *Proceedings of the National Academy of Sciences of the United States of America* 103(45), pp. 16806–16811.

Gao, C., Xiao, G. and Hu, J. 2014. Regulation of Wnt/β-catenin signaling by posttranslational modifications. *Cell & bioscience* 4(1), p. 13.

Gartel, A.L., Ye, X., Goufman, E., Shianov, P., Hay, N., Najmabadi, F. and Tyner, A.L. 2001. Myc represses the p21(WAF1/CIP1) promoter and interacts with Sp1/Sp3. *Proceedings of the National Academy of Sciences of the United States of America* 98(8), pp. 4510–4515.

Gebhardt, R., Baldysiak-Figiel, A., Krügel, V., Ueberham, E. and Gaunitz, F. 2007. Hepatocellular expression of glutamine synthetase: an indicator of morphogen actions as master regulators of zonation in adult liver. *Progress in histochemistry and cytochemistry* 41(4), pp. 201–266.

Gill, G. 2004. SUMO and ubiquitin in the nucleus: different functions, similar mechanisms? *Genes & development* 18(17), pp. 2046–2059.

Groll, N., Emele, F., Poetz, O. and Rothbauer, U. 2015. Towards multiplexed protein-protein interaction analysis using protein tag-specific nanobodies. *Journal of proteomics*.

Grompe, M. 2014. Liver stem cells, where art thou? *Cell stem cell* 15(3), pp. 257–258.

Gualdi, R., Bossard, P., Zheng, M.H., Hamada, Y., Coleman, J.R. and Zaret, K.S. 1996. Hepatic specification of the gut endoderm in vitro: Cell signaling and transcriptional control. *Genes & development* 10(13), pp. 1670–1682.

Guichard, C., Amaddeo, G., Imbeaud, S., Ladeiro, Y., Pelletier, L., Maad, I.B., Calderaro, J., et al. 2012. Integrated analysis of somatic mutations and focal copy-number changes identifies key genes and pathways in hepatocellular carcinoma. *Nature genetics* 44(6), pp. 694–698.

Guo, X., Ramirez, A., Waddell, D.S., Li, Z., Liu, X. and Wang, X.-F. 2008. Axin and GSK3-beta control Smad3 protein stability and modulate TGF-beta signaling. *Genes & development* 22(1), pp. 106–120.

Gwak, J., Cho, M., Gong, S.-J., Won, J., Kim, D.-E., Kim, E.-Y., Lee, S.S., et al. 2006. Protein-kinase-C-mediated beta-

catenin phosphorylation negatively regulates the Wnt/beta-catenin pathway. *Journal of cell science* 119(Pt 22), pp. 4702–4709.

Habib, S.J., Chen, B.-C., Tsai, F.-C., Anastassiadis, K., Meyer, T., Betzig, E. and Nusse, R. 2013. A localized Wnt signal orients asymmetric stem cell division in vitro. *Science (New York, N.Y.)* 339(6126), pp. 1445–1448.

Hadjihannas, M.V., Bernkopf, D.B., Brückner, M. and Behrens, J. 2012. Cell cycle control of Wnt/β-catenin signalling by conductin/axin2 through CDC20. *EMBO reports* 13(4), pp. 347–354.

Hadjihannas, M.V., Brückner, M. and Behrens, J. 2010. Conductin/axin2 and Wnt signalling regulates centrosome cohesion. *EMBO reports* 11(4), pp. 317–324.

Hadjihannas, M.V., Brückner, M., Jerchow, B., Birchmeier, W., Dietmaier, W. and Behrens, J. 2006. Aberrant Wnt/beta-catenin signaling can induce chromosomal instability in colon cancer. *Proceedings of the National Academy of Sciences of the United States of America* 103(28), pp. 10747–10752.

Haegele, L., Ingold, B., Naumann, H., Tabatabai, G., Ledermann, B. and Brandner, S. 2003. Wnt signalling inhibits neural differentiation of embryonic stem cells by controlling bone morphogenetic protein expression. *Molecular and cellular neurosciences* 24(3), pp. 696–708.

Hagen, T., Di Daniel, E., Culbert, A.A. and Reith, A.D. 2002. Expression and characterization of GSK-3 mutants and their effect on beta-catenin phosphorylation in intact cells. *The Journal of biological chemistry* 277(26), pp. 23330–23335.

Hall, J., Guo, G., Wray, J., Eyres, I., Nichols, J., Grotewold, L., Morfopoulou, S., et al. 2009. Oct4 and LIF/Stat3 Additively Induce Krüppel Factors to Sustain Embryonic Stem Cell Self-Renewal. *Cell stem cell* 5(6), pp. 597–609.

Harris, T.J.C. and Peifer, M. 2005. Decisions, decisions: β-catenin chooses between adhesion and transcription. *Trends in cell biology* 15(5), pp. 234–237.

Hayes, J.D. and Dinkova-Kostova, A.T. 2014. The Nrf2 regulatory network provides an interface between redox and intermediary metabolism. *Trends in biochemical sciences* 39(4), pp. 199–218.

He, T.C., Sparks, A.B., Rago, C., Hermeking, H., Zawel, L., da Costa, L.T., Morin, P.J., et al. 1998. Identification of c-MYC as a target of the APC pathway. *Science (New York, N.Y.)* 281(5382), pp. 1509–1512.

Hedgepeth, C.M., Conrad, L.J., Zhang, J., Huang, H.-C., Lee, V.M.Y. and Klein, P.S. 1997. Activation of the Wnt Signaling Pathway: A Molecular Mechanism for Lithium Action. *Developmental biology* 185(1), pp. 82–91.

Heeg-Truesdell, E. and LaBonne, C. 2006. Neural induction in Xenopus requires inhibition of Wnt-beta-catenin signaling. *Developmental biology* 298(1), pp. 71–86.

Hoess, R.H., Ziese, M. and Sternberg, N. 1982. P1 site-specific recombination: nucleotide sequence of the recombining sites. *Proceedings of the National Academy of Sciences of the United States of America* 79(11), pp. 3398–3402.

Hoshida, Y., Nijman, S.M.B., Kobayashi, M., Chan, J.A., Brunet, J.-P., Chiang, D.Y., Villanueva, A., et al. 2009. Integrative transcriptome analysis reveals common molecular subclasses of human hepatocellular carcinoma. *Cancer research* 69(18), pp. 7385–7392.

Hu, M., Kurobe, M., Jeong, Y.J., Fuerer, C., Ghole, S., Nusse, R. and Sylvester, K.G. 2007. Wnt/beta-catenin signaling in murine hepatic transit amplifying progenitor cells. *Gastroenterology* 133(5), pp. 1579–1591.

Huang, S.-M.A., Mishina, Y.M., Liu, S., Cheung, A., Stegmeier, F., Michaud, G.A., Charlat, O., et al. 2009. Tankyrase inhibition stabilizes axin and antagonizes Wnt signalling. *Nature* 461(7264), pp. 614–620.

Huch, M., Dorrell, C., Boj, S.F., van Es, J.H., Li, V.S.W., van de Wetering, M., Sato, T., et al. 2013. In vitro expansion of single Lgr5+ liver stem cells induced by Wnt-driven regeneration. *Nature* 494(7436), pp. 247–250.

Iida, I., Johkura, K., Teng, R.F., Kubota, S., Cui, L., Zhao, X., Ogiwara, N., et al. 2003. Immunohistochemical localization of hepatocyte growth factor activator (HGFA) in developing mouse liver tissues: Heterogeneous distribution of HGFA protein. *Journal of Histochemistry & Cytochemistry* 51(9), pp. 1139–1149.

Ikeda, S., Kishida, S., Yamamoto, H., Murai, H., Koyama, S. and Kikuchi, A. 1998. Axin, a negative regulator of the Wnt signaling pathway, forms a complex with GSK-3beta and beta-catenin and promotes GSK-3beta-dependent phosphorylation of beta-catenin. *The EMBO journal* 17(5), pp. 1371–1384.

Inoki, K., Ouyang, H., Zhu, T., Lindvall, C., Wang, Y., Zhang, X., Yang, Q., et al. 2006. TSC2 integrates Wnt and energy signals via a coordinated phosphorylation by AMPK and GSK3 to regulate cell growth. *Cell* 126(5), pp. 955–968.

Ireland, H., Houghton, C., Howard, L. and Winton, D.J. 2005. Cellular inheritance of a Cre-activated reporter gene to determine Paneth cell longevity in the murine small intestine. *Developmental dynamics : an official publication of the American Association of Anatomists* 233(4), pp. 1332–1336.

Ireland, H., Kemp, R., Houghton, C., Howard, L., Clarke, A.R., Sansom, O.J. and Winton, D.J. 2004. Inducible Cre-mediated control of gene expression in the murine gastrointestinal tract: effect of loss of beta-catenin. *Gastroenterology* 126(5), pp. 1236–1246.

Ishikawa, K.S., Masui, T., Ishikawa, K. and Shiojiri, N. 2001. Immunolocalization of hepatocyte growth factor and its receptor (c-Met) during mouse liver development. *Histochemistry and Cell Biology* 116(5), pp. 453–462.

Jho, E.-H., Zhang, T., Domon, C., Joo, C.-K., Freund, J.-N. and Costantini, F. 2002. Wnt/beta-catenin/Tcf signaling induces the transcription of Axin2, a negative regulator of the signaling pathway. *Molecular and cellular biology* 22(4), pp. 1172–1183.

Jung, J.N., Zheng, M.H., Goldfarb, M. and Zaret, K.S. 1999. Initiation of mammalian liver development from endoderm by fibroblast growth factors. *Science (New York, N.Y.)* 284(5422), pp. 1998–2003.

Jungermann, K. 1986. Dynamics of Zonal Hepatocyte Heterogeneity - Perinatal-Development and Adaptive Alterations During Regeneration After Partial-Hepatectomy, Starvation and Diabetes. *Acta Histochemica* 32, pp. 89–98.

Jungermann, K. and Katz, N. 1989. Functional specialization of different hepatocyte populations. *Physiological reviews* 69(3), pp. 708–764.

Kalkan, T. and Smith, A. 2014. Mapping the route from naive pluripotency to lineage specification. *Philosophical Transactions of the Royal Society of London B: Biological Sciences* 369(1657), p. 20130540.

Kaplan, D.D., Meigs, T.E., Kelly, P. and Casey, P.J. 2004. Identification of a role for beta-catenin in the establishment of a bipolar mitotic spindle. *The Journal of biological chemistry* 279(12), pp. 10829–10832.

Katoh, M. 2013. Wnt signaling in neoplasia. In: Gelmann, E. P., Sawyers, C. L., and Raucher, F. J., III eds. Cambridge University Press, pp. 243–257.

Keller, G.M. 1995. In vitro differentiation of embryonic stem cells. *Current Opinion in Cell Biology* 7(6), pp. 862–869.

Kelly, K.F., Ng, D.Y., Jayakumaran, G., Wood, G.A., Koide, H. and Doble, B.W. 2011. β-catenin enhances Oct-4 activity and reinforces pluripotency through a TCF-independent mechanism. *Cell stem cell* 8(2), pp. 214–227.

Kidder, B.L., Yang, J. and Palmer, S. 2008. Stat3 and c-Myc Genome-Wide Promoter Occupancy in Embryonic Stem Cells. *PloS one* 3(12), p. e3932.

Kielman, M.F., Rindapää, M., Gaspar, C., van Poppel, N., Breukel, C., van Leeuwen, S., Taketo, M.M., et al. 2002. Apc modulates embryonic stem-cell differentiation by controlling the dosage of β-catenin signaling. *Nature genetics* 32(4), pp. 594–605.

Kikuchi, A., Kishida, S. and Yamamoto, H. 2006. Regulation of Wnt signaling by protein-protein interaction and post-translational modifications. *Experimental & Molecular Medicine* 38(1), pp. 1–10.

Kikuchi, K., Niikura, Y., Kitagawa, K. and Kikuchi, A. 2010. Dishevelled, a Wnt signalling component, is involved in mitotic progression in cooperation with Plk1. *The EMBO journal* 29(20), pp. 3470–3483.

Kim, K., Pang, K.M., Evans, M. and Hay, E.D. 2000. Overexpression of -Catenin Induces Apoptosis Independent of Its Transactivation Function with LEF-1 or the Involvement of Major G1 Cell Cycle Regulators. *Molecular biology of the cell*.

Kim, M.J., Chia, I.V. and Costantini, F. 2008. SUMOylation target sites at the C terminus protect Axin from ubiquitination and confer protein stability. *The FASEB journal : official publication of the Federation of American Societies for Experimental Biology* 22(11), pp. 3785–3794.

Kim, S. and Jho, E.H. 2010. The Protein Stability of Axin, a Negative Regulator of Wnt Signaling, Is Regulated by Smad Ubiquitination Regulatory Factor 2 (Smurf2). *Journal of Biological Chemistry* 285(47), pp. 36420–36426.

Kim, S.-E., Huang, H., Zhao, M., Zhang, X., Zhang, A., Semonov, M.V., MacDonald, B.T., et al. 2013. Wnt stabilization of β-catenin reveals principles for morphogen receptor-scaffold assemblies. *Science (New York, N.Y.)* 340(6134), pp. 867–870.

Kishida, S., Yamamoto, H., Hino, S., Ikeda, S., Kishida, M. and Kikuchi, A. 1999. DIX domains of Dvl and Axin are necessary for protein interactions and their ability to regulate beta-catenin stability. *Molecular and cellular biology* 19(6), pp. 4414–4422.

Kishida, S., Yamamoto, H., Ikeda, S., Kishida, M., Sakamoto, I., Koyama, S. and Kikuchi, A. 1998. Axin, a negative regulator of the wnt signaling pathway, directly interacts with adenomatous polyposis coli and regulates the stabilization of beta-catenin. *The Journal of biological chemistry* 273(18), pp. 10823–10826.

Klaus, A. and Birchmeier, W. 2008. Wnt signalling and its impact on development and cancer. *Nature reviews. Cancer* 8(5), pp. 387–398.

Knudsen, E.S., Gopal, P. and Singal, A.G. 2014. The Changing Landscape of Hepatocellular Carcinoma: Etiology, Genetics, and Therapy. *The American journal of pathology* 184(3), pp. 574–583.

Kockeritz, L., Doble, B., Patel, S. and Woodgett, J.R. 2006. Glycogen synthase kinase-3--an overview of an over-achieving protein kinase. *Current drug targets* 7(11), pp. 1377–1388.

Kofron, M., Klein, P., Zhang, F., Houston, D.W., Schaible, K., Wylie, C. and Heasman, J. 2001. The Role of Maternal Axin in Patterning the Xenopus Embryo. *Developmental biology* 237(1), pp. 183–201.

Koo, B.-K., Stange, D.E., Sato, T., Karthaus, W., Farin, H.F., Huch, M., van Es, J.H., et al. 2011. Controlled gene expression in primary Lgr5 organoid cultures. *Nature Methods* 9(1), pp. 81–U197.

Krieghoff, E., Behrens, J. and Mayr, B. 2006. Nucleo-cytoplasmic distribution of beta-catenin is regulated by retention. *Journal of cell science* 119(Pt 7), pp. 1453–1463.

Kumagi, T., Hiasa, Y. and Hirschfield, G.M. 2009. Hepatocellular carcinoma for the non-specialist. *BMJ* 339(dec04 2), pp. b5039–b5039.

Kunieda, T., Xian, M., Kobayashi, E., Imamichi, T., Moriwaki, K. and Toyoda, Y. 1992. Sexing of mouse preimplantation embryos by detection of Y chromosome-specific sequences using polymerase chain reaction. *Biology of reproduction* 46(4), pp. 692–697.

La Coste, de, A., Romagnolo, B., Billuart, P., Renard, C.A., Buendia, M.A., Soubrane, O., Fabre, M., et al. 1998. Somatic mutations of the beta-catenin gene are frequent in mouse and human hepatocellular carcinomas. *Proceedings of the National Academy of Sciences of the United States of America* 95(15), pp. 8847–8851.

Lammi, L., Blagodatski, A., Somer, M., Jarvinen, H., Lahermo, P., Thesleff, I., Pirinen, S., et al. 2004. Mutations in AXIN2 cause familial tooth agenesis and predispose to colorectal cancer. *American journal of human genetics* 74(5), pp. 1043–1050.

Laurent-Puig, P., Legoix, P., Bluteau, O., Belghiti, J., Franco, D., Binot, F., Monges, G., et al. 2001. Genetic alterations associated with hepatocellular carcinomas define distinct pathways of hepatocarcinogenesis. *Gastroenterology* 120(7), pp. 1763–1773.

Lee, E., Salic, A., Krüger, R., Heinrich, R. and Kirschner, M.W. 2003. The roles of APC and Axin derived from experimental and theoretical analysis of the Wnt pathway. *PLoS biology* 1(1), p. E10.

Lee, J.M., Yang, J., Newell, P., Singh, S., Parwani, A., Friedman, S.L., Nejak-Bowen, K.N., et al. 2014. β-Catenin signaling in hepatocellular cancer: Implications in inflammation, fibrosis, and proliferation. *Cancer Letters* 343(1), pp. 90–97.

Leenders, M.-W. 2008. Mouse models in liver cancer research: A review of current literature. *World journal of gastroenterology : WJG* 14(45), p. 6915.

Lemaigre, F.P. 2009. Mechanisms of Liver Development: Concepts for Understanding Liver Disorders and Design of Novel Therapies. *Gastroenterology* 137(1), pp. 62–79.

Leong, T.Y.-M. and Leong, A.S.-Y. 2005. Epidemiology and carcinogenesis of hepatocellular carcinoma. *HPB : the official journal of the International Hepato Pancreato Biliary Association* 7(1), pp. 5–15.

Leung, J.Y., Kolligs, F.T., Wu, R., Zhai, Y., Kuick, R., Hanash, S., Cho, K.R., et al. 2002. Activation of AXIN2 expression by beta-catenin-T cell factor. A feedback repressor pathway regulating Wnt signaling. *The Journal of biological chemistry* 277(24), pp. 21657–21665.

Li, Q., Lin, S., Wang, X., Lian, G., Lu, Z., Guo, H., Ruan, K., et al. 2009. Axin determines cell fate by controlling the p53 activation threshold after DNA damage. *Nature cell biology* 11(9), pp. 1128–1134.

Li, S., Wang, C., Liu, X., Hua, S. and Liu, X. 2015. The roles of AXIN2 in tumorigenesis and epigenetic regulation. *Familial cancer* 14(2), pp. 325–331.

Li, V.S.W., Ng, S.S., Boersema, P.J., Low, T.Y., Karthaus, W.R., Gerlach, J.P., Mohammed, S., et al. 2012. Wnt Signaling through Inhibition of β-Catenin Degradation in an Intact Axin1 Complex. *Cell* 149(6), pp. 1245–1256.

Lickert, H., Domon, C., Huls, G., Wehrle, C., Duluc, I., Clevers, H., Meyer, B.I., et al. 2000. Wnt/(beta)-catenin signaling regulates the expression of the homeobox gene Cdx1 in embryonic intestine. *Development (Cambridge, England)* 127(17), pp. 3805–3813.

Lindsley, R.C., Gill, J.G., Kyba, M., Murphy, T.L. and Murphy, K.M. 2006. Canonical Wnt signaling is required for development of embryonic stem cell-derived mesoderm. *Development (Cambridge, England)* 133(19), pp. 3787–3796.

Liu, C., Li, Y., Semenov, M., Han, C., Baeg, G.H., Tan, Y., Zhang, Z., et al. 2002. Control of beta-catenin phosphorylation/degradation by a dual-kinase mechanism. *Cell* 108(6), pp. 837–847.

Liu, W., Rui, H., Wang, J., Lin, S., He, Y., Chen, M., Li, Q., et al. 2006. Axin is a scaffold protein in TGF-beta signaling that promotes degradation of Smad7 by Arkadia. *The EMBO journal* 25(8), pp. 1646–1658.

Liu, WG, Dong, X., Mai, M., Seelan, R., Taniguchi, K., Krishnadath, K., Halling, K., et al. 2000. Mutations in AXIN2 cause colorectal cancer with defective mismatch repair by activating beta-catenin/TCF signalling. *Nature genetics* 26(2), pp. 146–147.

Liu, Y.T., Dan, Q.J., Wang, J., Feng, Y., Chen, L., Liang, J., Li, Q., et al. 2011. Molecular Basis of Wnt Activation via the DIX Domain Protein Ccd1. *Journal of Biological Chemistry* 286(10), pp. 8597–8608.

Lloyd-Lewis, B. 2011. High-throughput screening for novel regulators of Beta-catenin in Wnt signalling. Cardiff University.

Logan, C.Y. and Nusse, R. 2004. The Wnt sigalling pathway in development and disease. *Annual review of cell and developmental biology* 20: 781-810.

Loh, K.M. and Lim, B. 2011. A precarious balance: pluripotency factors as lineage specifiers. *Cell stem cell* 8(4), pp. 363–369.

Louie, R.K., Bahmanyar, S., Siemers, K.A., Votin, V., Chang, P., Stearns, T., Nelson, W.J., et al. 2004. Adenomatous polyposis coli and EB1 localize in close proximity of the mother centriole and EB1 is a functional component of centrosomes. *Journal of cell science* 117(Pt 7), pp. 1117–1128.

Lu, W.-Y., Bird, T.G., Boulter, L., Tsuchiya, A., Cole, A.M., Hay, T., Guest, R.V., et al. 2015. Hepatic progenitor cells of biliary origin with liver repopulation capacity. *Nature cell biology* 17(8), pp. 971–983.

Lucey, B.C., Varghese, J.C. and Soto, J.A. 2006. Hepatic Disorders: Colorectal Cancer Metastases, Cirrhosis, and Hepatocellular Carcinoma. In: Medina, L. S. and Blackmore, C. C. eds. *Evidence-Based Imaging: Optimizing Imaging in Patient Care*. Springer.

Luche, H., Weber, O., Nageswara Rao, T., Blum, C. and Fehling, H.J. 2007. Faithful activation of an extra-bright red fluorescent protein in 'knock-in' Cre-reporter mice ideally suited for lineage tracing studies. 37(1), pp. 43–53.

Luckert, K., Gotschel, F., Sorger, P.K., Hecht, A., Joos, T.O. and Potz, O. 2011. Snapshots of Protein Dynamics and Post-translational Modifications In One Experiment-β-Catenin and Its Functions. *Molecular & Cellular Proteomics* 10(5), pp. M110.007377–M110.007377.

Luo, W. and Lin, S.-C. 2004. Axin: a master scaffold for multiple signaling pathways. 13(3), pp. 99–113.

Lustig, B., Jerchow, B., Sachs, M., Weiler, S., Pietsch, T., Karsten, U., van de Wetering, M., et al. 2002. Negative Feedback Loop of Wnt Signaling through Upregulation of Conductin/Axin2 in Colorectal and Liver Tumors. *Molecular and cellular biology* 22(4), pp. 1184–1193.

Lyashenko, N., Winter, M., Migliorini, D., Biechele, T., Moon, R.T. and Hartmann, C. 2011. Differential requirement for the dual functions of [beta]-catenin in embryonic stem cell self-renewal and germ layer formation. *Nature cell biology* 13(7), pp. 753–761.

MacDonald, B.T., Tamai, K. and He, X. 2009. Wnt/β-Catenin Signaling: Components, Mechanisms, and Diseases. *Developmental cell* 17(1), pp. 9–26.

Magami, Y., Azuma, T., Inokuchi, H., Kokuno, S., Moriyasu, F., Kawai, K. and Hattori, T. 2002. Cell proliferation and renewal of normal hepatocytes and bile duct cells in adult mouse liver. *Liver* 22(5), pp. 419–425.

Mao, J., Wang, J., Liu, B., Pan, W., Farr, G.H., Flynn, C., Yuan, H., et al. 2001. Low-density lipoprotein receptor-related protein-5 binds to Axin and regulates the canonical Wnt signaling pathway. *Molecular cell* 7(4), pp. 801–809.

Mao, J., Yuan, H., Xie, W., Simon, M.I. and Wu, D. 1998. Specific involvement of G proteins in regulation of serum response factor-mediated gene transcription by different receptors. *The Journal of biological chemistry* 273(42), pp. 27118–27123.

Marraffini, L.A. and Sontheimer, E.J. 2010. CRISPR interference: RNA-directed adaptive immunity in bacteria and archaea. *Nature reviews. Genetics* 11(3), pp. 181–190.

Marsh, V. 2008. Analysing the role of Pten in the murine small intestine. Cardiff University.

Martello, G. and Smith, A. 2014. The Nature of Embryonic Stem Cells. *Annual review of cell and developmental biology* 30(1), pp. 647–675.

Martello, G., Sugimoto, T., Diamanti, E., Joshi, A., Hannah, R., Ohtsuka, S., Göttgens, B., et al. 2012. Esrrb Is a Pivotal Target of the Gsk3/Tcf3 Axis Regulating Embryonic Stem Cell Self-Renewal. *Cell stem cell* 11(4), pp. 491–504.

Martin, G.R. 1981. Isolation of a pluripotent cell line from early mouse embryos cultured in medium conditioned by teratocarcinoma stem cells. *Proceedings of the National Academy of Sciences of the United States of America* 78(12), pp. 7634–7638.

Marvin, M.L., Mazzoni, S.M., Herron, C.M., Edwards, S., Gruber, S.B. and Petty, E.M. 2011. AXIN2-associated autosomal dominant ectodermal dysplasia and neoplastic syndrome. *American Journal of Medical Genetics Part A* 155(4), pp. 898–902.

Mazzoni, S.M. and Fearon, E.R. 2014. AXIN1 and AXIN2 variants in gastrointestinal cancers. *Cancer Letters* 355(1), pp. 1–8.

McGlynn, K.A., Tsao, L., Hsing, A.W., Devesa, S.S. and Fraumeni, J.F. 2001. International trends and patterns of primary liver cancer. *International journal of cancer. Journal international du cancer* 94(2), pp. 290–296.

Merrill, B.J. 2012. Wnt Pathway Regulation of Embryonic Stem Cell Self-Renewal. *Cold Spring Harbor perspectives in biology* 4(9), pp. a007971–a007971.

Merrill, B.J., Pasolli, H.A., Polak, L., Rendl, M., García-García, M.J., Anderson, K.V. and Fuchs, E. 2004. Tcf3: a transcriptional regulator of axis induction in the early embryo. *Development (Cambridge, England)* 131(2), pp. 263–274.

Michalopoulos, G.K. 2010. Liver regeneration after partial hepatectomy: critical analysis of mechanistic dilemmas.

The American journal of pathology 176(1), pp. 2–13.

Micsenyi, A., Tan, X., Sneddon, T., Luo, J.-H., Michalopoulos, G.K. and Monga, S.P.S. 2004. Beta-catenin is temporally regulated during normal liver development. *Gastroenterology* 126(4), pp. 1134–1146.

Mitalipov, S. and Wolf, D. 2009. Totipotency, pluripotency and nuclear reprogramming. In: Martin, U. ed. *Engineering of stem cells*. Advances in biochemical engineering/biotechnology, pp. 185–199.

Miyajima, A., Tanaka, M. and Itoh, T. 2014. Stem/Progenitor Cells in Liver Development, Homeostasis, Regeneration, and Reprogramming. *Cell stem cell* 14(5), pp. 561–574.

Miyoshi, Y., Iwao, K., Nagasawa, Y., Aihara, T., Sasaki, Y., Imaoka, S., Murata, M., et al. 1998. Activation of the beta-catenin gene in primary hepatocellular carcinomas by somatic alterations involving exon 3. *Cancer research* 58(12), pp. 2524–2527.

Moeini, A., Cornellà, H. and Villanueva, A. 2012. Emerging Signaling Pathways in Hepatocellular Carcinoma. *Liver Cancer* 1(2), pp. 83–93.

Molenaar, M., van de Wetering, M., Oosterwegel, M., Peterson-Maduro, J., Gadsave, S., Korinek, V., Roose, J., et al. 1996. XTcf-3 Transcription Factor Mediates beta-Catenin-Induced Axis Formation in Xenopus Embryos. *Cell* 86(3), pp. 391–399.

Monga, S.P.S., Monga, H.K., Tan, X., Mulé, K., Pediaditakis, P. and Michalopoulos, G.K. 2003. Beta-catenin antisense studies in embryonic liver cultures: role in proliferation, apoptosis, and lineage specification. *Gastroenterology* 124(1), pp. 202–216.

Moore, J.D. 2013. In the wrong place at the wrong time: does cyclin mislocalization drive oncogenic transformation? *Nature reviews. Cancer* 13(3), pp. 201–208.

Morrison, S.J., Shah, N.M. and Anderson, D.J. 1997. Regulatory Mechanisms in Stem Cell Biology. *Cell* 88(3), pp. 287–298.

Muto, Y., Maeda, T., Suzuki, K., Kato, T., Watanabe, F., Kamiyama, H., Saito, M., et al. 2014. DNA methylation alterations of AXIN2 in serrated adenomas and colon carcinomas with microsatellite instability. *BMC cancer* 14(1), p. 466.

Nakamura, T., Hamada, F., Ishidate, T., Anai, K., Kawahara, K., Toyoshima, K. and Akiyama, T. 1998. Axin, an inhibitor of the Wnt signalling pathway, interacts with beta-catenin, GSK-3beta and APC and reduces the beta-catenin level. *Genes to cells : devoted to molecular & cellular mechanisms* 3(6), pp. 395–403.

Nejak-Bowen, K.N. and Monga, S.P.S. 2011. Beta-catenin signaling, liver regeneration and hepatocellular cancer: sorting the good from the bad. *Seminars in cancer biology* 21(1), pp. 44–58.

Neo, S.Y., Zhang, Y., Yaw, L.P., Li, P. and Lin, S.C. 2000. Axin-induced apoptosis depends on the extent of its JNK activation and its ability to down-regulate beta-catenin levels. *Biochemical and biophysical research communications* 272(1), pp. 144–150.

Nguyen, V.T.T., Law, M.G. and Dore, G.J. 2009. Hepatitis B-related hepatocellular carcinoma: epidemiological characteristics and disease burden. *Journal of viral hepatitis* 16(7), pp. 453–463.

Nichols, J. and Smith, A. 2011. The origin and identity of embryonic stem cells. *Development (Cambridge, England)* 138(1), pp. 3–8.

Niehrs, C. and Acebron, S.P. 2012. Mitotic and mitogenic Wnt signalling. *The EMBO journal* 31(12), pp. 2705–2713.

Nishikawa, T., Ota, T. and Isogai, T. 2000. Prediction whether a human cDNA sequence contains initiation codon by combining statistical information and similarity with protein sequences. *Bioinformatics (Oxford, England)* 16(11), pp. 960–967.

Niwa, H. 2007. How is pluripotency determined and maintained? *Development (Cambridge, England)* 134(4), pp. 635–646.

Noutsou, M., Duarte, A.M.S., Anvarian, Z., Didenko, T., Minde, D.P., Kuper, I., de Ridder, I., et al. 2011. Critical

scaffolding regions of the tumor suppressor Axin1 are natively unfolded. *Journal of Molecular Biology* 405(3), pp. 773–786.

Nusse, R. and Varmus, H.E. 1982. Many tumors induced by the mouse mammary tumor virus contain a provirus integrated in the same region of the host genome. *Cell* 31(1), pp. 99–109.

Nusse, R., Fuerer, C., Ching, W., Harnish, K., Logan, C., Zeng, A., ten Berge, D., et al. 2008. Wnt signaling and stem cell control. *Cold Spring Harbor symposia on quantitative biology* 73, pp. 59–66.

Oinonen, T. and Lindros, K.O. 1998. Zonation of hepatic cytochrome P-450 expression and regulation. *Biochemical Journal* 329 (Pt 1), pp. 17–35.

Olmeda, D., Castel, S., Vilaró, S. and Cano, A. 2003. Beta-catenin regulation during the cell cycle: implications in G2/M and apoptosis. *Molecular biology of the cell* 14(7), pp. 2844–2860.

Onuma, K., Ochiai, M., Orihashi, K., Takahashi, M., Imai, T., Nakagama, H. and Hippo, Y. 2013. Genetic reconstitution of tumorigenesis in primary intestinal cells. *PNAS* 110(27), pp. 11127–11132.

Ootani, A., Li, X., Sangiorgi, E., Ho, Q.T., Ueno, H., Toda, S., Sugihara, H., et al. 2009. Sustained in vitro intestinal epithelial culture within a Wnt-dependent stem cell niche. *Nature medicine* 15(6), pp. 701–706.

Orford, K., Crockett, C., Jensen, J.P., Weissman, A.M. and Byers, S.W. 1997. Serine phosphorylation-regulated ubiquitination and degradation of beta-catenin. *The Journal of biological chemistry* 272(40), pp. 24735–24738.

Pagano, M. 1998. *Cell Cycle Control*. Pagano, M. ed. Springer.

Papkoff, J. and Aikawa, M. 1998. WNT-1 and HGF Regulate GSK3β Activity and β-Catenin Signaling in Mammary Epithelial Cells. *Biochemical and biophysical research communications* 247(3), pp. 851–858.

Park, C.S., Kim, S.I., Lee, M.S., Youn, C.-Y., Kim, D.J., Jho, E.-H. and Song, W.K. 2004. Modulation of beta-catenin phosphorylation/degradation by cyclin-dependent kinase 2. *The Journal of biological chemistry* 279(19), pp. 19592–19599.

Park, C.S., Lee, M.S., Oh, H.-J., Choi, K.Y., Yeo, M.G., Chun, J.-S. and Song, W.K. 2007. Modulation of beta-catenin by cyclin-dependent kinase 6 in Wnt-stimulated cells. *European journal of cell biology* 86(2), pp. 111–123.

Pálfy, M., Reményi, A. and Korcsmáros, T. 2012. Endosomal crosstalk: meeting points for signaling pathways. *Trends in cell biology* 22(9), pp. 447–456.

Pease, S., Braghetta, P., Gearing, D., Grail, D. and Williams, R.L. 1990. Isolation of embryonic stem (ES) cells in media supplemented with recombinant leukemia inhibitory factor (LIF). *Developmental biology* 141(2), pp. 344–352.

Pelton, R.W., Saxena, B., Jonnes, M., Moses, H.L. and Gold, L.I. 1991. Immunohistochemical Localization of Tgf-Beta-1, Tgf-Beta-2, and Tgf-Beta-3 in the Mouse Embryo - Expression Patterns Suggest Multiple Roles During Embryonic-Development. *The Journal of cell biology* 115(4), pp. 1091–1105.

Perry, W.L., Vasicek, T.J., Lee, J.J., Rossi, J.M., Zeng, L., Zhang, T., Tilghman, S.M., et al. 1995. Phenotypic and molecular analysis of a transgenic insertional allele of the mouse Fused locus. *Genetics* 141(1), pp. 321–332.

Piedra, J., Miravet, S., Castaño, J., Palmer, H.G., Heisterkamp, N., García de Herreros, A. and Duñach, M. 2003. p120 Catenin-associated Fer and Fyn tyrosine kinases regulate beta-catenin Tyr-142 phosphorylation and beta-catenin-alpha-catenin Interaction. *Molecular and cellular biology* 23(7), pp. 2287–2297.

Polakis, P. 2012. Wnt Signaling in Cancer. *Cold Spring Harbor perspectives in biology* 4(5), pp. a008052–a008052.

Pope, I., Langbein, W., Watson, P. and Borri, P. 2013. Simultaneous hyperspectral differential-CARS, TPF and SHG microscopy with a single 5 fs Ti:Sa laser. *Optics Express* 21(6), pp. 7096–7106.

Poulton, J.S., Mu, F.W., Roberts, D.M. and Peifer, M. 2013. APC2 and Axin promote mitotic fidelity by facilitating centrosome separation and cytoskeletal regulation. *Development (Cambridge, England)* 140(20), pp. 4226–4236.

Qian, L., Mahaffey, J.P., Alcorn, H.L. and Anderson, K.V. 2011. Tissue-specific roles of Axin2 in the inhibition and activation of Wnt signaling in the mouse embryo. *Proceedings of the National Academy of Sciences of the United*

States of America 108(21), pp. 8692–8697.

Qiao, L.J., Kang, K.L. and Heo, J.S. 2011. Simvastatin promotes osteogenic differentiation of mouse embryonic stem cells via canonical Wnt/β-catenin signaling. *Molecules and Cells* 32(5), pp. 437–444.

Qiu, Q., Hernandez, J.C., Dean, A.M., Rao, P.H. and Darlington, G.J. 2011. CD24-Positive Cells from Normal Adult Mouse Liver Are Hepatocyte Progenitor Cells. *Stem Cells and Development* 20(12), pp. 2177–2188.

Rabes, H.M. 1977. Kinetics of hepatocellular proliferation as a function of the microvascular structure and functional state of the liver. *Ciba Foundation symposium* (55), pp. 31–53.

Rada, P., Rojo, A.I., Offergeld, A., Feng, G.J., Velasco-Martín, J.P., González-Sancho, J.M., Valverde, Á.M., et al. 2015. WNT-3A regulates an Axin1/NRF2 complex that regulates antioxidant metabolism in hepatocytes. *Antioxidants & redox signaling* 22(7), pp. 555–571.

Ran, F.A., Hsu, P.D., Lin, C.-Y., Gootenberg, J.S., Konermann, S., Trevino, A.E., Scott, D.A., et al. 2013a. Double Nicking by RNA-Guided CRISPR Cas9 for Enhanced Genome Editing Specificity. *Cell* 154(6), pp. 1380–1389.

Ran, F.A., Hsu, P.D., Wright, J., Agarwala, V., Scott, D.A. and Zhang, F. 2013b. Genome engineering using the CRISPR-Cas9 system. *Nature protocols* 8(11), pp. 2281–2308.

Reya, T., Morrison, S.J., Clarke, M.F. and Weissman, I.L. 2001. Stem cells, cancer, and cancer stem cells. *Nature* 414(6859), pp. 105–111.

Robertson, E.J., Evans, M.J. and Kaufman, M.H. 1983. X-chromosome instability in pluripotential stem cell lines derived from parthenogenetic embryos. *Journal of embryology and experimental morphology* 74, pp. 297–309.

Rossi, J.M., Dunn, N.R., Hogan, B.L. and Zaret, K.S. 2001. Distinct mesodermal signals, including BMPs from the septum transversum mesenchyme, are required in combination for hepatogenesis from the endoderm. *Genes & development* 15(15), pp. 1998–2009.

Roura, S., Miravet, S., Piedra, J., García de Herreros, A. and Dunach, M. 1999. Regulation of E-cadherin/Catenin association by tyrosine phosphorylation. *The Journal of biological chemistry* 274(51), pp. 36734–36740.

Ruffner, H., Sprunger, J., Charlat, O., Leighton-Davies, J., Grosshans, B., Salathe, A., Zietzling, S., et al. 2012. R-Spondin Potentiates Wnt/β-Catenin Signaling through Orphan Receptors LGR4 and LGR5. *PloS one* 7(7), p. e40976.

Rui, H.L. 2002. SUMO-1 modification of the C-terminal KVEKVD of Axin is required for JNK activation but has no effect on Wnt signaling. *Journal of Biological Chemistry* 277(45), pp. 42981–42986.

Rui, Y., Xu, Z., Lin, S., Li, Q., Rui, H., Luo, W., Zhou, H.-M., et al. 2004. Axin stimulates p53 functions by activation of HIPK2 kinase through multimeric complex formation. *The EMBO journal* 23(23), pp. 4583–4594.

Saddic, L.A., Wirt, S., Vogel, H., Felsher, D.W. and Sage, J. 2011. Functional Interactions between Retinoblastoma and c-MYC in a Mouse Model of Hepatocellular Carcinoma. *PloS one* 6(5), p. e19758.

Sakaue-Sawano, A., Kobayashi, T., Ohtawa, K. and Miyawaki, A. 2011. Drug-induced cell cycle modulation leading to cell-cycle arrest, nuclear mis-segregation, or endoreplication. *BMC Cell Biology* 12(1), p. 2.

Salahshor, S. and Woodgett, J.R. 2005. The links between axin and carcinogenesis. *Journal of clinical pathology* 58(3), pp. 225–236.

Sato, N., Meijer, L., Skaltsounis, L., Greengard, P. and Brivanlou, A.H. 2004. Maintenance of pluripotency in human and mouse embryonic stem cells through activation of Wnt signaling by a pharmacological GSK-3-specific inhibitor. *Nature medicine* 10(1), pp. 55–63.

Sato, T., Vries, R.G., Snippert, H.J., van de Wetering, M., Barker, N., Stange, D.E., van Es, J.H., et al. 2009. Single Lgr5 stem cells build crypt-villus structures in vitro without a mesenchymal niche. *Nature* 459(7244), pp. 262–U147.

Satoh, S., Daigo, Y., Furukawa, Y., Kato, T., Miwa, N., Nishiwaki, T., Kawasoe, T., et al. 2000. AXIN1 mutations in hepatocellular carcinomas, and growth suppression in cancer cells by virus-mediated transfer of AXIN1. *Nature genetics* 24(3), pp. 245–250.

Schaub, J.R., Malato, Y., Gormond, C. and Willenbring, H. 2014. Evidence against a Stem Cell Origin of New Hepatocytes in a Common Mouse Model of Chronic Liver Injury. *CellReports* 8(4), pp. 933–939.

Schleicher, J., Tokarski, C., Marbach, E., Matz-Soja, M., Zellmer, S., Gebhardt, R. and Schuster, S. 2015. Zonation of hepatic fatty acid metabolism - The diversity of its regulation and the benefit of modeling. *Biochimica et biophysica acta* 1851(5), pp. 641–656.

Schmelzer, E., Wauthier, E. and Reid, L.M. 2006. The phenotypes of pluripotent human hepatic progenitors. *Stem cells (Dayton, Ohio)* 24(8), pp. 1852–1858.

Schmidt, E.E. and Schibler, U. 1995. Cell size regulation, a mechanism that controls cellular RNA accumulation: consequences on regulation of the ubiquitous transcription factors Oct1 and NF-Y and the liver-enriched transcription factor DBP. *The Journal of cell biology* 128(4), pp. 467–483.

Schneider, A.J., Branam, A.M. and Peterson, R.E. 2014. Intersection of AHR and Wnt signaling in development, health, and disease. *International Journal of Molecular Sciences* 15(10), pp. 17852–17885.

Schnuetgen, F., Stewart, A.F., Melchner, von, H. and Anastassiadis, K. 2006. Engineering embryonic stem cells with recombinase systems. *Methods in enzymology* 420, pp. 100–136.

Schuijers, J. and Clevers, H. 2012. Adult mammalian stem cells: the role of Wnt, Lgr5 and R-spondins. *The EMBO journal* 31(12), pp. 2685–2696.

Schwarz-Romond, T., Metcalfe, C. and Bienz, M. 2007. Dynamic recruitment of axin by Dishevelled protein assemblies. *Journal of cell science* 120(Pt 14), pp. 2402–2412.

Schwenk, F., Baron, U. and Rajewsky, K. 1995. A cre-transgenic mouse strain for the ubiquitous deletion of loxP-flanked gene segments including deletion in germ cells. *Nucleic Acids Research* 23(24), pp. 5080–5081.

Sekine, S., Gutierrez, P.J., Lan, B.Y., Feng, S. and Hebrok, M. 2007. Liver-specific loss of beta-catenin results in delayed hepatocyte proliferation after partial hepatectomy. *Hepatology (Baltimore, Md.)* 45(2), pp. 361–368.

Sekine, S., Lan, B.Y.-A., Bedolli, M., Feng, S. and Hebrok, M. 2006. Liver-specific loss of beta-catenin blocks glutamine synthesis pathway activity and cytochrome p450 expression in mice. *Hepatology (Baltimore, Md.)* 43(4), pp. 817–825.

Sharma, R.P. and Chopra, V.L. 1976. Effect of the Wingless (wg1) mutation on wing and haltere development in Drosophila melanogaster. *Developmental biology* 48(2), pp. 461–465.

Sheen, J. and Dickson, R. 2002. Overexpression of c-Myc alters G(1)/S arrest following ionizing radiation. *Molecular and cellular biology* 22(6), pp. 1819–1833.

Sheen, J.-H., Woo, J.-K. and Dickson, R.B. 2003. c-Myc alters the DNA damage-induced G2/M arrest in human mammary epithelial cells. *British journal of cancer* 89(8), pp. 1479–1485.

Sherman, M. 2010. Hepatocellular Carcinoma: Epidemiology, Surveillance, and Diagnosis. *Seminars in liver disease* 30(1), pp. 3–16.

Sheu, J.C., Sung, J.L., Chen, D.S., Yang, P.M., Lai, M.Y., Lee, C.S., Hsu, H.C., et al. 1985. Growth rate of asymptomatic hepatocellular carcinoma and its clinical implications. *Gastroenterology* 89(2), pp. 259–266.

Shibamoto, S., Higano, K., Takada, R., Ito, F., Takeichi, M. and Takada, S. 1998. Cytoskeletal reorganization by soluble Wnt-3a protein signalling. *Genes to cells : devoted to molecular & cellular mechanisms* 3(10), pp. 659–670.

Shiomi, K., Uchida, H., Keino-Masu, K. and Masu, M. 2003. Ccd1, a novel protein with a DIX domain, is a positive regulator in the Wnt signaling during zebrafish neural patterning. *Current Biology* 13(1), pp. 73–77.

Shtutman, M., Zhurinsky, J., Simcha, I., Albanese, C., D'Amico, M., Pestell, R. and Ben-Ze'ev, A. 1999. The cyclin D1 gene is a target of the beta-catenin/LEF-1 pathway. *Proceedings of the National Academy of Sciences of the United States of America* 96(10), pp. 5522–5527.

Sinner, D., Rankin, S., Lee, M. and Zorn, A.M. 2004. Sox17 and beta-catenin cooperate to regulate the transcription of endodermal genes. *Development (Cambridge, England)* 131(13), pp. 3069–3080.

Smith, A.G., Heath, J.K., Donaldson, D.D., Wong, G.G., Moreau, J., Stahl, M. and Rogers, D. 1988. Inhibition of pluripotential embryonic stem cell differentiation by purified polypeptides. *Nature* 336(6200), pp. 688–690.

Sokol, S.Y. 2011. Maintaining embryonic stem cell pluripotency with Wnt signaling. *Development (Cambridge, England)* 138(20), pp. 4341–4350.

Sokol, S.Y. 1993. Mesoderm formation in Xenopus ectodermal explants overexpressing Xwnt8: evidence for a cooperating signal reaching the animal pole by gastrulation. *Development (Cambridge, England)* 118(4), pp. 1335–1342.

Soriano, P. 1999. Generalized lacZ expression with the ROSA26 Cre reporter strain. *Nature genetics* 21(1), pp. 70–71.

Spelat, R., Ferro, F. and Curcio, F. 2012. Serine 111 phosphorylation regulates OCT4A protein subcellular distribution and degradation. *Journal of Biological Chemistry* 287(45), pp. 38279–38288.

Sternberg, N. and Hamilton, D. 1981. Bacteriophage P1 site-specific recombination. *Journal of Molecular Biology* 150(4), pp. 467–486.

Stolz, A., Neufeld, K., Ertych, N. and Bastians, H. 2015. Wnt-mediated protein stabilization ensures proper mitotic microtubule assembly and chromosome segregation. *EMBO reports* 16(4), pp. 490–499.

Strovel, E.T., Wu, D. and Sussman, D.J. 2000. Protein Phosphatase 2C Dephosphorylates Axin and Activates LEF-1-dependent Transcription. *Journal of Biological Chemistry* 275(4), pp. 2399–2403.

Stuart, K.E. and Stadler, Z. 2013. Primary Hepatic Carcinoma [Online]. Available at: http://emedicine.medscape.com/article/282814-overview#a0101 [Accessed: June 2015].

Sutherland, C. 2011. What are the bona fide GSK3 substrates? *International Journal of Alzheimer's Disease* 2011(2), pp. 1–23.

Suzuki, A., Raya, A., Kawakami, Y., Morita, M., Matsui, T., Nakashima, K., Gage, F.H., et al. 2006. Nanog binds to Smad1 and blocks bone morphogenetic protein-induced differentiation of embryonic stem cells. *PNAS* 103(27), pp. 10294–10299.

Tajiri, H., Tanaka, H., Brooks, S. and Takano, T. 2010. Reduction of hepatocellular carcinoma in childhood after introduction of selective vaccination against hepatitis B virus for infants born to HBV carrier mothers. *Cancer Causes & Control* 22(3), pp. 523–527.

Tan, X., Apte, U., Micsenyi, A., Kotsagrelos, E., Luo, J.-H., Ranganathan, S., Monga, D.K., et al. 2005. Epidermal growth factor receptor: a novel target of the Wnt/beta-catenin pathway in liver. *Gastroenterology* 129(1), pp. 285–302.

Tan, X., Behari, J., Cieply, B., Michalopoulos, G.K. and Monga, S.P.S. 2006. Conditional Deletion of β-Catenin Reveals Its Role in Liver Growth and Regeneration. *Gastroenterology* 131(5), pp. 1561–1572. Available at: http://www.gastrojournal.org/article/S0016-5085(06)01802-6/fulltext.

Taniguchi, K., Roberts, L.R., Aderca, I.N., Dong, X., Qian, C., Murphy, L.M., Nagorney, D.M., et al. 2002. Mutational spectrum of β-catenin, AXIN1, and AXIN2 in hepatocellular carcinomas and hepatoblastomas. *Oncogene* 21(31), pp. 4863–4871.

Tanimizu, N. 2004. Notch signaling controls hepatoblast differentiation by altering the expression of liver-enriched transcription factors. *Journal of cell science* 117(15), pp. 3165–3174.

Tannour-Louet, M., Porteu, A., Vaulont, S., Kahn, A. and Vasseur-Cognet, M. 2002. A tamoxifen-inducible chimeric Cre recombinase specifically effective in the fetal and adult mouse liver. *Hepatology (Baltimore, Md.)* 35(5), pp. 1072–1081.

Taurin, S., Sandbo, N., Qin, Y., Browning, D. and Dulin, N.O. 2006. Phosphorylation of beta-catenin by cyclic AMP-dependent protein kinase. *The Journal of biological chemistry* 281(15), pp. 9971–9976.

Taurin, S., Sandbo, N., Yau, D.M., Sethakorn, N. and Dulin, N.O. 2008. Phosphorylation of beta-catenin by PKA promotes ATP-induced proliferation of vascular smooth muscle cells. *American journal of physiology. Cell physiology* 294(5), pp. C1169–74.

ten Berge, D., Kurek, D., Blauwkamp, T., Koole, W., Maas, A., Eroglu, E., Siu, R.K., et al. 2011. Embryonic stem cells require Wnt proteins to prevent differentiation to epiblast stem cells. *Nature cell biology* 13(9), pp. 1070–1075.

Tetsu, O. and McCormick, F. 1999. beta-catenin regulates expression of cyclin D1 in colon carcinoma cells. *Nature* 398(6726), pp. 422–426.

Tremblay, K.D. and Zaret, K.S. 2005. Distinct populations of endoderm cells converge to generate the embryonic liver bud and ventral foregut tissues. *Developmental biology* 280(1), pp. 87–99.

van de Wetering, M., Cavallo, R., Dooijes, D., van Beest, M., van Es, J., Loureiro, J., Ypma, A., et al. 1997. Armadillo Coactivates Transcription Driven by the Product of the Drosophila Segment Polarity Gene dTCF. *Cell* 88(6), pp. 789–799.

Veeman, M.T., Slusarski, D.C., Kaykas, A., Louie, S.H. and Moon, R.T. 2003. Zebrafish Prickle, a Modulator of Noncanonical Wnt/Fz Signaling, Regulates Gastrulation Movements. *Current Biology* 13(8), pp. 680–685.

Vogelstein, B. and Kinzler, K.W. 2004. Cancer genes and the pathways they control. *Nature medicine* 10(8), pp. 789–799.

Wang, B., Zhao, L., Fish, M., Logan, C.Y. and Nusse, R. 2015. Self-renewing diploid Axin2+ cells fuel homeostatic renewal of the liver. *Nature* 524(7564), pp. 180–185.

Webster, M.T., Rozycka, M., Sara, E., Davis, E., Smalley, M., Young, N., Dale, T.C., et al. 2000. Sequence variants of the axin gene in breast, colon, and other cancers: an analysis of mutations that interfere with GSK3 binding. *Genes, chromosomes & cancer* 28(4), pp. 443–453.

Welcker, M., Singer, J., Loeb, K.R., Grim, J., Bloecher, A., Gurien-West, M., Clurman, B.E., et al. 2003. Multisite phosphorylation by Cdk2 and GSK3 controls cyclin E degradation. *Molecular cell* 12(2), pp. 381–392.

Wen, Y., Eng, C.H., Schmoranzer, J., Cabrera-Poch, N., Morris, E.J.S., Chen, M., Wallar, B.J., et al. 2004. EB1 and APC bind to mDia to stabilize microtubules downstream of Rho and promote cell migration. *Nature cell biology* 6(9), pp. 820–830.

Wend, P., Holland, J.D., Ziebold, U. and Birchmeier, W. 2010. Wnt signaling in stem and cancer stem cells. *Seminars in cell & developmental biology* 21(8), pp. 855–863.

Wiechens, N. 2003. Nucleo-cytoplasmic Shuttling of Axin, a Negative Regulator of the Wnt- -Catenin Pathway. *Journal of Biological Chemistry* 279(7), pp. 5263–5267.

Willert, K., Logan, C.Y., Arora, A., Fish, M. and Nusse, R. 1999. A Drosophila Axin homolog, Daxin, inhibits Wnt signaling. *Development (Cambridge, England)* 126(18), pp. 4165–4173.

Williams, R.L., Hilton, D.J., Pease, S., Willson, T.A., Stewart, C.L., Gearing, D.P., Wagner, E.F., et al. 1988. Myeloid leukaemia inhibitory factor maintains the developmental potential of embryonic stem cells. *Nature* 336(6200), pp. 684–687.

Wobus, A.M. 2005. Embryonic Stem Cells: Prospects for Developmental Biology and Cell Therapy. *Physiological reviews* 85(2), pp. 635–678.

Wordaz, A. and Nusse, R. 1998. Mechanisms of Wnt signaling in development. *Annual review of cell and developmental biology* 14, pp. 59–88.

Wu, C.-I., Hoffman, J.A., Shy, B.R., Ford, E.M., Fuchs, E., Nguyen, H. and Merrill, B.J. 2012a. Function of Wnt/β-catenin in counteracting Tcf3 repression through the Tcf3-β-catenin interaction. *Development (Cambridge, England)* 139(12), pp. 2118–2129.

Wu, G., Xu, G., Schulman, B.A., Jeffrey, P.D., Harper, J.W. and Pavletich, N.P. 2003. Structure of a beta-TrCP1-Skp1-beta-catenin complex: destruction motif binding and lysine specificity of the SCF(beta-TrCP1) ubiquitin ligase. *Molecular cell* 11(6), pp. 1445–1456.

Wu, Z.-Q.Z., Brabletz, T.T., Fearon, E.E., Willis, A.L.A., Hu, C.Y.C., Li, X.-Y.X. and Weiss, S.J.S. 2012b. The Canonical Wnt Suppressor, Axin2, Promotes Colon Carcinoma Oncogenic Activity. *Proceedings of the National Academy of Sciences of the United States of America* 109(28), pp. 11312–11317.

Xu, C., Kim, N.-G. and Gumbiner, B.M. 2009a. Regulation of protein stability by GSK3 mediated phosphorylation. *Cell Cycle* 8(24), pp. 4032–4039.

Xu, H., Wang, W., Li, C., Yu, H., Yang, A., Wang, B. and Jin, Y. 2009b. WWP2 promotes degradation of transcription factor OCT4 in human embryonic stem cells. *Cell research* 19(5), pp. 561–573.

Xu, H.-T., Wei, Q., Liu, Y., Yang, L.-H., Dai, S.-D., Han, Y., Yu, J.-H., et al. 2007. Overexpression of axin downregulates TCF-4 and inhibits the development of lung cancer. *Annals of surgical oncology* 14(11), pp. 3251–3259.

Yamamoto, H., Kishida, S., Kishida, M., Ikeda, S., Takada, S. and Kikuchi, A. 1999. Phosphorylation of Axin, a Wnt signal negative regulator, by glycogen synthase kinase-3 beta regulates its stability. *The Journal of biological chemistry* 274(16), pp. 10681–10684.

Yamamoto, H., Kishida, S., Uochi, T., Ikeda, S., Koyama, S., Asashima, M. and Kikuchi, A. 1998. Axil, a Member of the Axin Family, Interacts with Both Glycogen Synthase Kinase 3β and β-Catenin and Inhibits Axis Formation of Xenopus Embryos. *Molecular and cellular biology* 18(5), pp. 2867–2875.

Yamamoto, T., Suzuki, T., Kobayashi, A., Wakabayashi, J., Maher, J., Motohashi, H. and Yamamoto, M. 2008. Physiological Significance of Reactive Cysteine Residues of Keap1 in Determining Nrf2 Activity. *Molecular and cellular biology* 28(8), pp. 2758–2770.

Yang, J., Mowry, L.E., Nejak-Bowen, K.N., Okabe, H., Diegel, C.R., Lang, R.A., Williams, B.O., et al. 2014. Beta-catenin signaling in murine liver zonation and regeneration: A Wnt-Wnt situation! *Hepatology (Baltimore, Md.)* 60(3), pp. 964–976.

Yang, W., Shen, J., Wu, M., Arsura, M., FitzGerald, M., Suldan, Z., Kim, D.W., et al. 2001. Repression of transcription of the p27(Kip1) cyclin-dependent kinase inhibitor gene by c-Myc. *Oncogene* 20(14), pp. 1688–1702.

Yanger, K., Knigin, D., Zong, Y., Maggs, L., Gu, G., Akiyama, H., Pikarsky, E., et al. 2014. Adult hepatocytes are generated by self-duplication rather than stem cell differentiation. *Cell stem cell* 15(3), pp. 340–349.

Yi, F., Pereira, L., Hoffman, J.A., Shy, B.R., Yuen, C.M., Liu, D.R. and Merrill, B.J. 2011. Opposing effects of Tcf3 and Tcf1 control Wnt stimulation of embryonic stem cell self-renewal. *Nature cell biology* 13(7), pp. 762–770. Available at: http://http:/å/www.nature.com/doifinder/10.1038/ncb2283.

Ying, Q.-L., Wray, J., Nichols, J., Batlle-Morera, L., Doble, B., Woodgett, J., Cohen, P., et al. 2008. The ground state of embryonic stem cell self-renewal. *Nature* 453(7194), pp. 519–523.

Yu, H.-M.I., Jerchow, B., Sheu, T.-J., Liu, B., Costantini, F., Puzas, J.E., Birchmeier, W., et al. 2005. The role of Axin2 in calvarial morphogenesis and craniosynostosis. *Development (Cambridge, England)* 132(8), pp. 1995–2005.

Zeineddine, D., Hammoud, A.A., Mortada, M. and Boeuf, H. 2014. The Oct4 protein: more than a magic stemness marker. *American journal of stem cells* 3(2), pp. 74–82.

Zeng, G., Apte, U., Micsenyi, A., Bell, A. and Monga, S.P.S. 2006. Tyrosine residues 654 and 670 in beta-catenin are crucial in regulation of Met-beta-catenin interactions. *Experimental cell research* 312(18), pp. 3620–3630.

Zeng, L., Fagotto, F., Zhang, T., Hsu, W., Vasicek, T.J., Perry, W.L., Iii, Lee, J.J., et al. 1997. The mouse Fused locus encodes Axin, an inhibitor of the Wnt signaling pathway that regulates embryonic axis formation. *Cell* 90(1), pp. 181–192.

Zeng, X., Huang, H., Tamai, K., Zhang, X., Harada, Y., Yokota, C., Almeida, K., et al. 2008. Initiation of Wnt signaling: control of Wnt coreceptor Lrp6 phosphorylation/activation via frizzled, dishevelled and axin functions. *Development (Cambridge, England)* 135(2), pp. 367–375.

Zhang, Y., Liu, S., Mickanin, C., Feng, Y., Charlat, O., Michaud, G.A., Schirle, M., et al. 2011. RNF146 is a poly(ADP-ribose)-directed E3 ligase that regulates axin degradation and Wnt signalling. *Nature cell biology* 13(5), pp. 623–629.

Zhang, Y., Neo, S.Y., Han, J. and Lin, S.C. 2000. Dimerization choices control the ability of axin and dishevelled to activate c-Jun N-terminal kinase/stress-activated protein kinase. *The Journal of biological chemistry* 275(32), pp. 25008–25014.

Zhou, Q., Li, L. and Li, J. 2015. Stem cells with decellularized liver scaffolds in liver regeneration and their potential clinical applications. *Liver international : official journal of the International Association for the Study of the Liver* 35(3), pp. 687–694.

Zorn, A.M. 2008. *Liver development*. Schier, A. F. ed. Cambridge (MA): The Stem Cell Research Community, StemBook.

Zucman-Rossi, J. 2010. Molecular classification of hepatocellular carcinoma. *Digestive and Liver Disease* 42, pp. S235–S241.

Zucman-Rossi, J., Benhamouche, S., Godard, C., Boyault, S., Grimber, G., Balabaud, C., Cunha, A.S., et al. 2007. Differential effects of inactivated Axin1 and activated beta-catenin mutations in human hepatocellular carcinomas. *Oncogene* 26(5), pp. 774–780.

Zumbrunn, J., Kinoshita, K., Hyman, A.A. and Näthke, I.S. 2001. Binding of the adenomatous polyposis coli protein to microtubules increases microtubule stability and is regulated by GSK3β phosphorylation. *Current Biology* 11(1), pp. 44–49.

Appendices

Appendix 1: Plasmid Map

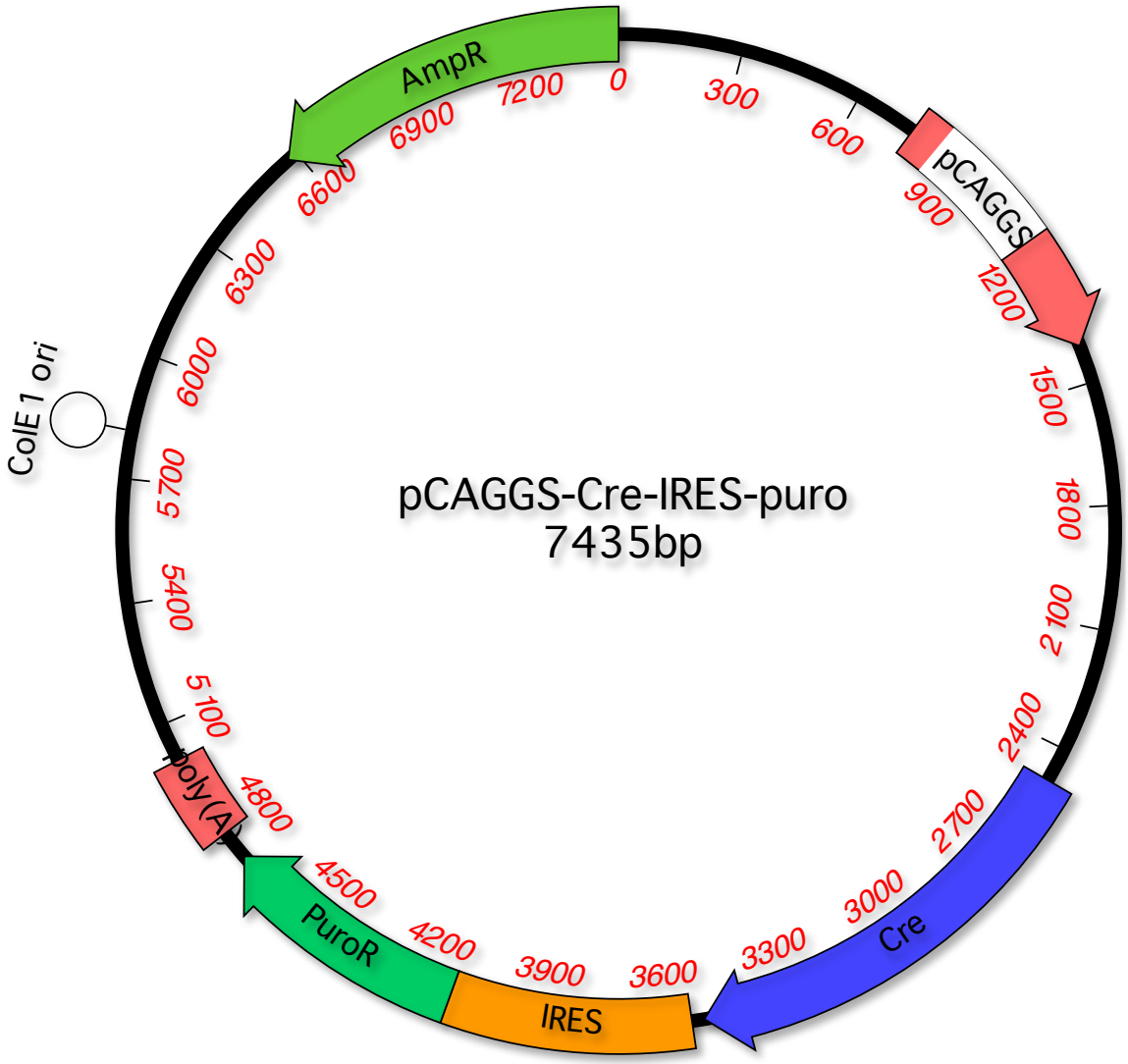

Figure A-1. Plasmid Map of pCAGGS-Cre-IRES-puro.

Appendix 2: CHARM setting

Table A-1. CHARM settings for the detection of liver organoids.

PARAMETER	SETTING
Edge detection sensitivity	1.6
Centre detection sensitivity	16.1
Soft colony diameter range	100-1500µm
Mid centre to centre separation	212µm
Circularity factor	26
Edge distance threshold	1
Number of spokes	32
Shape processing	Best fit circle
Colony diameter filter	100-1500µm
Colony density	0.05-2.00
Good edge factor	0
Overlap threshold	0.75

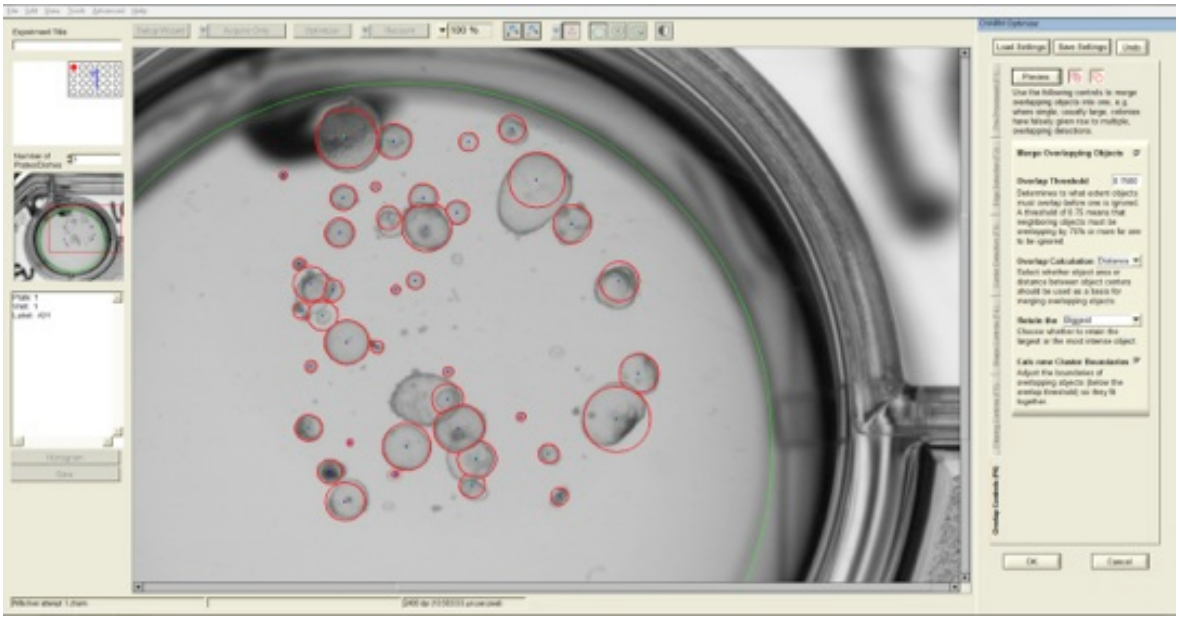

Figure A-2. Example of growth analysis data collection.
The GelCount™ was used to define a set of parameters to allow the program to identify and measure organoid size. Red circles indicate where the program has identified and determined the border of organoids. Dots have been identified as the centre points of organoids. Picture kindly provided by William Hill.

Appendix 3: Embryoid bodies

Cardiomyocyte assay

Movie A- 1. Cardiomyocyte assay in embryoid bodies.
Embryoid bodies of wt **(A)**; Axin1$^{\Delta/\Delta}$ **(B)**; Axin2$^{\Delta/\Delta}$ **(C)**; Axin2$^{lacZ/lacZ}$ **(D)**; Axin1$^{\Delta/\Delta}$, Axin2$^{\Delta/\Delta}$ **(E)**; Axin1$^{\Delta/\Delta}$, Axin2$^{lacZ/lacZ}$ **(F)**; GSK3α$^{\Delta/\Delta}$,GSK3β$^{\Delta/\Delta}$ **(G)**; and wt+ CHIR **(H)** cells were imaged on day 8 for spontaneously beating cardiomyocytes. Magnification = 4x. Videos can be viewed from the CD attached to this thesis or by following the above QR code or the link below:
https://www.youtube.com/playlist?list=PLK8osD0S9jry1mSuHo2kprQNyFIJ5sY-Q

H&E staining of EBs

A) wt

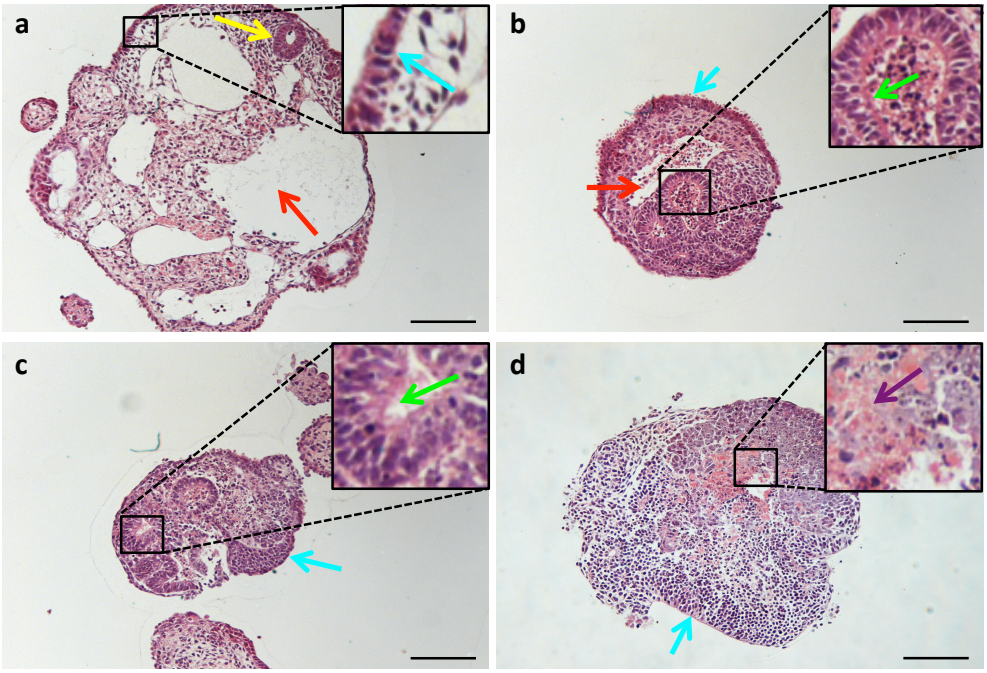

B) Axin1$^{\Delta/\Delta}$

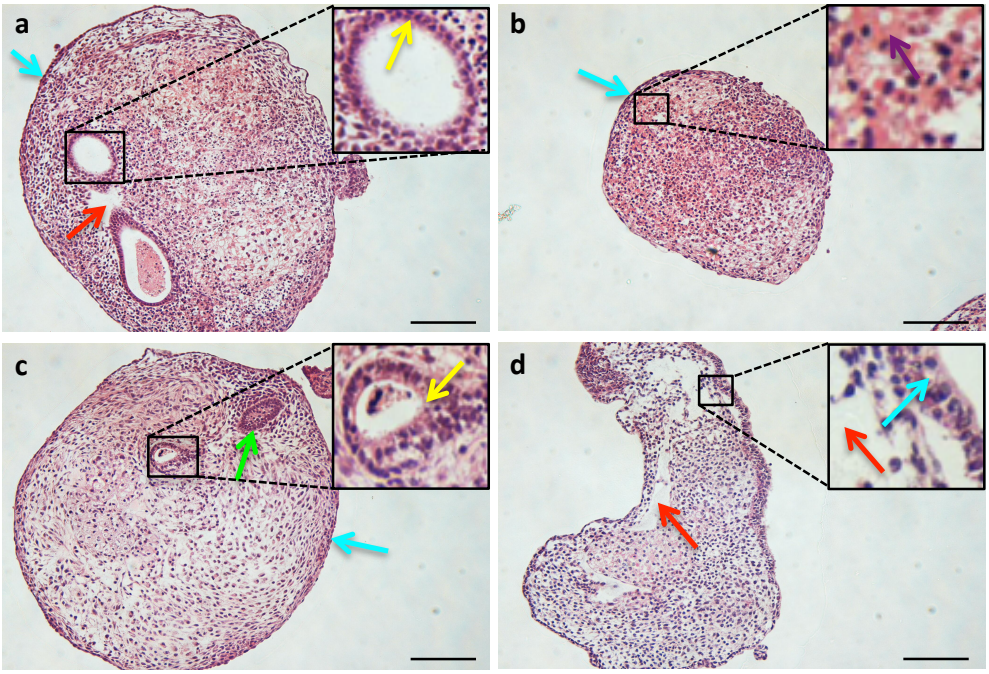

Figure A-3. H&E stains of embryoid bodies.
Selection of wild type **(A)** and Axin1$^{\Delta/\Delta}$ **(B)** embryoid bodies stained with Haematoxylin and Eosin on day 14. Differentiation into different germ layers is indicated by arrows: Parietal endoderm (blue,→); mesoderm/internal epithelia (yellow, →); ectoderm/columnar epithelia (possibly neural tubes) (green,→); internal cyst structures red,→); collagen and laminin matrix deposition (purple,→). Magnification = x32. Scale bars: 50 µm. Pictures were taken with the help of Kyle Hawker. (Figure continues on the following pages)

C) Axin2$^{\Delta/\Delta}$

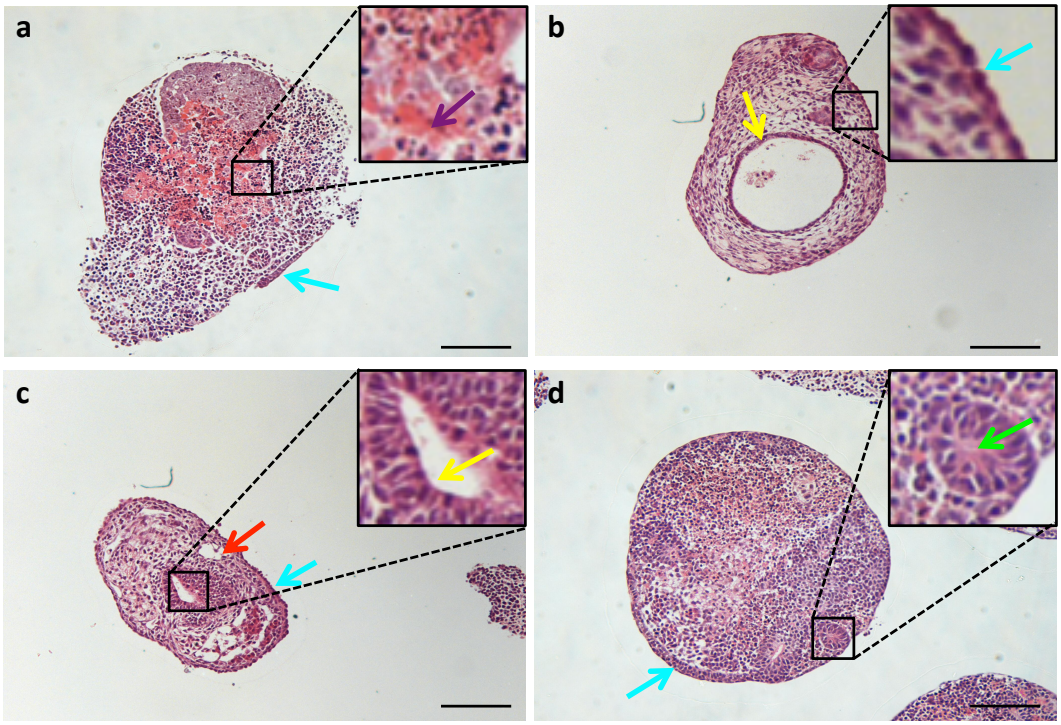

D) Axin2$^{lacZ/lacZ}$

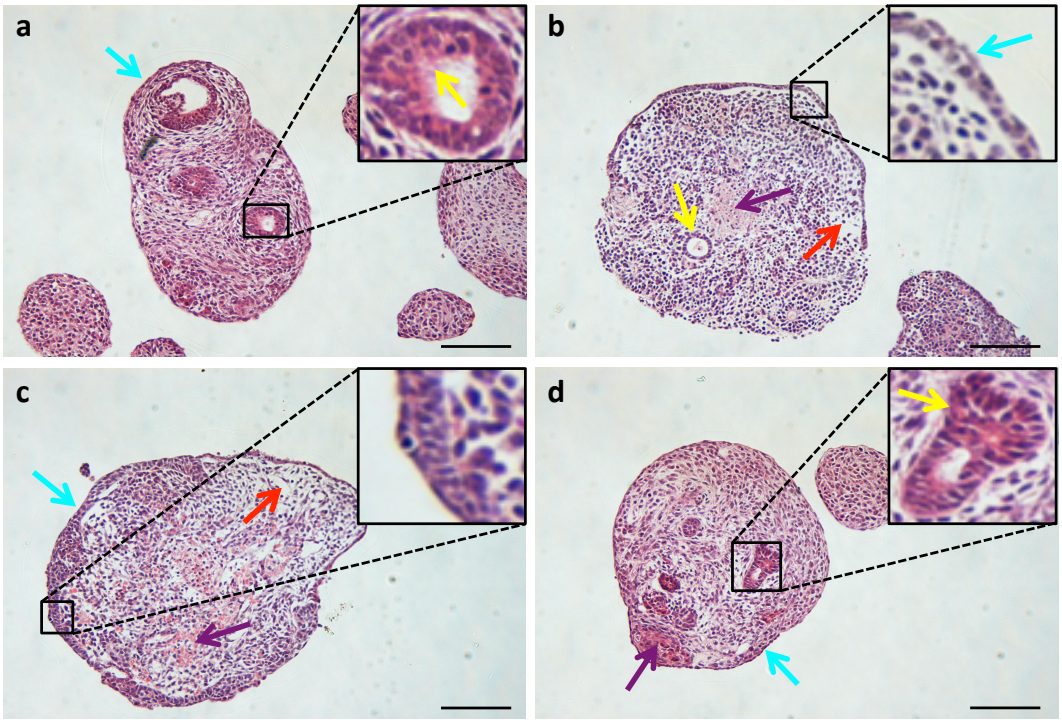

Figure A-3. (Continued) **H&E stains of embryoid bodies.**
Selection of Axin2$^{\Delta/\Delta}$ **(C)** and Axin2$^{lacZ.lacZ}$ **(D)** embryoid bodies stained with Haematoxylin and Eosin on day 14. Differentiation into different germ layers is indicated by arrows: Parietal endoderm (blue,→); mesoderm/internal epithelia (yellow, →); ectoderm/columnar epithelia (possibly neural tubes) (green,→); internal cyst structures red,→); collagen and laminin matrix deposition (purple,→). Magnification = x32. Scale bars = 50 µm. Pictures were taken with the help of Kyle Hawker. (Figure continues on the following pages)

E) Axin1$^{\Delta/\Delta}$, Axin2$^{\Delta/\Delta}$

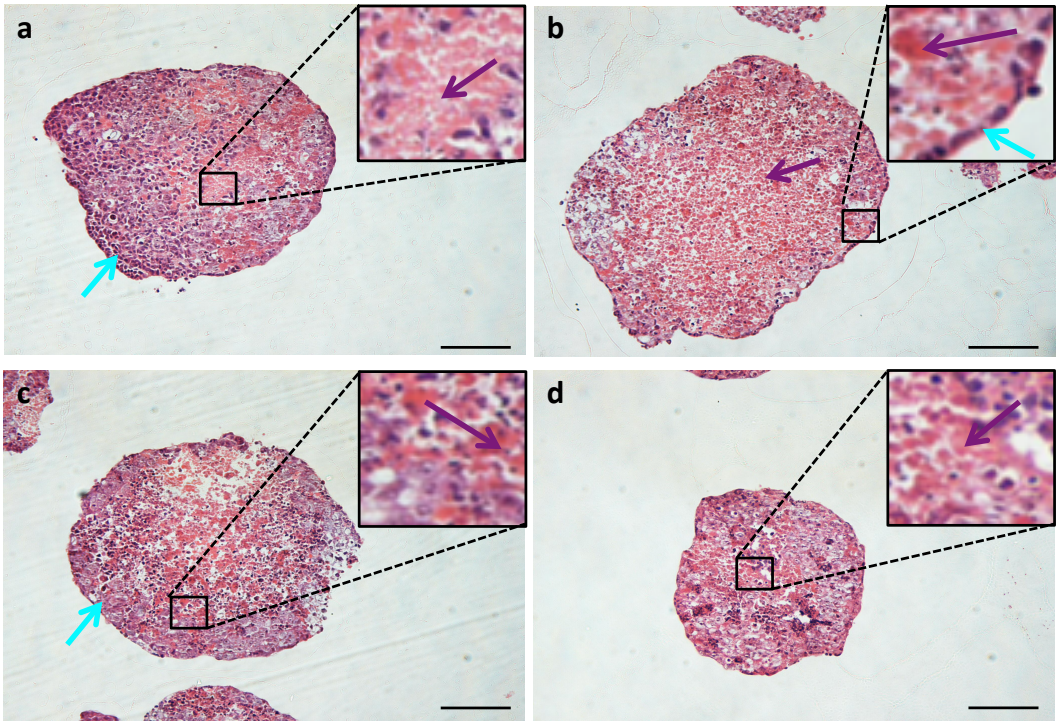

F) Axin1$^{\Delta/\Delta}$, Axin2$^{lacZ/lacZ}$

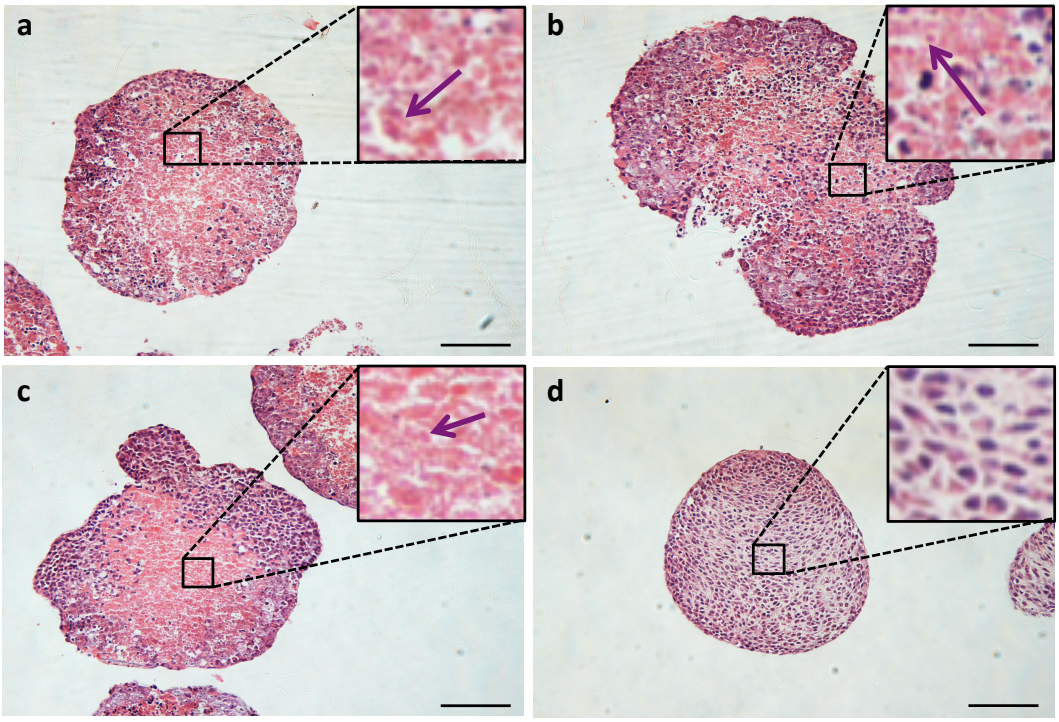

Figure A-3. (Continued) H&E stains of embryoid bodies.
Selection of Axin1$^{\Delta/\Delta}$,Axin2$^{\Delta/\Delta}$ **(E)** and Axin1$^{\Delta/\Delta}$,Axin2$^{lacZ.lacZ}$ **(F)** embryoid bodies stained with Haematoxylin and Eosin on day 14. Differentiation into different germ layers is indicated by arrows: Parietal endoderm (blue,→); mesoderm/internal epithelia (yellow, →); ectoderm/columnar epithelia (possibly neural tubes) (green,→); internal cyst structures red,→); collagen and laminin matrix deposition (purple,→). Magnification = x32. Scale bars = 50 µm. Pictures were taken with the help of Kyle Hawker. (Figure continues on the following page)

G) GSK3α$^{\Delta/\Delta}$, GSK3β$^{\Delta/\Delta}$

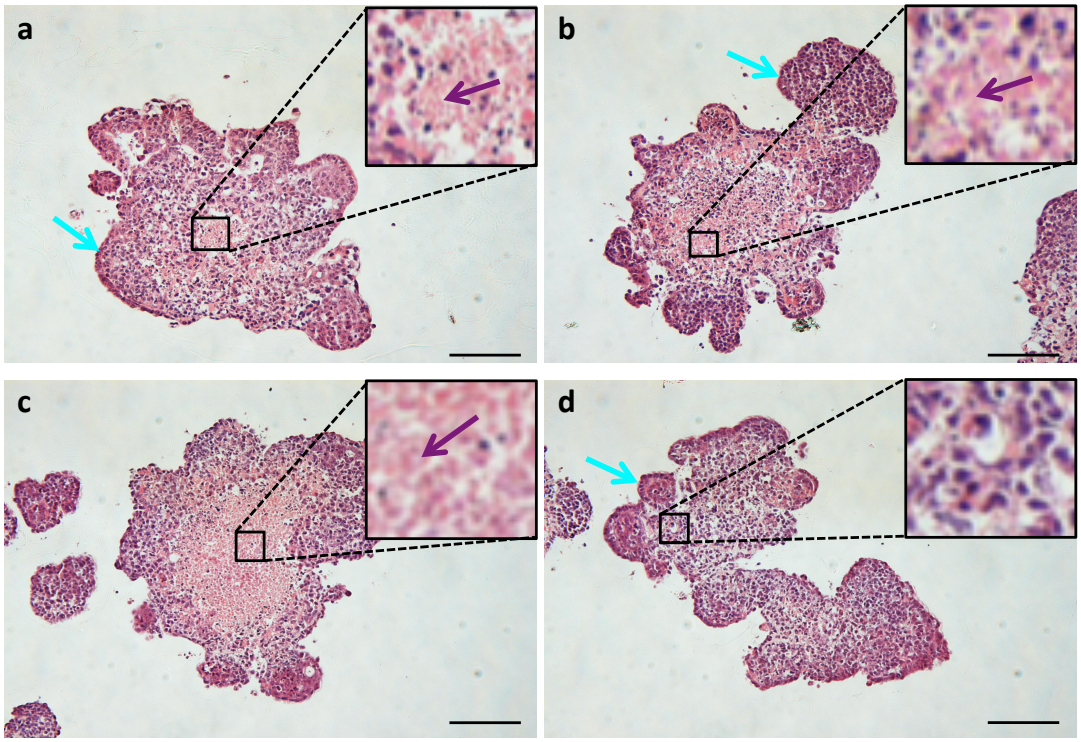

H) wt + CHIR

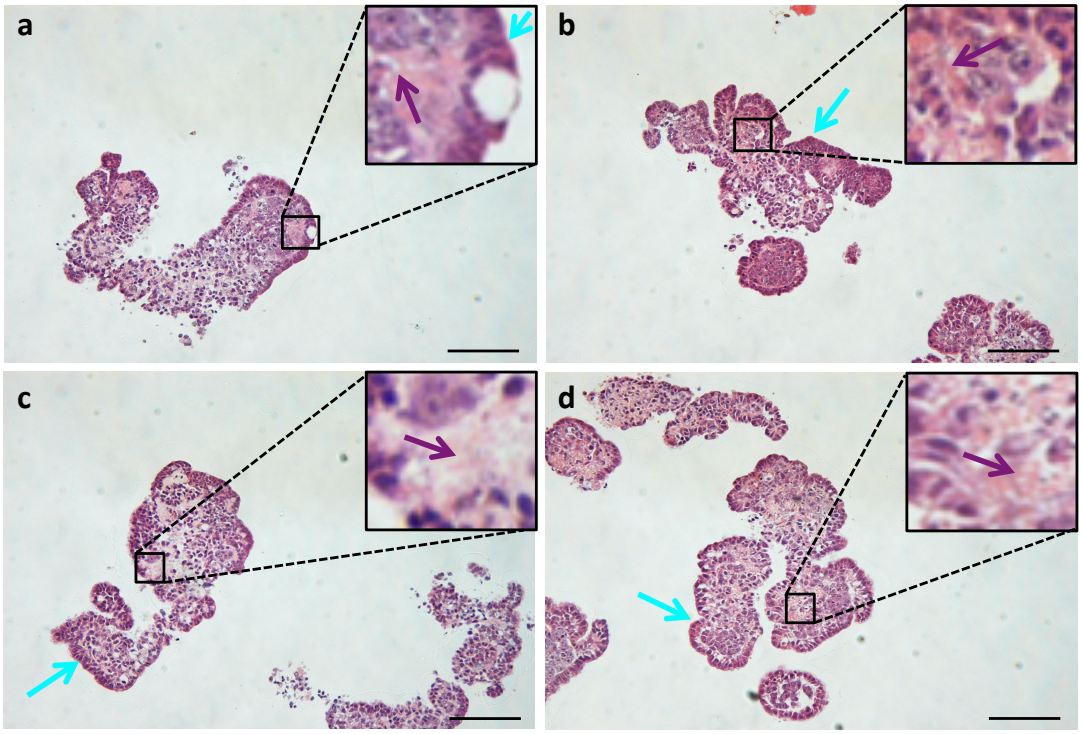

Figure A-3. (Continued) H&E stains of embryoid bodies.
Selection of GSK3a$^{\Delta/\Delta}$,GSK3b$^{\Delta/\Delta}$ **(G)** and Axin1$^{\Delta/\Delta}$,Axin2$^{lacZ.lacZ}$ **(H)** embryoid bodies stained with Haematoxylin and Eosin on day 14. Differentiation into different germ layers is indicated by arrows: Parietal endoderm (blue,→); mesoderm/internal epithelia (yellow, →); ectoderm/columnar epithelia (possibly neural tubes) (green,→); internal cyst structures (red,→); collagen and laminin matrix deposition (purple,→). Magnification = x32. Scale bars = 50 µm. Pictures were taken with the help of Kyle Halker.

Gene expression data fro the RT^2 PCR profiler array

Table A-2. Raw data from the RT^2 PCR Profiler Array performed on wt and $A1^{\Delta/\Delta}$, $A2^{\Delta/\Delta}$ EBs

GENE	$2^{-\Delta C_T}$ $A1^{fl/fl}$, $A2^{fl/fl}$ (wt)	$A1^{\Delta/\Delta}$, $A2^{\Delta/\Delta}$	FOLD UP/DOWN REGULATION	GENE GROUP
AFP	2.949158	0.026042	-113.24	Visceral Endoderm
Brix1	0.085447	0.252315	2.95	Stem Cell-Specific Genes
Cd34	0.003627	0.024709	6.81	Endothelial
Cd9	0.019096	0.068026	3.56	Stem Cell-Specific Genes
Cdh5	0.033889	0.001742	-19.45	Endothelial
Cdx2	0.00068	0.001626	2.39	Trophoblast
Col1a1	1.011883	0.55608	-1.82	Bone
Commd3	0.280287	0.012511	-22.4	Pluripotency and Self-Renewal
Crabp2	0.059388	0.002192	-27.09	Pluripotency and Self-Renewal
Dxd4	0.000116	0.000092	-1.26	Germ Cell
Des	0.04909	0.000179	-273.91	Muscle
Diap2	0.030435	0.000642	-47.44	Stem Cell-Specific Genes
Dnmt3b	0.004888	0.000146	-33.55	Stem Cell-Specific Genes
Ednrb	0.158582	0.004707	-33.69	Pluripotency and Self-Renewal
Eomes	0.003287	0.000967	-3.4	Trophoblast
Fgf4	0.000116	0.000463	4.01	Cytokines and Growth Factors
Fgf5	0.006931	0.000169	-41.05	Cytokines and Growth Factors
Flt1	0.004191	0.006101	1.46	Endothelial
Fn1	0.300987	0.022564	-13.34	Parietal Endoderm
Foxa2	0.003387	0.000774	-4.38	Extra-Embryonic Endoderm Markers
Foxd3	0.000116	0.000092	-1.26	'Stem-ness'
Gabrb3	0.001943	0.000766	-2.54	Pluripotency and Self-Renewal
Gal	0.000139	0.001126	8.08	Neural
Gata4	0.001559	0.004327	2.78	Extra-Embryonic Endoderm Markers
Gata6	0.148766	0.000825	-180.38	'Stem-ness'
Gbx2	0.001031	0.001274	1.24	'Stem-ness'
Gcg	0.000116	0.000092	-1.26	Pancreas
Gcm1	0.000116	0.002184	18.89	Trophoblast
Gdf3	0.000455	0.000684	1.5	Cytokines and Growth Factors
Grb7	0.001597	0.00392	2.46	Pluripotency and Self-Renewal
Hba-x	0.42248	0.030954	-13.65	Blood
Hbb-y	0.238328	0.092534	-2.58	Blood
Hck	0.003086	0.000094	-32.94	Pluripotency and Self-Renewal
Iapp	0.000204	0.000092	-2.21	Pancreas
Ifitm1	0.283296	0.011572	-24.48	Pluripotency and Self-Renewal
Ifitm2	0.13966	0.060703	-2.3	Stem Cell-Specific Genes
Igf2bp2	0.061717	0.011414	-5.41	Stem Cell-Specific Genes
Il6st	0.150765	0.023619	-6.38	Cytokines and Growth Factors
Ins2	0.000116	0.000092	-1.26	Pancreas
Kit	0.053739	0.008194	-6.56	Pluripotency and Self-Renewal
Krt1	0.007811	0.002123	-3.68	Trophoblast
Lama1	0.000401	0.144899	361.4	Parietal Endoderm
Lamb1	0.038957	0.164844	4.23	Parietal Endoderm
Lamc1	0.01705	0.093403	5.48	Parietal Endoderm
Lefty1	0.012041	0.003412	-3.53	Cytokines and Growth Factors
Lefty2	0.00156	0.000138	-11.3	Cytokines and Growth Factors
Lifr	0.002351	0.120479	51.24	Pluripotency and Self-Renewal

Table A-2. (Continued) Raw data from the RT^2 PCR Profiler Array performed on wt and A1$^{\Delta/\Delta}$, A2$^{\Delta/\Delta}$ EBs

GENE	2^-ΔC$_T$ A1$^{fl/fl}$, A2$^{fl/fl}$(wt)	A1$^{\Delta/\Delta}$, A2$^{\Delta/\Delta}$	FOLD UP/DOWN REGULATION	GENE GROUP
Lin28a	0.005295	0.006113	1.15	Stem Cell-Specific Genes
Myf5	0.000116	0.000092	-1.26	Muscle
Myod1	0.000119	0.000092	-1.29	Muscle
Nanog	0.000116	0.014755	127.62	'Stem-ness'
Nes	0.009897	0.001217	-8.13	Neural
Neurod1	0.001693	0.000092	-18.4	Neural
Nodal	0.000116	0.000092	-1.26	Pluripotency and Self-Renewal
Nog	0.000902	0.001974	2.19	Pluripotency and Self-Renewal
Nr5a2	0.00431	0.002245	-1.92	'Stem-ness'
Nr6a1	709.70681	0.041483	-17108.5	'Stem-ness'
Numb	0.009876	0.005724	-1.73	Pluripotency and Self-Renewal
Olig2	0.000116	0.000092	-1.26	Differentiation
Pax4	0.000116	0.000092	-1.26	Pancreas
Pax6	0.007389	0.000516	-14.31	Neural
Pdx1	0.000549	0.000092	-5.97	Pancreas
Pecam1	0.087733	0.035818	-2.45	Endothelial
Podxl	0.084437	0.217323	2.57	Stem Cell-Specific Genes
Pou5f1	0.033439	0.061983	1.85	'Stem-ness'
Pten	0.2996	0.053141	-5.64	Pluripotency and Self-Renewal
Ptf1a	0.00201	0.000092	-21.85	Extra-Embryonic Endoderm Markers
Rest	0.173505	0.20862	1.2	Stem Cell-Specific Genes
Runx2	0.001444	0.007689	5.32	Bone
Sema3a	0.017322	0.084621	4.89	Stem Cell-Specific Genes
Serpina1a	0.014966	0.002089	-7.16	Viseral Endoderm
Sfrp2	0.228316	0.08499	-2.69	Pluripotency and Self-Renewal
Sox17	0.000984	0.007944	8.07	Parietal Endoderm
Sox2	0.012419	0.006664	-1.86	'Stem-ness'
Sst	0.000516	0.000092	-5.61	Pancreas
Sycp3	0.000116	0.000092	-1.26	Germ Cell
T	0.004604	0.001608	-2.86	Mesoderm
Tat	0.001481	0.000092	-16.1	Differentiation
Tcfcp2l1	0.007051	0.030632	4.34	'Stem-ness'
Tdgf1	0.0135	0.009072	-1.49	Cytokines and Growth Factors
Tert	0.008094	0.010965	1.35	Stem Cell-Specific Genes
Utf1	0.010183	0.032823	3.22	'Stem-ness'
Wt1	0.062049	0.006389	-9.71	Mesoderm
Zfp42	0.004123	0.011553	2.8	'Stem-ness'
Acb	6.273595	6.055836	-1.04	Housekeeper
B2m	1.363732	1.293953	-1.05	Housekeeper
Gapdh	2.413381	2.088877	-1.16	Housekeeper
Gusb	0.097639	0.086543	-1.13	Housekeeper
Hsp90ab1	3.111874	4.275007	1.37	Housekeeper

Appendix 4: Alternative start codons of Axin$^{\Delta/\Delta}$

Start codons in Axin1

Table A 3. Initiation codons identified in Axin1 version 1 cDNA.

RELIABILITY	IDENTITY TO KOZAK RULE A/GXXATGG	START (bp)	FINISH (bp)	ORF Length (aa)	DOMAINS FOUND IN PROTEIN BLAST	SEQUENCE
0.33	cXXATGc	421	3024	868	TNKs-binding site RGS domain β-Catenin binding site DIX domain	MQSPKMNVQEQGFPLDLGASFTEDAPRPPVPGEEGELVSTDSRPVNHSFCSGKGTSIKSETSTATPRRSD LDLGYEPEGSASPTPPYLRWAESLHSLLDDQDGISLFRTFLKQEGCADLLDFWFACSGFRKLEPCDSNEEKR LKLARAIYRKYILDSNGIVSRQTKPATKSFIKDCVMKQQIDPAMFDQAQTEIQSTMEENTYPSFLKSDIYLEY TRTGSESPKVCSDQSSGSGTGKGMSGYLPTLNEDEEWKCDQDADEDDGRDPLPPSRLTQKLLLETAAPR APSSRRYNEGRELRYGSWREPVNPYYVNSGYALAPATSANDSEQQSLSSDADTLSLTDSSVDGIPPYRIRK QHRREMQESIQVNGRVPLPHIPRTYRMPKEIRVEPQKFAEELIHRLEAVQRTREAEEKLEERLKRVRMEEE GEDGEMPSGPMASHKLPSVPAWHHFPPRYVDMGCSGLRDAHEENPESILDEHVQRVMRTPGCQSPGP GHRSPDSGHVAKTAVLGGTASGHGKHVPKLGLKLDTAGLHHHRHVHHHVHHNSARPKEQMEAEVARR VQSSFSWGPETHGHAKPRSYSENAGTTLSAGDLAFGGKTSAPSKRNTKKAESGKNANAEVPSTTEDAEK NQKIMQWIIEGEKEISRHRKAGHGSSGLRKQQAHESSRPLSIERPGAVHPWVSAQLRNSVQPSHLFIQDP TMPPNPAPNPLTQLEEARRRLEEEEKRANKLPSKQRYVQAVMQRGRTCVRPACAPVLSVVPAVSDLELSE TETKSQRKAGGGSAPPCDSIVVAYYFCGEPIPYRTLVRGRAVTLGQFKELLTKKGSYRYYFKKVSDEFDCGV VFEEVREDEAVLPVFEEKIIGKVEKVD

The Axin1 cDNA sequence (Vega Genome Browser) was analysed using the online tool ATGpr (Nishikawa et al. 2000). Protein sequences were then blasted using NCBI's BLASTP to find protein domains.

Table A 4. Initiation codons identified in Axin1$^{\Delta/\Delta}$ cDNA

RELIABILITY	IDENTITY TO KOZAK RULE A/GXXATGG	START (bp)	FINISH (bp)	ORF Length (aa)	DOMAINS FOUND IN PROTEIN BLAST	SEQUENCE
0.55	cXXATGG	294	623	110	N/A	MGLAGPGARPRAAPPQPPRAGMDLGGSPSTPTTSTLAMPWPQPPVPMTVSSRACPVMLTRYPLRTVVW MESPHTGSVSSTEGRCRRVSKSMGGYLYLTFLALTECQRRSG
0.53	GXXATGc	542	2065	508	β-Catenin binding site DIX domain	MQESIQVNGRVPLPHIPRTYRMPKEIRVEPQKFAEELIHRLEAVQRTREAEEKLEERLKRVRMEEEGEDGEM PSGPMASHKLPSVPAWHHFPPRYVDMGCSGLRDAHEENPESILDEHVQRVMRTPGCQSPGPGHRSPDS GHVAKTAVLGGTASGHGKHVPKLGLKLDTAGLHHHRHVHHHVHHNSARPKEQMEAEVARRVQSSFSWG PETHGHAKPRSYSENAGTTLSAGDLAFGGKTSAPSKRNTKKAESGKNANAEVPSTTEDAEKNQKIMQWIIE GEKEISRHRKAGHGSSGLRKQQAHESSRPLSIERPGAVHPWVSAQLRNSVQPSHLFIQDPTMPPNPAPNPL TQLEEARRRLEEEEKRANKLPSKQRYVQAVMQRGRTCVRPACAPVLSVVPAVSDLELSETETKSQRKAGGG SAPPCDSIVVAYYFCGEPIPYRTLVRGRAVTLGQFKELLTKKGSYRYYFKKVSDEFDCGVVFEEVREDEAVLPV FEEKIIGKVEKVD
0.31	GXXATGc	1682	2065	128	DIX domain	MQRGRTCVRPACAPVLSVVPAVSDLELSETETKSQRKAGGGSAPPCDSIVVAYYFCGEPIPYRTLVRGRAVT LGQFKELLTKKGSYRYYFKKVSDEFDCGVVFEEVREDEAVLPVFEEKIIGKVEKVD
0.29	GXXATGt	1071	1430	120	N/A	MSTTMFTIIQLDLRSKWRLKLPAGSRAASRGAQKHMVMPSPGAIPRTQAPPSVLGIWPLVVKLVHLPKETP RRLNLGRMPMLRYPVPQRTLRRTRRSCSGSLRERRRSVDTGRQAMGLLG
0.28	AXXATGc	1562	2065	168	DIX domain	MPPNPAPNPLTQLEEARRRLEEEEKRANKLPSKQRYVQAVMQRGRTCVRPACAPVLSVVPAVSDLELSETE TKSQRKAGGGSAPPCDSIVVAYYFCGEPIPYRTLVRGRAVTLGQFKELLTKKGSYRYYFKKVSDEFDCGVVFE EVREDEAVLPVFEEKIIGKVEKVD
0.26	GXXATGG	357	623	89	N/A	MDLGGSPSTPTTSTLAMPWPQPPVPMTVSSRACPVMLTRYPLRTVVWMESPHTGSVSSTEGRCRRVSKS MGGYLYLTFLALTECQRRSG
0.23	GXXATGG	833	2065	411	β-Catenin binding site DIX domain	MGCSGLRDAHEENPESILDEHVQRVMRTPGCQSPGPGHRSPDSGHVAKTAVLGGTASGHGKHVPKLGLK LDTAGLHHHRHVHHHVHHNSARPKEQMEAEVARRVQSSFSWGPETHGHAKPRSYSENAGTTLSAGDLAF GGKTSAPSKRNTKKAESGKNANAEVPSTTEDAEKNQKIMQWIIEGEKEISRHRKAGHGSSGLRKQQAHESS RPLSIERPGAVHPWVSAQLRNSVQPSHLFIQDPTMPPNPAPNPLTQLEEARRRLEEEEKRANKLPSKQRYV QAVMQRGRTCVRPACAPVLSVVPAVSDLELSETETKSQRKAGGGSAPPCDSIVVAYYFCGEPIPYRTLVRGR AVTLGQFKELLTKKGSYRYYFKKVSDEFDCGVVFEEVREDEAVLPVFEEKIIGKVEKVD

Table A 4. (Continued) Initiation codons identified in Axin1$^{\Delta/\Delta}$ cDNA

RELIABILITY	IDENTITY TO KOZAK RULE A/GXXATGG	START (bp)	FINISH (bp)	ORF Length (aa)	DOMAINS FOUND IN PROTEIN BLAST	SEQUENCE
0.18	cXXATGG	1118	2065	316	DIX domain	MEAEVARRVQSSFSWGPETHGHAKPRSYSENAGTTLSAGDLAFGGKTSAPSKRNTKKAESGKNANAEVPS TTEDAEKNQKIMQWIIEGEKEISRHRKAGHGSSGLRKQQAHESSRPLSIERPGAVHPWVSAQLRNSVQPSH LFIQDPTMPPNPAPNPLTQLEEARRRLEEEEKRANKLPSKQRYVQAVMQRGRTCVRPACAPVLSVVPAVSD LELSETETKSQRKAGGGSAPPCDSIVVAYYFCGEPIPYRTLVRGRAVTLGQFKELLTKKGSYRYYFKKVSDEFD CGVVFEEVREDEAVLPVFEEKIIGKVEKVD
0.17	GXXATGG	233	286	18	N/A	MGAPQGRAPAVARPLSRR
0.14	AXXATGt	1083	1430	116	N/A	MFTIIQLDLRSKWRLKLPAGSRAASRGAQKHMVMPSPGAIPRTQAPPSVLGIWPLVVKLVHLPKETPRRLN LGRMPMLRYPVPQRTLRRTRRSCSGSLRERRRSVDTGRQAMGLLG

The Axin1 cDNA sequence (Vega Genome Browser) was analysed using the online tool ATGpr (Nishikawa et al. 2000). Protein sequences were then blasted using NCBI's BLASTP to find protein domains.

Start codons in Axin2

Table A 5. Initiation codons identified in Axin2 version 1 cDNA.

RELIABILITY	IDENTITY TO KOZAK RULE A/GXXATGG	START (bp)	FINISH (bp)	ORF Length (aa)	DOMAINS FOUND IN PROTEIN BLAST	SEQUENCE
0.28	AXXATGa	350	2869	840	TNKs-binding site RGS domain β-Catenin binding site DIX domain	MSSAVLVTLLPDPSSSFREDAPRPPVPGEEGETPPCQPSVGKVQSTKPMPVSSNARRNEDGLGEPEGRASPD SPLTRWTKSLHSLLGDQDGAYLFRTFLEREKCVDTLDFWFACNGFRQMNLKDTKTLRVAKAIYKRYIENNSVV SKQLKPATKTYIRDGIKKQQIGSVMFDQAQTEIQAVMEENAYQVFLTSDIYLEYVRSGGENTAYMSNGGLGSL KVLCGYLPTLNEEEEWTCADLKCKLSPTVVGLSSKTLRATASVRSTETAENGFRSFKRSDPVNPYHVGSGYVFA PATSANDSELSSDALTDDSMSMTDSSVDGVPPYRMGSKKQLQREMHRSVKANGQVSLPHFPRTHRLPKEM TPVEPAAFAAELISRLEKLKLELESRHSLEERLQQIREDEEKEGSEQALSSRDGAPVQHPLALLPSGSYEEDPQTIL DDHLSRVLKTPGCQSPGVGRYSPRSRSPDHHHQHHHHQQCHTLLPTGGKLPPVAACPLLGGKSFLTKQTTKH VHHHYIHHHAVPKTKEEIEAEATQRVRCLCPGGTDYYCYSKCKSHPKAPEPLPGEQFCGSRGGTLPKRNAKGT EPGLALSARDGGMSSAAGAPQLPGEEGDRSQDVWQWMLESERQSKSKPHSAQSIRKSYPLESACAAPGERV SRHHLLGASGHSRSVARAHPFTQDPAMPPLTPPNTLAQLEEACRRLAEVSKPQKQRCCVASQQRDRNHSAA GQAGASPFANPSLAPEDHKEPKKLASVHALQASELVVTYFFCGEEIPYRRMLKAQSLTLGHFKEQLSKKGNYRY YFKKASDEFACGAVFEEIWDDETVLPMYEGRILGKVERID

The Axin2 cDNA sequence (Vega Genome Browser) was analysed using the online tool ATGpr (Nishikawa et al. 2000). Protein sequences were then blasted using NCBI's BLASTP to find protein domains.

Table A 6. Initiation codons identified in Axin2$^{\Delta/\Delta}$ cDNA.

RELIABILITY	IDENTITY TO KOZAK RULE A/GXXATGG	START (bp)	FINISH (bp)	ORF Length (aa)	DOMAINS FOUND IN PROTEIN BLAST	SEQUENCE
0.55	GXXATGG	2557	2922	122	N/A	MGHPHPTPPPAMLLCLSQTSCGLVVTASSPLWGPSRVGEWGRLHPGAKGYTVRVVPEPVTALVVQASSASLGSEGFLFSFKNQSLDYGHQESTLAHLTLRGHGHPAAPLLCYLPLGDRSGLC
0.52	tXXATGt	332	1918	529	β-Catenin binding site DIX domain	MSMTDSSVDGVPPYRMGSKKQLQREMHRSVKANGQVSLPHFPRTHRLPKEMTPVEPAAFAAELISRLEKLKLELESRHSLEERLQQIREDEEKEGSEQALSSRDGAPVQHPLALLPSGSYEEDPQTILDDHLSRVLKTPGCQSPGVGRYSPRSRSPDHHHQHHHHQQCHTLLPTGGKLPPVAACPLLGGKSFLTKQTTKHVHHHYIHHHAVPKTKEEIEAEATQRVRCLCPGGTDYYCYSKCKSHPKAPEPLPGEQFCGSRGGTLPKRNAKGTEPGLALSARDGGMSSAAGAPQLPGEEGDRSQDVWQWMLESERQSKSKPHSAQSIRKSYPLESACAAPGERVSRHHLLGASGHSRSVARAHPFTQDPAMPPLTPPNTLAQLEEACRRLAEVSKPQKQRCCVASQQRDRNHSAAGQAGASPFANPSLAPEDHKEPKKLASVHALQASELVVTYFFCGEEIPYRRMLKAQSLTLGHFKEQLSKKGNYRYYFKKASDEFACGAVFEEIWDDETVLPMYEGRILGKVERID
0.42	GXXATGc	1442	1918	159	N/A	MPPLTPPNTLAQLEEACRRLAEVSKPQKQRCCVASQQRDRNHSAAGQAGASPFANPSLAPEDHKEPKKLASVHALQASELVVTYFFCGEEIPYRRMLKAQSLTLGHFKEQLSKKGNYRYYFKKASDEFACGAVFEEIWDDETVLPMYEGRILGKVERID
0.38	GXXATGc	2590	2922	111	N/A	MLLCLSQTSCGLVVTASSPLWGPSRVGEWGRLHPGAKGYTVRVVPEPVTALVVQASSASLGSEGFLFSFKNQSLDYGHQESTLAHLTLRGHGHPAAPLLCYLPLGDRSGLC
0.37	GXXATGa	482	1918	479	β-Catenin binding site DIX domain	MTPVEPAAFAAELISRLEKLKLELESRHSLEERLQQIREDEEKEGSEQALSSRDGAPVQHPLALLPSGSYEEDPQTILDDHLSRVLKTPGCQSPGVGRYSPRSRSPDHHHQHHHHQQCHTLLPTGGKLPPVAACPLLGGKSFLTKQTTKHVHHHYIHHHAVPKTKEEIEAEATQRVRCLCPGGTDYYCYSKCKSHPKAPEPLPGEQFCGSRGGTLPKRNAKGTEPGLALSARDGGMSSAAGAPQLPGEEGDRSQDVWQWMLESERQSKSKPHSAQSIRKSYPLESACAAPGERVSRHHLLGASGHSRSVARAHPFTQDPAMPPLTPPNTLAQLEEACRRLAEVSKPQKQRCCVASQQRDRNHSAAGQAGASPFANPSLAPEDHKEPKKLASVHALQASELVVTYFFCGEEIPYRRMLKAQSLTLGHFKEQLSKKGNYRYYFKKASDEFACGAVFEEIWDDETVLPMYEGRILGKVERID
0.25	GXXATGG	642	908	89	N/A	MEHRSSTPWPSYPPAAMKRTHKPFWTTTSPGSSRPPAVNPLVWVAIAHGPAPPTTTTSTTTISSVIPFFRLGASCPPWLLAPSLEARAS
0.25	tXXATGG	2523	2774	84	N/A	MVPAPPIDTCRNGSPPPHPTPRHAALLVTDVLWVGCDSIFTTLGTIQSGGVGETSPWSQRLHRTCSPRARHSPCGSSFFCLFRK

Table A 6 (Continued) Initiation codons identified in Axin2$^{\Delta/\Delta}$ cDNA.

RELIABILITY	IDENTITY TO KOZAK RULE A/GXXATGG	START (bp)	FINISH (bp)	ORF Length (aa)	DOMAINS FOUND IN PROTEIN BLAST	SEQUENCE
0.21	tXXATGa	338	1918	527	β-Catenin binding site DIX domain	MTDSSVDGVPPYRMGSKKQLQREMHRSVKANGQVSLPHFPRTHRLPKEMT PVEPAAFAAELISRLEKLKLELESRHSLEERLQQIREDEEKEGSEQALSSRDGAPVQHPLALLPSGSYEEDPQTILDDH LSRVLKTPGCQSPGVGRYSPRSRSPDHHHQHHHHQQCHTLLPTGGKLPPVAACPLLGGKSFLTKQTTKHVHHHYI HHHAVPKTKEEIEAEATQRVRCLCPGGTDYYCYSKCKSHPKAPEPLPGEQFCGSRGGTLPKRNAKGTEPGLALSAR DGGMSSAAGAPQLPGEEGDRSQDVWQWMLESERQSKSKPHSAQSIRKSYPLESACAAPGERVSRHHLLGASGH SRSVARAHPFTQDPAMPPLTPPNTLAQLEEACRRLAEVSKPQKQRCCVASQQRDRNHSAAGQAGASPFANPSLA PEDHKEPKKLASVHALQASELVVTYFFCGEEIPYRRMLKAQSLTLGHFKEQLSKKGNYRYYFKKASDEFACGAVFEEI WDDETVLPMYEGRILGKVERID
0.18	cXXATGG	377	1918	514	β-Catenin binding site DIX domain	MGSKKQLQREMHRSVKANGQVSLPHFPRTHRLPKEMTPVEPAAFAAELISRLEKLKLELESRHSLEERLQQIREDE EKEGSEQALSSRDGAPVQHPLALLPSGSYEEDPQTILDDHLSRVLKTPGCQSPGVGRYSPRSRSPDHHHQHHHHQ QCHTLLPTGGKLPPVAACPLLGGKSFLTKQTTKHVHHHYIHHHAVPKTKEEIEAEATQRVRCLCPGGTDYYCYSKCK SHPKAPEPLPGEQFCGSRGGTLPKRNAKGTEPGLALSARDGGMSSAAGAPQLPGEEGDRSQDVWQWMLESER QSKSKPHSAQSIRKSYPLESACAAPGERVSRHHLLGASGHSRSVARAHPFTQDPAMPPLTPPNTLAQLEEACRRLA EVSKPQKQRCCVASQQRDRNHSAAGQAGASPFANPSLAPEDHKEPKKLASVHALQASELVVTYFFCGEEIPYRRM LKAQSLTLGHFKEQLSKKGNYRYYFKKASDEFACGAVFEEIWDDETVLPMYEGRILGKVERID
0.18	GXXATGt	1187	1918	244	DIX domain	MSSAAGAPQLPGEEGDRSQDVWQWMLESERQSKSKPHSAQSIRKSYPLESACAAPGERVSRHHLLGASGHSRS VARAHPFTQDPAMPPLTPPNTLAQLEEACRRLAEVSKPQKQRCCVASQQRDRNHSAAGQAGASPFANPSLAPE DHKEPKKLASVHALQASELVVTYFFCGEEIPYRRMLKAQSLTLGHFKEQLSKKGNYRYYFKKASDEFACGAVFEEIW DDETVLPMYEGRILGKVERID

The Axin2 cDNA sequence without exon 2 (Vega Genome Browser) was analysed using the online tool ATGpr (Nishikawa et al. 2000). Protein sequences were then blasted using NCBI's BLASTP to find protein domains.

Appendix 5: CARS analysis of liver organoids

z-Stacks of EM and DM organoids

Movie A-2. CARS miscopy of liver organoids.
Liver organoids in EM **(A)** or DM **(B)** imaged using Coherent anti-Stokes Raman Scattering (CARS) microscopy at the lipid peak (2850 cm^{-1}). Z-stacks were taken in 0.5 µm steps with the help of Iestyn Pope. Imagine frame was 150 x 150 µm. Videos can be viewed from the CD attached to this thesis or by following the above QR code or the link below:
https://www.youtube.com/playlist?list=PLK8osD0S9jrxRC7b0KvNuTIBeL17r9lUg